Spatiotemporal Dynamics and Pattern Formation Analysis of Biological Species Interaction with Various Ecological Factors

THESIS

Submitted in partial fulfilment of the requirements for the degree of

DOCTOR OF PHILOSOPHY

by

ANSHU
ID No. 2019PHXF0404P

Under the Supervision of

PROF. BALRAM DUBEY

BITS Pilani
Pilani | Dubai | Goa | Hyderabad | Mumbai

BIRLA INSTITUTE OF TECHNOLOGY AND SCIENCE, PILANI

2024

BIRLA INSTITUTE OF TECHNOLOGY & SCIENCE, PILANI

CERTIFICATE

This is to certify that the thesis titled **"Spatiotemporal Dynamics and Pattern Formation Analysis of Biological Species Interaction with Various Ecological Factors"** submitted by **Ms. Anshu**, ID No. **2019PHXF0404P** for the award of Ph.D. of the institute embodies original work done by her under my supervision.

_____

Signature of the Supervisor
Name: **PROF. BALRAM DUBEY**
Designation: **Professor**

Date: **September 12, 2024**

Acknowledgments

First and foremost, I extend my gratitude to the Almighty for blessing me with the strength, purpose, enthusiasm, and confidence to reach so far and achieve my goals. I pray for continued blessings in my future endeavors.

I would like to express my sincere appreciation to my supervisor, Prof. Balram Dubey, whose guidance was instrumental in pursuing my research and completing this thesis. His insightful feedback, unwavering encouragement, and meaningful discussions motivated me to enhance my analytical skills, significantly aiding my research endeavors. I am genuinely grateful for his profound expertise and steadfast commitment to fostering my intellectual development as a researcher. I am forever indebted to his invaluable contributions to my research journey.

I wish to extend my heartfelt appreciation to the members of my Doctoral Advisory Committee (DAC), Prof. Ashish Tiwari and Prof. Bhupendra Kumar Sharma, for generously offering their expertise and knowledge to support this research endeavor. Their thoughtful feedback has been instrumental in refining my ideas, honing my focus, and enhancing my analytical abilities.

I am deeply grateful to Prof. Bhupendra Kumar Sharma (Former HoD) and Prof. Devendra Kumar, the current HoD of the Department of Mathematics, for their gracious guidance and support throughout this journey. I also acknowledge the faculty members and fellow research scholars for their invaluable assistance and cooperation during my research endeavors. The memories and relationships formed during this time hold a special place in my heart and will be cherished indefinitely. I extend my gratitude for their significant contributions to my academic growth.

Furthermore, I would like to express my thanks to the Vice-Chancellor, Director, Dean Academic (AGSRD), and Registrar of BITS Pilani for providing me an opportunity to achieve a challenging position in the respective field pertinent to my qualifications, which allowed me to use my skills to prove myself worthy.

I express my deepest gratitude to Dr. Sourav Kumar Sasmal of IIT Roorkee for his invaluable guidance, encouragement, and advice. I have gleaned significant insights from your wealth of experiences, expertise, and perspectives, and I appreciate the time and dedication you have invested in my growth. Your generosity in sharing your knowledge and insights has served as a wellspring of inspiration and motivation for me. Additionally, I express sincere appreciation and owe a debt of gratitude to my seniors, Dr. Ankit Kumar and Dr. Sajan, for their assistance in elucidating concepts and guiding me through the research process. Furthermore, I extend thanks to Ashvini, Masoom, Arjun, and Anand, who have brought new perspectives and energy

to our research discussions, inspiring me to keep pushing the boundaries of my research. I am truly fortunate to have collaborated with such talented and committed individuals, and I am grateful for their unwavering support and encouragement.

My family deserves special mention for their unwavering support and blessings. I want to acknowledge my parents, Mr. Maman Singh Mor and Mrs. Sunil Devi, to whom I owe all that I have ever accomplished. They have been a source of unconditional support, love, care, and motivation when needed. I want to express my deep gratitude to my brother Ashish Mor for his enduring love and encouragement throughout this journey. With heartfelt thanks, I extend special appreciation to my in-law's family members, my father-in-law, Mr. Om Prakash Kalkal, and my mother-in-law, Mrs. Kamlesh Kalkal, for their immense love and support. Completing this work would not have been possible without the steadfast support, patience, and understanding of my beloved husband, Manish Kalkal. His unwavering encouragement, affection, and faith in me have been my greatest pillars of strength throughout the journey of completing this thesis.

I am thankful to University Grants Commission (UGC), New Delhi for financial assistance during my Ph.D. tenure.

Place: BITS Pilani
Date: September 12, 2024

Anshu
(Department of Mathematics)

Abstract

Prey-predator dynamics is an elementary notion in ecology that enables us to comprehend population fluctuations and complex relationships between predators and their prey in ecosystems. Modeling these prey-predator interactions helps us to assess the status and viability of endangered species populations, facilitate sustainable management of natural resources, etc. Mathematically, these interactions can be modeled using differential equations. Through mathematical analysis and simulation, these models offer valuable insights into the mechanisms underlying predator-prey dynamics. Various ecological factors such as fear effect, hunting cooperation, prey refuge, carry-over effects, time delay, and random movement of individuals can significantly influence the prey-predator dynamics. Incorporating these factors into the models enhances the realism and intricacy of the ecological systems.

This thesis attempts to study various ecological models that depict the interaction between prey and predator species incorporating various environmental factors, which can significantly affect the system dynamics. This thesis consists of six chapters. The introductory chapter provides essential background information to facilitate understanding of the remaining chapters. The subsequent chapters formulate and analyze the various spatiotemporal models represented using ordinary, partial, or delay differential equations. The well-posedness and feasibility of multiple steady-states are investigated for all the proposed models. We analyzed the system dynamics using the stability theories for non-delayed and delayed models, bifurcation theory, chaos theory, and the theory for spatial models. Extensive numerical simulations are conducted to corroborate the analytical findings. The abstracts for all chapters are provided below.

Chapter 1 begins with the basic introduction to the subsequent chapters. It contains the background, objective, and motivation of the research work presented in the thesis. This chapter briefly discusses some fundamental concepts and mathematical tools used throughout the remaining chapters.

Cooperation among species is a ubiquitous behavior that helps us better understand the system dynamics from an ecological perspective. Hunting cooperation among predators can impose fear effects on the prey population, thereby decreasing the prey's birth rate. Considering this fact, in Chapter 2, we propose a model that incorporates hunting cooperation among predators and the fear induced birth reduction in the prey population. We have done the complete dynamical analysis, including boundedness of solutions, persistence of the system, existence of all equilibria and their local and global stability, existence of Hopf-bifurcation and its direction and stability, existence of saddle-node bifurcation. We analyzed Hopf-bifurcation with respect

to the hunting cooperation parameter and observed that system undergoes saddle-node bifurcation by varying the predation rate. Moreover, we analyzed the multi-stability of the system and observe that bi-stability occur in two different scenarios. In the spatially extended system, we provided detailed stability analysis and obtained the conditions for Turing instability. Various Turing patterns such as spots, holes, and stripes are obtained and discussed the biological significance of these patterns for the two-dimensional spatial model.

Recent studies indicate that the presence of prey refuge can help prolong the prey-predator interactions by decreasing the risk of extinction for prey species caused by predation. Chapter 3 presents a qualitative analysis of a modified Leslie-Gower prey-predator model with fear effect and prey refuge in the presence of diffusion and time delay. For the non-delayed temporal system, we examined the dissipativeness and persistence of the solutions. The existence of equilibria and stability analysis are performed to comprehend the complex behavior of the proposed model. Bifurcation of codimension-1 such as Hopf-bifurcation, saddle-node are investigated. In addition, it is observed that increasing the strength of fear may induce periodic oscillations, and a higher value of fear may lead to the extinction of prey species. The system shows a bistability attribute involving two stable equilibria. The impact of providing spatial refuge to the prey population is also examined. We noticed that prey refuge benefits both the species up to a specific threshold value beyond which it turns detrimental to predator species. For the non-spatial delayed system, the direction and stability of Hopf-bifurcation are investigated with the help of the center manifold theorem and normal form theory. We noticed that increasing the delay parameter may destabilize the system by producing periodic oscillations. For the spatiotemporal system, we derived the analytical conditions for Turing instability. We investigated the pattern dynamics driven by self-diffusion. The biological significance of various Turing patterns, such as cold spots, stripes, hot spots, and organic labyrinth, is examined. We analyzed the criterion for Hopf-bifurcation for the delayed spatiotemporal system. The impact of fear response delay on spatial patterns is investigated.

In ecology, carrying capacity is a crucial component that gives an idea about population size and resource availability. The past activities of the species influence the carrying capacity, and the impact is not immediate. Taking these facts in consideration, in Chapter 4, we attempt to study the temporal and spatiotemporal dynamics of a delayed prey-predator system with variable carrying capacity. Prey and predator interact via Holling Type-II functional response. A detailed dynamical analysis, including well-posedness and the possibility of coexistence equilibria has been performed for the temporal system. Local and global stability behavior of the co-existence equilibrium is discussed. Bistability behavior between two coexistence equilibria is demonstrated. The system undergoes Hopf-bifurcation with respect to the crucial parameter which affects the carrying capacity of the prey species. The delayed system exhibits

chaotic behavior. Maximal Lyapunov exponent and sensitivity analysis are done to confirm the chaotic dynamics. In the spatiotemporal system, the conditions for Turing instability are derived. Further, we analyzed the Turing pattern formation for different diffusivity coefficients for a two-dimensional spatial domain. Moreover, we investigated the spatiotemporal dynamics incorporating two discrete delays. The effect of the delay parameters in the transition of the Turing patterns is depicted. Various Turing patterns, such as hot-spot, cold-spot, patchy and labyrinth are obtained in the case of a two-dimensional spatial domain. This study shows that the key parameters significantly instigate the intriguing system dynamics and provide new insight into population dynamics. The findings in this chapter may help evaluate the biological revelations obtained from research on interactions between the species.

Allee effects play a crucial role in the extinction of small populations, exerting significant influence on population dynamics within ecosystems. In Chapter 5, we have investigated the temporal and spatiotemporal behavior of a prey-predator model with weak Allee effect in prey and the quality of being cannibalistic in a specialist predator. The parameters responsible for the Allee effect and cannibalism impact both the existence and stability of coexistence steady states of the temporal system. The temporal system exhibits various kinds of local bifurcations such as saddle-node, Hopf, Generalized Hopf (Bautin), Bogdanov-Takens, and global bifurcation like homoclinic, saddle-node bifurcation of limit cycles. For the model with self-diffusion, we establish the non-negativity and prior bounds of the solution. Subsequently, we derive the theoretical conditions in which self-diffusion leads to the destabilization of the interior equilibrium. Additionally, we explore the conditions under which cross-diffusion induces the Turing-instability where self-diffusion fails to do so. Further, we present different kinds of stationary and dynamic patterns on varying the values of diffusion coefficients to depict the spatiotemporal model's rich dynamics. It has been found that the addition of self and cross-diffusion in a prey-predator model with the Allee effect in prey and cannibalistic predator play essential roles in comprehending the pattern formation of a distributed population model.

The past interactions and experiences between prey and predator species can subsequently impact current behaviors, physiological states, or population dynamics. Chapter 6 aims to investigate a diffusive predator-prey system incorporating additional food for predators, prey refuge, fear effect, and its carry-over effects. For the temporal model, the well-posedness and persistence of the system have been discussed. We investigated the existence and the stability behavior of the various equilibria. Furthermore, we explored the bifurcations of co-dimension one including transcritical, saddle-node, and Hopf, with respect to the crucial parameters. The system also presents co-dimension two bifurcations such as Bogdanov-Takens and cusp bifurcation along with the global homoclinic bifurcation. We observed the bubbling phenomena,

which illustrates the fluctuations in the amplitudes of the periodic oscillations. For the spatiotemporal system, we established the non-negativity and boundedness of the solutions. We derived the conditions for the diffusion-driven instabilities in a confined region with Neumann boundary conditions. It is observed that incorporating cross-diffusion divides the bi-parametric plane into various sub-regions and dynamic patterns are analyzed in these different regions. The intricate spatiotemporal dynamics exhibited by prey-predator interactions are crucial for unraveling the intricacies within ecological systems.

Contents

List of Figures

List of Tables

Dedicated To

My

Beloved Family

Chapter 1

Introduction

1.1 Basic introduction and literature survey

Mathematical ecology constitutes a specialized field within ecology that employs mathematical models to study the dynamics and interactions of populations within ecosystems. Fundamentally, it aims to unravel the basic principles of ecological phenomena and forecast the responses of ecosystems to perturbations, changes in the environment, and human interventions. Mathematical modeling serves as a powerful tool for ecologists to comprehend a diverse range of ecological phenomena, such as population dynamics, prey-predator interactions, resource management, and ecosystem resilience. Prey-predator interaction is one of the most captivating themes in ecology and evolutionary biology that has piqued ecologists' interest for a good cause. In the realm of population dynamics, Thomas Robert Malthus [94] introduced a seminal concept in 1798. The well-known Malthusian growth model, which is derived from this idea and describes the dynamics of a single species, is given by:

$$\frac{dx}{dt} = rx,$$

where r is the per capita growth rate of population species. This model fails to reflect real-world scenarios as it doesn't account for the limited resources in nature, which may influence the exponential growth of the population. To address these shortcomings, in 1838, Pierre F Verhulst [174] proposed the logistic growth model incorporating a carrying capacity (K) to consider the environmental constraints on population size. The mathematical representation of the Verhulst model is given by:

$$\frac{dx}{dt} = rx\left(1 - \frac{x}{K}\right),$$

where r is the per capita growth rate of population and K is the carrying capacity of the environment. This model acknowledges the self-limiting nature of population growth in response to environmental constraints.

Although the Verhulst model offers a valuable framework for comprehending population growth within single species, the growing recognition of interdependent species within ecological communities underscores the necessity for a more intricate and responsive portrayal of prey-predator interactions. The Lotka-Volterra model, introduced by Alfred J. Lotka [91] and Vito Volterra [177], comprises a set of coupled differential equations that served as the foundation for modeling the dynamic prey-predator interactions, given by:

$$\frac{dx}{dt} = ax - bxy,$$
$$\frac{dy}{dt} = cxy - dy,$$

where x and y denote the population density of prey and predator at any time t, respectively. a is the per capita growth rate and b is the attack rate of predator on prey population. The parameters c, d respectively describe the effect of the presence of prey on predator's growth rate and predator's natural mortality rate. In the absence of predators, this model assumes that prey grows exponentially, which may not hold true in all ecological contexts due to limited food supply, and it can influence the model's ability to represent real-world dynamics accurately. Furthermore, the generalist behavior of predators is not taken into account by the Lotka-Volterra model. This restriction may affect the model's capacity to represent the intricacies of prey-predator interactions in heterogeneous environments where several prey species coexist and are pursued by the same predator species. Leslie [84, 85] introduced the prey-predator model in which the predator's carrying capacity is directly proportional to the prey density. The generalist behavior of predators can be addressed by the modified Leslie-Gower model by incorporating multiple food sources, allowing predators to adjust their feeding preferences dynamically.

In nature, prey-predator interactions often exhibit non-linear dynamics, such as saturation effects or functional responses, that can have varying consequences on population dynamics. A functional response is a measure of successfully attacked prey by the predator. In recent years, selecting an appropriate functional response has been a matter of subject in the ecological field. In a series of influential articles that began in the late 1950s, Holling established three broad categories of functional response [55, 56, 57]. Holling type I functional response assumes a linear increase in the intake rate of predators with increasing prey density, beyond which it

attains its maximum handling capacity. It is mathematically represented as:

$$f_1(x) = ax,$$

where a is the attack rate. This is the simplest and fundamental functional response used in the Lotka-Volterra prey-predator model. Despite the valuable foundation offered by this functional response, it has certain limitations. The assumption that predators can consume prey at a constant rate may not hold true in all ecological scenarios, as predators can face satiation, which influences their intake rate. To mitigate the drawbacks of type I functional response, Holling type II functional response is proposed, given by:

$$f_2(x) = \frac{ax}{1+ahx},$$

where a is the attack rate and h is the handling time. This functional response represents a predator's average feeding rate when the predator spends some time searching for prey and some time, apart from seeking, handling each captured prey.

Holling type III functional response is identical to Holling type II functional response at high levels of prey density. But for low values of prey density, the graphical representation between the number of prey consumed and prey density is a superlinearly increasing function of prey consumed by predators. It may be represented as:

$$f_3(x) = \frac{ax^2}{1+ahx^2}.$$

In nature, ecological factors can have a profound impact on population dynamics by influencing the interaction between prey and predators. In most cases, social interactions among conspecifics are beneficial to each other. In the context of hunting, cooperation refers to when two or more individuals work together to achieve a common goal to increase their fitness, or success and, consequently, their chances of survival and reproduction [6, 19]. There are numerous advantages of incorporating hunting cooperation among predators, including increased capture rate, a reduction in chasing distance, etc. [33]. In particular, many living organisms cooperate during hunting; for example, wild chimpanzees [17], lions [110], birds [54], wild dogs [33]. Cosner *et al.* [29], in 1999, initially derived a functional response depending on the spatial distribution of predators when the predators aggregate for hunting prey herd to increase their biomass. Berec [9] investigated a prey-predator system incorporating hunting cooperation and analyzed that when the encounter rate between the species is affected by hunting cooperation, it destabilizes the system dynamics. Alves and Hilker [2] examined a Lotka-Volterra model considering Berec's encounter-driven functional response. They found that cooperative hunting

produces oscillatory dynamics in the prey-predator model and improves the stability scenario of the coexistence steady-state, both of which are impossible without cooperative hunting.

In the early studies of prey-predator interactions, researchers relied on the long-held belief that predators can only impact prey populations by killing them directly. But later on, it was discovered that the mere presence of predators is enough for prey to exhibit anti-predator responses such as habitat relocation, reduced reproduction rate, foraging less, etc. In 2011, Zanette *et al.* [187] carried out an experiment on song sparrows and highlighted that the predation fear alone reduced the number of song sparrow *(Melospiza Melodia)* offsprings by 40%. In 2016, Wang *et al.* [180] proposed the very first prey-predator model incorporating fear phenomena and discovered that high levels of fear could stabilize the system dynamics by excluding the existence of periodic oscillations. Panday *et al.* [117] proposed a three-species food chain model considering the cost of fear and found that a sufficient value of fear might bring order to a system that would otherwise be chaotic.

In the presence of predators, it becomes imperative to protect prey species as part of efforts to manage and preserve biodiversity in ecosystems. Prey refuge serves as a buffer against predation risk by reducing the possibility of prey extinction due to predation. Kar [63] observed that spatial refugia, which conceal prey from predators and reduce the chance of extinction of prey, is a common feature of mite predator-prey interactions. In 2015, Sharma and Samanta [150] proposed an eco-epidemiological model and analyzed how the infected prey refuge can affect the constituent population dynamics. They remarked that prey refuge plays a crucial role in regulating the stability of populations.

The term “carry-over effect” was originally introduced from repeated clinical experiements. In the realm of prey-predator interactions, carry-over effect results from lingering consequences of species’ past interactions and experiences that might affect the current behaviors, physiological states, or population dynamics [107]. Experimental evidences show that the carry-over effect might occur within a single season and over a short time span in insects, amphibians, marine invertebrates, and marine fish [98, 162]. In a study examining the impact of the perceived risk of predation and its carry-over effects, Sasmal and Takeuchi [145] noted that changing the carry-over effect parameter can have a substantial impact on the stability of the coexistence equilibrium. Furthermore, they concluded that the “paradox of enrichment" might be completely eradicated with the appropriate choice of non-lethal effect parameters. Therefore, incorporating carry-over effects into population dynamics can facilitate comprehending the possible connection between the reproduction cost and trade-offs in life history strategies.

A correlation between population size or density and the mean individual fitness of a population or species defines the Allee effect. This concept was first established by ecologist Warder

Clyde Allee in 1931. Prey populations may expand at negative or positive rates at lower population densities, depending on the intensity of the Allee effect. The Allee effect can be categorized into two distinct types: strong and weak, depending on whether there is a negative or positive growth rate at lower population densities. Empirical evidence substantiating the existence of the Allee effect is observed in a diverse array of natural species, covering insects [80], plants [43], marine invertebrates [43], birds and mammals [30]. Notably, when the Allee effect occurs, populations may experience decreased growth rates at low densities, leaving individuals more vulnerable to cannibalism or predation. Cannibalism is a phenomenon that involves the killing and consumption of the whole or a part of an individual of the same species (conspecifics). Experimental zoologists have documented cases of cannibalism in a wide range of animal taxa, including fish, wolf spiders, house finches, bank voles, and zooplankton. With rates ranging from 8% in Belding's ground squirrels to 95% in dragonfly larvae, size-structured cannibalism—in which more prominent individuals of the same species devour smaller ones—may significantly contribute to overall mortality [128]. This indicates how it impacts community interactions and population dynamics [27, 134].

In nature, most of the biological processes entail a time lag. Incorporating time delays into a mathematical model can alter the system dynamics, rendering it more ecologically realistic [46, 74, 92]. Mathematically, delay differential equations can capture any past phenomena that can influence the present state within the system. These equations help us better comprehend the temporal dynamics of ecological systems and anticipate how the system behaves in response to environmental perturbations. A wide variety of research has been devoted to investigate the complex dynamics of a prey-predator model incorporating various discrete delays [8, 42, 118]. There are different types of delays that can ne introduced in a dynamical model to make it more robust such as maturation delay, gestation delay, fear response delay. Jana *et al.* [62] proposed and examined a dynamical model incorporating gestation delay and noticed that the discrete delay preserves system's stability. Panday *et al.* [119] analyzed a delayed prey-predator system and concluded that the delay parameter has both stabilizing and destabilizing effects on the system dynamics. Dubey *et al.* [42] investigated a multi-delayed prey-predator model and highlighted that system exhibits chaotic dynamics for sufficiently high value of the fear response delay.

The irregular movement of species across the space is ubiquitous. During prey-predator interactions, predators tend to diffuse in search of prey, and prey migrate to avoid predators, resulting in spatial variations [108]. As a result, because of the temporal and spatial interactions, the population disperses according to the erratic movements of every individual in the population. This irregular movement can result in a variety of intriguing spatial patterns. In 1952, Alan Turing [165] first proposed the concept of Turing instability, which arises when a stable

equilibrium point loses its stability in the presence of diffusion. Before recognizing this instability mechanism caused by the diffusion coefficients, it was usually presumed that diffusional effects stabilize the system. In the early 1970s, Segel and Jackson [146] and Levin and Segel [87] discovered Turing's concept that differential diffusion may lead to spatial patterns when acted upon a reacting system. In fact, spatial diffusion plays a significant role in population evolution, and there has been a growing focus and engagement in studying Turing patterns in the spatial population models [41, 99, 106, 121, 143, 168, 170, 171]. A broad range of spatiotemporal patterns, including stationary patterns like spots, labyrinthine patterns, and mixtures of stripes and spots, as well as non-stationary patterns like periodic, quasi-periodic, chaotic, and so on, can be produced by diffusive prey-predator systems. The study of Turing patterns in ecology can help one better understand the processes that govern the spatial pattern formation in natural systems as well as the variables affecting biodiversity and spatial heterogeneity. It is crucial to comprehend the emergence and evolution of Turing patterns in ecological systems in order to forecast ecosystem dynamics, manage natural resources, and preserve biodiversity.

1.2 Objectives of the thesis

This thesis aims to investigate certain ecological factors influencing the ecosystem's stability and addresses several issues related to biological population dynamics that may alter ecological stability. We delineated several gaps based on the abovementioned review of the existing literature, which we articulate as our thesis objectives.

1. To analyze the diffusive patterns in a predator-prey system with fear and hunting cooperation.

2. To study the consequences of fear effect and prey refuge on pattern formation in a delayed predator-prey system.

3. To investigate the spatiotemporal dynamics of a multi-delayed prey-predator system with variable carrying capacity.

4. To study the cannibalistic prey-predator system with Allee effect in prey under the presence of diffusion.

5. To explore the spatiotemporal dynamics in a diffusive predator-prey system incorporating a Holling type II functional response.

1.3 Mathematical preliminaries

Mathematically, most of the physical or ecological phenomena can be modelled using differential equations. It may be expressed as:

$$\frac{dw}{dt} = g(w), \quad w(t_0) = w_0, \tag{1.1}$$

where $w(t) = (w_1(t), w_2(t), ..., w_n(t))^T$, $g(w(t)) = (g_1, g_2, ..., g_n)^T$ and t_0 denotes the initial time. The enough smoothness of g ensures the existence and uniqueness of the solution to (1.1).

Definition 1.3.1. *The solution $w(t)$ of (1.1) is called a **stable** solution if, for each $\varepsilon > 0$, there exists a $\delta = \delta(\varepsilon) > 0$ such that, for any solution $\bar{w}(t) = w(t, t_0, \bar{w}_0)$ of (1.1), the inequality $||\bar{w}_0 - w_0|| \leq \delta$ implies $||\bar{w}(t) - w(t)|| < \varepsilon$ as $t \to \infty$.*

Definition 1.3.2. *The solution $w(t)$ of (1.1) is said to be **unstable** if it is not stable.*

Definition 1.3.3. *The solution $w(t)$ of (1.1) is said to be **locally asymptotically stable** if it is stable and there exists a $\delta_0 > 0$ such that $||\bar{w}_0 - w_0|| \leq \delta_0$ implies $||\bar{w}(t) - w(t)|| \to 0$ as $t \to \infty$.*

Definition 1.3.4. *A point $\hat{w} \in \mathbb{R}^n$ is called a **steady-state** or an **equilibrium point** of (1.1) if $g(\hat{w}) = 0$. This steady-state is said to be hyperbolic if $Dg(\hat{w})$ (Jacobian of g evaluated at $\hat{w}$) has no eigenvalue with zero real part.*

Definition 1.3.5. *An equilibrium point $\hat{w}$ of system (1.1) is called **sink** (stable) or **source** (unstable) if all the corresponding eigenvalues of $Dg(\hat{w})$ have negative or positive real parts, respectively. If at least one eigenvalue has the real component of the opposite sign from the other eigenvalues, the steady state is referred to as the **saddle point**.*

Definition 1.3.6. *A steady state $\hat{w}$ of system (1.1) is said to be **globally asymptotically stable** if every solution of the system, irrespective of the initial value, converges to $\hat{w}$.*

Definition 1.3.7. *A closed solution curve of (1.1) is said to be **periodic orbit** or **cycle** if the system returns to the same state at regular intervals of time. The stability of this cycle can be employed similar to the stability of an equilibrium point.*

Definition 1.3.8. *The **orbit** or **trajectory** $\psi(w_0)$ of (1.1) through w_0 is defined by*

$$\psi(w_0) = \{w \in \mathbb{R}^n : w = w(t, t_0, w_0),\ t \in \mathbb{R}\},$$

where $w(t,w_0)$ is any solution of (1.1) defined for every $t \in \mathbb{R}$. Similary, the positive and negative semiorbit of (1.1) through w_0 are described as

$$\psi^+(w_0) = \{w \in \mathbb{R}^n : w = w(t,t_0,w_0),\ t \in [0,\infty)\},$$

and

$$\psi^-(w_0) = \{w \in \mathbb{R}^n : w = w(t,t_0,w_0),\ t \in (-\infty,0]\}.$$

Definition 1.3.9. *The set of all limit points of $\psi^+(w_0)$ (or $\psi^-(w_0)$) is said to be $\omega-$ **limit set** $L(\psi^+)$ (or $\alpha-$ **limit set** $L(\psi^-)$), respectively. More precisely, a point $p \in L(\psi^+)$ is known as $\omega-$ limit point if $\exists$ a sequence $\{t_n\}$, $t_n \to \infty$ as $n \to \infty$ such that*

$$\lim_{n\to\infty} \psi(t_n,w_0) = p.$$

In a similar way, a point $q \in L(\psi^-)$ is known as $\alpha-$ limit point if $\exists$ a sequence $\{t_n\}$, $t_n \to -\infty$ as $n \to \infty$ such that

$$\lim_{n\to\infty} \psi(t_n,w_0) = q.$$

Definition 1.3.10. *A set $N \in \mathbb{R}^n$ is called an **invariant set** of (1.1) if for every solution $w(t)$, $w(t_0) \in N$ implies $w(t) \in N\ \forall\ t > t_0$.*

Definition 1.3.11. *A periodic solution Γ of (1.1) is said to be a **limit cycle** if it is either a ω or $\alpha-$ limit set of some other orbit. If a periodic orbit Γ is ω-limit set (or α-limit set) for every solution contained in its interior as well as exterior, then it is called stable limit cycle (or unstable limit cycle).*

Definition 1.3.12. *In the dynamical system, **multi-stability** refers to a situation wherein a system inhibits multiple stable states or attractors.*

Definition 1.3.13. ***Basin of attraction** is the collection of all initial points $w_0 \in \mathbb{R}^n$ for an attractor $\hat{A}$ of (1.1) if*

$$\lim_{t\to\infty} w(t,w_o) = \hat{A}.$$

Definition 1.3.14. *(**Sylvester's criterion**) Consider*

$$V(y) = y^T A y = \sum_{i,j=1}^{n} a_{ij} y_i y_j$$

be the quadratic form with the symmetric matrix $A = (a_{ij})$. The necessary and sufficient condition for $V(y)$ to be positive definite is that the symmetric matrix A has all the successive principal minors with the positive determinant.

Definition 1.3.15. ***Bifurcation*** *is the qualitative change that occur in the dynamical system by varying one or more parameters. Qualitative changes can encompass alterations in the number of steady states or modifications in their stability characteristics.*

Definition 1.3.16. *The number of parameters that need to be varied for a bifurcation to occur is known as its* ***codimension****.*

Definition 1.3.17. *In* ***transcritical*** *bifurcation, two steady states interchange their stability as the bifurcation parameter is varied.*

Definition 1.3.18. *The* ***saddle-node*** *bifurcation occurs when two steady states collide and annihilate each other with variation in the bifurcation parameter.*

Definition 1.3.19. ***Pitchfork*** *bifurcation occurs when a system transits from one steady state to three steady states.*

Definition 1.3.20. *The* ***Hopf****-bifurcation refers to the emergence of a periodic solution from a steady state or vice-versa as a parameter crosses a critical value. In* ***supercritical*** *Hopf-bifurcation, the stable steady state switches its stability and a stable limit cycle appears. The unstable steady state gains stability by creating unstable limit cycle in the case of* ***subcritical*** *Hopf-bifurcation.*

Definition 1.3.21. ***Homoclinic*** *bifurcation occurs when a limit cycle expands and collides with a saddle point, forming a homoclinic orbit. In the case of* ***heteroclinic*** *bifurcation, a limit cycle connects with two or more saddle points.*

Definition 1.3.22. *In bifurcation theory, a* ***Bogdanov–Takens*** *bifurcation is a co-dimension two bifurcation that involves the intersection of three co-dimension one bifurcation: saddle-node, Hopf, and homoclinic.*

Definition 1.3.23. *The* ***cusp*** *bifurcation occurs when two branches of the saddle-node bifurcation curve meet tangentially, forming a semicubic parabola.*

Definition 1.3.24. *The* ***Bautin or generalized Hopf*** *bifurcation is a bifurcation of codimension two that separates branches of supercritical and subcritical Hopf-bifurcation in the parameteric plane.*

Definition 1.3.25. ***Self-diffusion*** *refers to the random movement of individuals of the same species within the habitat. In contrast,* ***cross-diffusion*** *describes how the interaction between species affects the migration of individuals of different species.*

Definition 1.3.26. ***Homogenous Neumann*** *or* ***zero-flux*** *boundary conditions ensure that no member of the species can leave the domain of interaction nor can one enter it. It takes the following form:*

$$\frac{\partial u(x,t)}{\partial \eta} = 0, \ \ (t > 0,\ x \in \partial\Omega),$$

where $\partial\Omega$ is the smooth boundary of the bounded domain Ω in $\mathbb{R}^n$ and $\frac{\partial u(x,t)}{\partial \eta}$ is the directional derivative of u in the direction of η.

Definition 1.3.27. *A* ***delay differential equation*** *(DDE) is a differential equation using delays as the dependent variable. In other words, the rate of change of dependent variables at a given time is determined by their current and previous states. The general form of DDE is given by*

$$\frac{dw}{dt} = f(t, w(t), w_\tau),$$

where $w_\tau = \{w(\tau) : 0 \leq \tau \leq t\}$ represents the solution trajectories in the past.

Definition 1.3.28. ***Chaos*** *may be described as the unpredictable, non-repeating behavior observed in a deterministic system that exhibits sensitive dependence on initial conditions.*

Definition 1.3.29. *The solution is said to have* ***sensitive dependence on initial conditions*** *on Γ if there exists $\varepsilon > 0$ such that, for any $x \in \Gamma$ and any neighborhood Ω of x, there exist $y \in \Omega$ and $t > 0$ such that $|\psi(x,t) - \psi(y,t)| > \varepsilon$.*

1.4 Methodology

To investigate the properties such as persistence and permanence, stability, chaos, multi-stability, Turing instability, and bifurcation associated with our objectives defined by ordinary differential equations, partial differential equations, and delay differential equations, we employ the following distinct methodologies:

1. **Persistence and permanence:** Persistence and permanence are significant aspects of the system, as they depict its behavior over the long term. In a dynamical system, uniform persistence ensures the ultimate existence of all the species. The permanence of a system means the survival of all populations of the system in future time.

Assume that the ith component of the solution $w = w(t)$ of the deterministic dynamical system is $w_i(t)$, which represents the population density of the ith of a particular collection of species at time t, given by

$$\dot{w}_i = w_i f_i(w), \quad i = 1,2,3. \tag{1.2}$$

Uniform persistence of (1.2) implies there exists a positive number δ such that if, for each i, $w_i(0) > 0$, then

$$\liminf_{t\to\infty} w_i(t) \geq \delta. \tag{1.3}$$

Moreover, if there exists a constant K such that, $\forall\ w_i(t)$,

$$\limsup_{t\to\infty} w_i(t) \leq K, \tag{1.4}$$

then, system (1.2) is said to be dissipative or uniformly bounded. The system (1.2) is called permanent if both (1.3) and (1.4) hold true.

2. **Linearization of differential equations:** Let us consider that our system can be represented as follows

$$\frac{dY(t)}{dt} = G(Y(t)), \tag{1.5}$$

where $Y(t) = (y_1(t), y_2(t), ..., y_n(t))^T$, $G(Y(t)) = (g_1, g_2, ..., g_n)^T$ and $E^* = (y_1^*, y_2^*, ..., y_n^*)^T$ is the steady state corresponding to (1.5). Let $z_i(t) = y_i(t) - y_i^*$ and linearizing (1.5) about E^*, we obtain

$$\frac{dZ(t)}{dt} = DZ(t), \tag{1.6}$$

where D is Jacobian matrix corresponding to system (1.5) evaluated about E^*.

3. **Local stability:** The stability of an equilibrium point in its neighborhood is determined by computing the characteristic equation associated with the Jacobian matrix evaluated at the equilibrium point. Then, we assess the sign of the real parts of the eigenvalue of this equation. To facilitate this, we use the following theorem:

Theorem 1.4.1. ***(Hurwitz's theorem)*** *A necessary and sufficient condition for the negativity of the real parts of all the roots of the polynomial*

$$\lambda^n + A_1\lambda^{n-1} + ... + A_n = 0, \tag{1.7}$$

with real coefficients is the positivity of all principle diagonals of minors of the Hurwitz matrix

$$H_n = \begin{bmatrix} A_1 & 1 & 0 & 0 & 0 & 0 & 0 & \dots & 0 \\ A_3 & A_2 & A_1 & 1 & 0 & 0 & 0 & \dots & 0 \\ A_5 & A_4 & A_3 & A_2 & A_1 & 1 & 0 & \dots & 0 \\ \vdots & \vdots & \vdots & \vdots & \vdots & \vdots & \vdots & \vdots & \vdots \\ 0 & 0 & 0 & 0 & 0 & 0 & 0 & 0 & A_n \end{bmatrix},$$

Here, it should be noted that the elements of the Hurwitz matrix $H_n = (h_{ik})$ are given by $h_{ik} = A_{2i-k}$, the missing coefficients are replaced by zero.

The Hurwitz conditions for negative real parts of the solutions of (1.7) for the second, third and fourth degrees are applied as:

$$\begin{aligned} &n = 2,\ A_1 > 0,\ A_2 > 0, \\ &n = 3,\ A_1 > 0,\ A_2 > 0,\ A_3 > 0,\ \text{and}\ A_1A_2 - A_3 > 0, \\ &n = 4,\ A_1 > 0,\ A_2 > 0,\ A_3 > 0,\ A_4 > 0,\ \text{and}\ A_1A_2A_3 - A_3^2 - A_1^2A_4 > 0. \end{aligned}$$

This theorem becomes impractical for large n.

Remark: The characteristic polynomial (1.7) is said to be stable if all its roots have negative real parts.

4. **Non-linear Stability (Global Stability):** If the solution trajectory starting from anywhere in the given domain coverges to the same steady state, then that steady state is said to be globally stable. Here, we establish the sufficient conditions for the global Stability of the system around the critical point by choosing a suitable Lyapunov's function which is a positive definite function.
   Let us consider an autonomous system of differential equations:

$$\frac{dx}{dt} = f(x), \tag{1.8}$$

   where $f \in C[R^n, R^n]$ and $S_\rho = \{x \in R^n : ||x|| < \rho\}$ such that f is smooth enough to ensure the existence and uniqueness of (1.8) and x^* is the equilibrium point for it.
   We have some important results to lay down the ample conditions ensuring the global stability of the system and are stated below.

Theorem 1.4.2. *If there exists a scalar function $V(x)$ which is positive definite about x^* such that $V^*(x) < 0$ (derivative of $V(x)$ along (1.8) is negative definite) on S_ρ, then x^* is asymptotically stable.*

Theorem 1.4.3. *If there exists a scalar function $V(x)$ which is positive definite about x^* such that $V^*(x) \leq 0$ on S_ρ, then x^* is stable.*

Theorem 1.4.4. *If there exists a scalar function $V(x); V(0) = 0$ such that $\frac{dV}{dt} > 0$ on S_ρ and if in every neighbourhood N of the x^*, $N \subset S_\rho$, there is a point x_0 where $V(x_0) > 0$ then then x^* is unstable.*

5. **Bendixson–Dulac theorem:** Consider the system (1.5) with n=2 and assume there exists a continuously differentiable function $\phi(y_1, y_2)$ (called the **Dulac function**) such that the expression

$$\frac{\partial(\phi g_1)}{\partial y_1} + \frac{\partial(\phi g_2)}{\partial y_2}$$

has the same sign ($\neq 0$) almost everywhere in a simply connected region of the plane, then according to the Bendixson–Dulac theorem, system (1.5) (for n=2) has no nonconstant periodic solutions lying entirely within the region.

6. **Bifurcation theory:** If varying one or more parameters leads to a change in the qualitative behavior of the equilibrium point, the dynamical system is said to undergo bifurcation.
To demonstrate the occurrence of transcritical and saddle-node bifurcation, we illustrate the Sotomayor's theorem conditions by considering the following system:

$$\frac{dz}{dt} = g(z, \mu), \tag{1.9}$$

where μ is the bifurcation parameter. Assuming $z = z_0$ be the corresponding hyperbolic equilibrium of the system (1.9) at the critical point $\mu = \mu_0$ with p and q be the be the eigenvectors corresponding to the zero eigenvalue of $A = Dg(z_0, \mu_0)$ and A^T, respectively. Now, we procced with the subsequent theorems for different bifurcations.

Theorem 1.4.5. *Under the following conditions of the Sotomayor's theorem, the system (1.9) undergoes saddle-node bifurcation at the equilibrium point z_0 as the parameter μ passes through the bifurcation value $\mu = \mu_0$.*

- $q^T g_\mu(z_0, \mu_0) \neq 0$, *and*
- $q^T [D^2 g(z_0, \mu_0)(p, p)] \neq 0$.

Theorem 1.4.6. *The system* (1.9) *undergoes transcritical bifurcation at the equilibrium point z_0 as the parameter μ passes through the bifurcation value $\mu = \mu_0$, if the following conditions of the Sotomayor's theorem hold:*

- $q^T g_\mu(z_0, \mu_0) = 0$,
- $q^T [Dg_\mu(z_0, \mu_0)p] \neq 0$, *and*
- $q^T [D^2 g(z_0, \mu_0)(p, p)] \neq 0$.

$Dg(z_0, \mu_0)$ has a pair of complex eigenvalues in Hopf-bifurcation. The subcritical or supercritical Hopf-bifurcation occurs when the complex eigenvalues cross the imaginary axis as the bifurcation parameter varies. At the critical point, we get a pair of pure imaginary eigenvalues.
Let us consider a two-dimensional system

$$\frac{dz_1}{dt} = g_1(z_1, z_2, \mu), \quad \frac{dz_2}{dt} = g_2(z_1, z_2, \mu), \tag{1.10}$$

where μ is the bifurcation parameter. Now, let us assume that the jacobian matrix about $E^*(z_1^*, z_2^*)$ has eigenvalues $\lambda_{1,2}(\mu) = \alpha(\mu) + i\beta(\mu)$. Moreover, we consider that the following conditions hold at the critical point $\mu = \mu_0$:

- non-hyperbolicity condition:

$$\alpha(\mu_0) = 0, \quad \beta(\mu_0) = \omega > 0,$$

- tranversality condition:

$$\left.\frac{d\alpha(\mu)}{d\mu}\right|_{\mu=\mu_0} = d \neq 0,$$

then the system undergoes Hopf-bifurcation at $\mu = \mu_0$ about the equilibrium point E^*. Next, we determine the direction of the Hopf-bifurcation by evaluating the following:

$$\begin{aligned}\sigma =& \frac{1}{16}(g_{1_{z_1z_1z_1}} + g_{1_{z_1z_2z_2}} + g_{2_{z_1z_1z_2}} + g_{2_{z_2z_2z_2}}) + \frac{1}{16\omega}(g_{1_{z_1z_2}}(g_{1_{z_1z_1}} + g_{1_{z_2z_2}}) \\ & - g_{2_{z_1z_2}}(g_{2_{z_1z_1}} + g_{2_{z_2z_2}}) - g_{1_{z_1z_1}}g_{2_{z_1z_1}} + g_{1_{z_2z_2}}g_{2_{z_2z_2}}),\end{aligned}$$

where $g_{1_{z_1z_2}} = \left.\frac{\partial^2 g_1}{\partial z_1 \partial z_2}\right|_{E^*,\mu=\mu_0}$, and in the similar manner other derivates may be defined. Thus, the Hopf bifurcation obtained is considered subcritical (or supercritical) if σ is positive (or negative), respectively.

7. **Chaotic dynamical systems:** Some dynamical system shows the characteristic of chaos. In this, the system is highly sensitive to initial conditions. A small perturbation in the initial values causes a very significant change in the behavior of the system, which makes it unpredictable in the future. However, every system is not chaotic. For confirmation of chaos; we corresponding maximum Lyapunov exponent, λ, defined as

$$\lambda = \lim_{t\to\infty} \lim_{\delta Z_0 \to 0} \frac{1}{t} ln \frac{\delta Z(t)}{\delta Z_0},$$

where δZ_0 is the perturbation in the initial condition, and $\delta Z(t)$ is the resulting change in the solution.

Remark: For a system to be chaotic, the corresponding maximum Lyapunov exponent must be positive.

8. **Numerical simulation:** Most of the existing literature's mathematical models exhibit nonlinear characteristics; therefore, they cannot be solved analytically. This is where numerical methods and tools become indispensable for solving such equations. Every forthcoming chapter of this thesis comprises extensive numerical simulations carried out with the help of Mathematica/MATLAB to validate the theoretical results. In some sections, we have used the popular continuation toolbox MatCont, a MATLAB package. For the phase plane analysis, we frequently used Pplane8, which is another toolbox package of MATLAB. Most simulation codes are written from scratch and mainly use a few standard MATLAB solvers, ode45 and dde23, for the system of ODEs and DDEs. The resulting plots enable us to better comprehend population dynamics concerning essential ecological factors.

Chapter 2

Diffusive patterns in a predator-prey system with fear and hunting cooperation[1]

2.1 Introduction

Predator-prey interaction is a central topic in ecology and evolutionary biology that has piqued ecologists' interest for a good cause. Predation ultimately results in the eviction of prey individuals from biological systems, which can substantially impact prey population dynamics and ecosystems as a whole. The long-held belief is that predators can only have an impact on prey populations by killing them directly. On the other hand, theoretical biologists [89] contend that a broad understanding of predator-prey interactions necessitates knowledge of predators' behaviorally generated nonlethal consequences. When prey perceives predation risk, they exhibit a variety of anti-predator responses. For example, they may decide to leave their original high-risk environment and relocate to lower-risk areas, forage less, reducing the reproduction rate and affecting their survival through starvation, etc. [32, 34]. Moreover, Zanette *et al.* [187] experimented on song sparrows (*Melospiza melodia*) and discovered that the fear of predation could itself reduce the number of offspring production by 40%. Based on such experimental evidence, Wang *et al.* [180] proposed a model incorporating the fear effect and analysed that significant levels of fear can stabilize the predator-prey system by excluding the possibility of periodic solutions. Many researchers have now integrated the reduced prey growth rate due to predation risk in their mathematical models [141, 144, 145, 181].

Cooperation is a crucial aspect of animal social behavior and a critical component in ecology. There are numerous advantages of incorporating hunting cooperation among predators, including increased capture rate, a reduction in chasing distance, etc. [33]. In particular, many living organisms cooperate during hunting; for example, wild chimpanzees [17], lions [110], birds [54], wild dogs [33]. It was observed [9] that when the encounter rate between prey and

[1]This chapter is based on our paper published in *The European Physical Journal Plus*, **137**, 281, 2022.

predator is affected by hunting cooperation, it destabilizes the system dynamics. Pribylova and Peniaskova [132] studied a predator-prey system and analyzed that by introducing intra-specific cooperation among predators, prey and predator can coexist for specific rates. Still, it can have severe repercussions for the predators themselves in the majority of cases. Alves and Hilker [2] showed that adding hunting cooperation increases the attack rate and allows the predator to exist even when the prey population is insufficient to sustain them; however, it can also lead to a sudden predator population collapse.

The irregular movement of species across space is ubiquitous. During prey-predator interactions, predators tend to diffuse in search of prey, and prey migrate to avoid predators, resulting in spatial variations [108]. This irregular movement can result in a variety of intriguing spatial patterns. Alan Turing first proposed Turing instability in 1952 [165], which arises when a stable steady-state loses its stability in the presence of diffusion. In the early 1970s, Segel and Jackson [146] and Levin and Segel [87] discovered Turing's concept that differential diffusion may lead to spatial patterns when acted upon a reacting system. Dubey *et al.* [39] studied the effect of time dependent cross diffusivity in a Gause-type predator-prey model.

Considerably, many recent studies investigated the reaction-diffusion system that can induce stationary spatial patterns [41, 99, 106, 121, 143, 168, 170, 171]. Sasmal *et al.* [143] proposed a prey-predator model and concluded that non-Turing patterns arise as a combined effect of aposematic time and searching efficiency of prey. Recently, Kumar and Kumari [76] studied the diffusion-induced chaos in a spatially extended model.

In recent years, the combined effect of hunting cooperation and fear effect on the dynamics of the system has been studied extensively [90, 112, 113]. Very few researchers have investigated the combined effect of both the ecological factors in a diffusive predator-prey system [38]. The aim of this study is to analyze the dynamics of a diffusive model system incorporating both hunting cooperation and fear effect. In this paper, we consider the predator mortality rate as:

$$M(y) = \frac{\gamma + \delta y}{1 + y} \quad ; \quad 0 < \gamma < \delta,$$

i.e. $M(y)$ is a predator density-dependent function [184]. The current model has a benefit over more widely used models because the predator mortality rate is neither constant nor unbounded here. However, it increases with predator density due to intra-species competition. Moreover, we consider that increasing hunting cooperation among predators increases fear among prey, as a result prey's birth rate decreases.

The rest of the chapter is arranged in the following manner. In Section 2.2, we formulated our mathematical model with fear and hunting cooperation. Fundamental mathematical analysis like positivity, dissipativeness, and persistence of the system has been discussed in Section

2.3. In Section 2.4, we analyzed the existence, local stability, and global stability of all equilibria. Bifurcation analysis is presented in Section 2.5. In Section 2.6, we analyzed the local and global stability for the spatial model. We perform some extensive numerical simulations in Section 2.7. The paper ends with a discussion in Section 2.8.

2.2 Formulation of mathematical model

First, we assume that prey grows logistically, which can be divided into three parts, namely, the birth, natural death and death due to intra-species competition. Hence, in predators' absence, the prey dynamics can be governed by the following ODE:

$$\frac{dx}{dt} = rx - r_0 x - r_1 x^2, \tag{2.1}$$

where $x(t)$ is the prey population density at any given time t, r is the birth rate of prey, r_0 is the natural death rate of prey, r_1 is the death rate due to intra-species competition among the preys.

Now, we explicitly include the predator dynamics in (2.1). This paper considers that the predator-prey interaction follows a linear functional response. We also incorporated the hunting cooperation among predators, which benefited the predator population [2, 54]. Moreover, we consider that the prey's growth rate decreases due to fear of predation, which depends on the predator population density [180]. Hence, our prey-predator model becomes:

$$\begin{aligned}
\frac{dx}{dt} &= \left[\frac{r}{(1+k\alpha_1 y)} - r_0 - r_1 x - (\alpha_0 + \alpha_1 y)y\right] x, \\
\frac{dy}{dt} &= \left[c(\alpha_0 + \alpha_1 y)x - \frac{\gamma + \delta y}{1+y}\right] y, \\
x(0) &\geq 0,\ y(0) \geq 0.
\end{aligned} \tag{2.2}$$

Here, y(t) is the predator population density at any time t, α_0 is the predation rate (without hunting cooperation among predators), α_1 is the predator hunting cooperation parameter, c is the conversion coefficient from prey density to predator density, which should lie between 0 to 1. Here, the parameter k refers to the level of fear which reflects the reduction of prey growth rate due to the anti-predator behavior. Moreover, we considered that the level of fear increases due to hunting cooperation among predators i.e., prey's growth rate decreases as the hunting cooperation parameter α_1 increases. Thus we modify the fear function as $\frac{1}{1+k\alpha_1 y}$. We consider the predator mortality rate $M(y) = \frac{\gamma+\delta y}{1+y}$ to be predator density dependent function with the assumption $\gamma < \delta$. The advantage of using this function as mortality rate, is that it is neither a

constant nor an unbounded function, yet it is an increasing function with the predator density [184].

Now, if we consider spatial effects in prey and predator population, then the spatial prey-predator model can be written in the following reaction-diffusion equations:

$$\begin{aligned}\frac{\partial x}{\partial t} &= \left[\frac{r}{(1+k\alpha_1 y)} - r_0 - r_1 x - (\alpha_0+\alpha_1 y)y\right]x + D_1\nabla^2 x,\\ \frac{\partial y}{\partial t} &= \left[c(\alpha_0+\alpha_1 y)x - \frac{\gamma+\delta y}{1+y}\right]y + D_2\nabla^2 y,\end{aligned} \tag{2.3}$$

where $x \equiv x(u;v;t)$, $y \equiv y(u;v;t)$ denotes the prey and predator population density at the spatial coordinate $(u;v)$ and time t, respectively. $\nabla^2 = \frac{\partial^2}{\partial u^2} + \frac{\partial^2}{\partial v^2}$ is the Laplacian Operator in two dimensional space. D_1 and D_2 are the self-diffusion coefficients of prey and predator species, respectively, which describe that the individuals tend to migrate from higher to lower concentration regions.

The spatiotemporal dynamics (2.3) are subjected to non-zero initial conditions and Neumann boundary conditions (which means that no species can leave or enter through the boundary):

$$x(u;v;0) = x_0(u;v) > 0; y(u;v;0) = y_0(u;v) > 0; (u,v) \in \Omega = [0,L]\times[0,M], \text{ and } \frac{\partial x}{\partial \hat{n}} = \frac{\partial y}{\partial \hat{n}} = 0,$$

where $\hat{n}$ is the outward unit normal vector.

2.3 Mathematical analysis of non-spatial model

First, we will analyze model (2.2) which is without diffusion. We assume that all the parameters involved with the model (2.2) are positive.

2.3.1 Positivity and boundedness of the solutions

In particular, positivity of solutions implies that the species will exists. Model (2.2) can be written as:

$$\begin{aligned}\frac{dx}{dt} &= \Psi_1(t)x,\\ \frac{dx}{dt} &= \Psi_2(t)y,\end{aligned}$$

where

$$\Psi_1(t) = \frac{r}{(1+k\alpha_1 y)} - r_0 - r_1 x - (\alpha_0 + \alpha_1 y)y,$$
$$\Psi_2(t) = c(\alpha_0 + \alpha_1 y)x - \frac{\gamma + \delta y}{1+y}.$$

Thus,

$$x(t) = x(0)\exp\left[\int_0^t \psi_1(x(s), y(s))ds\right] \geq 0,$$
$$y(t) = y(0)\exp\left[\int_0^t \psi_2(x(s), y(s))ds\right] \geq 0,$$

which gives

$$x(t) \geq 0, \text{ and } y(t) \geq 0,$$

and implies the positivity of all the solutions.

Theorem 2.3.1. *System (2.2) is dissipative i.e. all the solutions are bounded above in $\mathbb{R}^2_+$ with the following properties:*

$$\limsup_{t\to\infty} x(t) \leq \frac{r - r_0}{r_1},$$
$$\limsup_{t\to\infty}\left(x(t) + \frac{1}{c}y(t)\right) \leq \begin{cases} \frac{r-r_0}{r_1} \text{ when } \gamma > r - r_0 \\ \\ \frac{(r-r_0+\gamma)^2}{4r_1\gamma} \text{ when } \gamma \leq r - r_0. \end{cases}$$

Proof. From the first equation of (2.2), we have

$$\frac{dx}{dt} = \frac{rx}{(1+k\alpha_1 y)} - r_0 x - r_1 x^2 - (\alpha_0 + \alpha_1 y)xy,$$
$$\leq (r - r_0)x - r_1 x^2.$$

Considering $r - r_0 > 0$ (for the survival of prey, otherwise $x(t) \to 0$ as $t \to \infty$), we have

$$\limsup_{t\to\infty} x(t) \leq \frac{r - r_0}{r_1}.$$

Now, we define $z(t) = x(t) + \frac{1}{c}y(t)$, then

$$\begin{aligned}
\frac{dz}{dt} &= \frac{rx}{1+k\alpha_1 y} - r_0 x - r_1 x^2 - \frac{(\gamma+\delta y)}{c(1+y)}y, \\
&\leq rx - r_0 x - r_1 x^2 - \frac{\gamma y}{c}, \qquad (\text{ as } \delta > \gamma \implies \frac{\gamma+\delta y}{1+y} > \gamma) \\
&= rx - r_0 x - r_1 x^2 - \gamma(z-x), \\
&= (r - r_0 + \gamma)x - r_1 x^2 - \gamma z.
\end{aligned}$$

Then similar to the proof of the theorem (2.1) in [144], our results follow. ∎

Theorem 2.3.2. *System (2.2) is uniformly persistent under the following conditions:*

(a) $r > (1+k\alpha_1 y_{max})(r_0 + \alpha_0 y_{max} + \alpha_1 y_{max}^2)$,

(b) $x_{min} > \frac{\delta}{c\alpha_0}$.

Proof.

$$\begin{aligned}
\frac{dx}{dt} &= \frac{rx}{(1+k\alpha_1 y)} - r_0 x - r_1 x^2 - (\alpha_0 + \alpha_1 y)xy \\
\frac{dx}{dt} &\geq x\left[\frac{r}{(1+k\alpha_1 y_{max})} - r_0 - r_1 x - (\alpha_0 + \alpha_1 y_{max})y_{max}\right] \\
&= x\left[\left(\frac{r}{(1+k\alpha_1 y_{max})} - r_0 - (\alpha_0 + \alpha_1 y_{max})y_{max}\right) - r_1 x\right],
\end{aligned}$$

$$\lim_{t\to\infty} \inf x(t) \geq \frac{1}{r_1}\left(\frac{r}{1+k\alpha_1 y_{max}} - r_0 - (\alpha_0 + \alpha_1 y_{max})y_{max}\right) = m^*.$$

Now,

$$\begin{aligned}
\frac{dy}{dt} &= y\left[c(\alpha_0 + \alpha_1 y)x - \frac{\gamma+\delta y}{1+y}\right] \\
\frac{dy}{dt} &\geq y[c\alpha_0 x + c\alpha_1 xy - \delta] \\
\frac{dy}{dt} &\geq y\left[(c\alpha_0 x_{min} - \delta) + c\alpha_1 x_{min} y\right].
\end{aligned}$$

Now, if $(c\alpha_0 x_{min} - \delta) > 0$, then $\frac{dy}{dt} \geq 0$. This implies that y is strictly increasing function of t, $\forall t > 0$. Thus, $y(t) > y(0)$, $\forall t > 0$.
Choosing, $\varepsilon = min\{m^*, y(0)\}$ we get

For $\varepsilon > 0$,

$$\begin{aligned} &\lim_{t\to\infty} \inf x(t) > \varepsilon, \\ &\lim_{t\to\infty} \inf y(t) > \varepsilon. \end{aligned} \tag{2.4}$$

Hence, this completes the proof. ∎

2.4 Equilibrium analysis

Model (2.2) has three non-negative equilibria:

1. The trivial extinction equilibrium $E_0 = (0,\ 0)$, which always exists.
2. The axial equilibrium, where only prey population survive is given by $E_1 = \left(\frac{r-r_0}{r_1}, 0\right)$, which exists if $r - r_0 > 0$.
3. Other non-negative interior steady states of (2.2) can be solved from the following equations

$$\begin{aligned} f(x,y) &:= \frac{r}{1+k\alpha_1 y} - r_0 - r_1 x - (\alpha_0 + \alpha_1 y)y = 0, \\ g(x,y) &:= c(\alpha_0 + \alpha_1 y)x - \frac{\gamma + \delta y}{1+y} = 0. \end{aligned} \tag{2.5}$$

From $g(x,y) = 0$, we can get the expression of x as follows:

$$x = \frac{(\gamma+\delta y)}{c(\alpha_0+\alpha_1 y)(1+y)}, \tag{2.6}$$

Now from $f(x,y) = 0$, we can get a $5th$ degree polynomial equation in y as follows:

$$\beta_0 y^5 + \beta_1 y^4 + \beta_2 y^3 + \beta_3 y^2 + \beta_4 y + \beta_5 = 0, \tag{2.7}$$

where

$$\begin{aligned} \beta_0 &= kc\alpha_1^3\ (>0), \\ \beta_1 &= c\alpha_1^2(1 + k\alpha_1 + 2k\alpha_0)\ (>0), \\ \beta_2 &= c\alpha_1(r_0 k\alpha_1 + \alpha_1 + 2\alpha_0 + 2k\alpha_0\alpha_1 + k\alpha_0^2)\ (>0), \\ \beta_3 &= r_0 ck\alpha_1^2 + r_1 k\alpha_1\delta + r_0 ck\alpha_0\alpha_1 + 2c\alpha_0\alpha_1 + c\alpha_0^2 + kc\alpha_0^2\alpha_1 - c\alpha_1(r-r_0), \\ \beta_4 &= r_0 ck\alpha_0\alpha_1 + r_1 k\alpha_1\gamma + r_1\delta + c\alpha_0^2 - c(r-r_0)(\alpha_0+\alpha_1), \\ \beta_5 &= r_1\gamma - c\alpha_0(r-r_0). \end{aligned}$$

Depending on the values of the parameter $\beta_i's$ for $i = 3,4,5$, our proposed system (2.2) would have none, one, two or three interior equilibria.

We have the following theorem for the number of interior equilibria corresponding to system (2.2).

Theorem 2.4.1. **(a)** *System (2.2) has no interior equilibrium if the following condition holds:*

$$0 < r - r_0 < \min\left\{\frac{\gamma r_1}{c\alpha_0}, \frac{r_1(\delta+k\gamma\alpha_1)+c\alpha_0(\alpha_0+r_0k\alpha_1)}{c(\alpha_0+\alpha_1)}, \frac{c[\alpha_0\alpha_1(2+k\alpha_0+kr_0)+\alpha_0^2+r_0k\alpha_1^2]+r_1k\alpha_1\delta}{c\alpha_1}\right\}.$$

(b) *System (2.2) has unique interior equilibrium if any one of the following two conditions holds:*

$$(i) \quad \frac{\gamma r_1}{c\alpha_0} < r - r_0 < \frac{c[\alpha_0\alpha_1(2+k\alpha_0+kr_0)+\alpha_0^2+r_0k\alpha_1^2]+r_1k\alpha_1\delta}{c\alpha_1}.$$
$$(ii) \quad \max\left\{\frac{\gamma r_1}{c\alpha_0}, \frac{r_1(\delta+k\gamma\alpha_1)+c\alpha_0(\alpha_0+r_0k\alpha_1)}{c(\alpha_0+\alpha_1)}\right\} < r - r_0.$$

(c) *System (2.2) has at most two interior equilibria if any one of the following two conditions holds:*

$$(i) \quad \frac{r_1(\delta+k\gamma\alpha_1)+c\alpha_0(\alpha_0+r_0k\alpha_1)}{c(\alpha_0+\alpha_1)} < r - r_0 < \frac{\gamma r_1}{c\alpha_0}.$$
$$(ii) \quad \frac{c[\alpha_0\alpha_1(2+k\alpha_0+kr_0)+\alpha_0^2+r_0k\alpha_1^2]+r_1k\alpha_1\delta}{c\alpha_1} < r - r_0 < \frac{\gamma r_1}{c\alpha_0}.$$

(d) *System (2.2) has at most three interior equilibria if the following condition holds:*

$$\max\left\{\frac{\gamma r_1}{c\alpha_0}, \frac{c[\alpha_0\alpha_1(2+k\alpha_0+kr_0)+\alpha_0^2+r_0k\alpha_1^2]+r_1k\alpha_1\delta}{c\alpha_1}\right\} < r - r_0 < \frac{r_1(\delta+k\gamma\alpha_1)+c\alpha_0(\alpha_0+r_0k\alpha_1)}{c(\alpha_0+\alpha_1)}.$$

Proof. The number of interior equilibria depends on the number of positive real roots of the equation (2.7), which depends on the sign of coefficients β_3, β_4 and β_5. By using 'Descartes' rule of signs' we can easily verify that the equation (2.7) has no positive real root if $\beta_i's > 0$, for $i = 3,4,5$, which gives

$$r - r_0 < \min\left\{\frac{\gamma r_1}{c\alpha_0}, \frac{r_1(\delta+k\gamma\alpha_1)+c\alpha_0(\alpha_0+r_0k\alpha_1)}{c(\alpha_0+\alpha_1)}, \frac{c[\alpha_0\alpha_1(2+k\alpha_0+kr_0)+\alpha_0^2+r_0k\alpha_1^2]+r_1k\alpha_1\delta}{c\alpha_1}\right\}.$$

Similarly, the system has unique interior equilibrium in any of the three set of conditions (i) $\beta_3 > 0$, $\beta_4 > 0$ and $\beta_5 < 0$, (ii) $\beta_3 > 0$, $\beta_4 < 0$ and $\beta_5 < 0$, (iii) $\beta_3 < 0$, $\beta_4 < 0$ and $\beta_5 < 0$.

Combining these three set of conditions we can easily simplify that the equation (2.7) has unique real positive roots if $\beta_3 > 0$ and $\beta_5 < 0$ or $\beta_4 < 0$ and $\beta_5 < 0$, i.e., if $\frac{\gamma r_1}{c\alpha_0} < r - r_0 < \frac{c[\alpha_0\alpha_1(2+k\alpha_0+kr_0)+\alpha_0^2+r_0k\alpha_1^2]+r_1k\alpha_1\delta}{c\alpha_1}$ or $\max\left\{\frac{\gamma r_1}{c\alpha_0}, \frac{r_1(\delta+k\gamma\alpha_1)+c\alpha_0(\alpha_0+r_0k\alpha_1)}{c(\alpha_0+\alpha_1)}\right\} < r - r_0$. Similarly, we can prove that when the system has at most two or three interior equilibria. ∎

Note: From Theorem 2.4.1, we can conclude that system (2.2) has atleast one interior equilibrium if any of the conditions (b) and (d) hold (the region above the black solid line in Fig. 2.1).

In Fig. 2.2, we fixed the parameters as $r = 2.7$, $r_0 = 0.2$, $r_1 = 0.1$, $k = 0.1$, $\alpha_1 = 0.006$, $c = 0.5$,

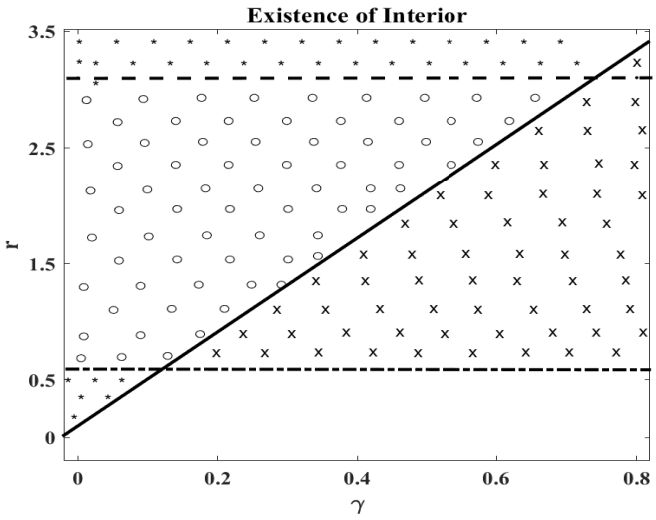

Fig. 2.1: Here we fix the parameter values as $r_0 = 0.2$, $r_1 = 0.1$, $k = 0.1$, $\alpha_0 = 0.05$, $\alpha_1 = 0.006$, $c = 0.5$, $\delta = 0.8$ and vary the parameters γ and r from 0 to 0.8, and 0 to 3.5, respectively. Here, (o) is for the existence of at most three interior equilibria (condition (d) in Theorem 2.4.1), $(\times)$ is for the existence of at most two interior equilibria (condition (c) in Theorem 2.4.1) and $(*)$ is for the existence of unique interior equilibrium (condition (b) in Theorem 2.4.1). Thus, Model (2.2) has at least one interior equilibrium in the region above black solid line.

$\gamma = 0.5$, $\delta = 0.8$ and vary the parameter α_0. For $\alpha_0 = 0.03$, we have no interior steady state. We get a unique interior steady state for $\alpha_0 = 0.05$. For $\alpha_0 = 0.04$ and $\alpha_0 = 0.045$, we have two and three interior steady states, respectively.

Next, we provide the following theorems regarding the stability of equilibria corresponding to system (2.2).

Theorem 2.4.2. *The extinction equilibrium E_0 is locally asymptotically stable if $r - r_0 < 0$. In fact, E_0 is globally asymptotically stable under this condition.*

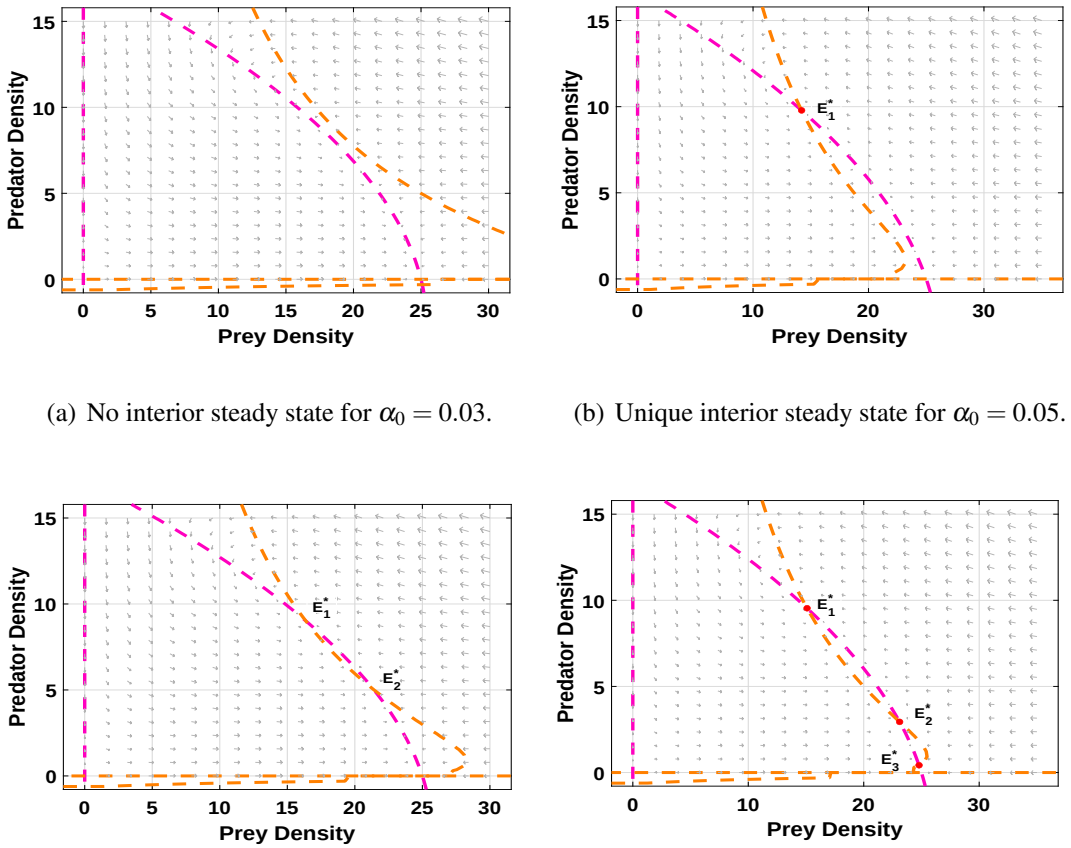

(a) No interior steady state for $\alpha_0 = 0.03$.

(b) Unique interior steady state for $\alpha_0 = 0.05$.

(c) Two interior steady states for $\alpha_0 = 0.04$.

(d) Three interior steady states for $\alpha_0 = 0.045$.

Fig. 2.2: Number of interior steady states for model (2.2) with varying α_0. The other parameter values are fixed as $r = 2.7$, $r_0 = 0.2$, $r_1 = 0.1$, $k = 0.1$, $\alpha_1 = 0.006$, $c = 0.5$, $\gamma = 0.5$, and $\delta = 0.8$.

Proof. The eigenvalues at the extinction equilibrium E_0 are given by $\lambda_1 = r - r_0$ and $\lambda_2 = -\gamma\,(< 0)$. Thus E_0 is locally asymptotically stable if $r - r_0 < 0$.

It is easy to show that the solution $(x(t), y(t))$ of (2.2) for any positive initial conditions in $\mathbb{R}^2_+$ tends to $E_0 = (0,0)$ when $r - r_0 < 0$. ∎

Theorem 2.4.3. *The axial equilibrium E_1 exists and is locally asymptotically stable if $0 < r - r_0 < \frac{\gamma r_1}{c\alpha_0}$. Moreover, E_1 is globally asymptotically stable if*

$$0 < r - r_0 < \min\left\{\frac{\gamma r_1}{c\alpha_0}, \frac{r_1(\delta + k\gamma\alpha_1) + c\alpha_0(\alpha_0 + r_0 k\alpha_1)}{c(\alpha_0 + \alpha_1)}, \frac{c[\alpha_0\alpha_1(2 + k\alpha_0 + kr_0) + \alpha_0^2 + r_0 k\alpha_1^2] + r_1 k\alpha_1\delta}{c\alpha_1}\right\}.$$

Proof. The eigenvalues at the axial equilibrium E_1 are given by $\lambda_1 = -(r - r_0)$ and $\lambda_2 = c\alpha_0\frac{(r-r_0)}{r_1} - \gamma$. Thus, E_1 is locally asymptotically stable if $0 < r - r_0 < \frac{\gamma r_1}{c\alpha_0}$.

Moreover, under the condition

$$0 < r - r_0 < \min\left\{ \frac{\gamma r_1}{c\alpha_0}, \frac{r_1(\delta+k\gamma\alpha_1)+c\alpha_0(\alpha_0+r_0k\alpha_1)}{c(\alpha_0+\alpha_1)}, \frac{c[\alpha_0\alpha_1(2+k\alpha_0+kr_0)+\alpha_0^2+r_0k\alpha_1^2]+r_1k\alpha_1\delta}{c\alpha_1} \right\},$$

the system does not have any interior equilibrium. The extinction equilibrium is always unstable (saddle) and E_1 is always locally stable under this condition. Also, all the solutions of system (2.2) remains positive and bounded. So, every solution ultimately tends to E_1. ∎

Theorem 2.4.4. *The interior equilibrium $E^* = (x^*, y^*)$ is locally asymptotically stable if $x^* < min\left(\frac{y^*(\delta-\gamma)}{(1+y^*)^2(c\alpha_1y^*-r_1)}, \frac{\delta-\gamma}{c\alpha_1(1+y^*)^2} + \frac{\alpha_0+\alpha_1 y}{r_1\alpha_1}\left[\frac{rk\alpha_1}{(1+k\alpha_1y^*)^2} + (\alpha_0+2\alpha_1y^*)\right] \right)$ and $y^* > \frac{r_1}{c\alpha_1}$.*

Proof. The Jacobian matrix at the interior equilibrium is given by

$$J_{E^*} = \begin{bmatrix} -r_1x^* & -x^*(\frac{rk\alpha_1}{(1+k\alpha_1y^*)^2} + (\alpha_0+2\alpha_1y^*)) \\ c(\alpha_0+\alpha_1y^*)y^* & c\alpha_1x^*y^* - \frac{y^*(\delta-\gamma)}{(1+y^*)^2} \end{bmatrix}.$$

The characteristic equation at the interior equilibrium is

$$\begin{aligned} &\lambda^2 - Tr(J_{E^*})\lambda + det(J_{E^*}) = 0, \\ &\implies \lambda^2 + \left[r_1x^* + \frac{y^*(\delta-\gamma)}{(1+y^*)^2} - c\alpha_1x^*y^* \right]\lambda \\ &+ r_1x^*y^*\left[\frac{(\delta-\gamma)}{(1+y^*)^2} - c\alpha_1x^*\right] + cx^*y^*(\alpha_0+\alpha_1y^*)\left[\frac{rk\alpha_1}{(1+k\alpha_1y^*)^2} + (\alpha_0+2\alpha_1y^*)\right] \quad = 0. \end{aligned}$$

Thus, the interior equilibrium $E^* = (x^*, y^*)$ is locally asymptotically stable if $Tr(J_{E^*}) < 0$ and $det(J_{E^*}) > 0$, i.e., if

$$\begin{aligned} &r_1x^* + \frac{y^*(\delta-\gamma)}{(1+y^*)^2} - c\alpha_1x^*y^* > 0 \\ &\text{and } r_1\left[\frac{(\delta-\gamma)}{(1+y^*)^2} - c\alpha_1x^*\right] + c(\alpha_0+\alpha_1y^*)\left[\frac{rk\alpha_1}{(1+k\alpha_1y^*)^2} + (\alpha_0+2\alpha_1y^*)\right] > 0. \end{aligned}$$

The above two inequalities satisfies if

$$x^* < min\left(\frac{y^*(\delta-\gamma)}{(1+y^*)^2(c\alpha_1y^*-r_1)}, \frac{\delta-\gamma}{c\alpha_1(1+y^*)^2} + \frac{\alpha_0+\alpha_1 y}{r_1\alpha_1}\left[\frac{rk\alpha_1}{(1+k\alpha_1y^*)^2} + (\alpha_0+2\alpha_1y^*)\right] \right) \text{ and } y^* > \frac{r_1}{c\alpha_1}.$$

∎

Remark: From the expressions of $Tr(J_{E^*})$ and $det(J_{E^*})$, the sufficient condition for the local stability of $E^*(x^*,y^*)$ is

$$\delta > \gamma + c\alpha_1 x^*(1+y^*)^2.$$

Next, we assume that we have a unique interior equilibrium under conditions (b) of Theorem 2.4.1. Now, we provide the following result for the global stability of the unique interior equilibrium.

Theorem 2.4.5. *The unique interior equilibrium E_1^* is globally asymptotically stable if the following condition holds:*

$$x^* < \frac{\delta-\gamma}{c\alpha_1(1+y_{max})(1+y^*)} - \frac{1}{4r_1\alpha_1\left(\frac{rk\alpha_1}{1+k\alpha_1}+\alpha_1 y^*\right)^2}.$$

Proof. Let us consider a positive definite function:

$$V(x,y) = \left(x - x^* - x^* ln\frac{x}{x^*}\right) + m\left(y - y^* - y^* ln\frac{y}{y^*}\right).$$

Differentiating $V(x,y)$ with respect to t and simplifying the expression, we get:

$$\begin{aligned}\dot{V} &= -r_1(x-x^*)^2 + (x-x^*)(y-y^*)\left[\frac{-rk\alpha_1}{(1+k\alpha_1 y)(1+k\alpha_1 y^*)} - \alpha_0 - \alpha_1(y+y^*) + mc\alpha_0 + mc\alpha_1 y\right] \\ &\quad - (y-y^*)^2\left[-mc\alpha_1 x^* - \frac{m\gamma}{(1+y)(1+y^*)} + \frac{m\delta}{(1+y)(1+y^*)}\right] \\ &= -a_{11}(x-x^*)^2 + a_{12}(x-x^*)(y-y^*) - a_{22}(y-y^*)^2.\end{aligned}$$

Using Sylvester's criteria, sufficient conditions for $\dot{V}$ to be negative definite are

$$\begin{gathered} a_{22} > 0, \text{ and } a_{12}^2 < 4a_{11}a_{22}, \\ a_{22} > 0 \text{ gives } \frac{m(\delta-\gamma)}{(1+y)(1+y^*)} > mc\alpha_1 x^* \\ \text{i.e., } x^* < \frac{\delta-\gamma}{c\alpha_1(1+y_{max})(1+y^*)}. \end{gathered}$$

Taking $m = \frac{1}{c}$ i.e., $mc = 1$, $a_{12}^2 < 4a_{11}a_{22}$ gives

$$\left(\frac{rk\alpha_1}{(1+k\alpha_1)} + \alpha_1 y^*\right)^2 < 4r_1\left(\frac{\delta-\gamma}{c(1+y_{max})(1+y^*)} - \alpha_1 x^*\right),$$

$$\text{i.e. } x^* < \frac{\delta-\gamma}{c\alpha_1(1+y_{max})(1+y^*)} - \frac{1}{4r_1\alpha_1}\left(\frac{rk\alpha_1}{1+k\alpha_1}+\alpha_1 y^*\right)^2.$$

Hence, $E_1(x^*,y^*)$ is globally asymptotically stable if

$$x^* < \min\left\{\frac{\delta-\gamma}{c\alpha_1(1+y_{max})(1+y^*)}, \frac{\delta-\gamma}{c\alpha_1(1+y_{max})(1+y^*)} - \frac{1}{4r_1\alpha_1}\left(\frac{rk\alpha_1}{1+k\alpha_1}+\alpha_1 y^*\right)^2\right\},$$

$$\text{i.e., if } x^* < \frac{\delta-\gamma}{c\alpha_1(1+y_{max})(1+y^*)} - \frac{1}{4r_1\alpha_1}\left(\frac{rk\alpha_1}{1+k\alpha_1}+\alpha_1 y^*\right)^2.$$

∎

In Fig. 2.3, we have shown the global stability region of the unique interior equilibrium in $\gamma - r$ parameter plane, by fixing the other parameter values as $r_0 = 0.2$, $r_1 = 0.1$, $k = 0.1$, $\alpha_0 = 0.05$, $\alpha_1 = 0.006$, $c = 0.5$, $\delta = 0.8$. In Fig. 2.4, we have shown the global stability of unique interior E_1^* by drawing the phase-portrait with different initial conditions by fixing the remaining two parameters $r = 1.5$ and $\gamma = 0.1$ in Fig. 2.3.

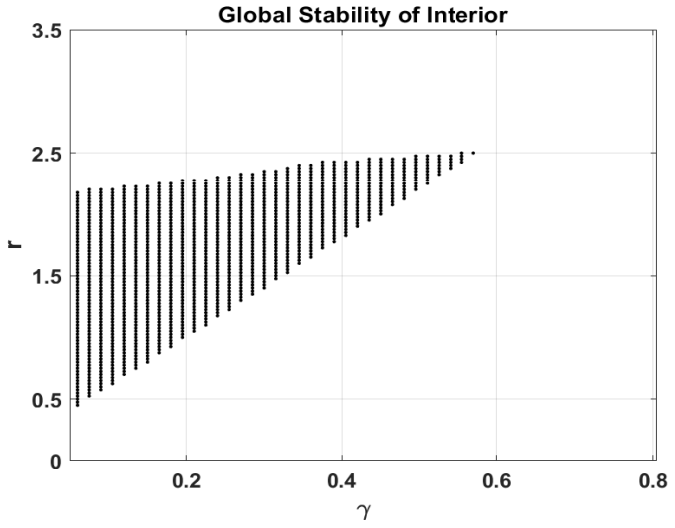

Fig. 2.3: Here, we fix the parameter values as $r_0 = 0.2$, $r_1 = 0.1$, $k = 0.1$, $\alpha_0 = 0.05$, $\alpha_1 = 0.006$, $c = 0.5$, $\delta = 0.8$ and vary the parameters γ and r from 0 to 0.8, and 0 to 3.5, respectively. The interior is globally asymptotically stable in black region (Theorem 2.4.5).

We summarize the existence, local stability and global stability conditions of all the equilibria in the Table 2.1.

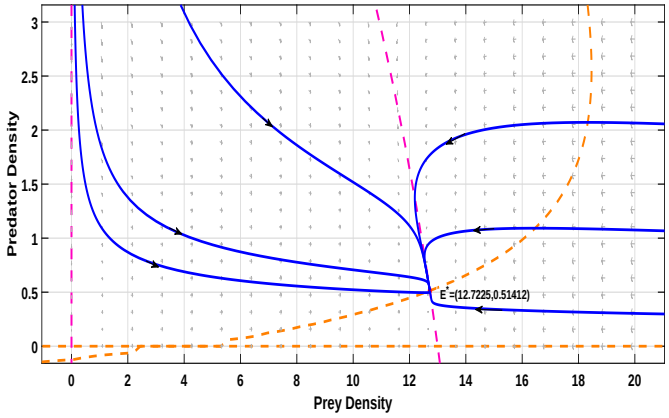

Fig. 2.4: Here, we fix the parameter values as $r = 1.5$, $r_0 = 0.2$, $r_1 = 0.1$, $k = 0.1$, $\alpha_0 = 0.05$, $\alpha_1 = 0.006$, $c = 0.5$, $\delta = 0.8$ and $\gamma = 0.1$. The unique interior equilibrium $E_1^* = (12.72, 0.51)$ is globally asymptotically stable.

2.5 Bifurcation analysis

Next, we investigate the possibility of Hopf-bifurcation at the interior equilibrium E_1^* by varying the hunting cooperation parameter α_1, as bifurcation parameter.

The interior equilibrium E_1^* loses its stability through Hopf-bifurcation when the eigenvalues are complex conjugate with zero real parts. We consider α_1 as the bifurcation parameter. Considering the characteristic equation evaluated from the Jacobian matrix at E_1^*, we have

$$\lambda^2 + B_1\lambda + B_2 = 0, \tag{2.8}$$

where

$$B_1 = -Tr(J_{E_1^*}) \quad \text{and,} \quad B_2 = det(J_{E_1^*}).$$

Let $\lambda(\alpha_1) = \lambda_r(\alpha_1) + i\lambda_i(\alpha_1)$ be an eigenvalue of above characteristic equation. Putting the value of $\lambda(\alpha_1)$ in Eq. (2.8) and comparing the real and imaginary parts, we get

$$\lambda_r^2 - \lambda_i^2 + B_1\lambda_r + B_2 = 0, \tag{2.9}$$

$$2\lambda_r\lambda_i + \lambda_i B_1 = 0. \tag{2.10}$$

Equilibrium	**Existence**	**Local Stability**	**Global Stability**
$E_0 = (0,0)$	Always	$r - r_0 < 0$	$r - r_0 < 0$
$E_1 = \left(\frac{r-r_0}{r_1}, 0\right)$	$r - r_0 > 0$	$r - r_0 < \frac{r_1\gamma}{c\alpha_0}$	$r - r_0 < \min\left\{\frac{\gamma r_1}{c\alpha_0}, \frac{r_1(\delta+k\gamma\alpha_1)+c\alpha_0(\alpha_0+r_0k\alpha_1)}{c(\alpha_0+\alpha_1)}, \frac{c[\alpha_0\alpha_1(2+k\alpha_0+kr_0)+\alpha_0^2+r_0k\alpha_1^2]+r_1k\alpha_1\delta}{c\alpha_1}\right\}$
$E^* = (x^*, y^*)$	Conditions (b)-(d) of Theorem 2.4.1	$x^* < min\left(\frac{y^*(\delta-\gamma)}{(1+y^*)^2(c\alpha_1y^*-r_1)}, \frac{\delta-\gamma}{c\alpha_1(1+y^*)^2} + \frac{\alpha_0+\alpha_1y}{r_1\alpha_1}\left[\frac{rk\alpha_1}{(1+k\alpha_1y^*)^2} + (\alpha_0+2\alpha_1y^*)\right]\right)$ and $y^* > \frac{r_1}{c\alpha_1}$	$x^* < \frac{\delta-\gamma}{c\alpha_1(1+y_{max})(1+y^*)} - \frac{1}{4r_1\alpha_1}\left(\frac{rk\alpha_1}{1+k\alpha_1} + \alpha_1y^*\right)^2$

Table 2.1: Existence, local and global stability conditions of equilibria for model (2.2).

For the Hopf- bifurcation to occur, we need $\lambda_r(\alpha_1) = 0$ at the bifurcating value $\alpha_1 = \alpha_h$. Thus,

$$\begin{aligned} -\lambda_i^2 + B_2 &= 0, \quad \lambda_i \in \mathbb{R}, \\ \lambda_i B_1 &= 0, \quad \lambda_i \neq 0. \end{aligned}$$

Thus,

$$B_2 > 0 \text{ and } B_1 = 0 \text{ at the bifurcating point } \alpha_h.$$

Now, from $B_1 = 0$, we have

$$\alpha_1 = \alpha_h = \frac{r_1}{cy^*} + \frac{(\delta-\gamma)}{cx^*(1+y^*)^2}.$$

Differentiating Eqs. (2.9) and (2.10) with respect to the bifurcating parameter α_1 and substituting $\lambda_r = 0$, we get

$$-2\lambda_i\frac{d\lambda_i}{d\alpha_1} + B_1\frac{d\lambda_r}{d\alpha_1} + \frac{dB_2}{d\alpha_1} = 0, \tag{2.11}$$

$$2\lambda_i\frac{d\lambda_r}{d\alpha_1} + \lambda_i\frac{dB_1}{d\alpha_1} + B_1\frac{d\lambda_i}{d\alpha_1} = 0. \tag{2.12}$$

Solving above two equations,

$$\left.\frac{d\lambda_r}{d\alpha_1}\right|_{\alpha_1=\alpha_h} = -\frac{(B_1\frac{dB_2}{d\alpha_1}+2\lambda_i^2\frac{dB_1}{d\alpha_1})}{B_1^2+4\lambda_i^2} \neq 0,$$

provided $B_1\frac{dB_2}{d\alpha_1}+2\lambda_i^2\frac{dB_1}{d\alpha_1} \neq 0$.

Therefore, the system undergoes Hopf-bifurcation at E_1^* if $B_2>0$ and $(B_1\frac{dB_2}{d\alpha_1}+2\lambda_i^2\frac{dB_1}{d\alpha_1}) \neq 0$ at the bifurcating point $\alpha_1=\alpha_h$.

In the next theorem we will discuss about the direction and stability of Hopf-bifurcation around the interior equilibrium point E_1^*.

Theorem 2.5.1. *Let L be defined as*

$$\begin{aligned} L := & \frac{1}{16}\left[\frac{\partial^3 H_1}{\partial z_1^3}+\frac{\partial^3 H_1}{\partial z_1\partial z_2^2}+\frac{\partial^3 H_2}{\partial z_1^2\partial z_2}+\frac{\partial^3 H_2}{\partial z_2^3}\right] \\ & +\frac{1}{16\sqrt{f_u g_v - f_v g_u}}\left[\frac{\partial^2 H_1}{\partial z_1\partial z_2}\left(\frac{\partial^2 H_1}{\partial z_1^1}+\frac{\partial^2 H_1}{\partial z_2^2}\right)-\frac{\partial^2 H_2}{\partial z_1\partial z_2}\left(\frac{\partial^2 H_2}{\partial z_1^2}+\frac{\partial^2 H_2}{\partial z_2^2}\right)-\frac{\partial^2 H_1}{\partial z_1^2}\frac{\partial^2 H_2}{\partial z_1^2}+\frac{\partial^2 H_1}{\partial z_2^2}\frac{\partial^2 H_2}{\partial z_2^2}\right]. \end{aligned}$$

Then the Hopf bifurcation is supercritical if $L<0$ and it is subcritical if $L>0$.

Proof. To find the stability and direction of Hopf bifurcation, we calculate the 1st Lyapunov coefficient. Let $u=x-x^*$ and $v=y-y^*$, then system (2.2) becomes

$$\begin{aligned} \frac{du}{dt} &= \frac{r(u+x^*)}{1+k\alpha_1(v+y^*)} - r_0(u+x^*) - r_1(u+x^*)^2 - (\alpha_0+\alpha_1(v+y^*))(u+x^*)(v+y^*) := f(u,v). \\ \frac{dv}{dt} &= c(\alpha_0+\alpha_1(v+y^*))(u+x^*)(v+y^*) - [\tfrac{\gamma+\delta(v+y^*)}{1+(v+y^*)}](v+y^*) := g(u,v). \end{aligned}$$

Now, expanding the above system in Taylor's series at $(u,v)=(0,0)$ upto 3rd order, we get

$$\begin{aligned} \frac{du}{dt} &= J_{11}u+J_{12}v+f_1(u,v), \\ \frac{dv}{dt} &= J_{21}u+J_{22}v+g_1(u,v), \end{aligned} \tag{2.13}$$

$f_1(u,v)$ and $g_1(u,v)$ are the higher order terms of u and v, given by

$$\begin{aligned} f_1(u,v) &= f_{uu}u^2+f_{uv}uv+f_{vv}v^2+f_{uuu}u^3+f_{uuv}u^2v+f_{uvv}uv^2+f_{vvv}v^3, \\ g_1(u,v) &= g_{uu}u^2+g_{uv}uv+g_{vv}v^2+g_{uuu}u^3+g_{uuv}u^2v+g_{uvv}uv^2+g_{vvv}v^3, \end{aligned}$$

where

$$
\begin{aligned}
f_u =& J_{11} = \frac{r}{1+k\alpha_1 y^*} - r_0 - 2r_1 x^* - (\alpha_0 + \alpha_1 y^*)y^*, \\
f_v =& J_{12} = -\frac{rk\alpha_1 x^*}{(1+k\alpha_1 y^*)^2} - x^*(\alpha_0 + 2\alpha_1 y^*), \\
f_{uu} =& -2r_1, \\
f_{uv} =& [\frac{-rk\alpha_1}{(1+k\alpha_1 y^*)^2} - (\alpha_0 + 2\alpha_1 y^*)], \\
f_{vv} =& 2x^*\alpha_1(\frac{rk^2\alpha_1}{(1+k\alpha_1 y^*)^3} - 1), \\
f_{uuu} =& 0, \\
f_{uuv} =& 0, \\
f_{uvv} =& 2(\frac{rk^2\alpha_1^2}{(1+k\alpha_1 y^*)^3} - \alpha_1), \\
f_{vvv} =& -\frac{6rk^3\alpha_1^3 x^*}{(1+k\alpha_1 y^*)^4},
\end{aligned}
$$

and

$$
\begin{aligned}
g_u =& J_{21} = c(\alpha_0 + \alpha_1 y^*)y^*, \\
g_v =& J_{22} = cx^*(2\alpha_1 y^* + \alpha_0) - \frac{\gamma + \delta y^*}{1+y^*} - y^*\frac{\delta - \gamma}{(1+y^*)^2}, \\
g_{uu} =& 0, \\
g_{uv} =& c(\alpha_0 + 2\alpha_1 y^*), \\
g_{vv} =& 2(c\alpha_1 x^* - \frac{\delta - \gamma}{(1+y^*)^3}), \\
g_{uuu} =& 0, \\
g_{uuv} =& 0, \\
g_{uvv} =& 2c\alpha_1, \\
g_{vvv} =& \frac{6(\delta - \gamma)}{(1+y^*)^4}.
\end{aligned}
$$

System (2.13) can be written as:

$$\dot{U} = J_{E_1^*}U + H(U),$$

where

$$\begin{aligned} U &= \Big(u,v\Big)^T, \\ H &= \Big(f_1(u,v), g_1(u,v)\Big)^T, \\ &= \Big(f_{uu}u^2 + f_{uv}uv + f_{vv}v^2 + f_{uvv}uv^2 + f_{vvv}v^3, g_{uv}uv + g_{vv}u^2 + g_{uvv}uv^2 + g_{vvv}v^3\Big)^T. \end{aligned}$$

Now, Hopf bifurcation occurs when $Tr(J_{E_1^*}) = 0$ and $det(J_{E_1^*}) > 0$, i.e., at the Hopf bifurcation point, the eigenvalue will be purely imaginary, which is given by $i\sqrt{f_u g_v - f_v g_u}$. Eigenvector corresponding to this eigenvalue $i\sqrt{f_u g_v - f_v g_u}$ is given by $\overline{v} = \Big(f_v, i\sqrt{f_u g_v - f_v g_u} - f_u\Big)^T$. Now, we define $S = \Big(Re(\overline{v}), -Im(\overline{v})\Big) = \begin{bmatrix} f_v & 0 \\ -f_u & -\sqrt{f_u g_v - f_v g_u} \end{bmatrix}$. Now, let $U = SZ$ or $Z = S^{-1}U$, where $Z = \Big(z_1, z_2\Big)^T$. Therefore, under this transformation, the system is reduced to

$$\dot{Z} = \Big(S^{-1} J_{E_1^*} S\Big) Z + S^{-1} H\Big(SZ\Big).$$

This can be written as

$$\begin{bmatrix} \dot{z_1} \\ \dot{z_2} \end{bmatrix} = \begin{bmatrix} 0 & -\sqrt{f_u g_v - f_v g_u} \\ \sqrt{f_u g_v - f_v g_u} & 0 \end{bmatrix} \begin{bmatrix} z_1 \\ z_2 \end{bmatrix} + \begin{bmatrix} H_1(z_1, z_2) \\ H_2(z_1, z_2) \end{bmatrix},$$

where $H_1(z_1, z_2)$ and $H_2(z_1, z_2)$ are given by

$$\begin{aligned} H_1(z_1,z_2) = &\frac{1}{f_v}\Big[f_{uu}f_v^2 z_1^2 - f_{uv}f_v z_1(f_u z_1 + \sqrt{f_u g_v - f_v g_u} z_2) + f_{vv}(f_u z_1 + \sqrt{f_u g_v - f_v g_u} z_2)^2 \\ &+ f_{uvv}f_v z_1(f_u z_1 + \sqrt{f_u g_v - f_v g_u} z_2)^2 - f_{vvv}(f_u z_1 + \sqrt{f_u g_v - f_v g_u} z_2)^3\Big], \end{aligned}$$

$$\begin{aligned} H_2(z_1,z_2) = &-\frac{1}{f_v\sqrt{f_u g_v - f_v g_u}}\Big[f_u(f_{uu}f_v^2 z_1^2 - f_{uv}f_v z_1(f_u z_1 + \sqrt{f_u g_v - f_v g_u} z_2) \\ &+ f_{vv}(f_u z_1 + \sqrt{f_u g_v - f_v g_u} z_2)^2 \\ &+ f_{uvv}f_v z_1(f_u z_1 + \sqrt{f_u g_v - f_v g_u} z_2)^2 - f_{vvv}(f_u z_1 + \sqrt{f_u g_v - f_v g_u} z_2)^3) \\ &+ f_v(-g_{uv}f_v z_1(f_u z_1 + \sqrt{f_u g_v - f_v g_u} z_2) + g_{vv}(f_u z_1 + \sqrt{f_u g_v - f_v g_u} z_2)^2 \\ &+ g_{uvv}f_v z_1(f_u z_1 + \sqrt{f_u g_v - f_v g_u} z_2)^2 - g_{vvv}(f_u z_1 + \sqrt{f_u g_v - f_v g_u} z_2)^3)\Big]. \end{aligned}$$

The direction of Hopf bifurcation is determined by the sign of the 1*st* Lyapunov coefficient, which is given by

$$L := \frac{1}{16}\left[\frac{\partial^3 H_1}{\partial z_1^3}+\frac{\partial^3 H_1}{\partial z_1 \partial z_2^2}+\frac{\partial^3 H_2}{\partial z_1^2 \partial z_2}+\frac{\partial^3 H_2}{\partial z_2^3}\right] + \frac{1}{16\sqrt{f_u g_v - f_v g_u}}\left[\frac{\partial^2 H_1}{\partial z_1 \partial z_2}\left(\frac{\partial^2 H_1}{\partial z_1^1}+\frac{\partial^2 H_1}{\partial z_2^2}\right)-\frac{\partial^2 H_2}{\partial z_1 \partial z_2}\left(\frac{\partial^2 H_2}{\partial z_1^2}+\frac{\partial^2 H_2}{\partial z_2^2}\right)-\frac{\partial^2 H_1}{\partial z_1^2}\frac{\partial^2 H_2}{\partial z_1^2}+\frac{\partial^2 H_1}{\partial z_2^2}\frac{\partial^2 H_2}{\partial z_2^2}\right].$$

∎

Now, the following theorem gives an insight for the occurrence of saddle-node bifurcation.

Theorem 2.5.2. *System* (2.2) *undergoes a saddle-node bifurcation around the steady state* $(\bar{x},\bar{y})$ *as the predation rate parameter* α_0 *passes through the bifurcation value* $\alpha_0 = \alpha_{0s}$ *if and only if*

$$-\left(1+c\frac{f_x}{g_x}\right)\neq 0,$$
$$\left[\left(f_{xx}-\frac{f_x}{f_y}(f_{xy}+f_{yx})+\frac{f_x^2}{f_y^2}f_{yy}\right)-\frac{f_x}{g_x}\left(g_{xx}-\frac{f_x}{f_y}(g_{xy}+g_{yx})+\frac{f_x^2}{f_y^2}g_{yy}\right)\right]\neq 0.$$

Proof. Let $\alpha_0 = \alpha_{0s}$ be the critical value for α_0 and $(\bar{x},\bar{y})$ be the interior equilibrium point.

The Jacobian matrix at the equilibrium point E$(\bar{x},\bar{y})$ is:

$$J_{E(\bar{x},\bar{y})} = \begin{bmatrix} -r_1\bar{x} & -\bar{x}\left(\frac{rk\alpha_1}{(1+k\alpha_1\bar{y})^2}+(\alpha_0+2\alpha_1\bar{y})\right) \\ c(\alpha_0+\alpha_1\bar{y})\bar{y} & c\alpha_1\bar{x}\bar{y}-\frac{\bar{y}(\delta-\gamma)}{(1+\bar{y})^2} \end{bmatrix}.$$

Now, the Jacobian matrix $J_{E(\bar{x},\bar{y})}$ has a zero eigenvalue at $\alpha_0 = \alpha_{0s}$. Therefore, the equilibrium point $E(\bar{x},\bar{y})$ is non-hyperbolic.

Now, differentiating the given model w.r.t. α_0, we get

$$F_{\alpha_0}(\bar{x}\bar{y}) = \begin{bmatrix} -\bar{x}\bar{y} \\ c\bar{x}\bar{y} \end{bmatrix},$$

$$A = Df(E(\bar{x},\bar{y}),\alpha_{0s}) = \begin{bmatrix} f_x & f_y \\ g_x & g_y \end{bmatrix},$$

where

$$\begin{aligned}
f_x =& -r_1\bar{x},\\
f_y =& -\bar{x}\Big(\frac{rk\alpha_1}{(1+k\alpha_1\bar{y})^2}+(\alpha_0+2\alpha_1\bar{y})\Big),\\
g_x =& c(\alpha_0+\alpha_1\bar{y})\bar{y},\\
g_y =& c\alpha_1\bar{x}\bar{y}-\frac{\bar{y}(\delta-\gamma)}{(1+\bar{y})^2}
\end{aligned}$$

$$D^2f(E(\bar{x},\bar{y}),\alpha_{0s}) = \begin{bmatrix} f_{xx} & f_{xy} & f_{yx} & f_{yy}\\ g_{xx} & g_{xy} & g_{yx} & g_{yy}\end{bmatrix},$$

where

$$\begin{aligned}
f_{xx} =& -r_1,\\
f_{xy} =& 0,\\
f_{yx} =& -\Big(\frac{rk\alpha_1}{(1+k\alpha_1\bar{y})^2}+(\alpha_0+2\alpha_1\bar{y})\Big),\\
f_{yy} =& -\bar{x}\Big(\frac{-2rk^2\alpha_1^2}{(1+k\alpha_1\bar{y})^3}+2\alpha_1\Big),\\
g_{xx} =& 0,\\
g_{xy} =& c(\alpha_0+2\alpha_1\bar{y}),\\
g_{yx} =& c\alpha_1\bar{y},
\end{aligned}$$

$$g_{yy} = c\alpha_1\bar{x}-\frac{(1-\bar{y})(\delta-\gamma)}{(1+\bar{y})^3}.$$

Eigenvector corresponding to $\lambda=0$ of matrix $A=Df(E(\bar{x},\bar{y}),\alpha_{0s})$ is $v=\begin{bmatrix}1 & \frac{-f_x}{f_y}\end{bmatrix}^T$. Similarly, we have the eigenvector corresponding to $\lambda=0$ of matrix $A^T=[Df(E(\bar{x},\bar{y}),\alpha_{0s})]^T$ as $w=\begin{bmatrix}1 & \frac{-f_x}{g_x}\end{bmatrix}^T$.

Using Sotomayor's Theorem [126] for saddle-node bifurcation, we get

$$w^TF_{\alpha_0}\Big(E(\bar{x},\bar{y}),\alpha_{0s}\Big) = -(\bar{x}\bar{y})\Big(1+c\frac{f_x}{g_x}\Big)\neq 0,$$

and

$$w^T\left[\left(D^2 f(E(\bar{x},\bar{y}),\alpha_{0s})\right)(v,v)\right] = \left[\left(f_{xx} - \frac{f_x}{f_y}(f_{xy}+f_{yx}) + \frac{f_x^2}{f_y^2}f_{yy}\right) - \frac{f_x}{g_x}\left(g_{xx} - \frac{f_x}{f_y}(g_{xy}+g_{yx}) + \frac{f_x^2}{f_y^2}g_{yy}\right)\right] \neq 0.$$

Therefore, the system undergoes saddle-node bifurcation iff

$$\bar{x}\bar{y}\left(1 + c\frac{f_x}{g_x}\right) \neq 0 \text{ i.e., if } 1 + c\frac{f_x}{g_x} \neq 0,$$

and

$$w^T\left[\left(D^2 f(E(\bar{x},\bar{y}),\alpha_{0s})\right)(v,v)\right] = \left[\left(f_{xx} - \frac{f_x}{f_y}(f_{xy}+f_{yx}) + \frac{f_x^2}{f_y^2}f_{yy}\right) - \frac{f_x}{g_x}\left(g_{xx} - \frac{f_x}{f_y}(g_{xy}+g_{yx}) + \frac{f_x^2}{f_y^2}g_{yy}\right)\right] \neq 0.$$

∎

2.6 Stability analysis of spatial model

Now, we consider the complete model with diffusion (2.3) and linearize it by taking the transformation

$$\begin{aligned} x &= x^* + X, \\ y &= y^* + Y, \end{aligned}$$

where (X,Y) is the small perturbation in (x,y), we get

$$\begin{aligned} \frac{\partial X}{\partial t} &= a_{11}X + a_{12}Y + D_1\left(\frac{\partial^2 X}{\partial u^2} + \frac{\partial^2 X}{\partial v^2}\right), \\ \frac{\partial Y}{\partial t} &= a_{21}X + a_{22}Y + D_2\left(\frac{\partial^2 Y}{\partial u^2} + \frac{\partial^2 Y}{\partial v^2}\right). \end{aligned}$$

where

$$
\begin{aligned}
a_{11} &= -r_1 x^*, \\
a_{12} &= -x^*\Big(\frac{rk\alpha_1}{(1+k\alpha_1 y^*)^2} + (\alpha_0 + 2\alpha_1 y^*)\Big), \\
a_{21} &= c(\alpha_0 + \alpha_1 y^*)y^*, \\
a_{22} &= c\alpha_1 x^* y^* - \frac{y^*(\delta-\gamma)}{(1+y^*)^2}.
\end{aligned}
$$

We look for the solution of the form

$$
\begin{aligned}
X &= Ae^{\lambda t} sin\Big(\frac{n\pi}{L}u\Big) cos\Big(\frac{m\pi}{M}v\Big), \\
Y &= Be^{\lambda t} sin\Big(\frac{n\pi}{L}u\Big) cos\Big(\frac{m\pi}{M}v\Big).
\end{aligned}
$$

From system (2.3), we get

$$
\begin{aligned}
\frac{\partial X}{\partial t} &= a_{11}X + a_{12}Y + D_1\Big(\Big(\frac{n\pi}{L}\Big)^2 + \Big(\frac{m\pi}{M}\Big)^2\Big), \\
\frac{\partial Y}{\partial t} &= a_{21}X + a_{22}Y + D_2\Big(\Big(\frac{n\pi}{L}\Big)^2 + \Big(\frac{m\pi}{M}\Big)^2\Big).
\end{aligned}
$$

Now, the Jacobian matrix of the above linearized system is

$$
M_{E^*} = \begin{bmatrix} m_{11} & m_{12} \\ m_{21} & m_{22} \end{bmatrix} = \begin{bmatrix} a_{11} - D_1\Big(\Big(\frac{n\pi}{L}\Big)^2 + \Big(\frac{m\pi}{M}\Big)^2\Big) & a_{12} \\ a_{21} & a_{22} - D_2\Big(\Big(\frac{n\pi}{L}\Big)^2 + \Big(\frac{m\pi}{M}\Big)^2\Big) \end{bmatrix}.
$$

Now,

$$
M_1 = -Tr(M^*) = -(m_{11}+m_{22}) = r_1 x^* - c\alpha_1 x^* y^* + y^*\frac{\delta-\gamma}{(1+y^*)^2} + (D_1+D_2)\Big[\Big(\frac{n\pi}{L}\Big)^2 + \Big(\frac{m\pi}{M}\Big)^2\Big],
$$

$$
M_2 = det(M^*) = m_{11}m_{22} - m_{12}m_{21},
$$

$$
\begin{aligned}
M_2 = {} & r_1 x^*\Big(-c\alpha_1 x^* y^* + y^*\frac{(\delta-\gamma)}{(1+y^*)^2}\Big) + c(\alpha_0+\alpha_1 y^*)\Big(\frac{rk\alpha_1}{(1+k\alpha_1 y^*)^2} + (\alpha_0+2\alpha_1 y^*)\Big)x^* y^* \\
& + \Big(\Big(\frac{n\pi}{L}\Big)^2 + \Big(\frac{m\pi}{M}\Big)^2\Big)\Big[D_1\Big(-c\alpha_1 x^* y^* + y^*\frac{(\delta-\gamma)}{(1+y^*)^2}\Big) + D_2\Big(r_1 x^* + D_1\Big(\Big(\frac{n\pi}{L}\Big)^2 + \Big(\frac{m\pi}{M}\Big)^2\Big)\Big)\Big].
\end{aligned}
$$

The characteristic equation for the Jacobian matrix M^* is

$$\lambda^2 + M_1\lambda + M_2 = 0. \tag{2.14}$$

The positive equilibrium point $E^*(x^*, y^*)$ of the system (2.3) is locally asymptotically stable if and only if

$$M_1 > 0, \;\; M_2 > 0$$

i.e., if

$$r_1x^* - c\alpha_1x^*y^* + y^*\frac{\delta-\gamma}{(1+y^*)^2} + (D_1+D_2)\left[\left(\frac{n\pi}{L}\right)^2 + \left(\frac{m\pi}{M}\right)^2\right] > 0,$$

and

$$r_1x^*\left(-c\alpha_1x^*y^* + y^*\frac{(\delta-\gamma)}{(1+y^*)^2}\right) + c(\alpha_0+\alpha_1y^*)\left(\frac{rk\alpha_1}{(1+k\alpha_1y^*)^2} + (\alpha_0+2\alpha_1y^*)\right)x^*y^* +$$
$$\left(\left(\frac{n\pi}{L}\right)^2 + \left(\frac{m\pi}{M}\right)^2\right)\left[D_1\left(-c\alpha_1x^*y^* + y^*\frac{(\delta-\gamma)}{(1+y^*)^2}\right) + D_2\left(r_1x^* + D_1\left(\left(\frac{n\pi}{L}\right)^2 + \left(\frac{m\pi}{M}\right)^2\right)\right)\right] > 0.$$

2.6.1 Conditions for Turing instability

In particular, from the characteristic equation (2.14) of the Jacobian matrix $J_{E_1^*}$, we have

$$M_1 = -Tr(J_{E_1^*}) + (D_1+D_2)\left(\left(\frac{n\pi}{L}\right)^2 + \left(\frac{m\pi}{M}\right)^2\right),$$

and

$$M_2 = D_1D_2\left[\left(\frac{n\pi}{L}\right)^2 + \left(\frac{m\pi}{M}\right)^2\right]^2 - (a_{11}D_2 + a_{22}D_1)\left[\left(\frac{n\pi}{L}\right)^2 + \left(\frac{m\pi}{M}\right)^2\right] + det\left(J_{E_1^*}\right), \tag{2.15}$$

where,

$$Tr(J_{E_1^*}) = -r_1x^* - \frac{y^*(\delta-\gamma)}{(1+y^*)^2} + c\alpha_1x^*y^*,$$
$$det(J_{E_1^*}) = r_1x^*y^*\left[\frac{(\delta-\gamma)}{(1+y^*)^2} - c\alpha_1x^*\right] + cx^*y^*(\alpha_0+\alpha_1y^*)\left(\frac{rk\alpha_1}{(1+k\alpha_1y^*)^2} + (\alpha_0+2\alpha_1y^*)\right).$$

The condition for Turing instability i.e., the diffusion driven instability can occur when $M_1 < 0$ or $M_2 < 0$.

As we can see from M_1, if $Tr(J_{E_1^*}) < 0$, then $M_1 > 0$.

The only possibility left for the occurrence of Turing instability is that $M_2 < 0$ when $det(J_{E_1^*}) > 0$.

Now, we define

$$H(\zeta) = D_1D_2\zeta^2 - (a_{11}D_2 + a_{22}D_1)\zeta + det(J_{E_1^*}), \tag{2.16}$$

where $\zeta = \left(\frac{n\pi}{L}\right)^2 + \left(\frac{m\pi}{M}\right)^2$.

So, for Turing instability $H(\zeta) < 0$

$$\text{i.e., } D_1D_2\zeta^2 - (a_{11}D_2 + a_{22}D_1)\zeta + det(J_{E_1^*}) < 0.$$

Above equation is a quadratic equation in ζ. Therefore, let at $\zeta = \zeta_m$, $H(\zeta)$ attains its minimum. Thus,

$$H'(\zeta_m) = 0 \Rightarrow 2D_1D_2\zeta_m - (a_{11}D_2 + a_{22}D_1) = 0,$$

$$\text{which gives } \zeta_m = \frac{(a_{11}D_2 + a_{22}D_1)}{2D_1D_2} > 0. \tag{2.17}$$

At $\zeta = \zeta_m$, the condition for diffusive instability is

$$\frac{(a_{11}D_2 + a_{22}D_1)^2}{4D_1D_2} - \frac{(a_{11}D_2 + a_{22}D_1)^2}{2D_1D_2} + det(J_{E_1^*}) < 0,$$
$$\text{i.e. } (a_{11}D_2 + a_{22}D_1)^2 - 4D_1D_2det(J_{E_1^*}) > 0.$$

Now, from equation (2.16), we get the roots of the quadratic equation

$$\zeta_{1,2} = \frac{(a_{11}D_2 + a_{22}D_1) \pm \sqrt{(a_{11}D_2 + a_{22}D_1)^2 - 4D_1D_2det(J_{E_1^*})}}{2D_1D_2}.$$

Thus,

$$H(\zeta) < 0 \quad \text{for} \quad \zeta_1 < \zeta < \zeta_2.$$

Also, we have

$$a_{11} + a_{22} < 0 \Rightarrow -\frac{a_{22}}{a_{11}} < 1.$$

From (2.17)

$$\frac{D_2}{D_1} < \frac{-a_{22}}{a_{11}} < 1$$
$$\Rightarrow D_2 < D_1 \quad \text{for Turing instability.}$$

Now, the following result will give the global stability of the unique interior point in the presence of diffusion.

Theorem 2.6.1. *If the interior equilibrium E^* of model (2.2) is globally asymptotically stable, then the corresponding uniform steady state of system (2.3) with the given boundary conditions is also globally asymptotically stable.*

Proof. We consider model system (2.3) and define $\Omega = \Big\{(u,v) : 0 \leq u \leq L, 0 \leq v \leq M\Big\}$. Considering

$$V(x,y) = \Big(x - x^* - x^* ln\frac{x}{x^*}\Big) + m\Big(y - y^* - y^* ln\frac{y}{y^*}\Big)$$

as a Lyapnuov function, define

$$V_2(t) = \iint_\Omega V(x,y)dxdy.$$

Then,

$$\begin{aligned}
\frac{dV_2}{dt} &= \iint_\Omega \left(\frac{\partial V}{\partial x}\frac{\partial x}{\partial t} + \frac{\partial V}{\partial y}\frac{\partial y}{\partial t}\right)dxdy,\\
\frac{dV_2}{dt} &= \iint_\Omega \left[\frac{\partial V}{\partial x}\Big(\frac{rx}{1+k\alpha_1 y} - r_0 x - r_1 x^2 - (\alpha_0 + \alpha_1 y)xy\Big) + \frac{\partial V}{\partial y}\Big(c(\alpha_0 + \alpha_1 y)xy - y\frac{\gamma + \delta y}{1+y}\Big)\right]dxdy\\
&\quad + \iint_\Omega \left(D_1\frac{\partial V}{\partial x}\nabla^2 x + D_2\frac{\partial V}{\partial y}\nabla^2 y\right)dA,\\
&= \iint_\Omega \frac{dV}{dt}dA + \iint_\Omega \left(D_1\frac{\partial V}{\partial x}\nabla^2 x + D_2\frac{\partial V}{\partial y}\nabla^2 y\right)dA,\\
&= I_1 + I_2.
\end{aligned}$$

Using Green's Identity

$$\iint_\Omega F\nabla^2 G dA = \int_{d\Omega} F\frac{\partial G}{\partial n}dS - \iint_\Omega (\nabla F.\nabla G)dA,$$

in the above equation, we get

$$\iint_\Omega \frac{\partial V}{\partial x}\nabla^2 x\,dA = 0 - \iint_\Omega \left(\nabla\left(\frac{\partial V}{\partial x}\right).\nabla x\right)dA$$

$$\nabla\left(\frac{\partial V}{\partial x}\right) = \frac{\partial}{\partial u}\left(\frac{\partial V}{\partial x}\right)\hat{i} + \frac{\partial}{\partial v}\left(\frac{\partial V}{\partial x}\right)\hat{j}$$

$$= \frac{\partial^2 V}{\partial x^2}.\frac{\partial x}{\partial u}\hat{i} + \frac{\partial^2 V}{\partial x^2}.\frac{\partial x}{\partial v}\hat{j}$$

$$\nabla x = \frac{\partial x}{\partial u}\hat{i} + \frac{\partial x}{\partial v}\hat{j}$$

$$\therefore \quad \nabla\left(\frac{\partial V}{\partial x}\right).\nabla x = \frac{\partial^2 V}{\partial x^2}\left(\frac{\partial x}{\partial u}\right)^2 + \frac{\partial^2 V}{\partial x^2}\left(\frac{\partial x}{\partial v}\right)^2$$

$$\Rightarrow \frac{dV_2}{dt} = \iint_\Omega \frac{dV}{dt}dA - \iint_\Omega D_1\left[\frac{\partial^2 V}{\partial x^2}\left(\frac{\partial x}{\partial u}\right)^2 + \frac{\partial^2 V}{\partial x^2}\left(\frac{\partial x}{\partial v}\right)^2\right]dA - \iint_\Omega D_2\left[\frac{\partial^2 V}{\partial y^2}\left(\frac{\partial y}{\partial u}\right)^2 + \frac{\partial^2 V}{\partial y^2}\left(\frac{\partial y}{\partial v}\right)^2\right]dA.$$

Therefore, if $\frac{dV}{dt} \leq 0$, then $\frac{dV_2}{dt} \leq 0$. ∎

2.7 Numerical simulations

2.7.1 Non-spatial model

In this section, first, we perform some extensive numerical simulations to understand the dynamics of system (2.2).

In Fig. 2.5, we fixed the parameters as $r = 3$, $r_0 = 2$, $r_1 = 0.2$, $k = 0.25$, $\alpha_0 = 0.5$, $c = 0.5$, $\gamma = 0.5$, and $\delta = 0.8$. For $\alpha_1 = 0.5$, system (2.2) has a stable unique interior equilibrium point i.e. $E_1^* = (1.529, 0.603)$ is a spiral sink (Fig. 2.5(a)) and for $\alpha_1 = 1.2$, system (2.2) has a stable limit cycle around the interior equilibrium point $E_1^* = (1.168, 0.424)$ i.e. E_1^* is a spiral source (Fig. 2.5(b)).

Next, when model (2.2) has two interior equilibrium points E_1^* and E_2^*, then the extinction equilibrium E_0 is always a saddle point and the axial equilibrium E_1 is always locally asymptotically stable. In Fig. 2.6, we fixed the parameters as $r = 3$, $r_0 = 2$, $r_1 = 0.12$, $k = 0.5$, $\alpha_1 = 0.5$, $c = 0.5$, $\gamma = 0.5$,and $\delta = 0.8$. For $\alpha_0 = 0.025$, system (2.2) has two interior equilibrium points $E_1^* = (4.244, 0.517)$ and $E_2^* = (5.657, 0.359)$. Here, E_1^* is a stable equilibrium and E_2^* is a saddle point (Fig. 2.6(a)). Now, by changing $\alpha_0 = 0.05$, we get a stable limit cycle around the equilibrium point $E_1^* = (3.645, 0.567)$ i.e. E_1^* is a spiral source and $E_2^* = (6.589, 0.238)$ is a saddle point (Fig. 2.6(b)). In this case there is a bi-stability between interior equilibrium point E_1^* and the axial equilibrium E_1.

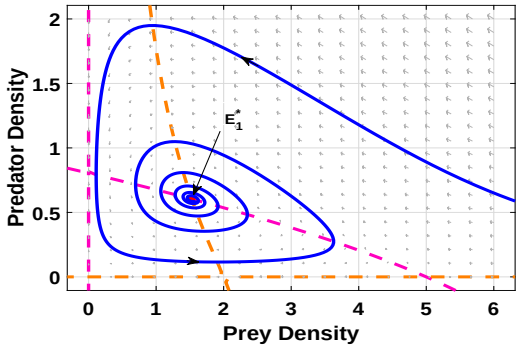

(a) $\alpha_1 = 0.5$, the unique interior equilibrium $E_1^* = (1.529, 0.603)$ is locally asymptotically stable.

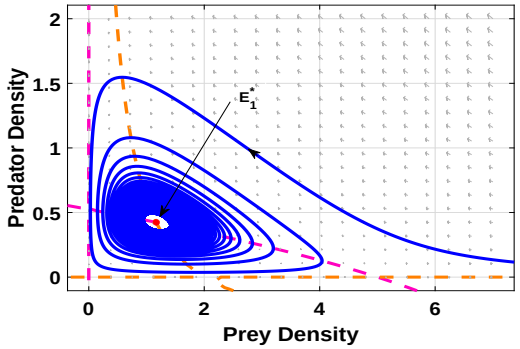

(b) $\alpha_1 = 1.2$, there is a stable limit cycle around the unique interior equilibrium $E_1^* = (1.168, 0.424)$.

Fig. 2.5: Here, all the parameters values are fixed as $r = 3$, $r_0 = 2$, $r_1 = 0.2$, $k = 0.25$, $\alpha_0 = 0.5$, $c = 0.5$, $\gamma = 0.5$, and $\delta = 0.8$. In this case, the other two equilibria E_0 and E_1 are always saddle.

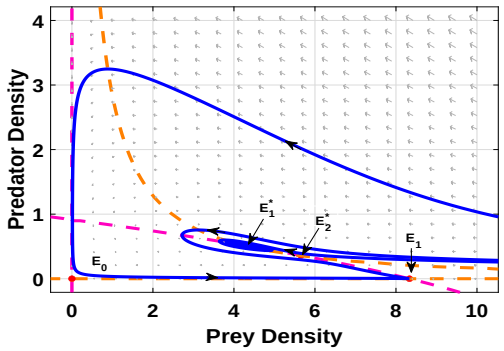

(a) $\alpha_0 = 0.025$, $E_1^* = (4.244, 0.518)$ is locally asymptotically stable and $E_2^* = (5.657, 0.359)$ is a saddle.

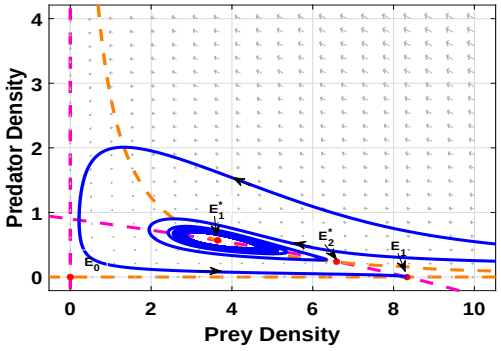

(b) $\alpha_0 = 0.05$, there is a stable limit cycle around $E_1^* = (3.645, 0.567)$ and $E_2^* = (6.589, 0.238)$ is a saddle.

Fig. 2.6: Here, we fixed the parameter values as $r = 3$, $r_0 = 2$, $r_1 = 0.12$, $k = 0.5$, $\alpha_1 = 0.5$, $c = 0.5$, $\gamma = 0.5$,and $\delta = 0.8$. In this case, axial equilibrium E_1 is always locally asymptotically stable, whereas the extinction equilibrium E_0 is always saddle point.

Now, if we fix the parameter values as $r = 2.7$, $r_0 = 0.2$, $r_1 = 0.1$, $k = 0.1$, $\alpha_0 = 0.045$, $\alpha_1 = 0.006$, $c = 0.5$, $\gamma = 0.5$ and $\delta = 0.8$, system (2.2) has three interior equilibrium points $E_1^* = (15.092, 9.540)$, $E_2^* = (23.110, 2.941)$, and $E_3^* = (24.791, 0.424)$. In this case, the extinction equilibrium $E_0 = (0, 0)$ and the axial equilibrium $E_1 = (25, 0)$ is always a saddle

point. In Fig. 2.7, the interior equilibrium $E_1^* = (15.092, 9.540)$ is a spiral sink and $E_3^* = (24.791, 0.424)$ is a nodal sink, i.e. both are locally asymptotically stable whereas the equilibrium $E_2^* = (23.110, 2.941)$ is a saddle point. Here, we notice bi-stability between two interior equilibrium points.

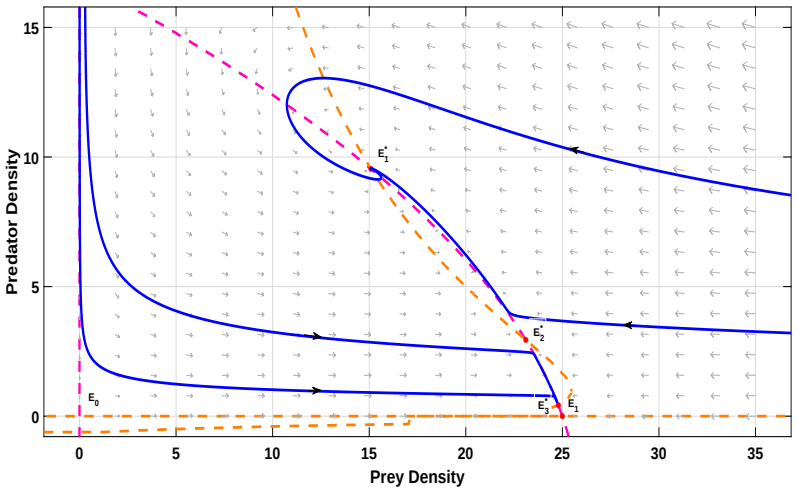

Fig. 2.7: $E_1^* = (15.0927, 9.5400)$ and $E_3^* = (24.7914, 0.4242)$ are locally asymptotically stable and $E_2^* = (23.1100, 2.9411)$ is a saddle point. Here, we fixed the parameter values as $r = 2.7$, $r_0 = 0.2$, $r_1 = 0.1$, $k = 0.1$,$\alpha_0 = 0.045$, $\alpha_1 = 0.006$, $c = 0.5$, $\gamma = 0.5$,and $\delta = 0.8$. In this case, axial equilibrium E_1 and the extinction equilibrium E_0 is always a saddle point.

In addition, we plot the existence of all the interior equilibria in Fig. 2.8. Here, we have fixed all the parameters as $r_0 = 0.2$; $r_1 = 0.1$; $k = 0.1$; $\alpha_1 = 0.006$; $c = 0.5$; $\gamma = 0.5$; $\delta = 0.8$ and varied the two parameters α_0 and r with the range 0 to 0.1 and 2 to 3, respectively. In blue region, no interior equilibrium exists. In green region, there is only one interior equilibrium which can be either source or stable. In yellow region, two interior equilibria exists of which one can be stable or source and other one is always saddle point. In red region, three interior equilibria exists of which two are always stable and one is always saddle.

Next, in Fig. 2.9, we analyze the basin of attraction for various equilibria. Here, we basically discussed the convergence region of the trajectories for a given set of initial conditions. In Fig. 2.9(a), we fixed the parameters as $r = 3$; $r_0 = 2$; $r_1 = 0.12$; $k = 0.5$; $\alpha_0 = 0.025$; $\alpha_1 = 0.5$; $c = 0.5$; $\gamma = 0.5$; $\delta = 0.8$. In this case, two interior equilibria exist and there is a bi-stability between the equilibria E_1 and E_1^*. Blue and yellow represent the convergence region of E_1 and E_1^*, respectively. In Fig. 2.9(b), we have fixed the parameters as $r = 2.7$; $r_0 = 0.2$; $r_1 = 0.1$; $k = 0.1$; $\alpha_0 = 0.045$; $\alpha_1 = 0.006$; $c = 0.5$; $\gamma = 0.5$; $\delta = 0.8$. Here, there are two attractors

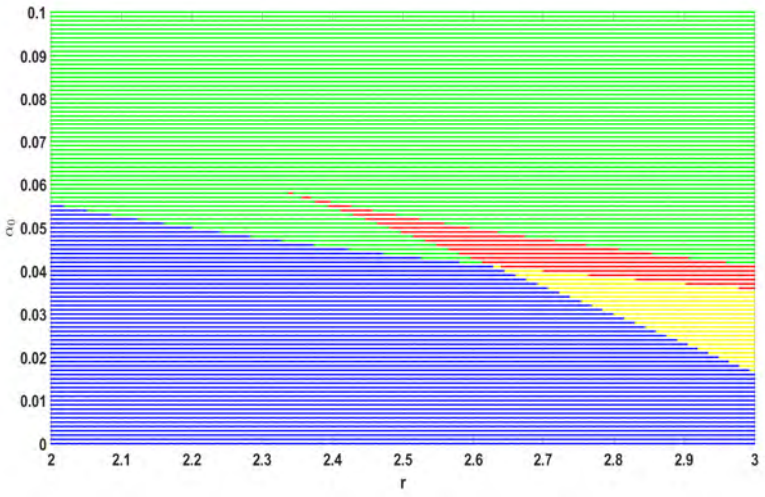

Fig. 2.8: Existence of all the interior equilibria in $\alpha_0 - r$ parameter plane. All the remaining parameters are fixed as $r_0 = 0.2$; $r1 = 0.1$; $k = 0.1$; $\alpha_1 = 0.006$; $c = 0.5$; $\gamma = 0.5$; $\delta = 0.8$. Blue: no interior equilibrium exists, green: only one interior equilibrium exists which can be either source or stable, yellow: two interior equilibria exists of which one can be stable or source and other one is always saddle point, red: three interior equilibria exists of which two are always stable and one is saddle.

E_1^* and E_3^* i.e., there is a bi-stability between E_1^* and E_3^*. Magenta and green represent the convergence region of E_1^* and E_3^*, respectively.

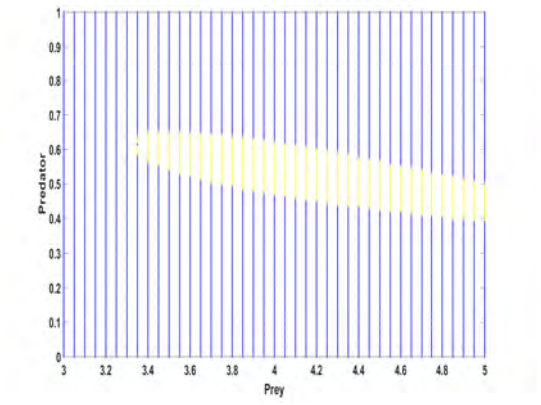

(a) Basin of attraction for the axial equilibrium E_1 and the interior equilibrium E_1^*. Blue and yellow represent the convergence region of E_1 and E_1^*, respectively.

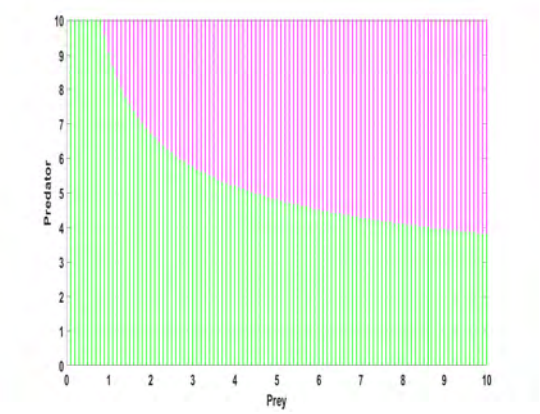

(b) Basin of attraction for the interior equilibrium E_1^* and the interior equilibrium E_3^*. Magenta and green represent the convergence region of E_1^* and E_3^*, respectively.

Fig. 2.9: Basin of attractions in the bistable region for the model (2.2).

In Fig. 2.10, we show the existence of all the interior equilibria and also discussed their

stability behavior with varying α_0. In Fig. 2.10(a), when there exists two interior equilibria, one is always saddle point and other one can be locally asymptotically stable or a source. In case of a unique interior equilibrium, it can be locally asymptotically stable or a source. Figure 2.10(b) shows that when there exists three interior equilibria, E_1^* and E_3^* are always locally asymptotically stable, and E_2^* is always a saddle point.

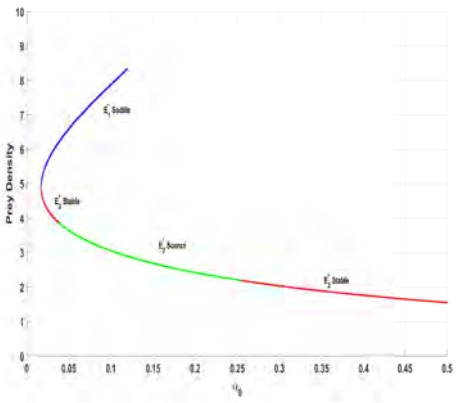

(a) α_0 v.s. prey density x at different equilibria. All the other parameters are fixed as $r = 3$, $r_0 = 2$, $r_1 = 0.12$, $k = 0.5$, $\alpha_1 = 0.5$, $c = 0.5$, $\gamma = 0.5$, $\delta = 0.8$.

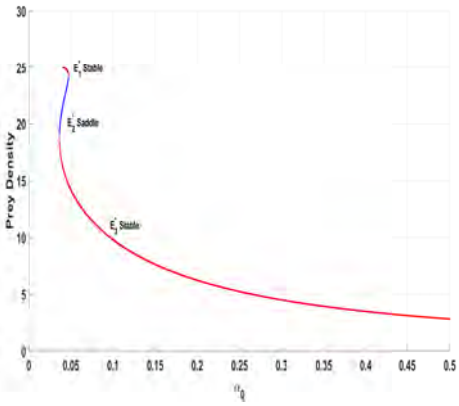

(b) α_0 v.s. prey population x at different equilibria. All the other parameters are fixed as $r = 2.7$, $r_0 = 0.2$, $r_1 = 0.1$, $k = 0.1$, $\alpha_1 = 0.006$, $c = 0.5$, $\gamma = 0.5$, $\delta = 0.8$.

Fig. 2.10: The figure shows the stability of interior equilibria (E_1^*, E_2^* and E_3^*) and describes the number of interior equilibria and their stability when α_0 changes from 0 to 0.5, where $y-$axis is the prey population at corresponding equilibria. Blue represents the saddle; green represents the source; and red represents the sink (stable).

Moreover, in Fig. 2.11, we plot the stability and instability region for the interior equilibria in the k-α_1 parameter plane. In this figure, we observe that for a fixed value of hunting cooperation parameter α_1, increasing the fear effect parameter k can make the system stable. Therefore, the value of k should be sufficiently large to rule out the existence of periodic solutions.

Next, we plot the bifurcation diagram of prey and predator with varying α_1 in Fig. 2.12. If the cooperation parameter α_1 is small, there is stable coexistence of both prey and predator species. As the cooperation parameter α_1 increases, Hopf-bifurcation occurs and the stable coexistence equilibrium loses its stability and a stable limit cycle emerges with increasing amplitude with α_1.

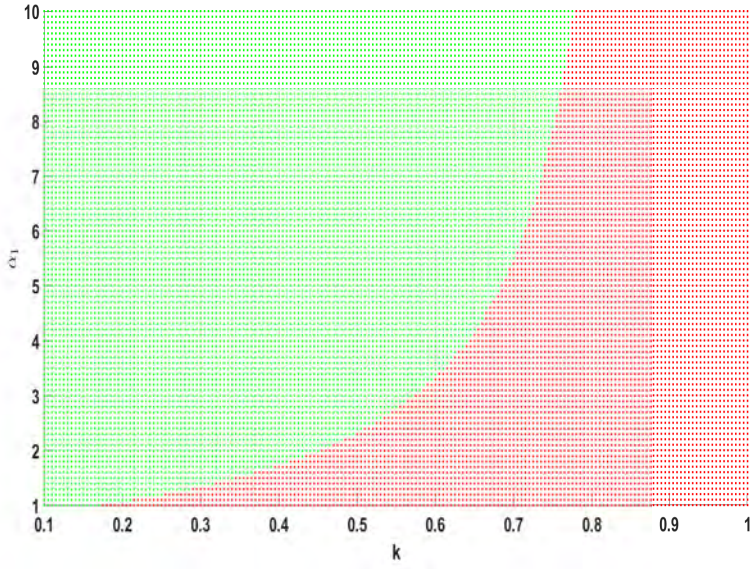

Fig. 2.11: Stablity and instability region of interior equilibria for the model (2.2) w.r.t. parameters k and α_1. Red indicates stablity region and green indicates instability region. All the other parameters are fixed as $r = 3$; $r_0 = 2$; $r_1 = 0.2$; $\alpha_0 = 0.5$; $c = 0.5$; $\gamma = 0.5$; and $\delta = 0.8$.

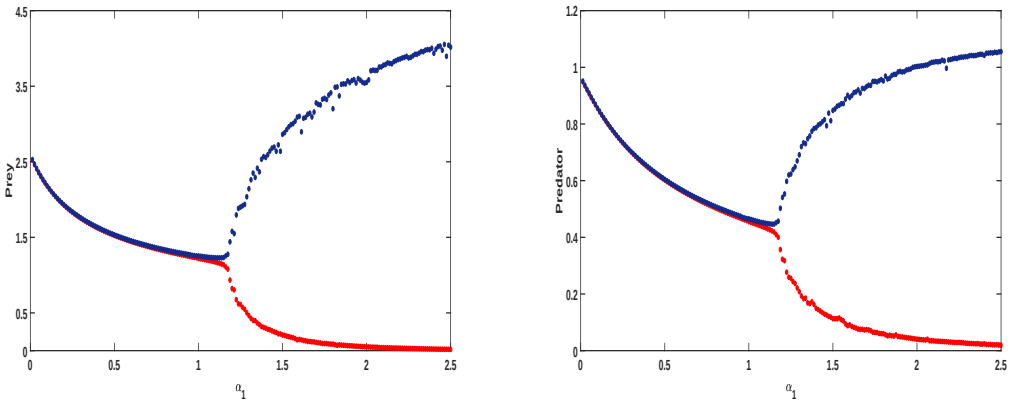

(a) For prey. (b) For predator.

Fig. 2.12: Bifurcation plot of prey and predator for the model 2.2 with varying cooperation parameter α_1. Here, all the parameters are fixed as $r = 3$; $r_0 = 2$; $r_1 = 0.2$; $k = 0.25$; $\alpha_0 = 0.5$; $c = 0.5$; $\gamma = 0.5$ and $\delta = 0.8$.

2.7.2 Pattern formation

Next, we show that there is a possibility of existence of diffusion induced instability in system (2.3). If an equilibrium is asymptotically stable without diffusion but unstable in the presence

of diffusion, it is said to be diffusion driven instability. Turing instabilities may cause patterns formation in a spatiotemporal model. Now, we check all the analytic conditions of Turing instability numerically. In Fig. 2.13, we plot $H(\zeta)$ vs ζ for different set of parameters for which system (2.2) has unique, two or three interior equilibria, respectively. In Fig. 2.13(a), we plot $H(\zeta)$ vs ζ for different values of r_0. Here, all the other parameters are fixed as $r = 2.8$, $r_1 = 0.2$, $k = 0.25$, $\alpha_0 = 0.5$, $\alpha_1 = 0.5$, $c = 0.5$, $\gamma = 0.5$, $\delta = 0.8$. This figure illustrates that as r_0 increases, the range of values for which the polynomial $H(\zeta)$ remains negative decreases and as a result the possibility for the existence of Turing instabilities decreases.

Similarly in Fig. 2.13(b), we plot $H(\zeta)$ vs ζ for different values of α_0. Here, all the other parameters are fixed as $r = 2.9$, $r_0 = 2$, $r_1 = 0.2$, $k = 0.5$, $\alpha_1 = 0.6$, $c = 0.8$, $\gamma = 0.5$, $\delta = 0.8$. From this figure, we observe that as the value α_0 increases, the possibility for the existence of Turing instability decreases. In Fig. 2.13(c), we plot $H(\zeta)$ vs ζ for different values of k with other parameters as $r = 2.57$, $r_0 = 0.2$, $r_1 = 0.1$, $\alpha_0 = 0.045$, $\alpha_1 = 0.006$, $c = 0.5$, $\gamma = 0.5$, $\delta = 0.8$. Here, we analyze that as the value of k increases, the range for which the polynomial $H(\zeta)$ remains negative increases. Hence, the possibility for the occurrence of diffusion induced instabilities increases as the value of k increases.

Turing patterns in two-dimensional spatial model (2.3)

Now, we perform some numerical simulation to obtain the Turing patterns in two-dimensional space. We will investigate Turing patterns obtained for different diffusive rates. The system of equations in (2.3) is numerically solved using the finite difference method to obtain the spatiotemporal dynamics in a two-dimensional spatial domain. For the reaction part, the forward difference Euler scheme is used, and for the two-dimensional diffusion terms, the standard five point explicit finite difference scheme is used with homogeneous Neumann boundary conditions. We consider a square domain $\omega = [0,200] \times [0,200]$ with the time step $\Delta t = 1/300$ and spatial grid sizes $\Delta x = \Delta y = 1/3$. For the numerical simulations, we introduce a small random perturbation near the equilibrium point $E^*(x^*, y^*)$ in the reaction-diffusion system. The initial condition is considered as

$$\begin{aligned} x(u,v,0) &= x^* + 5\varepsilon\xi_{i,j}, \\ y(u,v,0) &= y^* + 5\varepsilon\theta_{i,j}, \end{aligned} \tag{2.18}$$

where $\varepsilon_1 = 0.0001$ and $\xi_{i,j}$ and $\theta_{i,j}$ represents standard Gaussian white noise.

Next, we will investigate the effect of diffusion coefficients on the Turing patterns. We carry out the simulations at time $t = 1,00,000$ so that patterns will become stationary and will not change further with changing time. Figures 2.14, 2.15, and 2.16 depicts various Turing patterns

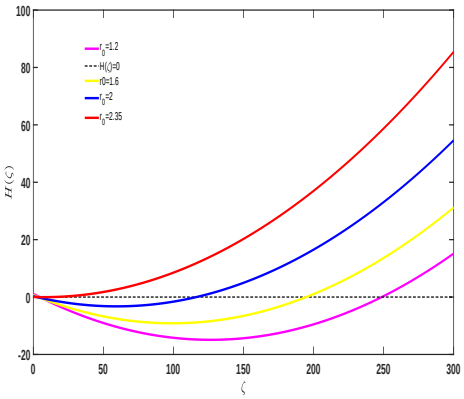

(a) $H(\zeta)$ vs ζ for different values of r_0.

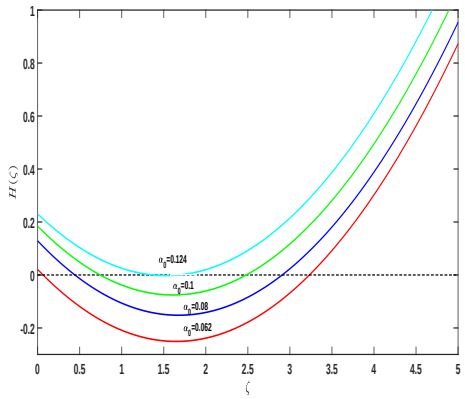

(b) $H(\zeta)$ vs ζ for different values of α_0.

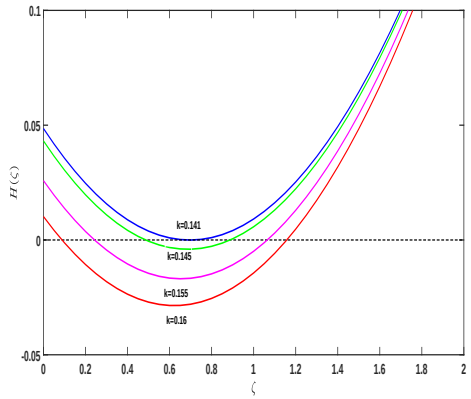

(c) $H(\zeta)$ vs ζ for different values of k.

Fig. 2.13: Plot of $H(\zeta)$ with respect to ζ for different values of α_0 and k, where black dashed line represents $H(\zeta) = 0$.

obtained for different diffusive rates. In Fig. 2.14, we obtain Turing patterns for the spatial model when the system has a unique interior equilibrium. Here, we observe that increase in diffusion may lead to decrease in spatial heterogeneity in population density of prey and predator. In this figure, the system dynamics shows holes patterns for the prey and spots pattern for the predator population, i.e. the prey population exists at low density in the isolated region and at high density in the remaining area, whereas the predator population resides at medium density in the isolated spots and at low density in the remaining region.

Figure 2.15 presents Turing pattern for the spatial system when there exists two interior equilibrium. Here, all the parameters are fixed as given in Table 2.2. The blue color signifies low population density, while the red color signifies high population density. This figure depicts the patterns of holes and spots for the prey and predator populations, respectively. Here, we

Fig No.	Number of Interior Equilibrium	Parameter values
2.14	Unique	$r = 3$, $r_0 = 2.5$, $r_1 = 0.2$, $k = 0.25$, $\alpha_0 = 0.5$, $\alpha_1 = 0.5$, $c = 0.5$, $\gamma = 0.5$, and $\delta = 0.8$
2.15	Two	$r = 2.9$, $r_0 = 2$, $r_1 = 0.2$, $k = 0.5$, $\alpha_0 = 0.08$, $\alpha_1 = 0.6$, $c = 0.8$, $\gamma = 0.5$, and $\delta = 0.8$
2.16	Three	$r = 2.62$, $r_0 = 0.2$, $r_1 = 0.1$, $k = 0.7$, $\alpha_0 = 0.045$, $\alpha_1 = 0.006$, $c = 0.5$, $\gamma = 0.5$, and $\delta = 0.8$

Table 2.2: Parameters values for Turing patterns used in Figs. 2.14, 2.15, 2.16

analyzed that the prey population has a spatial distribution in which the average and high population density occupy the majority of the domain. In contrast, the predator population occupies a considerable portion of low population density area.

Similarly, Fig. 2.16 depicts snapshots of Turing patterns obtained for prey and predator population in two dimensional spatial model. In this case, the system has three interior equilibria out of which one satisfies the analytic conditions of Turing instability. Figure 2.16 shows a mixture of spots and stripes patterns. As we increase the value of diffusion coefficients, the patterns start evolving.

2.8 Discussion and concluding remarks

In the present paper, we proposed a predator-prey model incorporating both hunting cooperation among predators and fear induced birth reduction in prey. Moreover, we assume that due to hunting cooperation. The fear induced in the prey is incorporated in the form of reduced birth rate of prey. We assume that predators consume prey through Type-I functional response [55]. Further, the temporal and spatial model systems are proposed and examined.

For the temporal model system (2.2), we discussed the positivity and boundedness of the solutions. We provided some sufficient conditions for the system to be persistent. Further, we derived the conditions for the existence of the number of interior equilibrium points and their local stability is analyzed. The global stability of the unique interior equilibrium point is investigated by choosing a suitable Lyapnuov function. We obtained the conditions for the existence of saddle-node bifurcation around the equilibrium point E^* for the bifurcation parameter α_0. Throughout this study, our primary concern is to analyze the effect of hunting cooperation on the system dynamics. As a result, we conducted a Hopf-bifurcation study of the system with respect to the hunting cooperation parameter α_1 and obtained a critical value of the parameter

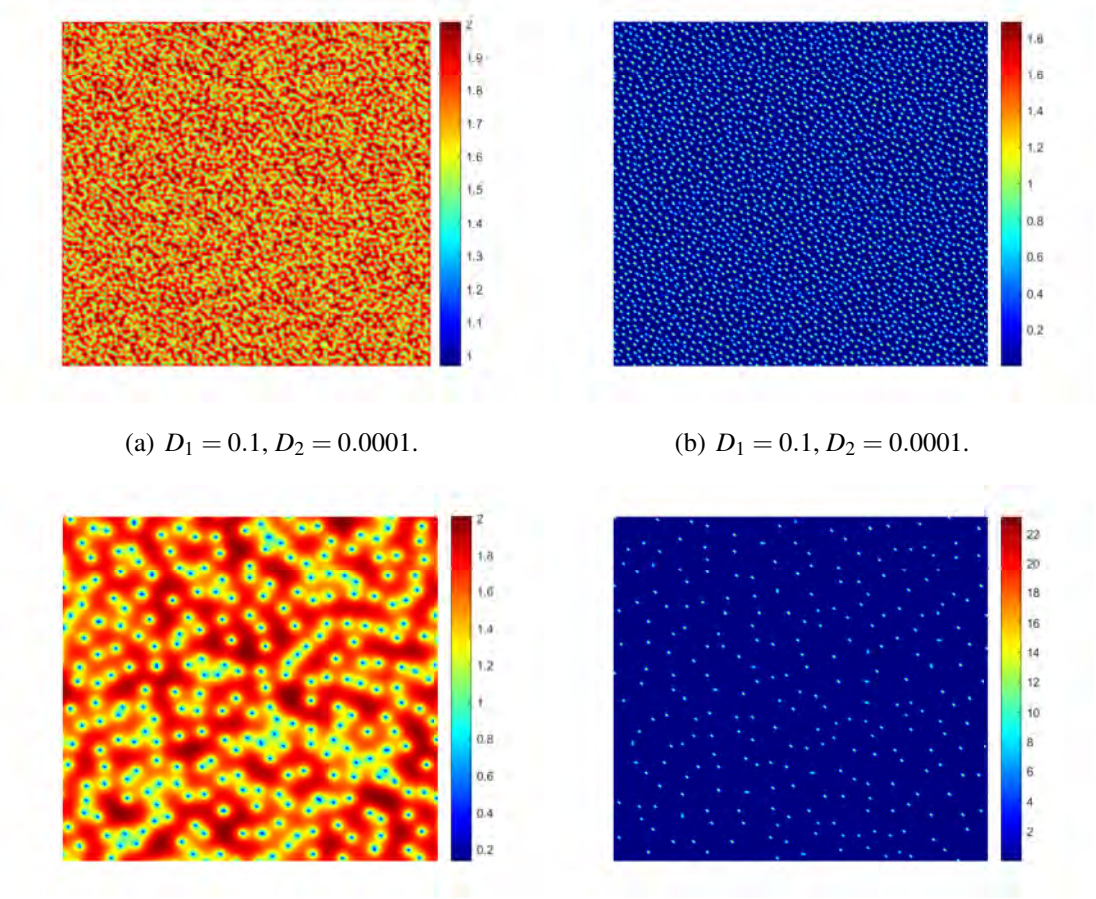

(a) $D_1 = 0.1, D_2 = 0.0001$.

(b) $D_1 = 0.1, D_2 = 0.0001$.

(c) $D_1 = 1, D_2 = 0.001$.

(d) $D_1 = 1, D_2 = 0.001$.

Fig. 2.14: Snapshots of prey and predator obtained for different diffusive rates in 2D(xy-plane). All the other parameters are fixed as mentioned in Table 2.2.

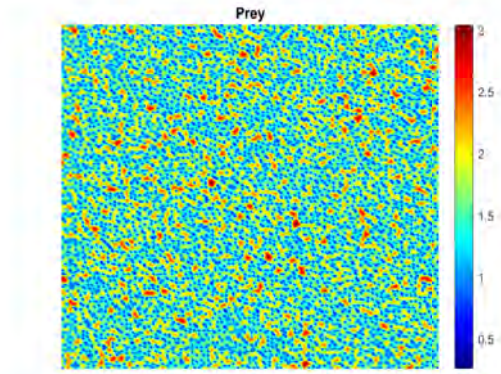

(a) $D_1 = 0.1, D_2 = 0.001$.

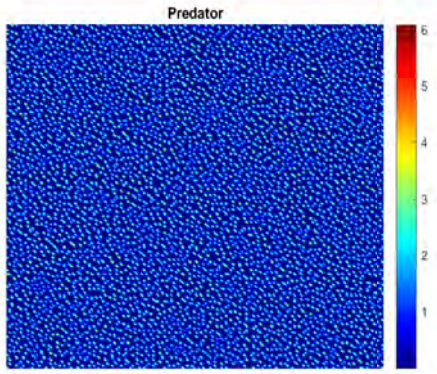

(b) $D_1 = 0.1, D_2 = 0.001$.

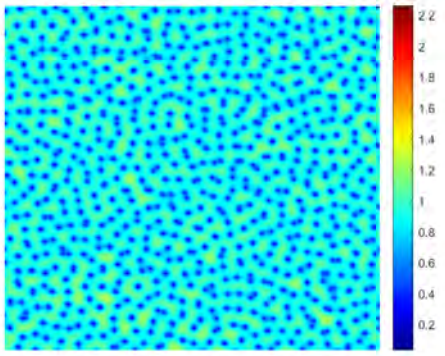

(c) $D_1 = 1, D_2 = 0.01$.

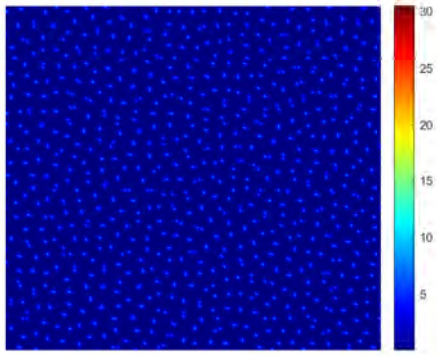

(d) $D_1 = 1, D_2 = 0.01$.

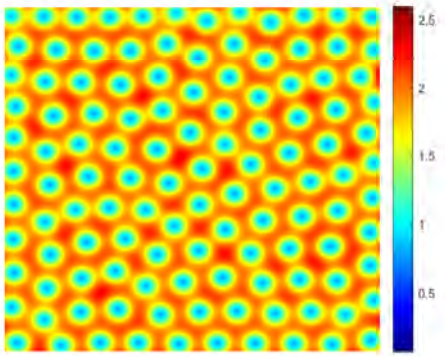

(e) $D_1 = 2, D_2 = 0.1$.

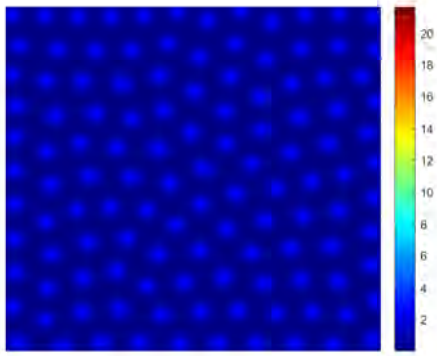

(f) $D_1 = 2, D_2 = 0.1$.

Fig. 2.15: Snapshots of prey and predator obtained for different diffusive rates in 2D(xy-plane). All the other parameters are fixed as mentioned in Table 2.2.

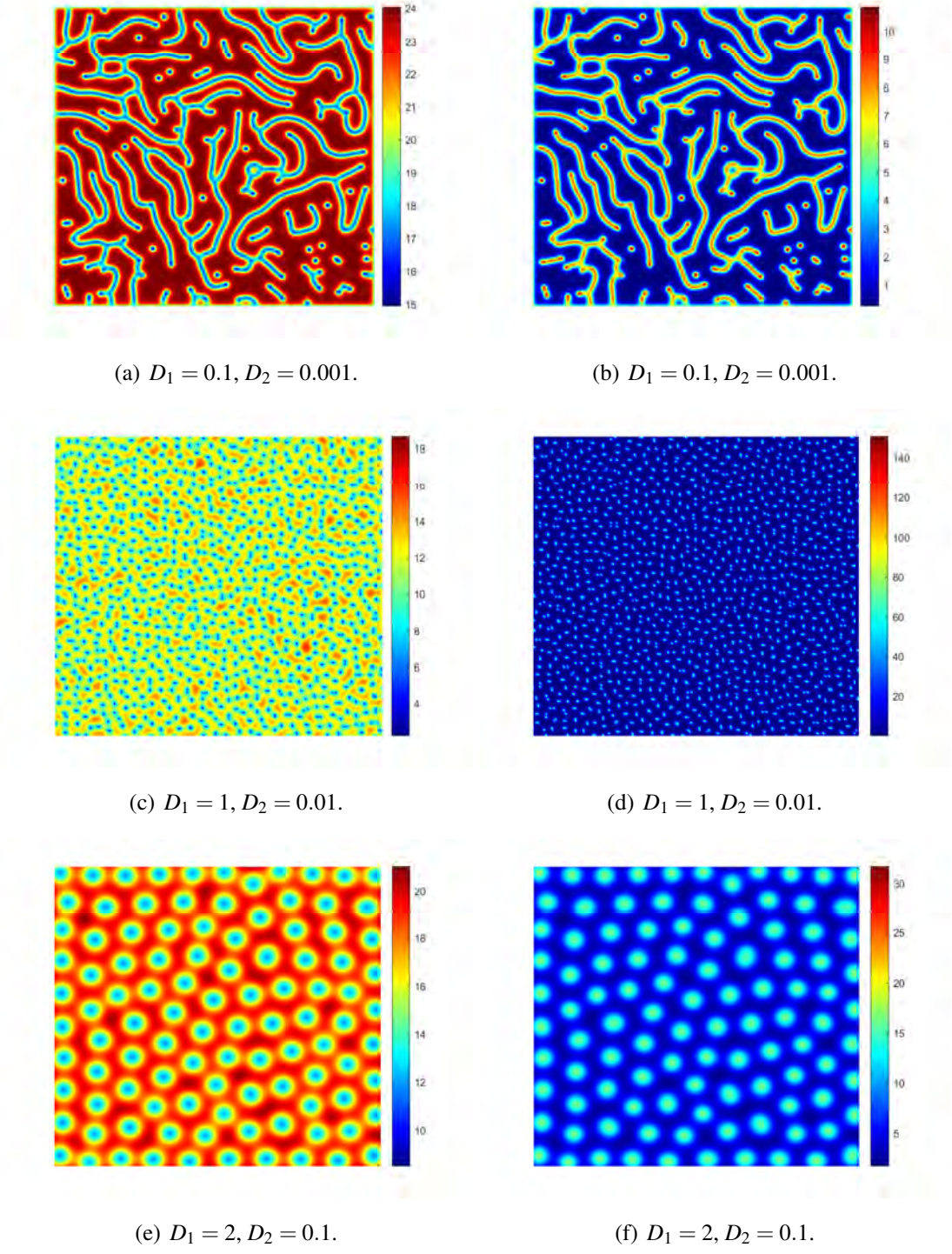

(a) $D_1 = 0.1, D_2 = 0.001$.

(b) $D_1 = 0.1, D_2 = 0.001$.

(c) $D_1 = 1, D_2 = 0.01$.

(d) $D_1 = 1, D_2 = 0.01$.

(e) $D_1 = 2, D_2 = 0.1$.

(f) $D_1 = 2, D_2 = 0.1$.

Fig. 2.16: Snapshots of prey and predator obtained for different diffusive rates in 2D(xy-plane). All the other parameters are fixed as mentioned in Table 2.2.

α_1 at which Hopf-bifurcation occurred and the system flips its stability behaviour. We analyze that increasing the hunting cooperation parameter may destabilize the system. Here, we notice that for a fixed value of hunting cooperation parameter, increasing the value of fear parameter can make the system stable. For the spatiotemporal model (2.3), we analyze the linear stability to determine the Turing instability conditions. Also, we provided the global stability analysis in the case of spatiotemporal model system.

We performed some numerical simulations to validate our analytical findings. We discuss about all the possible attractors of the system solutions in Figs. 2.5, 2.6, and 2.7. Moreover, we also depicted bistability between various equilibrium points in Figs. 2.6 and 2.7. We have analyzed and presented the basin of attractions in the bi-stable region for model (2.2) in Fig. 2.9. The model show a variety of complex dynamics, including one-parameter bifurcations such as saddle-node, and Hopf bifurcation which is illustrated in Figs. 2.10 and 2.12. Moreover, we performed simulations to better understand the movement of species and their spatial distribution across the domains. Turing instability conditions are satisfied for the set of parameters as given in Table 2.2. We obtained Turing patterns for different diffusive rates in case of two dimesional spatial model system. Spots, holes and stripes patterns are obtained as illustrated in Figs. 2.14, 2.15, and 2.16.

Chapter 3

Consequences of fear effect and prey refuge on the Turing patterns in a delayed predator-prey system[1]

3.1 Introduction

In ecology and theoretical biology, the dynamic interaction between predators and their prey is one of the most dominant themes due to its universal prevalence and significance [10]. Numerous prey-predator models have been investigated to comprehend the impact of prey density and predator feeding patterns on both species' stable and oscillatory coexistence. Leslie [84, 85] introduced the prey-predator model in which the predator's carrying capacity is directly proportional to the prey density. Many ecologists have been studying the predator-prey model based on the Leslie-Gower scheme in recent years [5, 65, 73, 105]. Aziz-Alaoui and Okiye [5] studied the dynamics of a Leslie-Gower scheme-based predator-prey system with Holling-type II functional response.

Prey refuge has been found useful in a predator-prey interaction by decreasing the risk of extinction due to predation [28]. Kar [63] highlighted that mite predator-prey interactions frequently exhibit spatial refugia, which provide refuge from predation and lower the risk of extinction for the prey. Chen *et al.* [24] and Cai *et al.* [20] analyzed the pattern formation in a Leslie-Gower prey-predator system with prey refuge. Kar *et al.* [66] proposed a model for two predators and one prey and showed that incorporating constant prey refuge may prevent prey extinction. In 2015, Sharma and Samanta [150] developed an eco-epidemiological model and studied how the infected prey refuge can affect the constituent population density. They concluded that prey refuge plays a vital role in controlling the stability of populations. Verma and Misra [175] investigated that increasing the prey refuge greater than a certain Allee threshold may prevent the situation of unconditional extinction.

[1]This chapter is based on our paper published in *Chaos: An Interdisciplinary Journal of Nonlinear Science*, **32**, 123132, 2022.

It has long been assumed that predators can only alter prey populations by killing them directly, as predatory incidents are relatively easy to detect [32, 34]. But recently, Zanette *et al.* [187] highlighted that the predation fear alone reduced the number of song sparrow (*Melospiza Melodia*) offsprings by 40%. Wang *et al.* [180] simulated a predator-prey interaction with fear effect and observed that high levels of fear could stabilize the system dynamics by excluding the existence of periodic oscillations. Wang *et al.* [179] examined a prey-predator system equipped with both prey refuge and fear. They analyzed that the gradual increments in fear might decrease the population density, and prey might become extinct.

In general, biological processes often involve delay factors. Incorporating time delays in a mathematical model can alter the system dynamics and makes it more realistic from an ecological perspective [74]. Few studies incorporated the fear response delay as far as the author is concerned. The amount of time it takes for predation fear to alter the density of prey populations is known as the fear response delay. Panday *et al.* [119] examined a delayed predator-prey model and concluded that the system exhibits multi-stability switching and chaotic dynamics for a significant increase in delay parameter. Dubey *et al.* [42] analyzed a multi-delayed predator-prey system and noticed that system eventually enters a chaotic phase for a significantly high value of the fear response delay. Therefore, motivated by the above works, in the present work, we propose a predator-prey model based on a modified Leslie-Gower scheme in which the prey population exhibits refuge. Here, we are interested in studying the complex dynamics of the spatial predator-prey system in which the number of prey in the refuge is proportional to the prey-predator interactions. Prey refuge proportional to both species can make the model more realistic as prey and predator densities can affect the prey refuge [52, 95, 102, 161]. Also, we assume the reduced birth rate of the prey population, which accounts for anti-predator behavior due to predation risk. Since the effect of predation is not instantaneous, we consider the fear response delay in the growth rate of the prey population. Hence, our model becomes

$$\begin{aligned}\frac{dx}{dt} &= \left[\frac{r}{(1+ky(t-\tau))} - r_0 - r_1 x - \frac{(\alpha(1-\beta y)y)}{a+(1-\beta y)x}\right]x,\\ \frac{dy}{dt} &= \left[(\mu - \frac{cy}{a+(1-\beta y)x})\right]y,\end{aligned} \tag{3.1}$$

subjected to the non-negative initial conditions

$$x(z) = \psi_1(z) \geq 0, \quad y(z) = \psi_2(z) \geq 0, \quad z \in [-\tau, 0],$$

where

$$\psi_j(z) \in \mathbb{C}([-\tau, 0] \to \mathbb{R}^+), \quad j = 1, 2.$$

Here, prey and predator densities are represented by x and y at any given time t, r and r_0

signifies birth rate and natural death rate of prey population, respectively. r_1 is the magnitude of intraspecies competitions among preys, α is the attack rate parameter, μ is the growth rate of predator population, a is the half-saturation constant, c is the maximum value of per capita reduction of x due to y, τ is the fear response delay. Here, we assume the number of prey refugia to be $x_r = \beta xy$, where β is the prey refuge coefficient. Thus, the available prey for predation is $x - \beta xy = x(1 - \beta y)$. Throughout this chapter, we consider $(1 - \beta y) \geq 0$ i.e., $y \leq \frac{1}{\beta}$. If $(1 - \beta y) < 0$, then it would imply that no prey species ia available for predation. All the parameters associated with the above model only assume positive values.

During prey-predator interaction, predators move to hunt prey, while prey migrates to avoid predators, resulting in spatial variations in population density. This irregular movement of species can be explained mathematically using Fick's law of diffusion [108]. This spread of species might lead to a variety of remarkable spatial patterns. The term Turing instability was first introduced by Alan Turing [165], which means that adding diffusion to a certain type of multispecies interaction can destabilize the system dynamics. Dubey *et al.* [39] examined the impact of time-varying cross-diffusion and analyzed that increasing the time variation amplitude might have a positive effect on the stabilizing tendency. Dubey *et al.* [41] investigated the mathematical aspects of the mechanism for pattern formation in a spatial prey-predator model. Many ecologists have intensively analyzed the spatiotemporal patterns induced by Turing instability in recent years [71, 72, 77]. Tang *et al.* [159] studied the dynamical properties of a diffusive prey-predator system with herd behavior. Chakraborty *et al.* [23] analyzed how the combined effects of prey refuge and additional food affect the dynamical properties and prey density in a diffusive prey-predator system. Upadhyay and Mishra [169] explored the dynamic consequences of incorporating predation fear in a two-dimensional spatial system. Sasmal *et al.* [143] examined the changes in Turing patterns as a result of aposematic time. Kumar and Kumari [76] analyzed the spatial dynamics of a diffusive predator-prey system and obtained various Turing and non-Turing patterns. Sasmal *et al.* [142] proposed and examined a diffusive prey-predator model exhibiting hunting cooperation with fear effect. They observed complex dynamical behaviors and obtained various Turing patterns for two-dimensional diffusion. Manna and Banerjee [97] investigated that prey and predator species may experience spatiotemporal chaos for a sufficiently large value of gestational delay. Tripathi *et al.* [164] analyzed a prey-predator model with time delay and concluded that diffusion facilitates the oscillatory coexistence of both species and may alter the bifurcation point. To understand the impact of prey refuge and predation fear on the system dynamics in a more pragmatic way, we spatially extend the proposed model system by adding two-dimensional diffusion. The following reaction-diffusion equations represent the extended proposed model considering the spatial

effects,

$$\begin{aligned}\frac{\partial x}{\partial t} &= \left[\frac{r}{(1+ky(t-\tau))} - r_0 - r_1 x - \frac{(\alpha(1-\beta y)y)}{a+(1-\beta y)x}\right] x + D_1\nabla^2 x,\\ \frac{\partial y}{\partial t} &= \left[(\mu - \frac{cy}{a+(1-\beta y)x})\right] y + D_2\nabla^2 y,\end{aligned} \tag{3.2}$$

subjected to the non-negative initial conditions

$$x(u,v,s) = \psi_1(u,v,s) \geq 0, \quad y(u,v,s) = \psi_2(u,v,s) \geq 0,$$

$$s \in [-\tau, 0] \quad \text{and} \quad \rho = \{(u,v) : 0 \leq u \leq M, 0 \leq v \leq N\},$$

and Neumann boundary conditions,

$$\frac{\partial x}{\partial n} = \frac{\partial y}{\partial n} = 0.$$

Here, ρ is the bounded domain in $\mathbb{R}^2_+$ with smooth boundary $\partial\rho$ and n is the outward normal vector to $\partial\rho$. $x(u,v,t)$ and $y(u,v,t)$ signifies the prey and predator densities at the spatial coordinates (u,v) and time t, respectively. All the other parameters have the same meaning as in model (3.1). Here, $\nabla^2 = \frac{\partial^2}{\partial u^2} + \frac{\partial^2}{\partial v^2}$ is the usual Laplacian operator in the two-dimensional domain. D_1 and D_2 are the self-diffusion coefficients for prey and predator, respectively. Neumann boundary conditions indicates that no species can enter or leave through the boundary.

The rest of this paper is structured as follows: In Section 3.2, we analyzed the complex dynamics of the non-delayed temporal model. We investigated the local stability behavior for the delayed system in Section 3.3. We have done the direction and stability analysis of Hopf-bifurcation using normal form theory and center manifold theorem. In Section 3.4, we derived the conditions for diffusion-driven instability and provided the global stability analysis for the coexistence equilibrium point. We have done the Hopf-bifurcation analysis for the delayed spatiotemporal system in Section 3.5. In Section 3.6, we performed extensive numerical simulations to corroborate the analytical results. Finally, in Section 3.7, we concluded our analytical findings and discussed the ecological significance of our obtained results.

3.2 Dynamics of non-delayed temporal model

In this section, we shall analyze the temporal model (3.1) without considering delay which may represented by the following system of ordinary differential equations:

$$\begin{aligned}\frac{dx}{dt} &= \left[\frac{r}{(1+ky)} - r_0 - r_1 x - \frac{\alpha(1-\beta y)y}{a+(1-\beta y)x}\right] x =: f(x,y),\\ \frac{dy}{dt} &= \left[(\mu - \frac{cy}{a+(1-\beta y)x})\right] y =: g(x,y),\end{aligned} \tag{3.3}$$

$$x(0) = x_0 \geq 0, \quad y(0) = y_0 \geq 0.$$

3.2.1 Mathematical preliminaries

First, we will prove that all the solutions are non-negative. We can write the model (3.3) as

$$\begin{aligned}\tfrac{dx}{dt} &= \Phi_1(t)x,\\ \tfrac{dy}{dt} &= \Phi_2(t)y,\end{aligned}$$

where

$$\begin{aligned}\Phi_1(t) &= \frac{r}{(1+ky)} - r_0 - r_1 x - \frac{\alpha(1-\beta y)y}{a+(1-\beta y)x},\\ \Phi_2(t) &= \mu - \frac{cy}{a+(1-\beta y)x}.\end{aligned}$$

Hence

$$x(t) = x(0)\exp\left[\int_0^t \Phi_1(x(s),y(s))ds\right] \geq 0,$$

$$y(t) = y(0)\exp\left[\int_0^t \Phi_2(x(s),y(s))ds\right] \geq 0,$$

which yields

$$x(t) \geq 0, \text{ and } y(t) \geq 0,$$

which indicates that all the solutions are non-negative.

Theorem 3.2.1. *The solutions of the system (3.3) are bounded above in $\mathbb{R}^2_+$ satisfying the given properties:*

$$\limsup_{t\to\infty} x(t) \leq \frac{r-r_0}{r_1} =: x_{max},$$
$$\limsup_{t\to\infty} y(t) \leq min\{\frac{1}{\beta}, \frac{\mu}{c}(a+\frac{r-r_0}{r_1})\} =: y_{max}.$$

Proof. System (3.3) gives us

$$\begin{aligned} \frac{dx}{dt} &= \frac{rx}{(1+ky)} - r_0x - r_1x^2 - \frac{\alpha(1-\beta y)xy}{a+(1-\beta y)x}, \\ &\leq (r-r_0)x - r_1x^2 \qquad (\text{as} \quad 1-\beta y \geq 0). \end{aligned}$$

Assuming $r-r_0>0$, we get

$$\limsup_{t\to\infty} x(t) \leq \frac{r-r_0}{r_1}.$$

Now,

$$\begin{aligned} \frac{dy}{dt} &= y\left(\mu - \frac{cy}{a+(1-\beta y)x}\right), \\ &\leq \mu y\left(1 - \frac{cy}{\mu(a+x_{max})}\right), \\ &= \mu y\left(1 - \frac{cy}{\mu(a+\frac{r-r_0}{r_1})}\right). \end{aligned}$$

Hence, the result follows. ∎

Theorem 3.2.2. *Under the following inequality:*

$$r > (1+ky_{max})(r_0 + \frac{\alpha y_{max}}{a}),$$

system (3.3) is uniformly persistent.

Proof.

$$\begin{aligned} \frac{dx}{dt} &= \frac{rx}{(1+ky)} - r_0x - r_1x^2 - \frac{\alpha(1-\beta y)xy}{a+(1-\beta y)x}, \\ \frac{dx}{dt} &\geq x\left[\frac{r}{(1+ky_{max})} - r_0 - r_1x - \frac{\alpha(1-\beta y_{max})y_{max}}{a}\right], \\ &\geq x\left[\frac{r}{(1+ky_{max})} - r_0 - r_1x - \frac{\alpha y_{max}}{a}\right], \\ &= x\left[\left(\frac{r}{(1+ky_{max})} - r_0 - \frac{\alpha y_{max}}{a}\right) - r_1x\right]. \end{aligned}$$

$$\implies \lim_{t\to\infty}\inf x(t) \geq \frac{1}{r_1}\left(\frac{r}{(1+ky_{max})} - r_0 - \left(\frac{\alpha y_{max}}{a}\right)\right) =: m^*.$$

Now,

$$\frac{dy}{dt} = y\left[\mu - \frac{cy}{a+(1-\beta y)x}\right],$$
$$\frac{dy}{dt} \geq y[\mu - \frac{c}{a}y].$$

Therefore,

$$\lim_{t\to\infty}\inf y(t) \geq \frac{\mu a}{c}.$$

Using the results of Theorem 3.2.1, we note that

$$0 < m^* \leq \liminf_{t\to\infty} x(t) \leq \limsup_{t\to\infty} x(t) \leq x_{max},$$
$$0 < \frac{\mu a}{c} \leq \liminf_{t\to\infty} y(t) \leq \limsup_{t\to\infty} y(t) \leq y_{max}.$$

This implies that system (3.3) is uniformly persistent. ∎

3.2.2 Equilibrium analysis

System (3.3) has four non-negative equilibria:

1. The extinction equilibrium $E_0 = (0,\ 0)$, which is always feasible.
2. The predator-free equilibrium $E_1 = \left(\frac{r-r_0}{r_1}, 0\right)$ exists if $r - r_0 > 0$.
3. The prey-free equilibrium is given by $E_2 = \left(0, \frac{\mu a}{c}\right)$, which always exists.
4. We can get interior equilibrium of (3.3) as solutions of the following algebraic equations

$$\begin{aligned} \psi_1(x,y) &:= \frac{r}{1+ky} - r_0 - r_1 x - \frac{\alpha(1-\beta y)y}{a+(1-\beta y)x} = 0, \\ \psi_2(x,y) &:= \mu - \frac{cy}{a+(1-\beta y)x} = 0. \end{aligned} \tag{3.4}$$

Solving for x from the second equation of (3.4), we get:

$$x = \frac{cy-\mu a}{\mu(1-\beta y)}, \tag{3.5}$$

Now, $\psi_1(x,y)=0$ yields the following cubic polynomial in y:

$$\gamma_0 y^3+\gamma_1 y^2+\gamma_2 y+\gamma_3=0, \tag{3.6}$$

where

$$\begin{aligned}
\gamma_0 &= \alpha k\mu^2\beta^2\ (>0),\\
\gamma_1 &= r_1kc^2+\alpha\mu^2\beta(\beta-2k)-cr_0\mu k\beta,\\
\gamma_2 &= cr\mu\beta+cr_0\mu(k-\beta)+r_1c(c-a\mu k)-\alpha\mu^2(2\beta-k),\\
\gamma_3 &= \mu[cr_0+\alpha\mu-cr-cr_1a].
\end{aligned}$$

Now, the sign of the coefficients $\gamma_i's$ for $i=1,2,3$ will decide whether the proposed system (3.3) will have no, unique, two or three positive equilibria.

The maximum number of coexistence equilibria is then determined using the Descartes' rule of sign, as stated below.

Theorem 3.2.3. **(a)** *Under the following condition:*

$$\frac{rc+r_1ac-\alpha\mu}{c}<r_0<\min\left\{\frac{1}{c\beta}\left(\frac{r_1kc^2+\alpha\mu^2\beta^2}{k\mu}-2\alpha\mu\beta\right),\ \frac{1}{c\mu(\beta-k)}\left(cr\mu\beta+r_1c^2-r_1ac\mu k-2\alpha\mu^2\beta+\alpha k\mu^2\right)\right\},$$

there exists no coexistence equilibrium.

(b) *Under any of the following two conditions:*

$$\begin{aligned}
&(i)\, r_0<\min\{\frac{rc+r_1ac-\alpha\mu}{c},\frac{1}{c\beta}\left(\frac{r_1kc^2+\alpha\mu^2\beta^2}{k\mu}-2\alpha\mu\beta\right)\},\\
&(ii)\,\frac{1}{c\mu(\beta-k)}\left(cr\mu\beta+r_1c^2-r_1ac\mu k-2\alpha\mu^2\beta+\alpha k\mu^2\right)<r_0<\frac{rc+r_1ac-\alpha\mu}{c},
\end{aligned}$$

there exists a unique coexistence equilibrium.

(c) *Under any of the following two conditions:*

$$\begin{aligned}
&(i) r_0>\max\left\{\frac{1}{c\beta}\left(\frac{r_1kc^2+\alpha\mu^2\beta^2}{k\mu}-2\alpha\mu\beta\right),\frac{rc+r_1ac-\alpha\mu}{c}\right\},\\
&(ii) r_0>\max\left\{\frac{1}{c\mu(\beta-k)}\left(cr\mu\beta+r_1c^2-r_1ac\mu k-2\alpha\mu^2\beta+\alpha k\mu^2\right),\frac{rc+r_1ac-\alpha\mu}{c}\right\},
\end{aligned}$$

there exists at most two coexistence equilibria.

(d) *Under the following condition:*

$$\frac{1}{c\beta}\left(\frac{r_1kc^2+\alpha\mu^2\beta^2}{k\mu}-2\alpha\mu\beta\right)<r_0<\min\left\{\frac{1}{c\mu(\beta-k)}\times\left(cr\mu\beta+r_1c^2-r_1ac\mu k-2\alpha\mu^2\beta+\alpha k\mu^2\right),\frac{rc+r_1ac-\alpha\mu}{c}\right\},$$

there exists at most three interior equilibria.

The existence region plot for each interior equilibria is shown in Fig. 3.1. The blue colour denotes the absence of an interior equilibrium. There is a unique interior equilibrium in the green region, while there are two interior equilibria in the yellow region.

The number of interior equilibria for different values of parameter a is depicted in Fig. 3.2 by fixing other parameter values. For $a = 0.23$, there is no interior equilibrium, for $a = 1$, there is a unique interior equilibrium, and the system has two interior equilibria for $a = 0.53$.

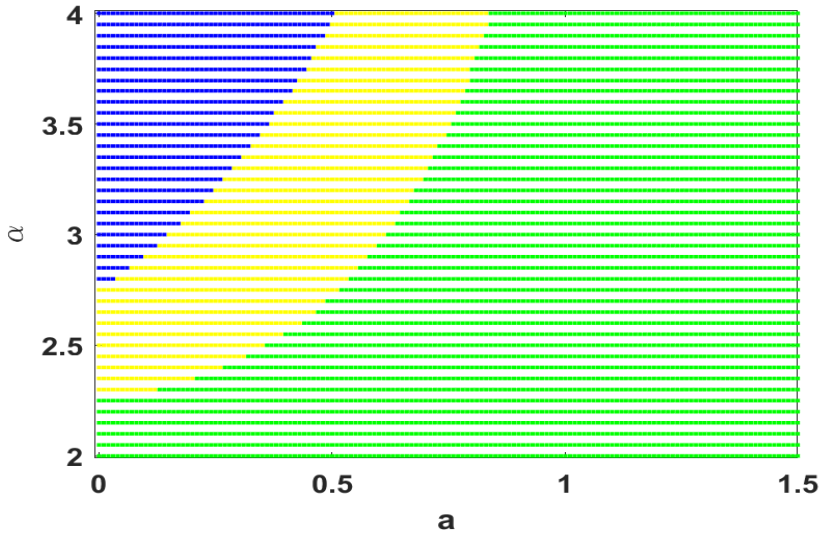

Fig. 3.1: Existence region for all the positive equilibria in $a-\alpha$ parameter plane. Blue indicates that no interior equilibrium occurs, green indicates that a unique interior equilibrium exists, and yellow indicates that two interior equilibria exist. Remaining parameters are considered as $r = 3$, $r_0 = 0.5$, $r_1 = 0.2$, $k = 0.5$, $\beta = 0.7$, $\mu = 1$, $c = 0.9$.

3.2.2.1 Local stability analysis

Next, the following results give us an insight into the system's dynamics around the corresponding equilibria.

Theorem 3.2.4. *The extinction equilibrium E_0 is a saddle point if $r - r_0 < 0$ and a source if $r - r_0 > 0$.*

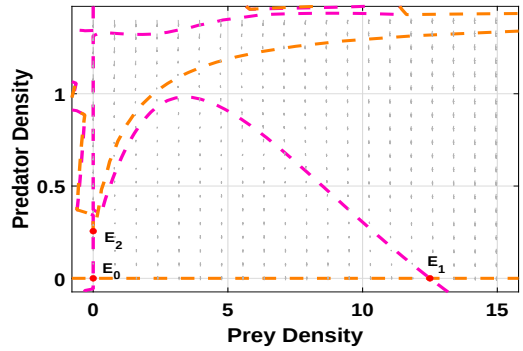

(a) No interior equilibrium for $a = 0.23$.

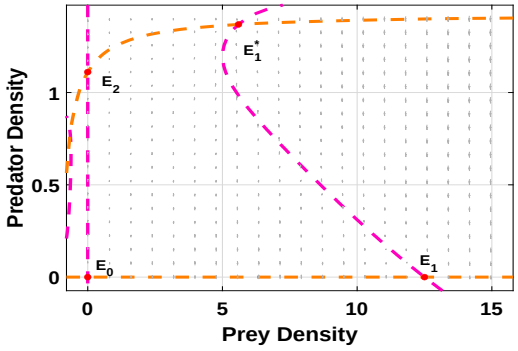

(b) Unique interior equilibrium for $a = 1$.

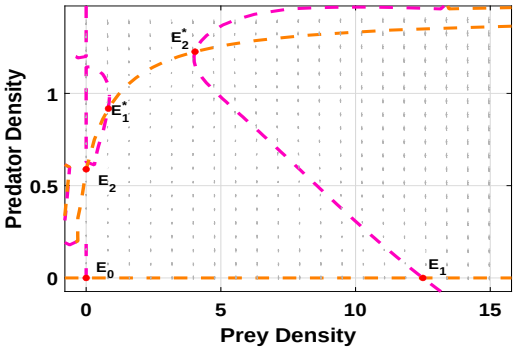

(c) Two interior equilibria for $a = 0.53$.

Fig. 3.2: Number of positive equilibria for system (3.3) with varying a. The remaining parameters take the values as $r = 3$, $r_0 = 0.5$, $r_1 = 0.2$, $k = 0.5$, $\alpha = 3.5$, $\beta = 0.7$, $\mu = 1$, $c = 0.9$.

Proof. At $E_0(0,0)$, eigenvalues are $\lambda_1 = r - r_0$ and $\lambda_2 = \mu\ (> 0)$. The behavior of the extinction equilibrium depends on the sign of $r - r_0$. Thus E_0 is saddle point if $r - r_0 < 0$ and a source if $r - r_0 > 0$. ∎

Theorem 3.2.5. *The predator-free equilibrium* $E_1 = \left(\frac{r-r_0}{r_1}, 0\right)$ *is always a saddle point, whenever it exists.*

Proof. At the equilibrium E_1, the eigenvalues are $\lambda_1 = -(r - r_0)(< 0)$ and $\lambda_2 = \mu(> 0)$. ∎

Theorem 3.2.6. *The prey-free equilibrium* E_2 *is locally asymptotically stable if* $\frac{rc}{c+k\mu a} - r_0 - \frac{\alpha\mu(c-\beta\mu a)}{c^2} < 0$.

Proof. At the axial equilibrium E_2, the eigenvalues are $\lambda_1 = \frac{rc}{c+k\mu a} - r_0 - \frac{\alpha\mu(c-\beta\mu a)}{c^2}$ and $\lambda_2 = -\mu(< 0)$. Thus, E_2 is locally asymptotically stable if $\frac{rc}{c+k\mu a} - r_0 - \frac{\alpha\mu(c-\beta\mu a)}{c^2} < 0$. ∎

Theorem 3.2.7. *The interior equilibrium $E^*(x^*,y^*)$, whenever it exists, is locally asymptotically stable if the following inequalities hold:*

$$\left(r_1x^* - \frac{\alpha(1-\beta y^*)^2x^*y^*}{(a+(1-\beta y^*)x^*)^2} + \frac{cy^*(a+x^*)}{(a+(1-\beta y^*)x^*)^2}\right) > 0, \quad \textit{and}$$
$$\left[\left(r_1x^* - \frac{\alpha(1-\beta y^*)^2x^*y^*}{(a+(1-\beta y^*)x^*)^2}\right)\left(\frac{cy^*(a+x^*)}{(a+(1-\beta y^*)x^*)^2}\right) + \left(\frac{rkx^*}{(1+ky^*)^2} + \frac{\alpha x^*[a(1-2\beta y^*)+x^*(1-\beta y^*)^2]}{(a+(1-\beta y^*)x^*)^2}\right)\left(\frac{cy^{*2}(1-\beta y^*)}{(a+(1-\beta y^*)x^*)^2}\right)\right] > 0.$$

Proof. The Jacobian matrix at $E^*(x^*,y^*)$ is given by

$$J_{E^*} = \begin{bmatrix} -r_1x^* + \frac{\alpha(1-\beta y^*)^2x^*y^*}{(a+(1-\beta y^*)x^*)^2} & \frac{-rkx^*}{(1+ky^*)^2} - \frac{\alpha x^*[a(1-2\beta y^*)+x^*(1-\beta y^*)^2]}{(a+(1-\beta y^*)x^*)^2} \\ \frac{cy^{*2}(1-\beta y^*)}{(a+(1-\beta y^*)x^*)^2} & \frac{-cy^*(a+x^*)}{(a+(1-\beta y^*)x^*)^2} \end{bmatrix}.$$

The characteristic equation is

$$\lambda^2 - trace(J_{E^*})\lambda + det(J_{E^*}) = 0,$$

where

$$trace(J_{E^*}) = -\left(r_1x^* - \frac{\alpha(1-\beta y^*)^2x^*y^*}{(a+(1-\beta y^*)x^*)^2} + \frac{cy^*(a+x^*)}{(a+(1-\beta y^*)x^*)^2}\right),$$
$$det(J_{E^*}) = \left(r_1x^* - \frac{\alpha(1-\beta y^*)^2x^*y^*}{(a+(1-\beta y^*)x^*)^2}\right)\left(\frac{cy^*(a+x^*)}{(a+(1-\beta y^*)x^*)^2}\right) + \left(\frac{rkx^*}{(1+ky^*)^2} + \frac{\alpha x^*[a(1-2\beta y^*)+x^*(1-\beta y^*)^2]}{(a+(1-\beta y^*)x^*)^2}\right)\left(\frac{cy^{*2}(1-\beta y^*)}{(a+(1-\beta y^*)x^*)^2}\right).$$

Under the conditions stated in the theorem, we note that $trace(J_{E^*}) < 0$ and $det(J_{E^*}) > 0$. Hence, all the eigenvalues of J_{E^*} will have negative real parts, and thus the theorem follows. ∎

Remark: The following gives us the sufficient condition for the local asymptotic stability of the interior equilibrium E^*:

$$r_1 > \frac{\alpha(1-\beta y^*)^2y^*}{(a+(1-\beta y^*)x^*)^2}.$$

3.2.2.2 Global stability analysis

Theorem 3.2.8. *Under the following inequality:*

$$\left[\frac{-rk}{(1+ky_{max})(1+ky^*)}+\frac{(ay^*(1+\alpha\beta)+(x^*(y^*-\alpha)(1-\beta y^*)-a\alpha)}{a(a+(1-\beta y^*)x^*)}\right]^2 < 4\left(r_1-\frac{\alpha y^*(1-\beta y^*)}{a(a+(1-\beta y^*)x^*}\right)\left(\frac{a+x^*}{a+x_{max}}\right),$$

the interior equilibrium point E^* is globally asymptotically stable.

Proof. Consider a positive definite function about $E^*(x^*,y^*)$ as

$$V_1(x,y)=\left(x-x^*-x^*ln\frac{x}{x^*}\right)+m\left(y-y^*-y^*ln\frac{y}{y^*}\right).$$

Choosing $m=\frac{a+(1-\beta y^*)x^*}{c}$, the time derivate of $V_1(x,y)$ along the solutions of the system (3.3) is given by

$$\dot{V_1} = -a_{11}(x-x^*)^2+a_{12}(x-x^*)(y-y^*)-a_{22}(y-y^*)^2,$$

where

$$a_{11}=\left[r_1-\frac{\alpha y^*(1-\beta y)(1-\beta y^*)}{(a+(1-\beta y)x)(a+(1-\beta y^*)x^*)}\right],$$
$$a_{12}=\left[\frac{-rk}{(1+ky)(1+ky^*)}+(\frac{ay^*(1+\beta(\alpha-y))+(x^*(y^*-\alpha))(1-\beta y^*)-a\alpha)(1-\beta y)}{(a+(1-\beta y)x)(a+(1-\beta y^*)x^*)})\right],$$
$$a_{22}=\left[\frac{(a+x^*)}{(a+(1-\beta y)x)}\right].$$

Applying Sylvester's criteria for $\dot{V_1}$ to be negative definite, we have

$$a_{11}>0, \quad a_{22}>0, \text{ and } a_{12}^2<4a_{11}a_{22}.$$

The above conditions are satisfied under the condition stated in Theorem 3.2.8. ∎

Figure 3.3 specifies the region (magenta) for the global asymptotic stability of the positive equilibrium in the $a-\alpha$ parameter plane. The remaining parameter values take the values as $r=3$, $r_0=0.5$, $r_1=0.2$, $k=0.5$, $\beta=0.7$, $\mu=1$, $c=0.9$.

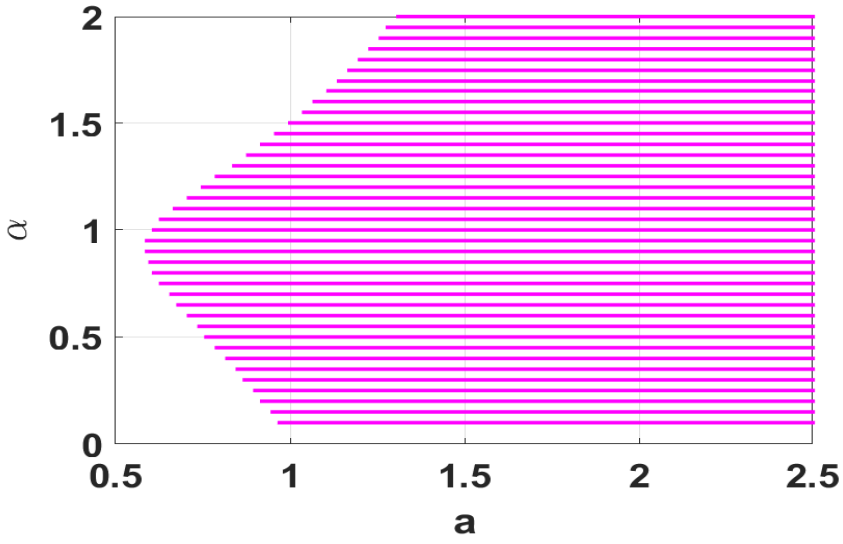

Fig. 3.3: Magenta colour signifies the global asymptotic stability region for the interior equilibrium (Theorem 3.2.8). The remaining parameters take the values as $r = 3$, $r_0 = 0.5$, $r_1 = 0.2$, $k = 0.5$, $\beta = 0.7$, $\mu = 1$, $c = 0.9$.

3.2.3 Bifurcation analysis

In this subsection, we shall explore the various bifurcations that system (3.3) exhibits. Bifurcation occurs when changing the value of a control parameter, causing a qualitative shift in the dynamics. Here, we have demonstrated that system (3.3) experiences Hopf and saddle-node bifurcation.

3.2.3.1 Hopf-bifurcation

Considering the fear parameter k as bifurcation parameter, we now examine the criteria for the occurence of Hopf-bifurcation around the positive equilibrium E^*.

At the equilibrium E^*, the Jacobian matrix yields the following characteristic equation:

$$\lambda^2 + A_1\lambda + A_2 = 0, \tag{3.7}$$

where

$$A_1 = -trace(J_{E^*}) \quad \text{and,} \quad A_2 = det(J_{E^*}).$$

Assuming the eigenvalue of the aforementioned equation to be of the form $\lambda_b(k) = \lambda_r(k) + i\lambda_{im}(k)$, we substitute $\lambda_b(k)$ in Eq. (3.7). Then, we obtain

$$\lambda_r^2 - \lambda_{im}^2 + A_1\lambda_r + A_2 = 0, \tag{3.8}$$

$$2\lambda_r\lambda_{im} + A_1\lambda_{im} = 0. \tag{3.9}$$

For the system to experience Hopf-bifuraction, we need $Re(\lambda_b(k)) = 0$ at the critical value $k = k_*$. Hence,

$$\begin{aligned} -\lambda_{im}^2 + A_2 &= 0, \quad \lambda_{im} \in \mathbb{R}, \\ \lambda_{im}A_1 &= 0, \quad \lambda_{im} \neq 0. \end{aligned}$$

Therefore,

$$A_2 > 0 \text{ and } A_1 = 0 \text{ at the critical value } k_*.$$

From $trace(J_{E^*}) = 0$, we get

$$k_* = \frac{1}{y^*}\left(\frac{r}{r_0 + 2r_1x^* - \mu - \frac{y^*(a(\alpha+2c)+2cx^*-\beta y^*(a\alpha+cx^*)}{(a+(1-\beta y^*)x^*)^2}} - 1\right).$$

Differentiating Eqs. (3.8) and (3.9) with respect to k and substituting $\lambda_r = 0$, we obtain

$$-2\lambda_{im}\frac{d\lambda_{im}}{dk} + A_1\frac{d\lambda_r}{dk} + \frac{dA_2}{dk} = 0, \tag{3.10}$$

$$2\lambda_{im}\frac{d\lambda_r}{dk} + \lambda_{im}\frac{dA_1}{dk} + A_1\frac{d\lambda_{im}}{dk} = 0. \tag{3.11}$$

On solving the above equations, we have

$$\left.\frac{d\lambda_r}{dk}\right|_{k=k_*} = -\frac{(A_1\frac{dA_2}{dk} + 2\lambda_{im}^2\frac{dA_1}{dk})}{A_1^2 + 4\lambda_{im}^2} \neq 0,$$

provided $A_1\frac{dA_2}{dk} + 2\lambda_{im}^2\frac{dA_1}{dk} \neq 0$.

Therefore, the system experiences Hopf-bifurcation around the positive equilibrium E^* if $A_2 > 0$ and $(A_1\frac{dA_2}{dk} + 2\lambda_{im}^2\frac{dA_1}{dk}) \neq 0$ at the critical value $k = k_*$. Thus, we can state the following theorem.

Theorem 3.2.9. *The necessary and sufficient condition for system (3.3) to experience Hopf-bifurcation around the interior E^* is that there exists $k = k_*$ such that*

1. $A_1(k_*) = 0$,
2. $\left.\frac{d\lambda_r}{dk}\right|_{k=k_*} \neq 0$.

3.2.3.2 Saddle-node bifurcation

Theorem 3.2.10. *If the following conditions hold true:*

$$\left(\alpha(1-\beta y^*)x^* - \frac{f_x}{g_x}cy^*\right) \neq 0,$$

and

$$\left[\left(f_{xx} - \frac{f_x}{f_y}(f_{xy}+f_{yx}) + \frac{f_x^2}{f_y^2}f_{yy}\right) - \frac{f_x}{g_x}\left(g_{xx} - \frac{f_x}{f_y}(g_{xy}+g_{yx}) + \frac{f_x^2}{f_y^2}g_{yy}\right)\right] \neq 0,$$

system (3.3) experiences a saddle-node bifurcation around the positive equilibrium as the half-saturation constant a crosses the critical value $a = a_s$.

Proof. At the positive equilibrium $E^*(x^*, y^*)$, the Jacobian matrix is

$$J_{E^*(x^*,y^*)} = \begin{bmatrix} -r_1x^* + \frac{\alpha(1-\beta y^*)^2x^*y^*}{(a+(1-\beta y^*)x^*)^2} & \frac{-rkx^*}{(1+ky^*)^2} - \frac{\alpha x^*[a(1-2\beta y)+x^*(1-\beta y^*)^2]}{(a+(1-\beta y^*)x^*)^2} \\ \frac{cy^{*2}(1-\beta y^*)}{(a+(1-\beta y^*)x^*)^2} & \frac{-cy^*(a+x^*)}{(a+(1-\beta y^*)x^*)^2} \end{bmatrix}.$$

At $a = a_s$, $det(J_{E^*}) = 0$.

Now, we can easily show that the above Jacobian matrix has a zero eigenvalue at $a = a_s$. Let $F = (f,g)^T$. Taking derivative of the given system (3.3) with respect to a, we obtain

$$F_a(x^*, y^*) = \begin{bmatrix} \frac{\alpha(1-\beta y^*)x^*y^*}{(a+(1-\beta y^*)x^*)^2} \\ \frac{c(y^*)^2}{(a+(1-\beta y^*)x^*)^2} \end{bmatrix},$$

$$A = DF(E^*(x^*, y^*), a_s) = \begin{bmatrix} f_x & f_y \\ g_x & g_y \end{bmatrix},$$

where

$$\begin{aligned} f_x &= -r_1x^* + \frac{\alpha(1-\beta y^*)^2x^*y^*}{(a_s+(1-\beta y^*)x^*)^2}, \\ f_y &= \frac{-rkx^*}{(1+ky^*)^2} - \frac{\alpha x^*[a_s(1-2\beta y)+x^*(1-\beta y^*)^2]}{(a_s+(1-\beta y^*)x^*)^2}, \\ g_x &= \frac{cy^{*2}(1-\beta y^*)}{(a_s+(1-\beta y^*)x^*)^2}, \\ g_y &= \frac{-cy^*(a_S+x^*)}{(a_s+(1-\beta y^*)x^*)^2}. \end{aligned}$$

$$D^2F(E(\bar{x},\bar{y}), a_s) = \begin{bmatrix} f_{xx} & f_{xy} & f_{yx} & f_{yy} \\ g_{xx} & g_{xy} & g_{yx} & g_{yy} \end{bmatrix},$$

where

$$
\begin{aligned}
f_{xx} &= -r_1 + \frac{\alpha(1-\beta y)^2 y(a-(1-\beta y)x)}{(a+(1-\beta y^*)x^*)^3},\\
f_{xy} &= \frac{-x\alpha(1-\beta y)[a(1-3\beta y)+x(1-\beta y)^2]}{(a+(1-\beta y^*)x^*)^3},\\
f_{yx} &= \frac{-kr}{(1+ky)^2} + \frac{-a(a+x)\alpha+a}{den},\\
f_{yy} &= x\left(\frac{2k^2 r}{(1+ky)^3} + \frac{2a(a+x)\alpha\beta}{(a+(1-\beta y)x)^3}\right),\\
g_{xx} &= \frac{2cy^2(1-\beta y)^2}{(a+(1-\beta y)x)^3},\\
g_{xy} &= \frac{cy[2(a+x)-3(a+x)\beta y+xy^2\beta^2]}{(a+(1-\beta y)x)^3},\\
g_{yx} &= \frac{cy(a+x-(2a+x)\beta y)}{(a+(1-\beta y)x)^3},\\
g_{yy} &= \frac{-c(a+x)(a+x+x\beta y)}{(a+(1-\beta y)x)^3}.
\end{aligned}
$$

Now, $v = \begin{bmatrix} 1 & \frac{-f_x}{f_y} \end{bmatrix}^T$ and $w = \begin{bmatrix} 1 & \frac{-f_x}{g_x} \end{bmatrix}^T$ are the eigenvectors corresponding to the zero eigenvalue of the matrix $A = DF(E^*(x^*,y^*),a_s)$ and $A^T = [DF(E^*(x^*,y^*),a_s)]^T$, respectively.

Applying Sotomayor's Theorem [126] gives us

$$
w^T F_a\Big(E^*(x^*,y^*),a_s\Big) = \frac{y^*}{(a_s+(1-\beta y^*)x^*)^2}\left[\alpha(1-\beta y^*)x^* - \frac{f_x}{g_x}cy^*\right] \neq 0,
$$

and

$$
w^T\left[\Big(D^2F(E(\bar{x},\bar{y}),a_s)\Big)(v,v)\right] = \left[\left(f_{xx} - \frac{f_x}{f_y}(f_{xy}+f_{yx}) + \frac{f_x^2}{f_y^2}f_{yy}\right) - \frac{f_x}{g_x}\left(g_{xx} - \frac{f_x}{f_y}(g_{xy}+g_{yx}) + \frac{f_x^2}{f_y^2}g_{yy}\right)\right] \neq 0.
$$

Hence, the system experiences saddle-node bifurcation under the following conditions:

$$
\alpha(1-\beta y^*)x^* - \frac{f_x}{g_x}cy^* \neq 0,
$$

and

$$
\left[\left(f_{xx} - \frac{f_x}{f_y}(f_{xy}+f_{yx}) + \frac{f_x^2}{f_y^2}f_{yy}\right) - \frac{f_x}{g_x}\left(g_{xx} - \frac{f_x}{f_y}(g_{xy}+g_{yx}) + \frac{f_x^2}{f_y^2}g_{yy}\right)\right] \neq 0.
$$

■

3.3 Dynamics of delayed temporal model

In this part, we shall look into the dynamics of the non-spatial delayed system (3.1).

3.3.1 Local stability and Hopf-bifurcation analysis

Considering $x = x^* + X$, $y = y^* + Y$, we linearize system (3.1) near the interior equilibrium $E^*(x^*, y^*)$. The corresponding linear system is given by

$$\frac{dV}{dt} = Z_1 V(t) + Z_2 V(t-\tau),$$

where

$$Z_1 = \left(\frac{\partial F}{\partial U(t)}\right)_{E^*}, \quad Z_2 = \left(\frac{\partial F}{\partial U(t-\tau)}\right)_{E^*}, \quad \textit{and} \quad V(t) = (X(t), Y(t))^T.$$

Now, calculating the Jacobian matrix for system (3.1), we get

$$J_{E^*} = Z_1 + Z_2 e^{-\lambda\tau},$$

$$J_{E^*} = \begin{bmatrix} a_1 & a_2 + a_5 e^{-\lambda\tau} \\ a_3 & a_4 \end{bmatrix},$$

where

$$\begin{aligned}
a_1 &= \frac{r}{1+ky^*} - r_0 - 2r_1 x^* - \frac{\alpha a(1-\beta y^*)y^*}{(a+(1-\beta y^*)x^*)^2}, \\
a_2 &= -\frac{\alpha x^*[a(1-2\beta y^*) + x^*(1-\beta y^*)^2]}{(a+(1-\beta y^*)x^*)^2}, \\
a_3 &= \frac{cy^{*2}(1-\beta y^*)}{(a+(1-\beta y^*)x^*)^2}, \\
a_4 &= \mu - \frac{cy^*(2a+2x^*-\beta x^* y^*)}{(a+(1-\beta y^*)x^*)^2}, \\
a_5 &= \frac{-rkx^*}{(1+ky^*)^2}.
\end{aligned}$$

Above Jacobian matrix yields the following characteristic equation:

$$\lambda^2 + p_1\lambda + (p_2 + p_3 e^{-\lambda\tau}) = 0, \tag{3.12}$$

$$\text{where} \quad p_1 = -(a_1 + a_4), \quad p_2 = (a_1 a_4 - a_2 a_3), \quad p_3 = -a_3 a_5.$$

Case (1): Characteristic equation for $\tau = 0$ is

$$\lambda^2 + p_1\lambda + (p_2 + p_3) = 0. \tag{3.13}$$

Remark: The above characteristic equation is the same as for system (3.3).

The characteristic equation (3.13) will have all the roots with negative real parts if and only if **(H1):** $p_1 > 0$, $p_2 + p_3 > 0$.

Case (2): $\tau > 0$. Assuming $i\omega(\omega > 0)$ to be a root of Eq. (3.12), we obtain

$$\begin{aligned} -\omega^2 + p_1 i\omega + (p_2 + p_3 e^{-i\omega\tau}) &= 0, \\ -\omega^2 + p_1 i\omega + p_2 + p_3(cos(\omega\tau) - isin(\omega\tau)) &= 0. \end{aligned}$$

Comparing real and imaginary parts,

$$\begin{aligned} p_3 cos(\omega\tau) &= \omega^2 - p_2, \\ p_3 sin(\omega\tau) &= p_1\omega, \end{aligned} \tag{3.14}$$

leading to

$$\begin{aligned} & z^2 + p'z + q' = 0, \\ \text{where} \quad & p' = p_1^2 - 2p_2, \quad q' = p_2^2 - p_3^2, \quad z = \omega^2. \end{aligned} \tag{3.15}$$

Let $\phi(z) = z^2 + p'z + q'$.

(H2): $p' > 0$, $q' > 0$.

Remark:

- Equation (3.15) has no positive roots if (H2) holds. Therefore, all the roots of Eq. (3.12) have negative real parts and thus, E^* is asymptotically stable for $\tau > 0$ if (H1) and (H2) hold.
- $E^*(x^*, y^*)$ is unstable for all $\tau > 0$ if any one of (H1) or (H2) does not hold true.

(H3): $q' < 0$.

Equation (3.15) has a unique positive root ω_0^2 if (H3) holds. Substituting in Eq. (3.14), we get:

$$p_3 cos(\omega_0 \tau) = \omega_0^2 - p_2,$$
$$p_3 sin(\omega_0 \tau) = p_1 \omega_0,$$

which gives us

$$\tau_i = \frac{1}{\omega_0}\left[cos^{-1}\left(\frac{\omega_0^2 - p_2}{p_3}\right)\right] + \frac{2i\pi}{\omega_0} \quad ; \quad i = 0, 1, 2, ... \tag{3.16}$$

(H4): $p' < 0$, $q' > 0$ and $p'^2 > 4q'$.

If (H4) holds true, then Eq. (3.15) has two distinct positive roots ω_1^2 and ω_2^2. From (3.14), we get

$$\tau_j^{1,2} = \frac{1}{\omega_{1,2}}\left[cos^{-1}\left(\frac{\omega_{1,2}^2 - p_2}{p_3}\right)\right] + \frac{2j\pi}{\omega_{1,2}} \quad ; \quad j = 0, 1, 2, ... \tag{3.17}$$

Let us assume that Eq. (3.12) has a root $\lambda(\tau)$ such that Re($\lambda(\tau)$)=0. Now from Eq. (3.12), we have

$$\left(\frac{d\lambda}{d\tau}\right)^{-1} = \frac{(2\lambda + p_1)e^{\lambda\tau}}{p_3\lambda} - \frac{\tau}{\lambda},$$
$$\left[\frac{d\lambda}{d\tau}\right]^{-1}_{\lambda=i\omega_0} = \frac{(2i\omega_0 + p_1)(cos(\omega_o\tau) + isin(\omega_o\tau))}{p_3 i\omega_0} - \frac{\tau}{i\omega_0},$$
$$Re\left[\frac{d\lambda}{d\tau}\right]^{-1}_{\lambda=i\omega_0} = \frac{2\omega_0 cos(\omega_o\tau) + p_1 sin(\omega_o\tau)}{p_3\omega_0}.$$

We know that

$$cos(\omega_o\tau) = \frac{\omega_0^2 - p_2}{p_3}, \quad sin(\omega_o\tau) = \frac{p_1\omega_0}{p_3}.$$

Therefore, after simplifying it a little, we get

$$Re\left[\frac{d\lambda}{d\tau}\right]^{-1}_{\lambda=i\omega_0} = \frac{2(\omega_0^2 - p_2) + p_1^2}{p_3^2}.$$

However,

$$\text{sign}\left[\frac{d}{d\tau}Re(\lambda)\right]_{\lambda=i\omega_0} = \text{sign}\left[Re\left(\frac{d\lambda}{d\tau}\right)\right]_{\lambda=i\omega_0}.$$

(H5): $2(\omega_0^2 - p_2) + p_1^2 \neq 0$.

Hence, if (H5) holds true, then $\left[\frac{d}{d\tau}Re(\lambda)\right]_{\lambda=i\omega_0} \neq 0$.
Now, we can state the following result.

Theorem 3.3.1. *Assuming (H1), (H3) and (H5) hold true for system (3.1), then there exist a positive number τ_0 such that the interior equilibrium $E^*(x^*,y^*)$ is locally asymptotically stable for $\tau < \tau_0$ and unstable for $\tau > \tau_0$. Also, system (3.1) experiences Hopf-bifurcation at the interior equilibrium $E^*(x^*,y^*)$ for $\tau = \tau_0$.*

3.3.2 Direction and stability of Hopf-bifurcation

This subsection presents a complete analysis of the characteristics of bifurcated periodic solutions using the center manifold theorem and normal form theory.

Let $\tau = \tau_0 + \mu, \mu \in \mathbb{R}$ such that Hopf-bifurcation occurs at $\mu = 0$ and $C = C([-1,0],\mathbb{R}^2)$ denotes the space of continuous real valued function. Using the transformation

$$\bar{x_1}(t) = x(t) - x^*, \quad \bar{y_1}(t) = y(t) - y^*$$

and still denoting $\bar{x_1}(t), \bar{y_1}(t)$ by $x(t), y(t)$, our delayed system (3.1) is reduced to functional differential equation in C as

$$\frac{dX}{dt} = L_\mu X_t + f(\mu, X_t), \tag{3.18}$$

where

$$\begin{aligned} X(t) &= [x(t), y(t)]^T \in \mathbb{R}^2, \\ L_\mu : C \to \mathbb{R}^2, &\quad f : \mathbb{R} \times C \to \mathbb{R}^2, \\ X_t(\theta) &= X(t+\theta), \quad \theta \in [-1,0], \end{aligned}$$

$$L_\mu = (\tau_0 + \mu)[Z_1\phi(0) + Z_2\phi(-1)], \tag{3.19}$$

$$L_\mu = (\tau_0 + \mu)\begin{bmatrix} a_1 & a_2 \\ a_3 & a_4 \end{bmatrix}\begin{bmatrix} \phi_1(0) \\ \phi_2(0) \end{bmatrix} + (\tau_0 + \mu)\begin{bmatrix} 0 & a_5 \\ 0 & 0 \end{bmatrix}\begin{bmatrix} \phi_1(-1) \\ \phi_2(-1) \end{bmatrix}, \tag{3.20}$$

$$f(\mu,\phi) = (\tau_0 + \mu)\begin{bmatrix} r_1\phi_1(0)^2 - \frac{\alpha(1-\beta\phi_2(0))\phi_1(0)\phi_2(0)}{a+(1-\beta\phi_2(0))\phi_1(0)} \\ \frac{-c\phi_2(0)^2}{a+(1-\beta\phi_2(0))\phi_1(0)} \end{bmatrix}.$$

By Reisz representation theorem, there exists a matrix whose components are bounded variation function $\eta(\theta,\mu)$ in [-1,0] such that

$$L_\mu = \int_{-1}^{0} d\eta(\theta,\mu)\phi(\theta), \quad \phi \in C([-1,0],\mathbb{R}^2). \tag{3.21}$$

In fact, we may choose

$$\eta(\theta,\mu) = (\tau_0+\mu)[Z_1\delta(\theta) - Z_2\delta(\theta+1)], \tag{3.22}$$

where δ represents Dirac-delta function defined by

$$\delta(\theta) = \begin{cases} 0 & : \theta = 0, \\ 1 & : \theta \neq 0. \end{cases} \tag{3.23}$$

For $\phi \in C^1([-1,0],\mathbb{R}^2)$, we define

$$A(\mu)\phi(\theta) = \begin{cases} \frac{d\phi(\theta)}{d\theta} & : -1 \leq \theta < 0, \\ \int_{-1}^{0} d\eta(\xi,\mu)\phi(\xi) & : \theta = 0. \end{cases}$$

$$\text{and,} \quad R(\mu)\theta = \begin{cases} 0 & : \theta \in [-1,0), \\ f(\mu,\phi) & : \theta = 0. \end{cases}$$

Then, system (3.1) is equivalent to the following operation differential equation of the form:

$$\dot{X(t)} = A(\mu)X_t + R(\mu)X_t, \tag{3.24}$$

where

$$X(t) = X(t+\theta), \qquad \theta \in [-1,0].$$

The adjoint operator A^* of A is defined by

$$A^*\psi(s) = \begin{cases} \frac{-d\psi(s)}{ds} & : s \in (0,1], \\ \int_{-1}^{0} \psi(-\xi)d\eta^T(\xi,0) & : s = 0, \end{cases}$$

associated with a bilinear form

$$< \psi(s), \phi(s) >= \bar{\psi}(0)\phi(0) - \int_{-1}^{0}\int_{\xi=0}^{\theta} \bar{\psi}(\zeta-\theta)d\eta(\theta)\phi(\xi)d\zeta,$$

where $\eta(\theta) = \eta(\theta,0)$, $A = A(0)$ and A^* are adjoint operators.

Following the above discussion, we can easily get $\pm i\omega_0\tau_0$ as the eigenvalues of $A(0)$ and hence, the eigenvalues of A^*.

Moreover, it can be easily verified that $A(0)$ and A^* has following eigenvectors corresponding to the eigenvalues $i\omega_0\tau_0$ and $-i\omega_0\tau_0$, respectively.

$$q(\theta) = (1,\sigma_1)^T e^{i\omega_0\tau_0\theta} \quad (\theta \in [-1,0]),$$
$$q^*(s) = M(1,\sigma_1^*)e^{i\omega_0\tau_0 s} \quad (s \in [0,1]),$$

where

$$\sigma_1 = \frac{i\omega_0 - a_1}{a_2 + a_5 e_{i\omega_0\tau_0}},$$
$$\sigma_1^* = \frac{-(i\omega_0 + a_1)}{a_3}.$$

Now,

$$< q^*(\theta), q(\theta) >= 1, \quad < q^*(s), \bar{q}(\theta) >= 1,$$
$$\bar{M} = \frac{1}{1 + \sigma\sigma^* - \tau_0 a_5 \sigma_1 e^{-i\omega_0\tau_0}}.$$

Following the computational process explained in [155] for obtaining Hopf-bifurcation properties, we get the following:

$$g_{20} = 2\left(\frac{-\alpha\sigma_1}{a} - \frac{cM\bar{\sigma_1}^*\sigma_1^2\tau_0}{a} - Mr_1\tau_0\right),$$
$$g_{11} = \left(\frac{-\alpha\bar{\sigma_1}}{a} - \frac{\alpha\sigma_1}{a} - 2Mr_1\tau_0 - \frac{2cM\bar{\sigma_1}\bar{\sigma_1}^*\sigma_1\tau_0}{a}\right),$$
$$g_{02} = 2\left(\frac{-\alpha\bar{\sigma_1}}{a} - \frac{cM\bar{\sigma_1}^2\bar{\sigma_1}^*\tau_0}{a} - Mr_1\tau_0\right),$$
$$g_{21} = \frac{\alpha\bar{\sigma_1}}{a} + \frac{2\alpha\sigma_1}{a^2} + \frac{2\alpha\beta\bar{\sigma_1}\sigma_1}{a} + \frac{\alpha\beta\sigma_1^2}{a} + \frac{2cM\bar{\sigma_1}\bar{\sigma_1}^*\sigma_1\tau_0}{a^2} + \frac{cM\bar{\sigma_1}^*\sigma_1^2\tau_0}{a^2} - \frac{\alpha\sigma_1 W_{11}^{(0)}(0)}{a}$$
$$- 2Mr_1\tau_0 W_{11}^{(1)}(0) - \frac{\alpha W_{11}^{(2)}(0)}{a} - \frac{2cM\bar{\sigma_1}^*\sigma_1\tau_0 W_{11}^{(2)}(0)}{a} - \frac{\alpha\sigma_1\bar{W_{20}^{(1)}}(0)}{2a} - Mr_1\tau_0 W_{20}^{(2)}(0)$$
$$- \frac{\alpha W_{20}^{(2)}(0)}{2a} - \frac{cM\bar{\sigma_1}\bar{\sigma_1}^*\tau_0 W_{20}^{(2)}(0)}{a},$$

where

$$W_{20}(\theta) = \frac{ig_{20}}{\omega_0\tau_0}q(0)e^{i\omega_0\tau_0\theta} + \frac{i\bar{g_{02}}}{3\omega_0\tau_0}q(\bar{0})e^{-i\omega_0\tau_0\theta} + \hat{E_1}e^{2i\omega_0\tau_0\theta},$$
$$W_{11}(\theta) = \frac{-ig_{11}}{\omega_0\tau_0}q(0)e^{i\omega_0\tau_0\theta} + \frac{i\bar{g_{11}}}{\omega_0\tau_0}q(\bar{0})e^{-i\omega_0\tau_0\theta} + \hat{E_2},$$

where $\hat{E_1} = (\hat{E_1}^{(1)}, \hat{E_1}^{(2)}) \in \mathbb{R}^2$ and $\hat{E_2} = (\hat{E_2}^{(1)}, \hat{E_2}^{(2)}) \in \mathbb{R}^2$ are constant vectors, calculated as

$$\hat{E_1} = \begin{bmatrix} 2i\omega_0 - a_1 & -a_2 - a_5e^{-2i\omega_0\tau_0} \\ -a_3 & 2i\omega_0\tau_0 - a_4 \end{bmatrix}^{-1} \begin{bmatrix} r_1 + \frac{\alpha(1-\beta\sigma_1)\sigma_1}{a} \\ \frac{c\sigma_1^2}{a} \end{bmatrix},$$
$$\hat{E_2} = \begin{bmatrix} -a_1 & -a_2 - a_5 \\ -a_3 & -a_4 \end{bmatrix}^{-1} \begin{bmatrix} r_1 + \frac{\alpha Re(\sigma_1) - \alpha\beta|\sigma_1|^2}{a} \\ \frac{c|\sigma_1|^2}{a} \end{bmatrix}.$$

Eventually, g_{ij} can be written in terms of parameters and delay parameter τ_0. Hence, standard results may be computed as

$$c_1(0) = \frac{i}{2\omega_0\tau_0}\left(g_{20}g_{11} - 2|g_{11}|^2 - \frac{|g_{02}|^2}{3}\right) + \frac{g_{21}}{2},$$
$$\mu_2 = -\frac{Re(c_1(0))}{Re(\lambda(\tau_0))},$$
$$\beta_2 = 2Re(c_1(0)),$$
$$T_2 = -\frac{Im(c_1(0)) + \mu_2 Im(\lambda(\tau_0))}{\omega_0\tau_0}.$$

The preceding terms describe a bifurcating periodic solution in the center manifold theorem for system (3.1) at $\tau = \tau_0$, that is given in the next theorem.

Theorem 3.3.2. *1. The direction of Hopf-bifurcation depends on the sign of μ_2. Hopf-bifurcation is supercritical (subcritical) if $\mu_2 > 0 (< 0)$.*

2. The bifurcated periodic solutions are unstable (stable) if $\beta_2 > 0 (< 0)$.

3. If $T_2 > 0 (< 0)$, then the period increases (decreases).

3.4 Stability analysis of non-delayed spatiotemporal model

Here, we shall investigate the following model which is without delay:

$$\begin{aligned}\frac{\partial x}{\partial t} &= \left[\frac{r}{(1+ky)} - r_0 - r_1 x - \frac{(\alpha(1-\beta y)y)}{a+(1-\beta y)x}\right]x + D_1\nabla^2 x,\\ \frac{\partial y}{\partial t} &= \left[(\mu - \frac{cy}{a+(1-\beta y)x})\right]y + D_2\nabla^2 y.\end{aligned} \tag{3.25}$$

Taking the transformation

$$\begin{aligned}X &= x - x^*,\\ Y &= y - y^*,\end{aligned}$$

system (3.25) reduces to

$$\begin{aligned}\frac{\partial X}{\partial t} &= A_{11}X + A_{12}Y + D_1\left(\frac{\partial^2 X}{\partial u^2} + \frac{\partial^2 X}{\partial v^2}\right),\\ \frac{\partial Y}{\partial t} &= A_{21}X + A_{22}Y + D_2\left(\frac{\partial^2 Y}{\partial u^2} + \frac{\partial^2 Y}{\partial v^2}\right),\end{aligned}$$

where

$$\begin{aligned}A_{11} &= -r_1 x^* + \frac{\alpha(1-\beta y^*)^2 x^* y^*}{(a+(1-\beta y^*)x^*)^2},\\ A_{12} &= \frac{-rkx^*}{(1+ky^*)^2} - \frac{\alpha x^*[a(1-2\beta y) + x^*(1-\beta y^*)^2]}{(a+(1-\beta y^*)x^*)^2},\\ A_{21} &= \frac{cy^{*2}(1-\beta y^*)}{(a+(1-\beta y^*)x^*)^2},\\ A_{22} &= \frac{-cy^*(a+x^*)}{(a+(1-\beta y^*)x^*)^2}.\end{aligned}$$

We take into account the solution of the form

$$\begin{aligned}X &= Ae^{\lambda t}sin\left(\frac{n\pi}{M}u\right)cos\left(\frac{m\pi}{N}v\right),\\ Y &= Be^{\lambda t}sin\left(\frac{n\pi}{M}u\right)cos\left(\frac{m\pi}{N}v\right).\end{aligned}$$

From system (3.25), we have

$$\frac{\partial X}{\partial t} = A_{11}X + A_{12}Y + D_1\left[\left(\frac{n\pi}{M}\right)^2 + \left(\frac{m\pi}{N}\right)^2\right],$$
$$\frac{\partial Y}{\partial t} = A_{21}X + A_{22}Y + D_2\left[\left(\frac{n\pi}{M}\right)^2 + \left(\frac{m\pi}{N}\right)^2\right].$$

The Jacobian matrix for the above system is

$$M_{E^*} = \begin{bmatrix} A_{11} - D_1\left(\left(\frac{n\pi}{M}\right)^2 + \left(\frac{m\pi}{N}\right)^2\right) & A_{12} \\ A_{21} & A_{22} - D_2\left(\left(\frac{n\pi}{M}\right)^2 + \left(\frac{m\pi}{N}\right)^2\right) \end{bmatrix},$$

Now,

$$M_1' = -trace(M_{E^*}) = r_1x^* - \frac{\alpha(1-\beta y^*)^2x^*y^*}{(a+(1-\beta y^*)x^*)^2} + \frac{cy^*(a+x^*)}{(a+(1-\beta y^*)x^*)^2} + (D_1+D_2)\left[\left(\frac{n\pi}{M}\right)^2 + \left(\frac{m\pi}{N}\right)^2\right],$$

$$\begin{aligned} M_2' =& det(M_{E^*}) = \left(r_1x^* - \frac{\alpha(1-\beta y^*)^2x^*y^*}{(a+(1-\beta y^*)x^*)^2}\right)\left(\frac{cy^*(a+x^*)}{(a+(1-\beta y^*)x^*)^2}\right) \\ &+ \left(\frac{rkx^*}{(1+ky^*)^2} + \frac{\alpha x^*[a(1-2\beta y)+x^*(1-\beta y^*)^2]}{(a+(1-\beta y^*)x^*)^2}\right)\left(\frac{cy^{*2}(1-\beta y^*)}{(a+(1-\beta y^*)x^*)^2}\right) \\ &+ \left(\left(\frac{n\pi}{M}\right)^2 + \left(\frac{m\pi}{N}\right)^2\right)\left[D_1\left(\frac{cy^*(a+x^*)}{(a+(1-\beta y^*)x^*)^2}\right)\right. \\ &\left. + D_2\left(r_1x^* - \frac{\alpha(1-\beta y^*)^2x^*y^*}{(a+(1-\beta y^*)x^*)^2} + D_1\left(\left(\frac{n\pi}{M}\right)^2 + \left(\frac{m\pi}{N}\right)^2\right)\right)\right]. \end{aligned}$$

The characteristic equation of M_{E^*} evaluated at E^* is

$$\lambda^2 + M_1'\lambda + M_2' = 0. \tag{3.26}$$

The equilibrium E^* of model (3.25) is locally asymptotically stable if and only if

$$M_1' > 0, \;\; M_2' > 0,$$

i.e., if

$$r_1x^* - \frac{\alpha(1-\beta y^*)^2x^*y^*}{(a+(1-\beta y^*)x^*)^2} + \frac{cy^*(a+x^*)}{(a+(1-\beta y^*)x^*)^2} + (D_1+D_2)\left[\left(\frac{n\pi}{M}\right)^2 + \left(\frac{m\pi}{N}\right)^2\right] > 0,$$

and

$$\begin{aligned}
&\left(r_1x^* - \frac{\alpha(1-\beta y^*)^2x^*y^*}{(a+(1-\beta y^*)x^*)^2}\right)\left(\frac{-cy^*(a+x^*)}{(a+(1-\beta y^*)x^*)^2}\right)\\
&+\left(\frac{rkx^*}{(1+ky^*)^2} + \frac{\alpha x^*[a(1-2\beta y)+x^*(1-\beta y^*)^2]}{(a+(1-\beta y^*)x^*)^2}\right)\left(\frac{cy^{*2}(1-\beta y^*)}{(a+(1-\beta y^*)x^*)^2}\right)\\
&+\left(\left(\frac{n\pi}{M}\right)^2 + \left(\frac{m\pi}{N}\right)^2\right)\left[D_1\left(\frac{cy^*(a+x^*)}{(a+(1-\beta y^*)x^*)^2}\right)\right.\\
&\left.+D_2\left(r_1x^* - \frac{\alpha(1-\beta y^*)^2x^*y^*}{(a+(1-\beta y^*)x^*)^2} + D_1\left(\left(\frac{n\pi}{M}\right)^2 + \left(\frac{m\pi}{N}\right)^2\right)\right)\right] > 0.
\end{aligned}$$

Remark: In a temporal system, the interior equilibrium is unstable if either $trace(J_{E^*}) > 0$ or $det(J_{E^*}) < 0$.

- **Case-I:** If $trace(J_{E^*}) > 0$, then the corresponding equilibrium in spatiotemporal system can be made stable by gradually increasing the value of D_1 and D_2 to a sufficiently large value.
- **Case-II:** If $det(J_{E^*}) < 0$, then the corresponding equilibrium in spatiotemporal system can be made stable by gradually increasing the value of D_1 to a sufficiently large value.

3.4.1 Conditions for diffusion-driven instability

The characteristic equation (3.26) yields

$$M_1' = -trace(J_{E^*}) + (D_1+D_2)\left[\left(\frac{n\pi}{M}\right)^2 + \left(\frac{m\pi}{N}\right)^2\right],$$

$$M_2' = D_1D_2\left[\left(\frac{n\pi}{M}\right)^2 + \left(\frac{m\pi}{N}\right)^2\right]^2 - (A_{11}D_2 + A_{22}D_1)\left[\left(\frac{n\pi}{M}\right)^2 + \left(\frac{m\pi}{N}\right)^2\right] + det\left(J_{E^*}\right), \tag{3.27}$$

where

$$trace(J_{E^*}) = -r_1x^* + \frac{\alpha(1-\beta y^*)^2x^*y^*}{(a+(1-\beta y^*)x^*)^2} - \frac{cy^*(a+x^*)}{(a+(1-\beta y^*)x^*)^2},$$
$$det(J_{E^*}) = \left(r_1x^* - \frac{\alpha(1-\beta y^*)^2x^*y^*}{(a+(1-\beta y^*)x^*)^2}\right)\left(\frac{-cy^*(a+x^*)}{(a+(1-\beta y^*)x^*)^2}\right) + \left(\frac{rkx^*}{(1+ky^*)^2} + \frac{\alpha x^*[a(1-2\beta y)+x^*(1-\beta y^*)^2]}{(a+(1-\beta y^*)x^*)^2}\right)\left(\frac{cy^{*2}(1-\beta y^*)}{(a+(1-\beta y^*)x^*)^2}\right).$$

Turing instability, i.e., diffusion driven instability occurs if either $M_1' < 0$ or $M_2' < 0$ holds. Clearly $M_1' > 0$ if $trace(J_{E^*}) < 0$. Now the only condition left for Turing instability to occur is $M_2' < 0$ with $det(J_{E^*}) > 0$.

Next, we define a function

$$H(\xi) = D_1D_2\xi^2 - (A_{11}D_2 + A_{22}D_1)\xi + det(J_{E^*}), \tag{3.28}$$

where $\xi = \left(\frac{n\pi}{M}\right)^2 + \left(\frac{m\pi}{N}\right)^2$.

Under the condition $H(\xi) < 0$, Turing instability occurs, i.e.,

$$D_1D_2\xi^2 - (A_{11}D_2 + A_{22}D_1)\xi + det(J_{E^*}) < 0.$$

Assuming that $H(\xi)$ attains its minimum at $\xi = \xi_m$. Thus,

$$H'(\xi_m) = 0 \Rightarrow 2D_1D_2\xi_m - (A_{11}D_2 + A_{22}D_1) = 0,$$

which gives us

$$\xi_m = \frac{(A_{11}D_2 + A_{22}D_1)}{2D_1D_2} > 0. \tag{3.29}$$

Condition for diffusion driven instability at $\xi = \xi_m$ is

$$\frac{(A_{11}D_2 + A_{22}D_1)^2}{4D_1D_2} - \frac{(A_{11}D_2 + A_{22}D_1)^2}{2D_1D_2} + det(J_{E^*}) < 0,$$
$$\text{i.e., } (A_{11}D_2 + A_{22}D_1)^2 - 4D_1D_2det(J_{E^*}) > 0.$$

The roots of the quadratic equation (3.28) is given by

$$\xi_{1,2} = \frac{(A_{11}D_2 + A_{22}D_1) \pm \sqrt{(A_{11}D_2 + A_{22}D_1)^2 - 4D_1D_2Det(J_{E^*})}}{2D_1D_2}.$$

Thus,

$$H(\xi) < 0 \quad \text{for} \quad \xi_1 < \xi < \xi_2.$$

Since $trace(J_{E^*}) < 0$ and, hence,

$$A_{11} + A_{22} < 0.$$

Since A_{22} is always negative, therefore

$$-\frac{A_{11}}{A_{22}} < 1.$$

Also, from Eq. (3.29), we have

$$A_{11}D_2 + A_{22}D_1 > 0,$$

$$\Rightarrow A_{11}D_2 > -A_{22}D_1,$$

$$\frac{-A_{11}}{A_{22}} > \frac{D_1}{D_2}. \tag{3.30}$$

From Eqs. (3.29) and (3.30), we obtain

$$\frac{D_1}{D_2} < \frac{-A_{11}}{A_{22}} < 1,$$

$$\Rightarrow D_1 < D_2 \quad \text{for Turing instability.}$$

Theorem 3.4.1. *The unique interior equilibrium E^* of the model system (3.25) is globally asymptotically stable provided the corresponding equilibrium of model (3.3) is globally asymptotically stable.*

Proof. Let us consider the model (3.25). We take the same Lyapnuov function as used in the proof of Theorem (3.2.8):

$$V_1(x,y) = \left(x - x^* - x^* ln\frac{x}{x^*}\right) + m\left(y - y^* - y^* ln\frac{y}{y^*}\right).$$

Let

$$V_2(t) = \iint_\rho V_1(x,y)dxdy,$$

$$\Rightarrow \frac{dV_2}{dt} = \iint_\rho \left(\frac{\partial V_1}{\partial x}\frac{\partial x}{\partial t} + \frac{\partial V_1}{\partial y}\frac{\partial y}{\partial t}\right)dxdy,$$

$$\Rightarrow \frac{dV_2}{dt} = \iint_\rho \left[\frac{\partial V_1}{\partial x}\Big(\frac{rx}{1+ky} - r_0x - r_1x^2 - \frac{\alpha(1-\beta y)xy}{a+(1-\beta y)x}\Big) + \frac{\partial V_1}{\partial y}\Big(\mu y - \frac{cy^2}{a+(1-\beta y)x}\Big)\right]dxdy$$
$$+ \iint_\rho \left(D_1\frac{\partial V_1}{\partial x}\nabla^2 x + D_2\frac{\partial V_1}{\partial y}\nabla^2 y\right)dA,$$
$$= \iint_\rho \frac{dV_1}{dt}dA + \iint_\rho \left(D_1\frac{\partial V_1}{\partial x}\nabla^2 x + D_2\frac{\partial V_1}{\partial y}\nabla^2 y\right)dA,$$
$$= J_1 + J_2,$$

where $J_1 = \iint_\rho \frac{dV_1}{dt}dA, \quad J_2 = \iint_\rho \left(D_1\frac{\partial V_1}{\partial x}\nabla^2 x + D_2\frac{\partial V_1}{\partial y}\nabla^2 y\right)dA.$

Applying Green's identity, we obtain

$$\iint_\rho \frac{\partial V_1}{\partial x}\nabla^2 x dA = 0 - \iint_\rho \Big(\nabla\Big(\frac{\partial V_1}{\partial x}\Big).\nabla x\Big)dA.$$
$$\nabla\Big(\frac{\partial V_1}{\partial x}\Big) = \frac{\partial}{\partial u}\Big(\frac{\partial V_1}{\partial x}\Big)\hat{i} + \frac{\partial}{\partial v}\Big(\frac{\partial V_1}{\partial x}\Big)\hat{j},$$
$$= \frac{\partial^2 V_1}{\partial x^2}.\frac{\partial x}{\partial u}\hat{i} + \frac{\partial^2 V_1}{\partial x^2}.\frac{\partial x}{\partial v}\hat{j}.$$
$$\nabla x = \frac{\partial x}{\partial u}\hat{i} + \frac{\partial x}{\partial v}\hat{j}.$$
$$\therefore \quad \nabla\Big(\frac{\partial V_1}{\partial x}\Big).\nabla x = \frac{\partial^2 V_1}{\partial x^2}\Big(\frac{\partial x}{\partial u}\Big)^2 + \frac{\partial^2 V_1}{\partial x^2}\Big(\frac{\partial x}{\partial v}\Big)^2.$$

$$\Rightarrow \frac{dV_2}{dt} = \iint_\rho \frac{dV_1}{dt}dA - \iint_\rho D_1\frac{\partial^2 V_1}{\partial x^2}\left[\Big(\frac{\partial x}{\partial u}\Big)^2 + \Big(\frac{\partial x}{\partial v}\Big)^2\right]dA$$
$$- \iint_\rho D_2\frac{\partial^2 V_1}{\partial y^2}\left[\Big(\frac{\partial y}{\partial u}\Big)^2 + \Big(\frac{\partial y}{\partial v}\Big)^2\right]dA.$$

Here,

$$\frac{\partial^2 V_1}{\partial x^2} = \frac{x^*}{x^2} > 0, \frac{\partial^2 V_1}{\partial y^2} = \frac{my^*}{y^2} > 0$$

Hence, $\frac{dV_2}{dt} < 0$ provided $\frac{dV_1}{dt} < 0$. ∎

Remark: If $\frac{dV_1}{dt} > 0$ i.e. the interior equilibrium is unstable in temporal system, then the corresponding equilibrium can be made globally asymptotiocally stable in spatiotemporal system by increasing the value of D_1 and D_2 to a sufficiently large value.

3.5 Dynamics of delayed spatiotemporal system

In this section, we analyze the delayed system with diffusion. We shall analyze the combined effects of delay and diffusion on Hopf-bifurcation.

Consider system (3.2) and take the transformation $\bar{x}(u,v,t) = x(u,v,t) - x^*$, $\bar{y}(u,v,t) = y(u,v,t) - y^*$. By linearizing the above system (ignoring the bar from variables to simplify the symbol marks), we have

$$\begin{array}{rcl} \frac{\partial x(u,v,t)}{\partial t} & = & J_{11}x(u,v,t) + J_{12}y(u,v,t) + J_{13}y(u,v,t-\tau) + D_1\nabla^2 x(u,v,t), \\ \frac{\partial y(u,v,t)}{\partial t} & = & J_{21}x(u,v,t) + J_{22}y(u,v,t) + D_2\nabla^2 y(u,v,t). \end{array} \tag{3.31}$$

We take the solution of the form (perturbing the interior equilibrium in both time and space)

$$\begin{aligned} x =& Ae^{\lambda t} sin\left(\frac{n\pi}{M}u\right) cos\left(\frac{m\pi}{N}v\right), \\ y =& Be^{\lambda t} sin\left(\frac{n\pi}{M}u\right) cos\left(\frac{m\pi}{N}v\right). \end{aligned}$$

Substituting the above solution in system (3.31) and simplifying, we obtain:

$$J = \begin{bmatrix} J_{11} - D_1\left(\left(\frac{n\pi}{M}\right)^2 + \left(\frac{m\pi}{N}\right)^2\right) & J_{12} \\ J_{21} & J_{22} - D_2\left(\left(\frac{n\pi}{M}\right)^2 + \left(\frac{m\pi}{N}\right)^2\right) \end{bmatrix} + \begin{bmatrix} 0 & J_{13} \\ 0 & 0 \end{bmatrix} e^{-\lambda\tau},$$

$$\Rightarrow J = \begin{bmatrix} J_{11} - D_1\chi^2 & J_{12} + J_{13}e^{-\lambda\tau} \\ J_{21} & J_{22} - D_2\chi^2 \end{bmatrix},$$

where

$$\begin{aligned} \chi &= \sqrt{\left(\frac{n\pi}{M}\right)^2 + \left(\frac{m\pi}{N}\right)^2}, \\ J_{11} &= -r_1x^* + \frac{\alpha(1-\beta y^*)^2x^*y^*}{(a+(1-\beta y^*)x^*)^2}, \\ J_{12} &= \frac{-rkx^*}{(1+ky^*)^2} - \frac{\alpha x^*[a(1-2\beta y) + x^*(1-\beta y^*)^2]}{(a+(1-\beta y^*)x^*)^2}, \\ J_{21} &= \frac{cy^{*2}(1-\beta y^*)}{(a+(1-\beta y^*)x^*)^2}, \\ J_{22} &= \frac{-cy^*(a+x^*)}{(a+(1-\beta y^*)x^*)^2}, \\ J_{13} &= \frac{-rkx^*}{(1+ky^*)^2}. \end{aligned}$$

Now, we have the following characteristic equation:

$$\lambda^2 + N_1\lambda + N_2 - N_3 e^{-\lambda\tau} = 0, \tag{3.32}$$

where

$$\begin{aligned} N_1 &= (D_1 + D_2)\chi^2 - (J_{11} + J_{22}), \\ N_2 &= (J_{11}J_{22} - J_{21}J_{12}) - (J_{11}D_2 + J_{22}D_1)\chi^2 + D_1D_2\chi^4, \\ N_3 &= J_{21}J_{13}. \end{aligned}$$

For $\lambda = i\omega(\omega > 0)$, we have

$$\begin{aligned} N_2 - \omega^2 &= N_3 cos(\omega\tau), \\ N_1\omega &= N_3 sin(\omega\tau). \end{aligned} \tag{3.33}$$

On squaring and adding the above two equations and simplifying, we get

$$\begin{aligned} &\omega^4 + R\omega^2 + S = 0, \\ \text{where} \quad &R = N_1^2 - 2N_2, \quad S = N_2^2 - N_3^2. \end{aligned} \tag{3.34}$$

We can divide the expression S into two parts

$$S = S_1S_2 = (N_2 + N_3)(N_2 - N_3),$$

where

$$\begin{aligned} S_1 &= (J_{11}J_{22} - J_{21}J_{12}) - (J_{11}D_2 + J_{22}D_1)\chi^2 + D_1D_2\chi^4 + J_{21}J_{13}, \\ S_2 &= (J_{11}J_{22} - J_{21}J_{12}) - (J_{11}D_2 + J_{22}D_1)\chi^2 + D_1D_2\chi^4 - J_{21}J_{13}. \end{aligned}$$

From the local stability conditions of $E^*(x^*, y^*)$ for the non-delayed model, $S_2 > 0$ always holds true.

Taking $z = \omega^2$, Eq. (3.34) gives

$$\begin{aligned} z^2 + Rz + S &= 0. \\ z^{\pm} &= \frac{-R \pm \sqrt{R^2 - 4S}}{2}. \end{aligned} \tag{3.35}$$

Next, we have the following cases:

(H1′): Let $R > 0$, $S_1 > 0$, $R^2 - 4S > 0$.

Then Eq. (3.35) has no positive root. Therefore, all the roots of Eq. (3.32) has negative real parts for any χ when $\tau > 0$.

(H2′): If $\exists$ a constant $\chi_0 \in \mathbb{N}$ such that

$$S_1(\chi_0) = D_1D_2{\chi_0}^4 - (J_{11}D_2 + J_{22}D_1){\chi_0}^2 + (J_{11}J_{22} - J_{21}J_{12}) + J_{21}J_{13} < 0$$

holds, then $\omega^+ = \sqrt{z^+}$ is a unique positive root of Eq. (3.35).

By substituting $\omega = \omega^+$ in Eq. (3.33),

$$\begin{aligned} cos(\omega^+\tau) &= \frac{N_2 - {\omega^+}^2}{N_3} \cong H_1(\omega^+), \\ sin(\omega^+\tau) &= \frac{N_1\omega^+}{N_3} \cong H_2(\omega^*+), \end{aligned} \tag{3.36}$$

and the corresponding bifurcation parameter is calculated as

$$\tau^j_{\chi_0} = \frac{1}{\omega^+}\left[cos^{-1}\left(\frac{N_2 - {\omega^+}^2}{N_3}\right)\right] + \frac{2j\pi}{\omega_0} \quad ; \quad j = 0,1,2,...$$

Let us assume that $\lambda(\tau)$ be a root of Eq. (3.32) such that $Re(\lambda(\tau)) = 0$ and $\lambda(\tau) = i\omega^+$. From Eq. (3.32), we have

$$\begin{aligned} \left(\frac{d\lambda}{d\tau}\right)^{-1} &= -\left[\frac{(2\lambda + N_1)e^{\lambda\tau}}{N_3\lambda} - \frac{\tau}{\lambda}\right], \\ \left[\frac{d\lambda}{d\tau}\right]^{-1}_{\lambda=i\omega^+} &= \frac{(2i\omega^+ + N_1)(cos(\omega^+\tau) + isin(\omega^+\tau))}{N_3 i\omega^+} - \frac{\tau}{i\omega^+}, \\ Re\left[\frac{d\lambda}{d\tau}\right]^{-1}_{\lambda=i\omega^+} &= \frac{2\omega^+ cos(\omega^+\tau) + N_1 sin(\omega^+\tau)}{N_3\omega^+}. \end{aligned}$$

Substituting the values of $cos(\omega^+\tau)$ and $sin(\omega^+\tau)$ from Eqs. (3.36), we get

$$Re\left[\frac{d\lambda}{d\tau}\right]^{-1}_{\lambda=i\omega_0} = \frac{2N_2 - 2{\omega^+}^2 + N_1^2}{N_3^2}.$$

Also,

$$\text{sign}\left[\frac{d}{d\tau}Re(\lambda)\right]_{\lambda=i\omega^+} = \text{sign}\left[Re\left(\frac{d\lambda}{d\tau}\right)\right]_{\lambda=i\omega^+}.$$

(H3′): $2N_2 - 2\omega^{+2} + N_1^2 \neq 0$.

Under (H3′), transversality condition holds.

From the preceding discussion, we can conclude the following result.

Theorem 3.5.1. *For the delayed diffusive system, the following conclusions can be made:*

1. *If (H1′) holds, then $E^*(x^*, y^*)$ is locally asymptotically stable for all $\tau > 0$ and for any value of χ.*

2. *If (H2′) holds:*

   (i) The positive equilibrium $E^*(x^*, y^*)$ is locally asymptotically stable for $\tau \in (0, \tau^0_{\chi_0})$ and unstable for $\tau > \tau^0_{\chi_0}$.

   (ii) When $\tau = \tau^i_{\chi_0}$, $\quad i = 0, 1, 2, 3, \ldots$, system (3.2) experiences Hopf-bifurcation around E^* and we get a family of periodic solutions bifurcating from E^*.

3.6 Numerical simulations

This section carries out extensive numerical simulations to corroborate the analytical findings obtained in the preceding sections. We use MATLAB R2019b to simulate the analytical findings.

3.6.1 Non-delayed temporal model

In this part, numerical simulation has been performed to better understand the impact of refuge parameter and the fear parameter on the dynamics of our proposed system (3.3).

In Fig. 3.4, we have shown the phase portrait when the system has unique interior equilibrium. For k=0.5, the interior equilibrium $E_1^*(4.4352, 1.0211)$ is locally asymptotically stable. While for k=1, the interior equilibrium has a stable limit cycle i.e., $E_1^*(0.6955, 0.5257)$ is a spiral source. In both the cases, the extinction equilibrium is a source while the axial equilibria $E_1(12.5, 0)$ and $E_2(0, 0.2620)$ are saddle points. The remaining parameters take the values as $r = 3$, $r_0 = 0.5$, $r_1 = 0.2$, $\alpha = 3.5$, $\beta = 0.7$, $\mu = 0.3$, $c = 0.5$, $a = 0.4367$.

Figure 3.5(a) depicts the phase portrait when the system has two interior equilibrium. Here system (3.3) exhibits bistability attribute between the axial equilibrium $E_2(0, 0.5556)$ and the interior equilibrium $E_1^*(3.8882, 1.2116)$. In addition, the extinction equilibrium is a source while the axial equilibrium $E_1(12.5, 0)$ and the interior equilibrium $E_2^*(0.9760, 0.9323)$ are saddle points. In Fig. 3.5(b), we have plotted basin of attractions which shows that solutions starting anywhere from red region converge to E_2 and from the green region converge to E_1^*.

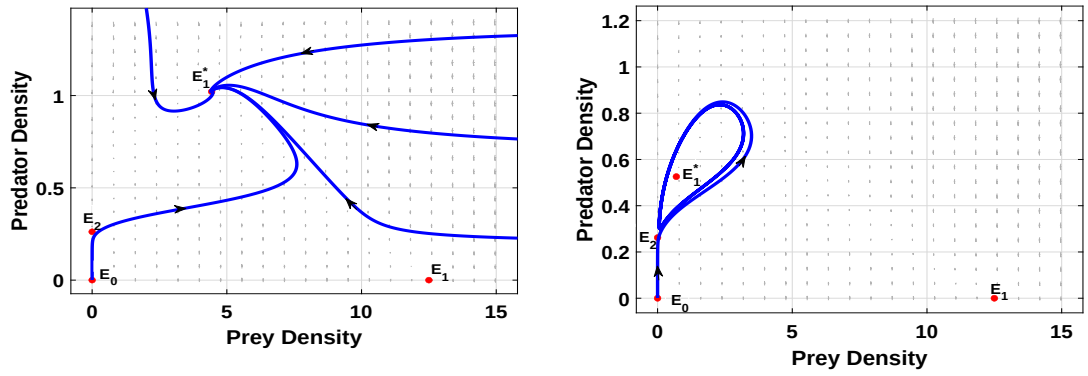

(a) $k = 0.5$ (b) $k = 1$

Fig. 3.4: Phase portrait depicting the stability behavior when there exists a unique interior equilibrium. Parameter values are taken as $r = 3$, $r_0 = 0.5$, $r_1 = 0.2$, $\alpha = 3.5$, $\beta = 0.7$, $\mu = 0.3$, $c = 0.5$, $a = 0.4367$.

The remaining parameters take the values as $r = 3$, $r_0 = 0.5$, $r_1 = 0.2$, $\alpha = 3.5$, $\beta = 0.7$, $\mu = 1$, $c = 0.9$, $a = 0.5$ and $k = 0.5$.

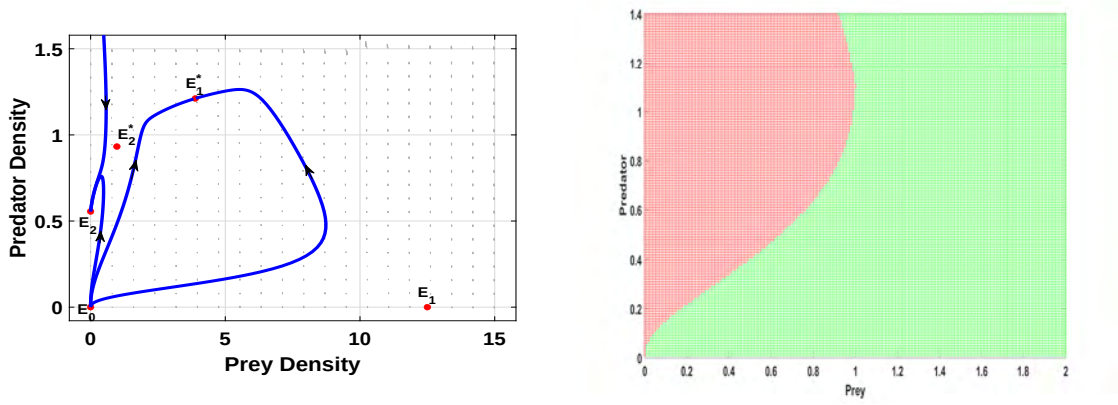

(a) $E_2 = (0, 0.556)$ and $E_1^* = (3.889, 1.211)$ are locally asymptotically stable, whereas $E_0 = (0,0)$ is nodal source, $E_1(12.5, 0)$ and $E_2^*(0.9760, 0.9323)$ are saddle points.

(b) Basin of attraction for $E_2 = (0, 0.556)$ and $E_1^* = (3.889, 1.211)$. Red: convergence region for E_2 while green for E_1^*.

Fig. 3.5: Bistability attribute involving two equilibria E_2 and E_1^*. The remaining parameters take the values as $r = 3$, $r_0 = 0.5$, $r_1 = 0.2$, $\alpha = 3.5$, $\beta = 0.7$, $\mu = 1$, $c = 0.9$, $a = 0.5$ and $k = 0.5$.

Moreover, Fig. 3.6 shows bifurcation of codimension one obtained by varying a as bifurcation parameter. The model system (3.3) exhibits saddle-node bifurcation at the interior equilibrium (2.43,1.07) at $a = 0.3627$, that is, coexistence equilibria vanish after colliding. In

this figure, red colour represents stable node and blue signifies saddle point. The remaining parameters take the values as $r = 3$, $r_0 = 0.5$, $r_1 = 0.2$, $\alpha = 3.5$, $\beta = 0.7$, $\mu = 1$, $c = 0.5$, $k = 0.5$.

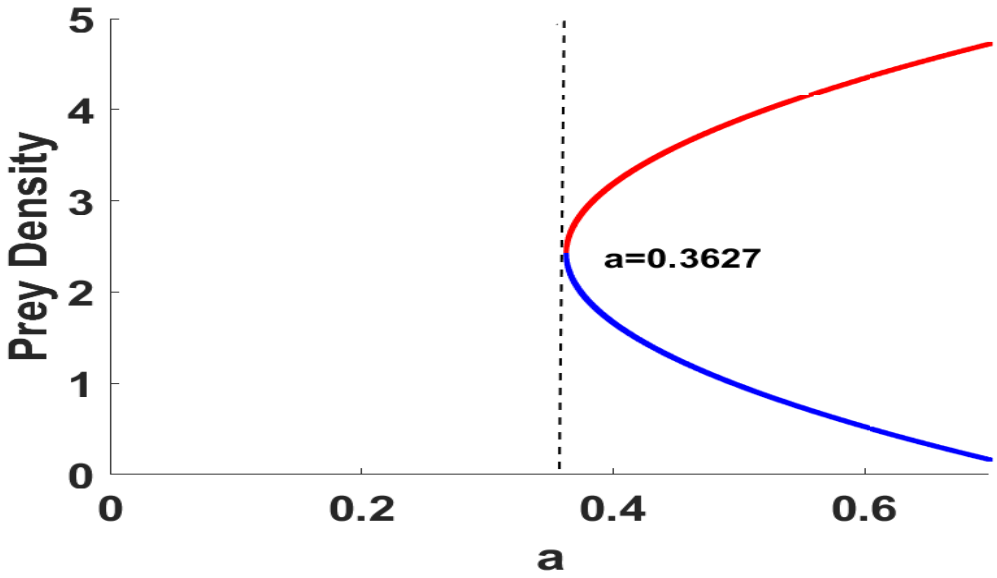

Fig. 3.6: Saddle-node bifurcation with respect to the parameter a. The remaining parameters take the values as $r = 3$, $r_0 = 0.5$, $r_1 = 0.2$, $\alpha = 3.5$, $\beta = 0.7$, $\mu = 1$, $c = 0.5$, $k = 0.5$. Red colour represents stable node and blue signifies saddle point.

Next, we draw the bifurcation diagram for both prey and predator species in Fig. 3.7. This figure depicts that for small values of fear parameter k, both prey and predator populations have a stable coexistence. As we increase the value of k, the stable coexistence loses its stability, and periodic oscillations arise, ensuring Hopf-bifurcation's existence. On further increasing the value of k, the limit cycle loses its stability and stable coexistence of both the species is observed. If the value of fear parameter is high $(k > 1.2)$, then prey population can not survive.

Figure 3.8 illustrates the stability and instability region in the $k - \alpha$ parameter plane. Here, magenta colour represents stability region and cyan colour signifies instability region. In addition, white region depicts no interior equilibrium region. All the other parameters are fixed as $r = 3$, $r_0 = 0.5$, $r_1 = 0.2$, $\beta = 0.7$, $\mu = 0.3$, $c = 0.5$, $a = 0.4367$. We also observe that to rule out periodic oscillations, a significant value of the fear parameter k is required.

Now, Fig. 3.9 indicates the effect of the refuge parameter β on the dynamics of the model system (3.3) . The prey density grows with the refuge parameter, but the predator population initially increases with β but then decreases after a threshold value. It can be observed that, up to a certain value, the refuge parameter β has a positive impact on both species. Beyond this threshold value, it can be destructive to the predator population.

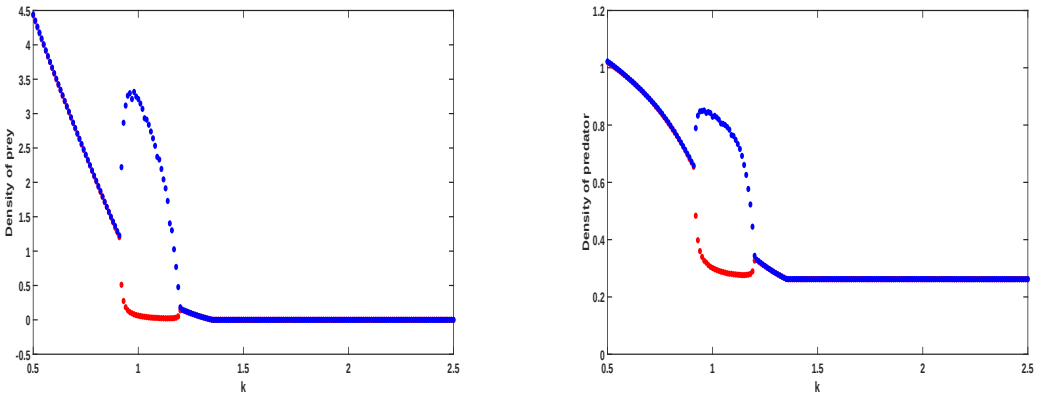

(a) Bifurcation diagram of prey.

(b) Bifurcation diagram of predator.

Fig. 3.7: Bifurcation diagrams for prey and predator illustrating double Hopf-bifurcation for the model (3.1) with respect to the fear parameter k. The remaining parameters take the values as $r = 3$, $r_0 = 0.5$, $a = 0.4367$, $r_1 = 0.2$, $\alpha = 3.5$, $\beta = 0.7$, $\mu = 0.3$, $c = 0.5$

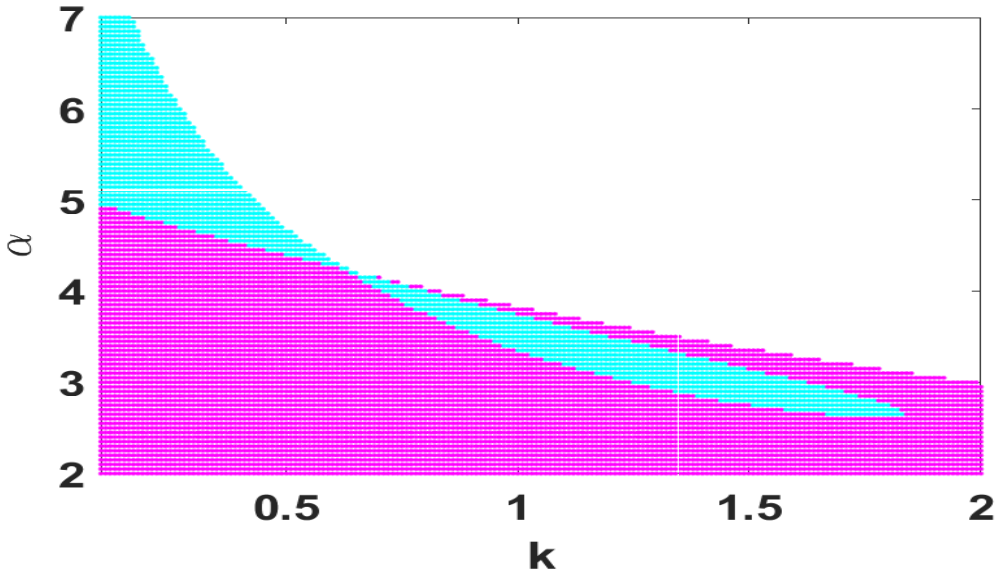

Fig. 3.8: Plot of stable and unstable region for the interior equilibrium with respect to the parameters k and α . Remaining fixed parameters are $r = 3$, $r_0 = 0.5$, $r_1 = 0.2$, $\beta = 0.7$, $\mu = 0.3$, $c = 0.5$, $a = 0.4367$. Magenta colour represents stability and cyan signifies instability regions. White depicts no interior equilibrium.

3.6.2 Non-spatial delayed model

In this section, the impact of the delay parameter τ on the dynamics of system (3.1) is investigated using numerical simulations. Incorporating fear response delay does not change

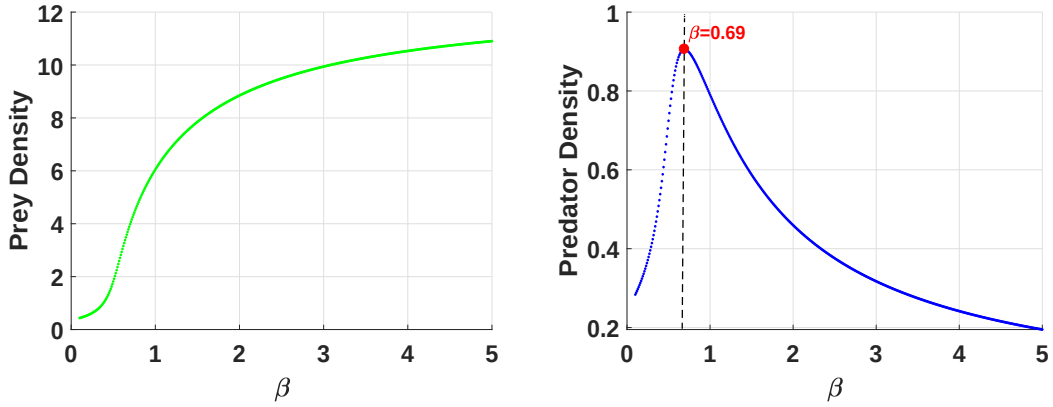

Fig. 3.9: Impact of prey refuge β on the prey and predator species. The remaining parameters take the values as $r = 3$, $r_0 = 0.5$, $r_1 = 0.2$, $\alpha = 3.5$, $a = 0.05$, $\mu = 0.3$, $c = 0.5$, and $k = 0.5$

the interior equilibrium. Hence, for the set of parameters as $r = 4$, $r_0 = 1$, $r_1 = 0.2$, $\alpha = 3.5$, $\beta = 0.7$, $a = 0.4367$, $\mu = 0.3$, $c = 0.5$, and $k = 1$, system (3.1) has a unique interior equilibrium $E^*(1.40, 0.69)$. Hypotheses stated in the analysis (H1) and (H3) hold for the given parameter values. In addition, considering $i = 0$ in the Eq. (3.16), we obtain

$$\omega_0 = 0.5466, \quad \tau_0 = 0.4680.$$

Figure 3.10 depicts the time series and phase portrait for the delay parameter $\tau = 0.4 < \tau_0$. Here, system shows stable dynamics around the interior equilibrium E^*. For $\tau = 0.5 > \tau_0$, the system exhibits a stable limit cycle around the interior equilibrium as shown in Fig. 3.11. As τ exceeds τ_0, the interior equilibrium $E^*(1.40, 0.69)$ becomes unstable.

Hopf-bifurcation plot for both prey and predator species with respect to the fear-response delay parameter is illustrated in Fig. 3.12. Here, we observe that for $\tau < 0.4680$, all the trajectories are converging to the stable interior equilibrium E^*. The model system (3.1) exhibits oscillating behavior around the interior equilibrium E^* when the delay parameter τ increases.

3.6.3 Turing instabilities and pattern formation

Turing instability may lead to stationary pattern (also called Turing pattern) in a spatiotemporal model. The model system (3.25) is solved numerically using the finite difference scheme to get the patterns. The forward difference Euler scheme is used for the reaction part, and the conventional five-point explicit finite difference scheme with homogeneous Neumann boundary conditions is implemented for the 2D diffusion [142].

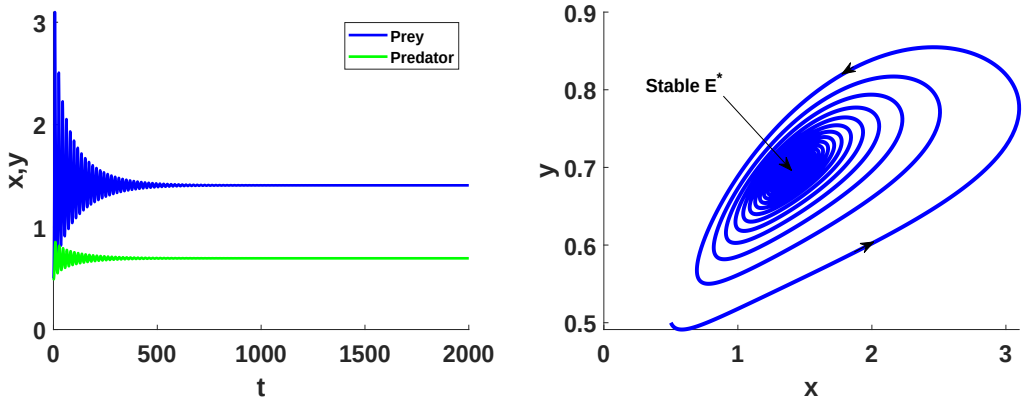

Fig. 3.10: For $\tau = 0.4$, system exhibits stable dynamics. Considered parameter values are $r = 4$, $r_0 = 1$, $r_1 = 0.2$, $\alpha = 3.5$, $\beta = 0.7$, $a = 0.4367$, $\mu = 0.3$, $c = 0.5$, and $k = 1$

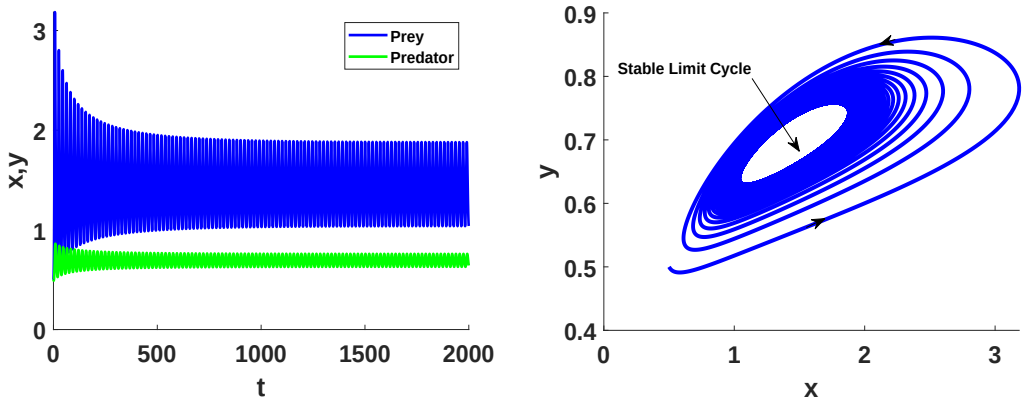

Fig. 3.11: For $\tau = 0.5$, system is unstable and have a stable limit cycle. Considered parameter values are $r = 4$, $r_0 = 1$, $r_1 = 0.2$, $\alpha = 3.5$, $\beta = 0.7$, $a = 0.4367$, $\mu = 0.3$, $c = 0.5$, and $k = 1$.

First, we investigate the possibility of diffusion-driven instabilities in the model system (3.25). To ensure this, all analytical conditions for Turing instability are numerically verified. Figures 3.13(a) and 3.13(b) illustrate $H(\xi)$ (Eq. 3.28) vs. ξ plot for different values of fear parameter k and prey refuge parameter β. We can see from these plots that initially, the probability of Turing instability increases as k or β increases, but further increments in these parameter values reduce the possibility of diffusion-driven instability. Figure (3.14) depicts the region for different Turing patterns. Here, the blue region corresponds to Turing instability.

Next, we obtain the Turing patterns for the 2D-spatial domain. Figure 3.15 depicts the effect of fear parameter k on the spatial distribution of prey species. Here, we observed that the Turing patterns obtained for prey and predator species have a one-to-one correspondence;

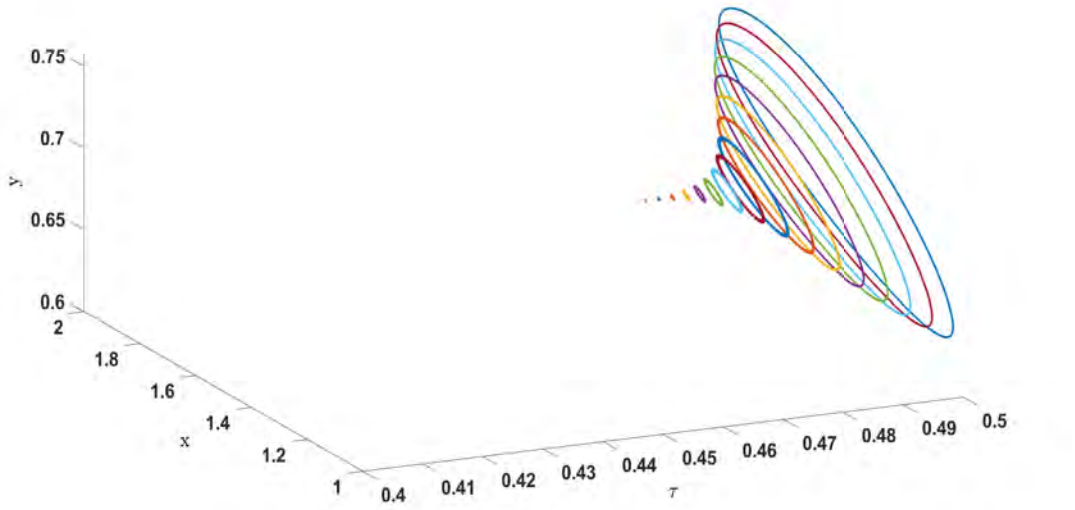

Fig. 3.12: Hopf-bifurcation with respect to the delay parameter τ. Remaining parameter values are $r = 4$, $r_0 = 1$, $r_1 = 0.2$, $\alpha = 3.5$, $a = 0.4367$, $\beta = 0.7$, $\mu = 0.3$, $c = 0.5$ and $k = 1$.

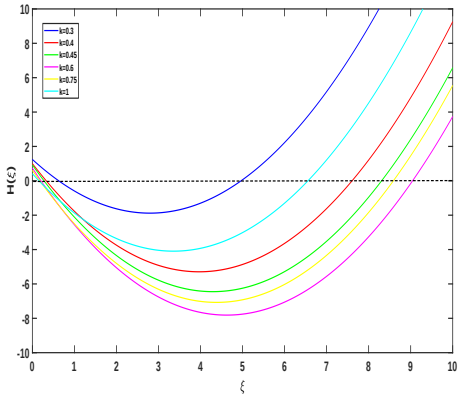

(a) $H(\xi)$ vs ξ for various $k's$. Here, $\beta = 0.2$.

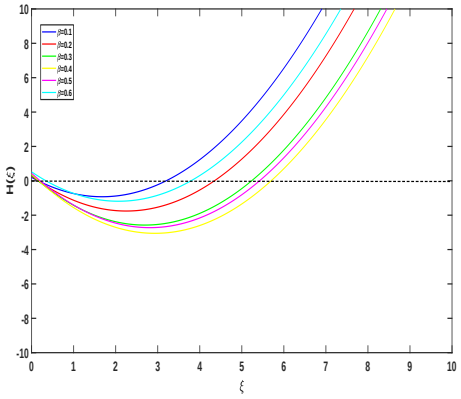

(b) $H(\xi)$ vs ξ for various $\beta's$. Here, $k = 1.2$

Fig. 3.13: $H(\xi)$ plotted against ξ for various values of β and k, with the black dashed line representing $H(\xi) = 0$. All parameter values are fixed as $r = 5$, $r_0 = 1$, $r_1 = 0.5$, $\alpha = 2.2$, $a = 0.3$, $\mu = 1$, $c = 0.9$ except k and β. Also, D_1 and D_2 takes the value as 0.1 and 4, respectively.

thus, we only show the patterns exhibited by the prey population. Blue indicates a low-density region, while red signifies a high-density area. In Fig. 3.15(a), the system dynamics show the cold-spots pattern for a small value of the fear parameter, i.e., the population is sparse in isolated areas whereas high in the remaining region. From an ecological viewpoint, when the

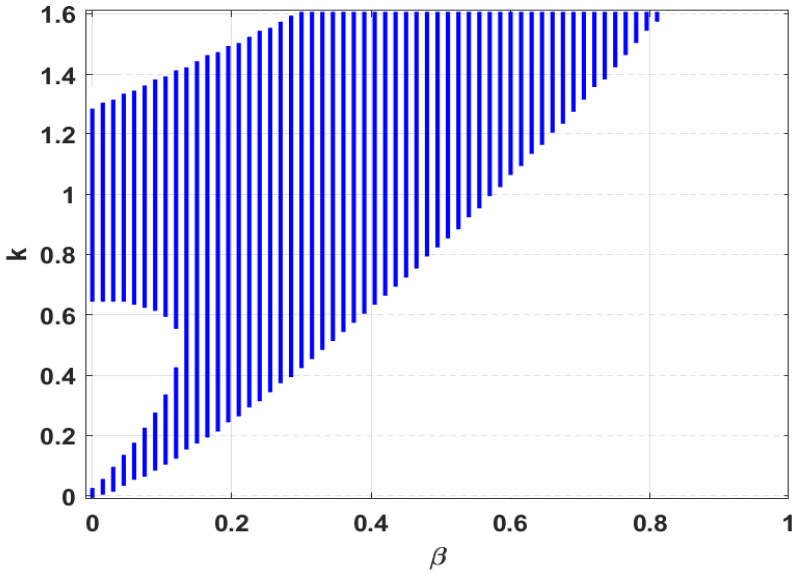

Fig. 3.14: Plot depicting Turing instability region. All other parameters take the same values as in Fig. 3.13.

strength of fear is low, the predator population is outcompeted by the prey population resulting in the formation of the cold spots pattern. Now, increasing the fear parameter k, the patterns changes from "cold spots" to "a mixture of stripes and holes" through "stripes" and then further increments in k leads to "stripes-spots" $\rightarrow$ "hot spots" patterns. As the fear induced by predator population increases, there is a decline observed in prey density resulting in hot spots pattern. The effect of prey refuge is illustrated in Fig. 3.16. In Fig. 3.16(a), the prey population is at a higher density in the isolated area, whereas it resides at a low density in the remaining region. On increasing the prey refuge parameter β, the prey population increases and occupies the major portion of the spatial domain, which is justified from an ecological perspective (Fig. 3.16(b)).

Now, we analyze the effect of diffusive coefficients on the spatial distribution. Figure 3.17 shows the spatial pattern distribution for the prey species at the stationary state. It is observed that the upper bound of the prey species changes with change in diffusion coefficients. Figure 3.17(a) depicts the hot spots pattern. From the ecological perspective, prey population lies in an isolated region with high density, and the rest is occupied with low density. As we decrease the diffusive rate in prey population, we observe that "hot spots" pattern changes to "organic labyrinth" pattern. We discovered that low population density occupies a significant portion of the domain; however, average and high population density occupies the remaining region.

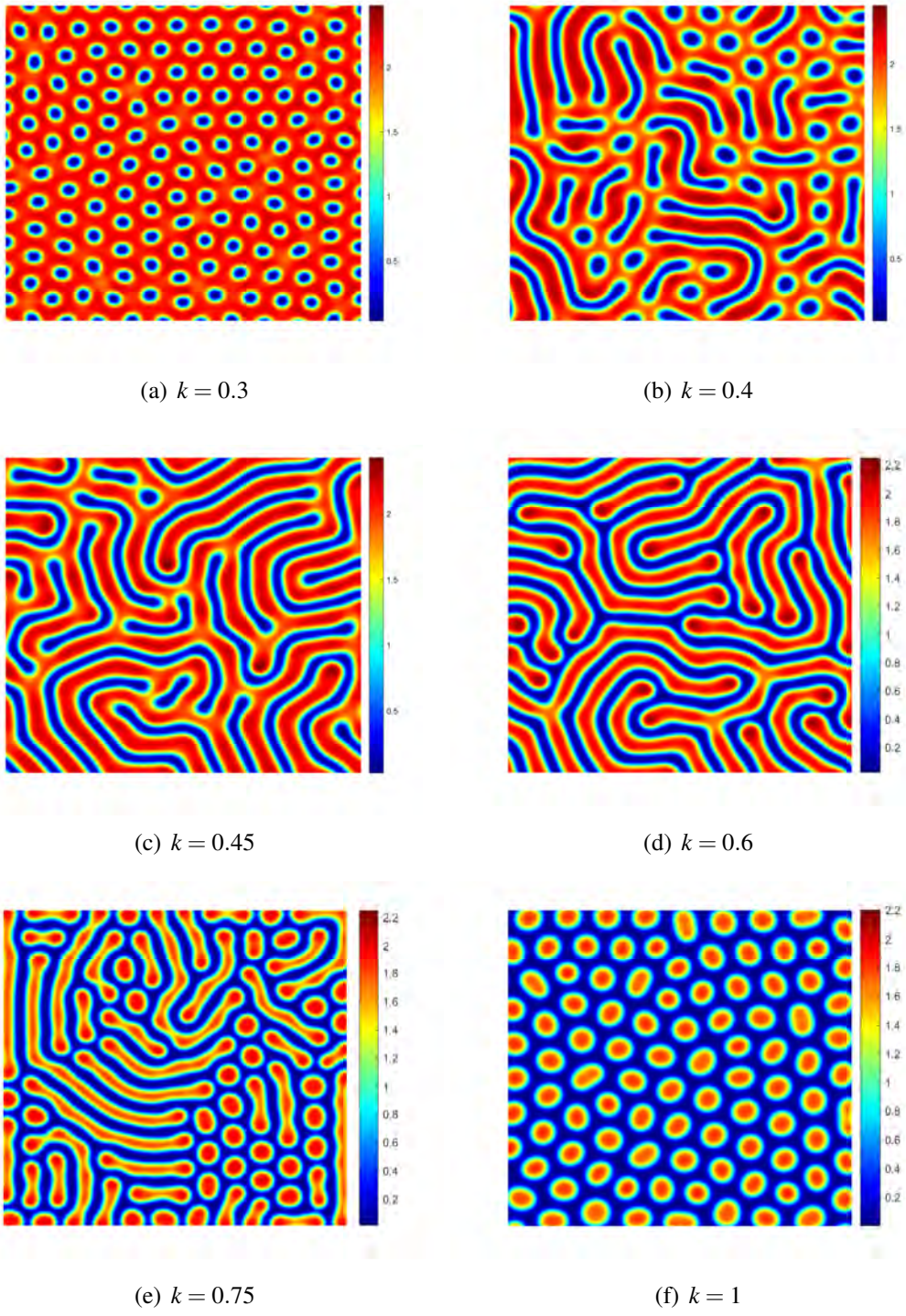

(a) $k = 0.3$ (b) $k = 0.4$

(c) $k = 0.45$ (d) $k = 0.6$

(e) $k = 0.75$ (f) $k = 1$

Fig. 3.15: Turing patterns obtained for prey population in 2D (xy-plane) to illustrate the impact of fear parameter. The remaining parameters take the values same as in Fig. 3.13 except k.

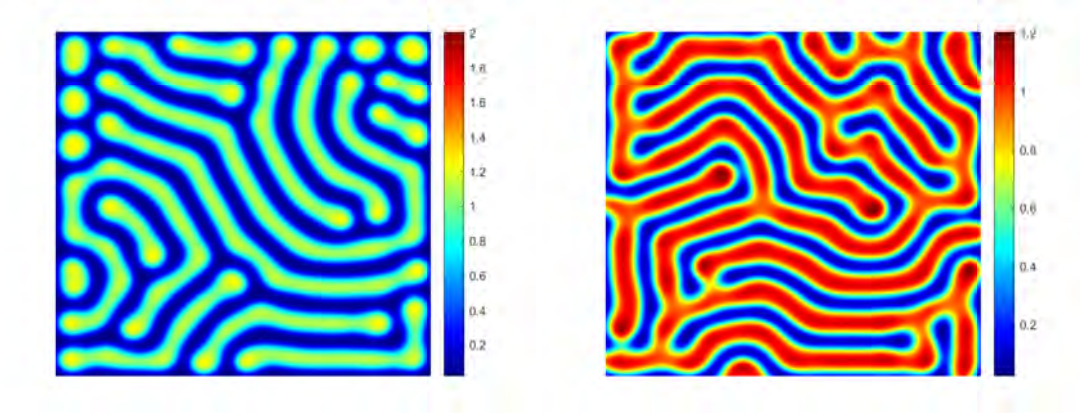

(a) $\beta = 0.7$ (b) $\beta = 0.75$

Fig. 3.16: Impact of prey refuge on Turing patterns exhibited by prey population in 2D (xy-plane). The remaining parameters take the values as $r = 3.5$, $r_0 = 1$, $r_1 = 0.5$, $\alpha = 2.2$, $a = 0.3$, $\mu = 1$, $c = 0.9$, $k = 0.6$. Also, D_1 and D_2 are 0.1 and 4, respectively.

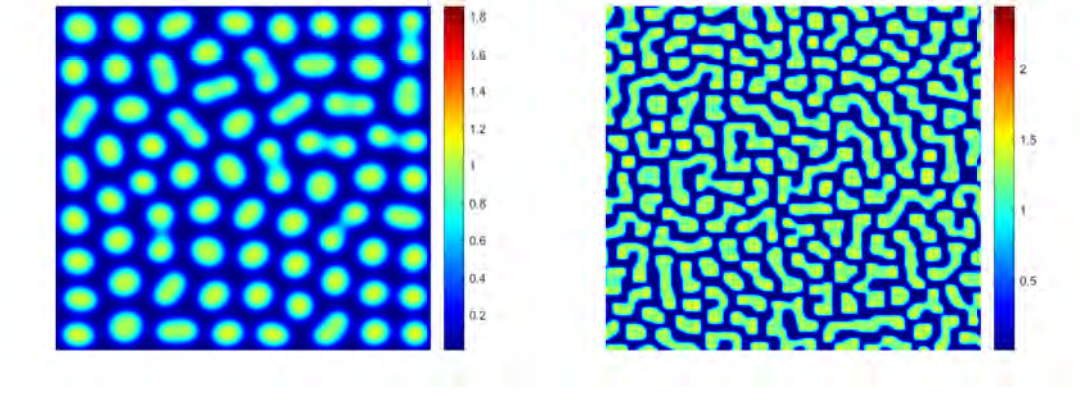

(a) $D_1 = 0.1, \quad D_2 = 4$ (b) $D_1 = 0.01, \quad D_2 = 4$

Fig. 3.17: Impact of diffusion coefficients on Turing patterns exhibited by prey population in 2D (xy-plane). Considered parameter values are $r = 3.5$, $r_0 = 1$, $r_1 = 0.5$, $\alpha = 2$, $\beta = 0.7$, $a = 0.3$, $\mu = 1$, $c = 0.9$ and $k = 0.8$.

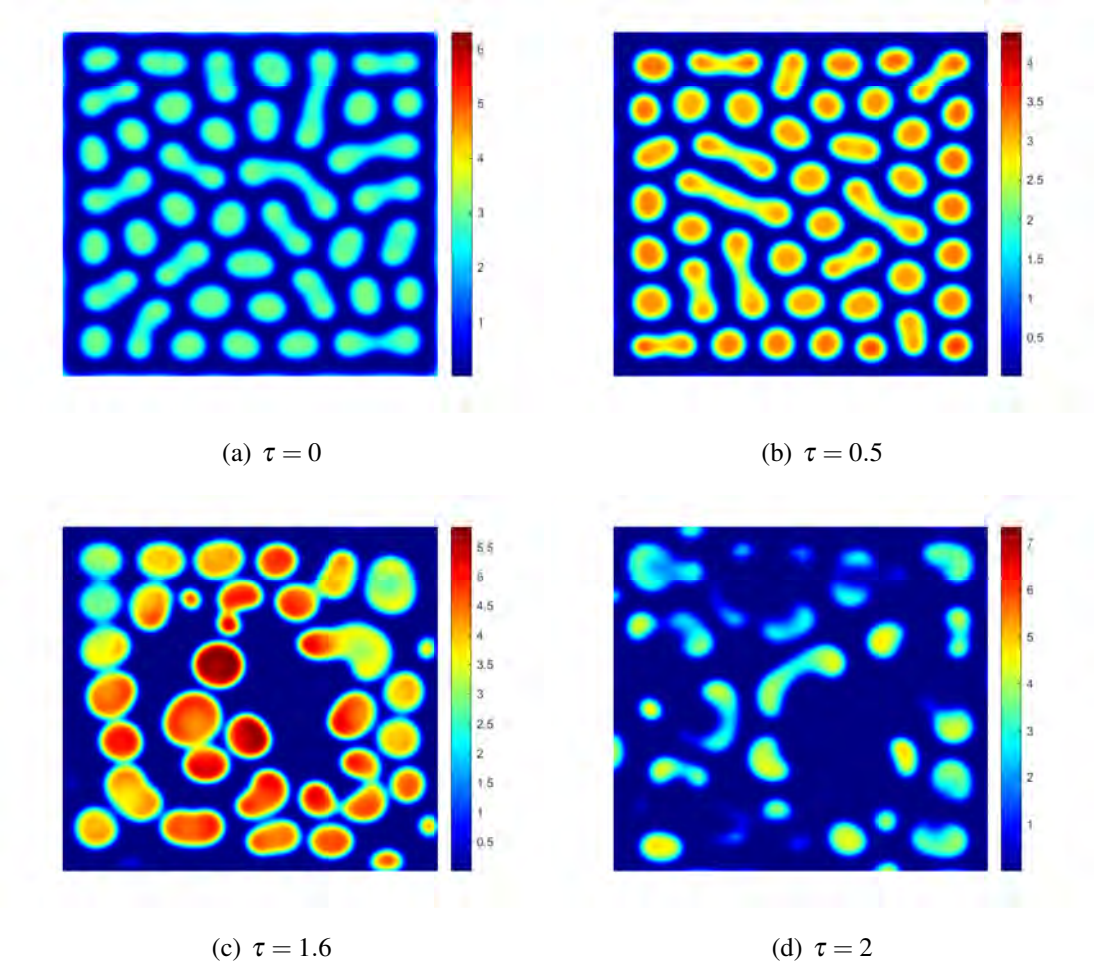

(a) $\tau = 0$ (b) $\tau = 0.5$

(c) $\tau = 1.6$ (d) $\tau = 2$

Fig. 3.18: Snapshots of prey species obtained over space for different values of fear response delay τ. All the parameter take the same values as in Fig. 3.11 except for fear parameter k (here k=1.5).

3.6.4 Spatiotemporal pattern with delay

In this part, we aim to provide numerical results of how the fear response delay affects the Turing patterns (Fig. 3.18). The parameter values chosen here lie inside the Turing domain satisfying all the analytical conditions for Turing instability. Figure 3.18(a) presents the "cold-spots" pattern obtained for the delayed system (3.2). As we increase the value of delay parameter τ, the "cold-spots pattern" changes to "hot-spots pattern" (Fig. 3.18(b)). Further gradual increments in τ leads to "loss of patterns" as illustrated in Figs. 3.18(c) and 3.18(d).

3.7 Discussion and concluding remarks

In the present chapter, we considered a delayed spatial predator-prey model based on a modified Leslie-Gower scheme incorporating fear induced by the predator population and non-constant prey refuge. The main focus of this study is to analyze how the fear induced in the prey population and prey refuge can affect the dynamics of the model in the presence of both diffusion and time delay. Thus, behaviors of temporal and spatiotemporal model systems are thoroughly investigated with and without time delay. First, we discussed the well-posedness of the proposed model by stating the positivity and boundedness of solutions and the prerequisites for the system to survive. The conditions for the number and existence of ecologically relevant equilibria are derived for the non-delayed temporal system, and their local stability behavior is investigated. In addition, we also studied the global asymptotic stability of the unique interior equilibrium. Taking a (the half-saturation constant) as the bifurcation parameter, we determined the criterion for the occurence of saddle-node bifurcation around the positive equilibrium E^*. We observed that the system exhibits bistability behavior between prey-free and coexistence equilibrium. Following that, we are interested in analyzing how fear affects population dynamics. So, we plotted the bifurcation diagram considering k (fear effect parameter) as the bifurcation parameter. We noticed that the system experiences a Hopf-bifurcation, and the stability flips from stable to periodic oscillations as the parameter k gradually increases. Moreover, on further increasing the fear parameter, the system experiences another Hopf-bifurcation and becomes stable from periodic oscillations. As a result, the system exhibits double Hopf-bifurcations with respect to the fear effect parameter k. A study done by Wang *et al.* [179] reveals that increasing the strength of fear may decrease the population densities and lead to prey extinction. They explored that incorporating the cost of fear may destabilize the system and further increment in fear strength stabilizes the system dynamics by excluding the possibility of a limit cycle. In the absence of delay parameter, the results remarked by Wang *et al.* [179] are in accordance with the findings of the present study. The effect of the refuge parameter on the system's dynamics is also explored, and it is discovered that preserving prey individuals below a certain threshold benefits both species. However, if we continue to preserve them, it will have a negative impact on predators. This result agrees with the recent findings demonstrated by Gupta *et al.* [48]. They assumed the prey refuge proportional to only prey density and investigated that providing refugia to prey population up to a certain value is lucrative for both species. On the other hand, we considered prey refuge proportional to prey-predator interactions to make the system more realistic from the ecological point of view.

Next, we investigated the rich and complex dynamics of non-spatial delayed system analytically and numerically. We observed that introducing fear response delay in the system can

induce a limit cycle via Hopf-bifurcation. We derived a critical value for the delay parameter such that if $\tau < \tau_0$, the positive equilibrium E^* remains stable. If the delay parameter crosses the value τ_0, a stable limit cycle is generated via Hopf-bifurcation.

For the non-delayed spatiotemporal model, we analyzed the local stability and derived the conditions for diffusion-driven instability. We investigated the global stability for the unique interior equilibrium. Various Turing patterns are obtained, which can better explain the spatial distribution of species with time. We explored that the fear effect and prey refuge have a considerable impact on creating spatial patterns, similar to temporal dynamics. Turing patterns show a transition from “cold-spots” to “a combination of holes and stripes" to “stripes” and then back to “hot-spots” on increasing the fear parameter. We also noticed that an increase in the refuge parameter might alter the density of prey population. Also, the impact of diffusive coefficients on the distribution patterns is explored. Han *et al.* [52] studied the formation of the Turing pattern in a diffusive predator-prey system incorporating prey refuge in proportion to both species with Beddington–DeAngelis functional response. To take one step closer to reality, we examined the consequences of fear response delay on pattern formation in the present study. Moreover, the existence of Hopf-bifurcation is also investigated for the delayed spatiotemporal system analytically.

The present study can help us better understand how the fear imposed on the prey population and prey refuge can affect species’ extinction and coexistence from an ecological perspective. It also explains how changing parameters can affect the constituent population’s distribution pattern.

Chapter 4

Spatiotemporal dynamics of a multi-delayed prey-predator system with variable carrying capacity[1]

4.1 Introduction

The study of the dynamic relationship between prey and predator has become a hot issue in both ecology and mathematical biology. Most biological phenomena involve a time delay to provide a realistic perspective. The time needed for any biological process to manifest itself is known as a time delay. Incorporating time delay in ecological models could provide more intriguing dynamics than non-delayed models [46, 74, 92]. A wide variety of research has been devoted to investigate the complex dynamics of a prey-predator model incorporating various discrete delays [8, 42, 118]. Gestation delay is the time the predator species takes to digest their prey completely and reproduce their progeny. Jana *et al.* [62] proposed and analyzed a mathematical model with prey refuge and gestation delay and observed that the discrete delay preserves stability. Zhang *et al.* [191] examined a Gause-type two prey and one predator system and concluded that the gestation delay destabilizes the system dynamics. Dubey and Kumar [40] studied a stage-structured dynamical system and found that incorporating multiple discrete delays switches the system's stability. Bhargava *et al.* [11] investigated a prey-predator model system and observed that the system exhibits chaotic behavior with respect to the multiple discrete delays. Pal *et al.* [115] explored a dynamical system with two discrete delays and noticed that the system switches stability for the higher delay parameter values. Bhunia *et al.* [13] explored the explicit impacts of delay parameter and harvesting on a fractional prey-predator system.

A functional response is a measure of successfully attacked prey by the predator. In recent years, selecting an appropriate functional response has been a matter of subject in the ecological field. In a series of influential articles that began in the late 1950s, Holling established three

[1]This chapter is based on our paper published in *Chaos: An Interdisciplinary Journal of Nonlinear Science*, **33**, 113116, 2023.

broad categories of functional response [55, 56, 57]. A lot of research has been done since then using Holling functional response [37, 59, 81, 194]. Holling Type II functional response represents a predator's average feeding rate when the predator spends some time searching for prey and some time, apart from seeking, handling each captured prey [11, 26, 147].

The distribution of species across the spatial domain is ubiquitous in ecology. The species disperse in the pursuit of food, shelter, mates, etc., forming many fascinating spatial patterns [103, 160]. Pattern formation can help predict biological incursions and promote conservation efforts for endangered species [124]. Turing [165] first gave the concept of Turing Instability, which can lead to the formation of time-independent spatial patterns in a homogenous environment. Kumari [77] investigated a tri-trophic food chain model and examined Turing and non-Turing patterns for the spatially extended system. Tripathi *et al.* [163] proposed a diffusive predator-prey model with prey reserve and explored the stabilizing effects of diffusion coefficients on the spatio-temporal dynamics. Manna and Banerjee [97] analyzed a delayed prey-predator system with the Allee effect and concluded that a high value of gestation delay might produce spatiotemporal chaos in the system. Song *et al.* [154] examined the stability and diffusion-induced instability regions in a spatially extended prey-predator system with hunting cooperation. Zhang *et al.* [189] studied the spatiotemporal pattern formation induced by the delay parameter in a dynamical system incorporating the fear effect. Sasmal *et al.* [142] explored the spatiotemporal dynamics and analyzed the Turing patterns in a spatially extended prey-predator system with hunting cooperation and fear effect. Anshu *et al.* [4] investigated the combined effects of fear and prey refuge on the pattern formation in a delayed prey-predator system. Also, they explored how the delay parameter affects the spatiotemporal dynamics. Han *et al.* [50] examined all possible stationary patterns in a spatiotemporal system with the Allee effect and hunting cooperation. They determined spatiotemporal chaos as time and space-varying solutions. Souna *et al.* [156] studied the spatial patterns in a prey-predator system with Holling III functional response and found that the predator-taxis coefficient gives rise to either a supercritical or subcritical Turing bifurcation.

To the best of the authors' knowledge, the dynamics of a prey-predator system in a diffusive environment with variable carrying capacity and multiple delays have not been considered. Thus, in the next section, we explain the formulation of the model.

4.2 Formulation of mathematical model

The complex prey-predator interactions in ecology are ubiquitous as well as inherently fascinating. Various mathematical models have been proposed and analyzed to understand ecological

complexity. In the present study, we consider a dynamical model to study the complex interactions of prey-predator environment given by the following pair of coupled non-linear equations:

$$\begin{aligned} \frac{dx}{dt} &= rx\left(1-\frac{x}{K_0}\right)-\frac{\alpha xy}{a+x}, \\ \frac{dy}{dt} &= \frac{c\alpha xy}{a+x}-\delta_0 y-\delta_1 y^2, \end{aligned} \tag{4.1}$$

where $x(t)$ and $y(t)$ represent the prey and predator densities at any given time t, respectively. The present work assumes that prey and predator interact via the Holling-II type functional response. Considering Holling type-II functional response makes the system more ecologically realistic as the resources are limited. Here, r is the intrinsic growth rate of the prey population, α is the attack rate, K_0 is the carrying capacity of prey, a is the half-saturation constant, c is the conversion efficiency, δ_0 is the natural mortality rate of predator population and δ_1 is the death rate of predator population due to intraspecies competition. All the aforementioned parameters take only positive values.

The maximum density of the species that the ecosystem can sustain depending on the resources available and changing environmental conditions is the carrying capacity of the particular species. Many ecological models have been framed, treating carrying capacity as a constant. But if the basic needs, such as adequate food, water, shelter, etc., are not met due to limited resources, then the population starts decreasing until resources rebound. Environmental factors such as climate change can significantly affect the prey population and the carrying capacity of the ecosystem. For example, the Dust Bowl during the 1930s significantly affected water availability, natural vegetation, and habitat loss, resulting in the decline of the prey population and, hence, the environmental carrying capacity in the affected areas [182]. Hence, changing environmental conditions may vary the carrying capacity over time. It has also been observed that the carrying capacity depends upon the past population size and their associated activities [185, 186]. Many prey activities contribute towards resource conservation, which can positively affect the carrying capacity of the environment. For example, the phenomena of selective grazing leads to the coexistence of a variety of plants, which promotes biodiversity. In such cases, the carrying capacity can be considered as an increasing function of the prey population. However, some activities of the prey population may cause a decrease in the carrying capacity. For example, considering the case of the Kaibab Plateau and the Bison Population (early 1900s) [133], the increased population of mule deer led to overgrazing and habitat degradation, which affected the environmental carrying capacity. In such situations, the carrying capacity can be taken as a decreasing function of the prey population. Thus, it is ecologically justified to consider varying carrying capacity. Several researchers have analyzed a prey-predator system with varying carrying capacities [85, 86, 135, 151]. This work assumes that past activities of

the species can significantly influence the intrinsic carrying capacity of an ecosystem. But the effect of the past activities on the induced carrying capacity is not instantaneous. Therefore, there is a time lag involved. Also, a time lag is involved in prey consumption and predators reproducing their progeny, referred to as gestation delay. Ganguli *et al.*[44] proposed a prey-predator model with a carrying capacity that varies with time. They concluded that no limit cycle exists for the constant carrying capacity. Motivated by the abovementioned scenarios, the prey-predator interaction is depicted with the following delay differential equations:

$$\begin{aligned} \frac{dx}{dt} &= rx\left(1-\frac{x}{K_0+\beta x(t-\tau_1)}\right)-\frac{\alpha xy}{a+x}, \\ \frac{dy}{dt} &= \frac{c\alpha x(t-\tau_2)y(t-\tau_2)}{a+x(t-\tau_2)}-\delta_0 y-\delta_1 y^2, \end{aligned} \tag{4.2}$$

where β measures the effect of past activities on the current carrying capacity K_0, it may assume positive or negative values depending on whether the activities are constructive ($\beta > 0$) or destructive ($\beta < 0$). The effect of the past activities is delayed by a time lag τ_1, and τ_2 is the gestation delay.

To take into consideration the spatial variations in the population densities, the proposed system is spatially extended. The following pair of parabolic partial differential equations govern the corresponding spatiotemporal model:

$$\begin{aligned} \frac{\partial x}{\partial t} &= \left[rx\left(1-\frac{x}{K_0+\beta x(t-\tau_1)}\right)-\frac{\alpha xy}{a+x}\right]+D_1\nabla^2 x, \\ \frac{\partial y}{\partial t} &= \left[\frac{c\alpha x(t-\tau_2)y(t-\tau_2)}{a+x(t-\tau_2)}-\delta_0 y-\delta_1 y^2\right]+D_2\nabla^2 y, \end{aligned} \tag{4.3}$$

subjected to the non-negative initial conditions,
$x(u,v,s)=\phi_1(u,v,s)\geq 0,\ \ y(u,v,s)=\phi_2(u,v,s)\geq 0,\ \ s\in[-\tau,0]$ where $\tau=\max\{\tau_1,\tau_2\},\quad \phi_i\in \mathbb{C}([-\tau,0])\rightarrow\mathbb{R}^+(i=1,2),$

$$\Omega=\{(u,v):0\leq u\leq M',0\leq v\leq N'\},\quad \frac{\partial x}{\partial \eta}=\frac{\partial y}{\partial \eta}=0.$$

Here, D_1 and D_2 represent the self-diffusion coefficients for prey and predator species, respectively. The rectangular habitat $\Omega\subseteq\mathbb{R}^2$ is a bounded domain with the smooth boundary $\partial\Omega$ and η is the unit outward normal to $\partial\Omega$. The homogenous Neumann boundary conditions are used which ensure that the boundary is impermeable.

We make the system non-dimensional by introducing the dimensionless variables as $\bar{x}=\frac{x}{K_0}$, $\bar{y}=\frac{y}{K_0}$, $\bar{t}=tr$, $\bar{\tau}_1=\tau_1 r$, $\bar{\tau}_2=\tau_2 r$ and the dimensionless model is given by the following pair of

reaction-diffusion equations (after dropping bars):

$$\begin{aligned} \frac{\partial x}{\partial t} &= \left[x\left(1-\frac{x}{1+\beta x(t-\tau_1)}\right)-\frac{mxy}{b+x}\right]+D_x\nabla^2 x, \\ \frac{\partial y}{\partial t} &= \left[\frac{cmx(t-\tau_2)y(t-\tau_2)}{b+x(t-\tau_2)}-\gamma_0 y-\gamma_1 y^2\right]+D_y\nabla^2 y, \end{aligned} \tag{4.4}$$

where $m=\frac{\alpha}{r}$, $b=\frac{a}{K_0}$, $D_x=\frac{D_1K_0}{r}$, $D_y=\frac{D_2K_0}{r}$, $\gamma_0=\frac{\delta_0}{r}$, and $\gamma_1=\frac{\delta_1K_0}{r}$.

In the present chapter, we extended the model proposed by Pati and Ghosh [122] in which they analyzed a delayed prey-predator system with variable carrying capacity. They considered that prey and predator interact via linear functional response. In this manuscript, we assumed a Holling type II functional response, which is ecologically justified as it reflects the constraints and complexities of prey-predator interaction in natural ecosystems, including limited resource availability and predator satiation. Incorporating the gestation delay for predators enables us to unveil the intriguing dynamics of species interactions where reproductive responses are not instantaneous. Further, this study demonstrated how the local interactions between the species and diffusive phenomena within a specified habitat give rise to self-organizing structures. Spatial dynamics enhance the complexity of the findings, which are explained with the help of numerical simulations.

4.3 Mathematical analysis of temporal model

4.3.1 Positivity and boundedness of the solutions

We consider the model (4.4) without delay without diffusion which can be written as

$$\begin{aligned} \frac{dx}{dt} &= \left[x\left(1-\frac{x}{1+\beta x}\right)-\frac{mxy}{b+x}\right], \\ \frac{dy}{dt} &= \left[\frac{cmxy}{b+x}-\gamma_0 y-\gamma_1 y^2\right]. \end{aligned} \tag{4.5}$$

It is easy to see that all the solutions of the system (4.5) with non-negative initial conditions are always non-negative. In the next theorem, we shall show that all the solutions are bounded.

Theorem 4.3.1. *All the solutions of the system (4.5) are bounded above with the mentioned properties:*

1. *If $\beta>0$, then*

$$\limsup_{t\to\infty}\left(x(t)+\frac{y(t)}{c}\right)\leq\frac{(2-\beta(1+\gamma_0))-2\sqrt{1-\beta(1+\gamma_0)}}{\gamma_0\beta^2},$$

provided $(1-\beta(1+\gamma_0))>0$.

2. *If* $\beta<0$, *then*

$$\limsup_{t\to\infty} x(t) \le \min\{1,\frac{1}{\alpha^*}\}, \qquad \textit{where}\ \ \alpha^*=-\beta,$$
$$\limsup_{t\to\infty} y(t) \le \frac{1}{\gamma_1}\left(\frac{cmx_{max}}{b}-\gamma_0\right).$$

Proof. **Case I.** Let $\beta>0$.

Let us assume $z(t)=x(t)+\frac{1}{c}y(t)$. Now, from system (4.5), we have

$$\frac{dx}{dt}+\frac{1}{c}\frac{dy}{dt}=x\left(1-\frac{x}{1+\beta x}\right)-\frac{\gamma_0}{c}y-\frac{\gamma_1}{c}y^2,$$
$$\frac{dx}{dt}+\frac{1}{c}\frac{dy}{dt}<(1+\gamma_0)x-\frac{x^2}{1+\beta x}-\gamma_0 z.$$

Let $h(x)=(1+\gamma_0)x-\frac{x^2}{1+\beta x}$.

We find the maxima for the function $h(x)$; i.e., $h_{max}=\frac{(2-\beta(1+\gamma_0))-2\sqrt{1-\beta(1+\gamma_0)}}{\beta^2}$. Then similar to the proof of Theorem (2.1) in [144], our results follow.

Case II. If $\beta<0$

From the first equation of the model (4.5), we have

$$\frac{dx}{dt}=\left[x\left(1-\frac{x}{1+\beta x}\right)-\frac{mxy}{b+x}\right],$$
$$\frac{dx}{dt}\le x(1-x),$$

$$\lim_{t\to\infty}\sup x(t) \ \le\ 1. \tag{4.6}$$

Also,

$$1-\alpha^* x>0, \quad \textit{where}\ \ \alpha^*=-\beta, \quad x<\tfrac{1}{\alpha^*}. \tag{4.7}$$

From (4.6) and (4.7), we obtain

$$\limsup_{t\to\infty} x(t) \le \min\{1,\frac{1}{\alpha^*}\}, \qquad \text{where}\ \ \alpha^*=-\beta.$$

Similarly, we obtain the upper bound for the predator population; i.e.,

$$\limsup_{t\to\infty} y(t) \leq \frac{1}{\gamma_1}\left(\frac{cmx_{max}}{b} - \gamma_0\right).$$

■

4.3.2 Existence of equilibria

We have the following possibilities for different equilibria of the system (4.5).

- The extinction equilibrium $E_0(0,0)$, which always exists.
- The prey-only equilibrium $E_1(\frac{1}{1-\beta},0)$, which exists if $1-\beta > 0$.
- We can find the coexistence equilibrium by solving the following pair of equations:

$$\begin{aligned} \left(1 - \tfrac{x}{1+\beta x}\right) - \tfrac{my}{b+x} &= 0, \\ \tfrac{cmx}{b+x} - \gamma_0 - \gamma_1 y &= 0. \end{aligned} \tag{4.8}$$

  Solving the above pair of equations leads to a cubic polynomial in x given by

$$F(x) = A_0x^3 + A_1x^2 + A_2X + A_3 = 0, \tag{4.9}$$

  where

$$A_0 = \gamma_1(\beta - 1), \tag{4.10}$$
$$A_1 = (\gamma_1 - 2b\gamma_1 + 2b\gamma_1\beta - cm^2\beta + m\gamma_0\beta), \tag{4.11}$$
$$A_2 = 2b\gamma_1 - \gamma_1 b^2 + \gamma_1\beta b^2 - cm^2 + m\gamma_0 + m\gamma_0\beta b, \tag{4.12}$$
$$A_3 = \gamma_1 b^2 + m\gamma_0 b \ (> 0). \tag{4.13}$$

  Using Descarte's rule of sign for the cubic polynomial in x, we state the following theorem for the number of coexistence equilibria.

Theorem 4.3.2. **(a)** *The system possess no coexistence equilibrium under the following condition:*

$$\beta > \max\left\{1, \frac{\gamma_1(2b-1)}{2b\gamma_1 + m(\gamma_0 - cm)}, \frac{\gamma_1 b(b-2) - m(\gamma_0 - cm)}{(\gamma_1 b + m\gamma_0)b}\right\}.$$

(b) *The system possess unique coexistence equilibrium if any of the following two conditions are satisfied:*

$$(i)\frac{\gamma_1 b(b-2)-m(\gamma_0-cm)}{(\gamma_1 b+m\gamma_0)b}<\beta<1,$$
$$(ii)\beta<\min\left\{1,\frac{\gamma_1(2b-1)}{2b\gamma_1+m(\gamma_0-cm)}\right\}.$$

(c) *The system possess at most two coexistence equilibria if any of the following two conditions are satisfied:*

$$(i)1<\beta<\frac{\gamma_1(2b-1)}{2b\gamma_1+m(\gamma_0-cm)},$$
$$(ii)1<\beta<\frac{\gamma_1 b(b-2)-m(\gamma_0-cm)}{(\gamma_1 b+m\gamma_0)b}.$$

(d) *The system possess at most three coexistence equilibria under the following condition:*

$$\frac{\gamma_1(2b-1)}{2b\gamma_1+m(\gamma_0-cm)}<\beta<\min\left\{1,\frac{\gamma_1 b(b-2)-m(\gamma_0-cm)}{(\gamma_1 b+m\gamma_0)b}\right\}.$$

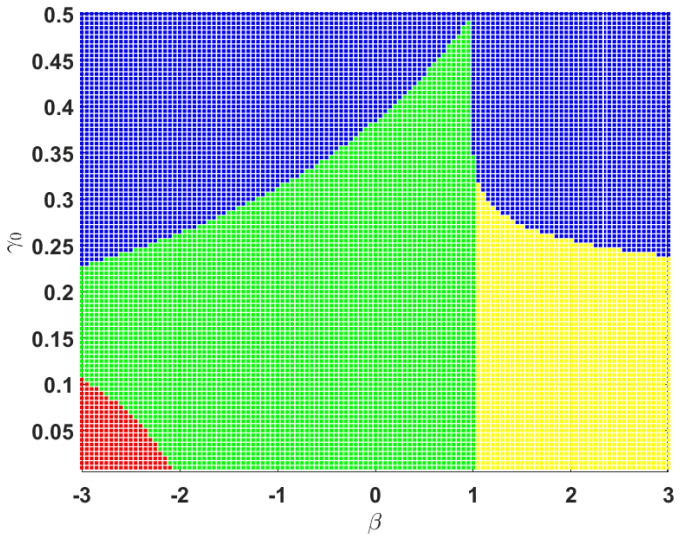

Fig. 4.1: Plot for the possible number of coexistence equilibria in the $\beta-\gamma_0$ parameter plane. This figure has $m=2$; $b=0.3$; $c=0.25$; $\gamma_1=0.3$ as fixed parameters and remaining two parameters β and γ_0 are varied.

Figure 4.1 depicts the plot for the number of possible coexistence equilibria in the $\beta - \gamma_0$ parameter plane for the system (4.5). Here, blue colour depicts no coexistence equilibrium, green region depicts region for unique coexistence equilibrium, yellow for two coexistence equilibria region, red gives the region for three coexistence equilibria.

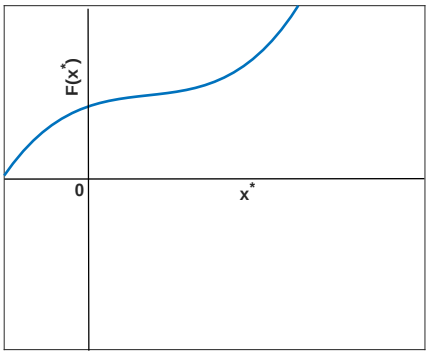

(a) No roots.

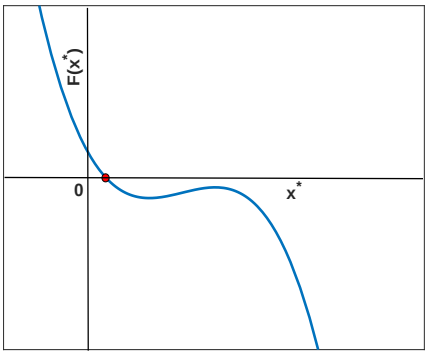

(b) Unique root.

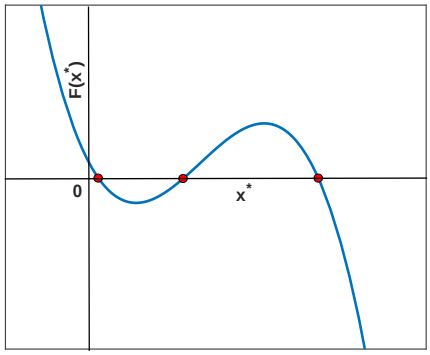

(c) Three roots.

Fig. 4.2: Number of possible roots of $F(x^*)$ given by (4.9) with varying γ_0 and β. Here, all the other parameters are fixed as $m = 2$, $b = 0.3$, $c = 0.25$, $\gamma_1 = 0.3$. γ_0 and β take the values as (a) $\gamma_0 = 0.3$, $\beta = 2$, (b) $\gamma_0 = 0.2$, $\beta = -1$ and, (c) $\gamma_0 = 0.05$, $\beta = -2.5$

.

In Fig. (4.2), we illustrated the possible roots of $F(x^*)$ given by (4.9) for different values of γ_0 and β. The red dots indicate the roots of $F(x^*)$ for the chosen set of parameters.

For the system to be dissipative, $\beta < \frac{1}{1+\gamma_0}$ $(if\ \beta > 0)$. Under this condition, the system (4.5) can have either no, unique or three coexistence equlibria as depicted in Fig. (4.3). For $\gamma_0 = 0.4$ and $\beta = 0.1$, the system has no coexistence equilibrium point. The system possesses a unique coexistence equilibrium for $\gamma_0 = 0.2$ and $\beta = 0.7$. Further, the system has three coexistence equilibria $\gamma_0 = 0.05$ and $\beta = -2.5$.

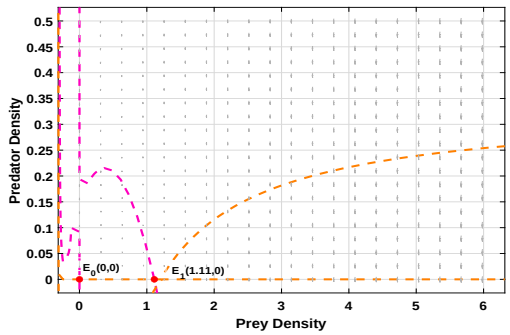

(a) No coexistence equilibrium for $\gamma_0 = 0.4$ and $\beta = 0.1$.

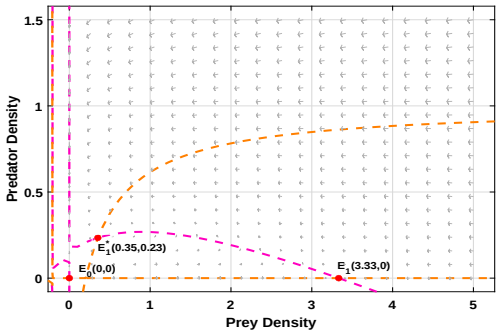

(b) Unique coexistence equilibrium for $\gamma_0 = 0.2$ and $\beta = 0.7$.

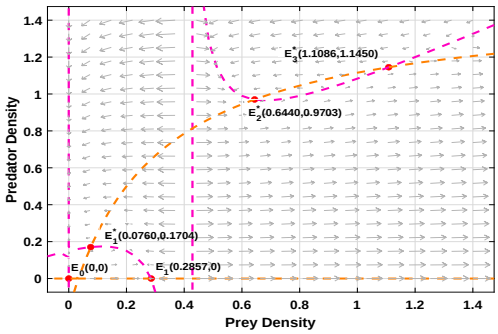

(c) Three coexistence equilibrium for $\gamma_0 = 0.05$ and $\beta = -2.5$.

Fig. 4.3: Number of possible coexistence equilibria with varying γ_0 and β. Here, $m = 2$, $b = 0.3$, $c = 0.25$ and $\gamma_1 = 0.3$ are the fixed parameters.

4.3.3 Stability analysis of various equilibria

First, we shall analyze the behavior of the system in the neighborhood of a particular equilibrium point.

4.3.3.1 Local stability analysis

For the local stability behavior, we linearize the system near the desired equilibrium and then determine the conditions for the negative real parts of the corresponding eigenvalues calculated from the Jacobian matrix. Keeping this in view, we state the following resuts for the local stability behavior of the concerned equilibria.

Theorem 4.3.3. *The extinction equilibrium $E_0(0,0)$ is always a saddle point.*

Proof. The eigenvalues associated with the extinction equilibrium are $\lambda_1 = 1(>0)$ and $\lambda_2 = -\gamma_0(<0)$. Hence, the result follows. ∎

Theorem 4.3.4. *The prey-only equilibrium $E_1(\frac{1}{1-\beta},0)$, whenever it exists, is locally asymptotically stable if and only if $cm < \gamma_0(b(1-\beta)+1)$.*

Proof. Eigenvalues associated with the equilibrium point $E_1(\frac{1}{1-\beta},0)$ are
$\lambda_1 = (\beta-1)(<0$ whenever E_1 exists) and $\lambda_2 = \frac{cm}{b(1-\beta)+1} - \gamma_0$. The prey-only equilibrium is locally asymptotically stable if and only if $\frac{cm}{b(1-\beta)+1} - \gamma_0 < 0$. Thus, our result follows. ∎

Theorem 4.3.5. *The coexistence equilibrium $E^*(x^*,y^*)$ is locally asymptotically stable if the following two conditions are satisfied:*

1. $\left(\frac{-bmy^*}{(b+x^*)^2} + \frac{(1+x^*(\beta-1)(2+\beta x^*)}{(1+\beta x^*)^2} - \gamma_1 y^*\right) < 0,$
2. $\left[\left(\frac{-bmy^*}{(b+x^*)^2} + \frac{(1+x^*(\beta-1)(2+\beta x^*)}{(1+\beta x^*)^2}\right)(-\gamma_1 y^*) + \left(\frac{bcmy^*}{(b+x^*)^2}\right)\left(\frac{mx^*}{(b+x^*)}\right)\right] > 0.$

Proof. The variational matrix at the coexistence equilibrium is

$$J_{E^*} = \begin{bmatrix} \frac{-bmy^*}{(b+x^*)^2} + \frac{(1+x^*(\beta-1)(2+\beta x^*)}{(1+\beta x^*)^2} & \frac{-mx^*}{(b+x^*)} \\ \frac{bcmy^*}{(b+x^*)^2} & -\gamma_1 y^* \end{bmatrix}.$$

Characteristic equation of the above matrix is given by

$$\lambda^2 - trace(J_{E^*})\lambda + det(J_{E^*}) = 0,$$

where

$$trace(J_{E^*}) = \left(\frac{-bmy^*}{(b+x^*)^2} + \frac{(1+x^*(\beta-1)(2+\beta x^*)}{(1+\beta x^*)^2} - \gamma_1 y^*\right),$$
$$det(J_{E^*}) = \left(\frac{-bmy^*}{(b+x^*)^2} + \frac{(1+x^*(\beta-1)(2+\beta x^*)}{(1+\beta x^*)^2}\right)(-\gamma_1 y^*) + \left(\frac{bcmy^*}{(b+x^*)^2}\right)\left(\frac{mx^*}{(b+x^*)}\right).$$

Using the Routh-Hurwitz criterion, the coexistence equilibrium $E^*(x^*,y^*)$ is locally asymptotically stable if and only if $trace(J_{E^*}) < 0$ and $det(J_{E^*}) > 0$, which proves the required result.

Remark: It is easy to see that if $x^* > \frac{1}{1-\beta}$, then both conditions (i) and (ii) are satisfied. This shows that $E^*(x^*,y^*)$ is locally symptotically stable if $x^* > \frac{1}{1-\beta}$. ∎

4.3.3.2 Global stability analysis for coexistence equilibrium

Theorem 4.3.6. *The coexistence equilibrium point $E^*(x^*,y^*)$, whenever it exists uniquely, is globally asymptotically stable under the following inequalities:*

(i) $b(b+x^*) > my_{max}(1+\beta x_{max})(1+\beta x^*)$ *when* $\beta > 0$,

(ii) $b(b+x^*) > my_{max}(1+\beta x^*)$ *when* $\beta < 0$.

Proof. Let us choose an appropriate Lyapunov function given by

$$W(x,y) = \left(x - x^* - x^* ln\tfrac{x}{x^*}\right) + \delta\left(y - y^* - y^* ln\tfrac{y}{y^*}\right).$$

Differentiating the above function w.r.t. time t and simplifying, we get

$$\dot{W} = -A_{11}(x-x^*)^2 + A_{12}(x-x^*)(y-y^*) - A_{22}(y-y^*)^2,$$

where

$$\begin{aligned} A_{11} &= \frac{1}{(1+\beta x)(1+\beta x^*)} - \frac{my}{(b+x)(b+x^*)}, \\ A_{12} &= \frac{m}{(b+x^*)}\left[\frac{\delta cb}{(b+x)} - 1\right], \\ A_{22} &= \delta\gamma_1. \end{aligned}$$

Using Sylvester's criterion for $\frac{dW}{dt}$ to be negative definite, we have $A_{11} > 0$, $A_{22} > 0$ and $A_{12}^2 < 4A_{11}A_{22}$.

It may be noted that conditions (i) and (ii) implies $A_{11} > 0$ when $\beta > 0$ and $\beta < 0$, respectively. Following $A_{11} > 0$ and maximizing A_{12}, if we choose $\delta = \frac{1}{c}$, then $A_{12}^2 < 4A_{11}A_{22}$ automatically holds true.

Hence, our result follows. ∎

Figure 4.4(a) illustrates the region (magenta) for the global stability behavior of the unique coexistence equilibria in the $\beta - \gamma_0$ plane. Further, the global stability of the unique coexistence equilibrium is depicted in phase portrait (Fig. 4.4(b)) for a chosen set of parameters.

4.3.4 Bifurcation analysis

4.3.4.1 Hopf-bifurcation analysis

The Jacobian matrix J_{E^*} at the coexistence equilibrium is calculated in the proof of Theorem 4.3.5.

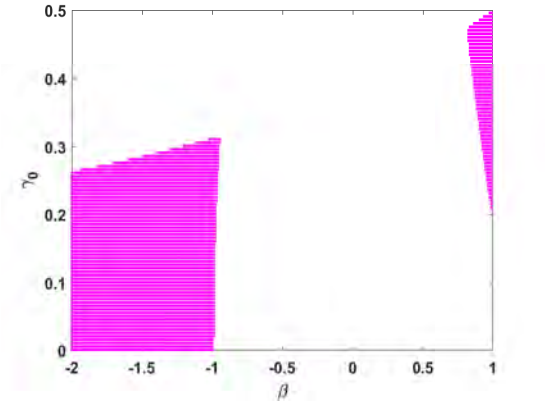

(a) Region for Global Stablility of unique coexistence eqilibrium in $\beta - \gamma_0$ parameter plane. Here, $m = 2$, $b = 0.3$, $c = 0.25$ and $\gamma_1 = 0.3$ are the fixed parameters.

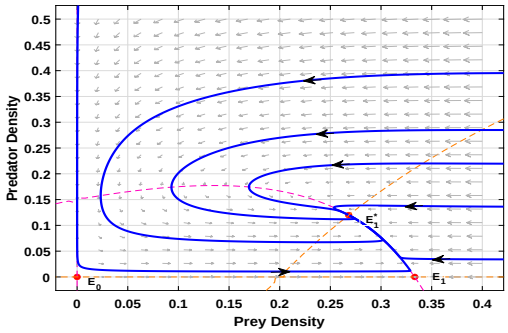

(b) Phase portrait depicting the global stability behavior of unique coexistence equilibrium. The parameters are fixed as $m = 2$, $b = 0.3$, $c = 0.25$, $\gamma_1 = 0.3$, $\beta = -2$ and $\gamma_0 = 0.2$.

Fig. 4.4: Global stability analysis of unique coexistence equilibrium.

The aforementioned matrix has the following characteristic equation:

$$\lambda^2 - trace(J_{E^*})\lambda + det(J_{E^*}) = 0. \tag{4.14}$$

We assume that the eigenvalues of the above equation takes the form as $\lambda(\beta) = \lambda_r(\beta) + i\lambda_{im}(\beta)$ and then, separating the real and imaginary parts, we get

$$\lambda_r^2 - \lambda_{im}^2 - trace(J_{E^*})\lambda_r + det(J_{E^*}) = 0, \tag{4.15}$$

$$2\lambda_r\lambda_{im} - trace(J_{E^*})\lambda_{im} = 0. \tag{4.16}$$

Now, we have $Re(\lambda(\beta)) = 0$ for Hopf-bifurcation to occur reducing the above pair of equations to

$$\begin{aligned} -\lambda_{im}^2 + det(J_{E^*}) &= 0, \quad \lambda_{im} \in \mathbb{R}, \\ -\lambda_{im} trace(J_{E^*}) &= 0, \quad \lambda_{im} \neq 0. \end{aligned}$$

Thus,

$$det(J_{E^*}) > 0 \text{ and } trace(J_{E^*}) = 0 \text{ at the critical value } \beta = \beta^*.$$

From $trace(J_{E^*}) = 0$, we obtain

$$\beta^* = \frac{(-2+x^*)(b+x^*)^2+2bmy^*+(b+x^*)(2(b+x^*)\gamma_1 y^* \pm \sqrt{x}\sqrt{(4+x^*)(b+x^*)^2-4bmy^*-4(b+x^*)^2\gamma_1 y^*})}{2x^*(-(b+x^*)^2+bmy^*+(b+x^*)^2 y^*\gamma_1)}.$$

Differentiating Eqs. (4.15) and (4.16) with regard to β and substituting $\lambda_r(\beta) = 0$, we get

$$-2\lambda_{im}\frac{d\lambda_{im}}{d\beta} - trace(J_{E^*})\frac{d\lambda_r}{d\beta} + \frac{d(det(J_{E^*}))}{d\beta} = 0, \tag{4.17}$$

$$2\lambda_{im}\frac{d\lambda_r}{d\beta} - \lambda_{im}\frac{d(trace(J_{E^*}))}{d\beta} - trace(J_{E^*})\frac{d\lambda_{im}}{d\beta} = 0. \tag{4.18}$$

Solving the preceding equations at the critical value $\beta = \beta^*$ gives us the following:

$$\left.\frac{d\lambda_r}{d\beta}\right|_{\beta=\beta^*} = \frac{1}{2}\left(\frac{d(trace(J_{E^*}))}{d\beta}\right) \neq 0,$$

provided $\frac{d(trace(J_{E^*}))}{d\beta} \neq 0$.

4.4 Dynamics of delayed temporal model

4.4.1 Local stability and Hopf-bifurcation analysis

In this section, we examined the dynamics of the following delayed non-spatial system:

$$\begin{aligned} \frac{dx}{dt} &= \left[x\left(1 - \frac{x}{1+\beta x(t-\tau_1)}\right) - \frac{mxy}{b+x}\right], \\ \frac{dy}{dt} &= \left[\frac{cmx(t-\tau_2)y(t-\tau_2)}{b+x(t-\tau_2)} - \gamma_0 y - \gamma_1 y^2\right]. \end{aligned} \tag{4.19}$$

We can rewrite the above model as

$$\frac{dW(t)}{dt} = F(W(t), W(t-\tau_1), W(t-\tau_2)),$$

where

$$W(t) = [x(t), y(t)]^T,$$
$$W(t-\tau_i) = [x(t-\tau_i), y(t-\tau_i)]^T, \quad i = 1, 2.$$

Let $x(t) = x^* + x'(t)$, $y(t) = y^* + y'(t)$. Now, we linearize the system (4.19) around the coexistence equilibrium $E^*(x^*, y^*)$, we obtain

$$\frac{dU}{dt} = PU(t) + QU(t-\tau_1) + RU(t-\tau_2),$$

where

$$P = \frac{\partial F}{\partial U(t)}_{E^*}, Q = \frac{\partial F}{\partial U(t-\tau_1)}_{E^*}, R = \frac{\partial F}{\partial U(t-\tau_2)}_{E^*}, U(t) = [x'(t), y'(t)]^T.$$

The variational matrix of the model (4.19) is given as follows:

$$J = P + Qe^{-\lambda\tau_1} + Re^{-\lambda\tau_2}.$$

Simplifying the aforementioned matrix, we get

$$J_{E^*} = \begin{bmatrix} a_1 + a_5 e^{-\lambda\tau_1} & a_2 \\ a_3 + a_6 e^{-\lambda\tau_2} & a_4 + a_7 e^{-\lambda\tau_2} \end{bmatrix},$$

where

$$\begin{aligned} a_1 &= 1 - \frac{2x^*}{1+\beta x^*} - \frac{mby^*}{(b+x^*)^2}, \quad a_2 = \frac{-mx^*}{b+x^*}, \quad a_3 = 0, \quad a_4 = -\gamma_0 - 2\gamma_1 y^*, \\ a_5 &= \frac{\beta x^{*2}}{(1+\beta x^*)^2}, \quad a_6 = \frac{cmby^*}{(1+\beta x^*)^2}, \quad a_7 = \frac{cmx^*}{(b+x^*)}. \end{aligned} \tag{4.20}$$

The corresponding characteristic equation:

$$\lambda^2 - [(a_1 + a_5 e^{-\lambda\tau_1}) + (a_4 + a_7 e^{-\lambda\tau_2})]\lambda + [(a_1 + a_5 e^{-\lambda\tau_1})(a_4 + a_7 e^{-\lambda\tau_2}) - a_2(a_3 + a_6 e^{-\lambda\tau_2})] = 0.$$

Simplifying the above equation leads to

$$\lambda^2 + p_1\lambda + p_2 + (p_3 + p_4\lambda)e^{-\lambda\tau_1} + (p_5 + p_6\lambda)e^{-\lambda\tau_2} + p_7 e^{-\lambda(\tau_1+\tau_2)} = 0, \tag{4.21}$$

where

$$\begin{aligned} p_1 = -(a_1 + a_4), \quad p_2 = (a_1 a_4 - a_2 a_3), \quad p_3 = a_4 a_5, \\ p_4 = -a_5, \quad p_5 = (a_1 a_7 - a_2 a_6), \quad p_6 = -a_7, \quad p_7 = a_5 a_7. \end{aligned}$$

Remark: If $\tau_1 = 0,\ \tau_2 = 0$, then the characteristic equation (4.21) becomes

$$\lambda^2 + (p_1 + p_4 + p_6)\lambda + (p_2 + p_3 + p_5 + p_7) = 0,$$

which is same as characteristic equation in case of non-delayed system.

(H1): $p_1 + p_4 + p_6 > 0,\ p_2 + p_3 + p_5 + p_7 > 0.$

All the roots of Eq. (4.21) have negative real parts if and only if (H_1) holds.

Case (1): $\tau_1 = 0,\ \tau_2 > 0.$

Then Eq. (4.21) becomes

$$\lambda^2 + (p_1 + p_4)\lambda + (p_2 + p_3) + (p_5 + p_7 + p_6\lambda)e^{-\lambda\tau_2} = 0. \tag{4.22}$$

Let us assume that above equation has a roots of the form $i\omega(\omega > 0)$ such that

$$\begin{aligned} -\omega^2 + (p_1 + p_4)i\omega + (p_2 + p_3) + (p_5 + p_7 + i\omega p_6)e^{-i\omega\tau_2}) = 0, \\ -\omega^2 + (p_1 + p_4)i\omega + (p_2 + p_3) + (p_5 + p_7 + i\omega p_6)(cos(\omega\tau_2) - isin(\omega\tau_2)) = 0. \end{aligned}$$

Simplifying and then separating real and imaginary parts,

$$\begin{aligned} (p_5 + p_7)cos(\omega\tau_2) + \omega p_6 sin(\omega\tau_2) &= \omega^2 - (p_2 + p_3), \\ \omega p_6 cos(\omega\tau_2) - (p_5 + p_7)sin(\omega\tau_2) &= -\omega(p_1 + p_4). \end{aligned} \tag{4.23}$$

The above-mentioned equations are squared and added to obtain

$$z^2 + b_1 z + b_2 = 0, \tag{4.24}$$

where $b_1 = (p_1 + p_4)^2 - 2(p_2 + p_3) - p_6^2, \quad b_2 = (p_2 + p_3)^2 - (p_5 + p_7)^2, \quad z = \omega^2$. Assuming $h(z) = z^2 + b_1 z + b_2$.

(H2): $b_1 > 0,\ b_2 > 0.$

If (H_2) holds true, then (4.24) has no positive roots i. e., no such ω exists. Hence, $E^*(x^*, y^*)$ is asymptotically stable for all $\tau_2 > 0$ if (H_1) and (H_2) hold true.

(H3): $b_2 < 0.$

If (H3) holds true, then Eq. (4.24) has a unique positive root ω_0^2. On substituting ω_0 in Eq. (4.23), we get

$$\begin{aligned} (p_5 + p_7)cos(\omega_0\tau_2) + \omega_0 p_6 sin(\omega_0\tau_2) &= {\omega_0}^2 - (p_2 + p_3), \\ \omega_0 p_6 cos(\omega_0\tau_2) - (p_5 + p_7)sin(\omega_0\tau_2) &= -\omega_0(p_1 + p_4), \end{aligned}$$

which leads to

$$\tau_{2i} = \frac{1}{\omega_0}\left[cos^{-1}\left(\frac{(p_5+p_7)[{\omega_0}^2-(p_2+p_3)]-{\omega_0}^2 p_6(p_1+p_4)}{[(p_5+p_7)^2+{\omega_0}^2{p_6}^2]}\right)\right]+\frac{2\pi i}{\omega_0} \quad ; \quad i=0,1,2,..... \tag{4.25}$$

(H4): $b_1<0$, $b_2>0$ and ${b_1}^2>4b_2$.

If (H1) and (H4) hold, then Eq. (4.24) has two distinct positive roots $\omega_{\pm}^2$. Substituting in Eq. (4.23), we obtain

$$\tau_{2j}^{\pm} = \frac{1}{\omega_{\pm}}\left[cos^{-1}\left(\frac{(p_5+p_7)({\omega_{\pm}}^2-(p_2+p_3))-{\omega_{\pm}}^2 p_6(p_1+p_4)}{((p_5+p_7)^2+{\omega_{\pm}}^2{p_6}^2)}\right)\right]+\frac{2j\pi}{\omega_{\pm}} \quad ; \quad j=0,1,2,..... \tag{4.26}$$

Let $\lambda(\tau_{2i})=i\omega_0$ be a root of Eq. (4.22). Then, differentiating Eq. (4.22) w.r.t. τ_2, we have

$$\left(\frac{d\lambda}{d\tau_2}\right)^{-1} = \frac{(2\lambda+p_1+p_4)e^{\lambda\tau_2}+p_6}{(p_5+p_7+p_6\lambda)\lambda}-\frac{\tau_2}{\lambda},$$

$$\left[\frac{d\lambda}{d\tau_2}\right]^{-1}_{\lambda=i\omega_0} = \frac{((p_1+p_4)cos(\omega_0\tau_2)-2\omega_0 sin(\omega_0\tau_2)+p_6)+i(2\omega_0 cos(\omega_0\tau_2)+(p_1+p_4)sin(\omega_0\tau_2))}{-{p_6}^2+\imath\omega_0(p_5+p_7)} - \frac{\tau_2}{i\omega_0},$$

$$Re\left[\frac{d\lambda}{d\tau_2}\right]^{-1}_{\lambda=i\omega_0} = \frac{(p_1+p_4)^2-{p_6}^2+2{\omega_0}^2-2(p_2+p_3)}{(p_5+p_7)^2+{p_6}^2{\omega_0}^2},$$

$$Re\left[\frac{d\lambda}{d\tau_2}\right]^{-1}_{\lambda=i\omega_0} = \frac{h'(\omega_0^2)}{(p_5+p_7)^2+{p_6}^2{\omega_0}^2}.$$

(H_{5A})**:** $h'({\omega_0}^2)>0$.

Then, $\left[\frac{d}{d\tau_2}Re(\lambda)\right]_{\lambda=i\omega_0}>0$ holds under assumption (H_{5A}).

Similarly, let us consider that Eq. (4.22) has roots $\lambda=i\omega_{\pm}$.

(H_{5B})**:** $h'({\omega_+}^2)>0$ $(resp.\ h'({\omega_-}^2)<0)$ holds, then

$\left[\frac{d}{d\tau_2}Re(\lambda)\right]_{\lambda=i\omega_+}>0$ $(resp.\ \left[\frac{d}{d\tau_2}Re(\lambda)\right]_{\lambda=i\omega_-}<0)$ hold under assumption (H_{5B}).

Now, the following theorem can be stated to summarize the above analysis.

Theorem 4.4.1. *If $\tau_1=0$ and $\tau_2>0$ for the model system (4.19), then we can conclude the following:*

- *$E^*(x^*,y^*)$ is locally asymptotically stable for all $\tau_2>0$ under (H_1) and (H_2).*
- *$E^*(x^*,y^*)$ is unstable for all $\tau_2>0$ if (H_1) fails to hold and (H_2) holds true.*

- *Under* (H_1), (H_3) *and* (H_{5A}), $E^*(x^*,y^*)$ *is asymptotically stable for all* $\tau_2 < \tau_{20}$ *and unstable* $\tau_2 > \tau_{20}$ *and the system undergoes Hopf-bifurcation at* $\tau_2 = \tau_{20}$.
- *If* (H_1), (H_4), *and* (H_{5B}) *hold then the coexistence equilibrium* $E^*(x^*,y^*)$ *is locally asymptotically stable in the intervals* $\tau_2 \in [0,\tau_{20}^+) \cup (\tau_{20}^-,\tau_{21}^+) \cup ..... \cup (\tau_{2(n-1)}^-,\infty)$ *and for the interval range* $\tau_2 \in (\tau_{20}^+,\tau_{20}^-) \cup ..... \cup (\tau_{2(n)}^+,\infty)$, $E^*(x^*,y^*)$ *is unstable. The system* (4.19) *experiences Hopf-bifurcation at* $\tau_2 = \tau_{2j}^{\pm}$ *for j=1,2,3,...*

Case (2): $\tau_1 > 0,\ \tau_2 = 0$. In this case, analysis is similar to case(1), and thus we state the following theorem.

Theorem 4.4.2. *For* $\tau_1 > 0,\ \tau_2 = 0$, *the system undergoes Hopf-bifurcation at* $\tau_1 = \tau_{10}$. *The coexistence* E^* *is locally asymptotically stable for* $\tau_1 < \tau_{10}$ *and unstable when* $\tau_1 > \tau_{10}$, *where* τ_{10} *is given by*

$$\tau_{10} = \frac{1}{\omega_0}\left[cos^{-1}\left(\frac{(p_3+p_7)[{\omega_0}^2-(p_2+p_5)]-{\omega_0}^2p_4(p_1+p_6)}{[(p_3+p_7)^2+{\omega_0}^2{p_4}^2]}\right)\right]. \tag{4.27}$$

Case (3): $\tau_1 > 0,\ \tau_2 > 0$. Now, we can consider that τ_1 lies in the stable interval $(0,\tau_{10})$ and τ_2 is treated as a parameter. Assuming that the Eq. (4.21) has a root $i\omega(\omega > 0)$, then substituting back in Eq. (4.21) and comparing real and imaginary parts, we obtain

$$\begin{aligned}\omega^2 - p_2 - p_3cos(\omega\tau_1) - p_4\omega sin(\omega\tau_1) =& cos(\omega\tau_2)[p_5 + p_7cos(\omega\tau_1)] \\ &+ sin(\omega\tau_2)[p_6\omega - p_7sin(\omega\tau_1)],\end{aligned} \tag{4.28}$$

$$\begin{aligned}-p_1\omega - p_4\omega cos(\omega\tau_1 + p_3sin(\omega\tau_1)) =& cos(\omega\tau_2)[p_6\omega - p_7sin(\omega\tau_1)] \\ &+ sin(\omega\tau_2)[-p_5 - p_7cos(\omega\tau_1)].\end{aligned} \tag{4.29}$$

Eliminating τ_2 from above equations will give us

$$\begin{aligned}(\omega^2-p_2)^2 + p_3^2 + p_4^2\omega^2 + p_1^2\omega^2 - p_6^2\omega^2 - p_7^2 + [p_1p_4\omega^2 - 2p_3(\omega^2-p_2) - 2p_5p_7]cos(\omega\tau_1) - \\ [p_4\omega(\omega^2-p_2) + p_1p_3\omega + 2p_6p_7\omega]sin(\omega\tau_1) = 0.\end{aligned} \tag{4.30}$$

The above equation is a transcedental equation. Therefore, it is not easy to predict the nature of its roots. Therefore, we assume that Eq. (4.30) has atleast one root (ω_0). Equations (4.28) and (4.29) can be re-written as:

$$A_1 = B_1cos(\omega_0\tau_2) + B_2sin(\omega_0\tau_2), \tag{4.31}$$

$$A_2 = B_2cos(\omega_0\tau_2) - B_1sin(\omega_0\tau_2), \tag{4.32}$$

where

$$\begin{aligned}
A_1 &= \omega_0^2 - p_2 - p_3 cos(\omega_0\tau_1) - p_4\omega_0 sin(\omega_0\tau_1),\\
B_1 &= p_5 + p_7 cos(\omega_0\tau_1),\\
A_2 &= -p_1\omega_0 - p_4\omega_0 cos(\omega_0\tau_1) + p_3 sin(\omega_0\tau_1),\\
B_2 &= p_6\omega_0 - p_7 sin(\omega_0\tau_1).
\end{aligned}$$

Solving above equations lead to

$$\tau_{2i} = \frac{1}{\omega_0}\left[cos^{-1}\left(\frac{A_1B_1 + A_2B_2}{A_1^2 + B_1^2}\right)\right] + \frac{2\pi i}{\omega_0}; \quad i = 0,1,2,3,...$$

Now, we verify the transversality condition by substituting $\lambda = \xi + i\omega$ in Eq. (4.21) and then differentiating it w.r.t. τ_2, and putting $\tau_2 = \tau_2^*$, $\omega = \omega_0^*$, $\xi = 0$, we get

$$\begin{aligned}
Q_1\left[\frac{d\xi}{d\tau_2}\right]_{\tau_2=\tau_{20}} + Q_2\left[\frac{d\omega}{d\tau_2}\right]_{\tau_2=\tau_{20}} &= R_1,\\
-Q_2\left[\frac{d\xi}{d\tau_2}\right]_{\tau_2=\tau_{20}} + Q_1\left[\frac{d\omega}{d\tau_2}\right]_{\tau_2=\tau_{20}} &= R_2,
\end{aligned} \tag{4.33}$$

where

$$\begin{aligned}
Q_1 &= p_1 - p_3\tau_1 cos(\omega\tau_1) + p_4 cos(\omega\tau_1) - p_4\omega\tau_1 sin(\omega\tau_1) - p_5\tau_2 cos(\omega\tau_2) + p_6 cos(\omega\tau_2)\\
&\quad - p_6\omega\tau_2 sin(\omega\tau_2) - p_7(\tau_1+\tau_2)cos(\omega(\tau_1+\tau_2)),\\
Q_2 &= -2\omega - p_3\tau_1 sin(\omega\tau_1) + p_4\omega cos(\omega\tau_1)\tau_1 + p_4 sin(\omega\tau_1) + p_5\tau_2 sin(\omega\tau_2)\\
&\quad + p_6 sin(\omega\tau_2) + p_6\omega\tau_2 cos(\omega\tau_2) - p_7(\tau_1+\tau_2)sin(\omega(\tau_1+\tau_2)),\\
R_1 &= -p_5\omega sin(\omega\tau_2) - p_6\omega^2 cos(\omega\tau_2) + p_7\omega sin(\omega(\tau_1+\tau_2)),\\
R_2 &= p_5\omega cos(\omega\tau_2) + p_6\omega^2 sin(\omega\tau_2) + p_7\omega cos(\omega(\tau_1+\tau_2)).
\end{aligned}$$

Solving Eq. (4.33) for $\left[\frac{d\xi}{d\tau_2}\right]_{\tau_2=\tau_{20}}$, we get

$$\left[\frac{d\xi}{d\tau_2}\right]_{\tau_2=\tau_{20},\omega=\omega^*} = \frac{R_1Q_1 - R_2Q_2}{Q_1^2 + Q_2^2},$$

(H_6): $R_1Q_1 - R_2Q_2 \neq 0$.

Theorem 4.4.3. *For system (4.19), let (H_1) and (H_6) hold true with τ_1 being in the stable interval $(0,\tau_{10})$. Then, E^* is locally asymptotically stable when $\tau_2 \in (0,\tau_{20})$ and the system undergoes Hopf-bifurcation at E^* when $\tau_2 = \tau_{20}$.*

Case (4): $\tau_1 > 0,\ \tau_2 > 0$, and we assume that τ_2 lies in the stable interval $(0, \tau_{20})$ and τ_1 is treated as a parameter. Assuming that the Eq. (4.21) has a root $i\omega(\omega > 0)$, then substituting back in Eq. (4.21) and comparing real and imaginary parts, we obtain

$$\begin{aligned} -\omega^2 + p_2 + p_5 cos(\omega\tau_2) + p_6\omega sin(\omega\tau_2) &= cos(\omega\tau_1)[-p_3 - p_7 cos(\omega\tau_2)] \\ &\quad + sin(\omega\tau_1)[-p_4\omega + p_7 sin(\omega\tau_2)], \qquad (4.34) \\ p_1\omega + p_6\omega cos(\omega\tau_2) - p_5 sin(\omega\tau_2) &= cos(\omega\tau_1)[-p_4\omega + p_7 sin(\omega\tau_2)] \\ &\quad + sin(\omega\tau_1[p_3 + p_7 cos(\omega\tau_2)]. \qquad (4.35) \end{aligned}$$

The above pair of equations can be re-written as

$$\begin{aligned} Pcos(\omega\tau_1) + Qsin(\omega\tau_1) &= R, \\ -Qcos(\omega\tau_1) + Psin(\omega\tau_1) &= S, \end{aligned} \qquad (4.36)$$

where

$$\begin{aligned} P &= -p_4\omega + p_7 sin(\omega\tau_2), \\ Q &= p_3 + p_7 cos(\omega\tau_2), \\ R &= p_1\omega + p_6\omega cos(\omega\tau_2) - p_5 sin(\omega\tau_2), \\ S &= -\omega^2 + p_2 + p_5 cos(\omega\tau_2) + p_6\omega sin(\omega\tau_2). \end{aligned}$$

Solving Eq. (4.36) give us

$$\tau_{1j}^* = \frac{1}{\omega}\left[cos^{-1}\left(\frac{PR - QS}{P^2 + Q^2}\right)\right] + \frac{2j\pi}{\omega}; \quad j = 0, 1, 2, 3, ...$$

Theorem 4.4.4. *For system (4.19), considering that τ_2 lies in the stable interval $(0, \tau_{20})$ and τ_1 is treated as a parameter, the system undergoes Hopf-bifurcation at $\tau_1 = \tau_{10}^*$.*

4.5 Dynamics of spatiotemporal model

In this section, we analyze the dynamics of spatio-temporal model given as

$$\begin{aligned} \frac{\partial x}{\partial t} &= \left[x\left(1 - \frac{x}{1+\beta x}\right) - \frac{mxy}{b+x}\right] + D_x\nabla^2 x, \\ \frac{\partial y}{\partial t} &= \left[\frac{cmxy}{b+x} - \gamma_0 y - \gamma_1 y^2\right] + D_y\nabla^2 y. \end{aligned} \qquad (4.37)$$

Considering the transformation

$$\begin{aligned} x &= x^* + X, \\ y &= y^* + Y, \end{aligned}$$

where (X,Y) are small perturbations in (x,y), the linearized system is given by

$$\begin{aligned} \frac{\partial X}{\partial t} &= A_1 X + A_2 Y + D_x\left(\frac{\partial^2 X}{\partial u^2} + \frac{\partial^2 X}{\partial v^2}\right), \\ \frac{\partial Y}{\partial t} &= A_3 X + A_4 Y + D_y\left(\frac{\partial^2 Y}{\partial u^2} + \frac{\partial^2 Y}{\partial v^2}\right), \end{aligned}$$

where

$$A_1 = \frac{-bmy^*}{(b+x^*)^2} + \frac{(1+x^*(\beta-1)(2+\beta x^*)}{(1+\beta x^*)^2},\ A_2 = \frac{-mx^*}{(b+x^*)},\ A_3 = \frac{bcmy^*}{(b+x^*)^2},\ A_4 = -\gamma_1 y^*.$$

Looking for the solution of the form

$$\begin{aligned} X =& A' e^{\lambda t} sin\left(\frac{j\pi}{M'}u\right) cos\left(\frac{i\pi}{N'}v\right), \\ Y =& B' e^{\lambda t} sin\left(\frac{j\pi}{M'}u\right) cos\left(\frac{i\pi}{N'}v\right), \end{aligned}$$

the system (4.37) leads to

$$\begin{aligned} \frac{\partial X}{\partial t} =& A_1 X + A_2 Y + D_x\left[\left(\frac{j\pi}{M'}\right)^2 + \left(\frac{i\pi}{N'}\right)^2\right], \\ \frac{\partial Y}{\partial t} =& A_3 X + A_4 Y + D_y\left[\left(\frac{j\pi}{M'}\right)^2 + \left(\frac{i\pi}{N'}\right)^2\right]. \end{aligned}$$

The variational matrix for the spatial system is as follows:

$$J_s^* = \begin{bmatrix} A_1 - D_x\left(\left(\frac{j\pi}{M'}\right)^2 + \left(\frac{i\pi}{N'}\right)^2\right) & A_2 \\ A_3 & A_4 - D_y\left(\left(\frac{j\pi}{M'}\right)^2 + \left(\frac{i\pi}{N'}\right)^2\right) \end{bmatrix}.$$

Now,

$$\begin{aligned} J_1' = -trace(J_s^*) =& \frac{bmy^*}{(b+x^*)^2} - \frac{(1+x^*(\beta-1)(2+\beta x^*)}{(1+\beta x^*)^2} + \gamma_1 y^* + (D_x + D_y)\left[\left(\frac{j\pi}{M'}\right)^2 + \left(\frac{i\pi}{N'}\right)^2\right], \\ J_2' = det(J_s^*) =& \left(\frac{bmy^*}{(b+x^*)^2} - \frac{(1+x^*(\beta-1)(2+\beta x^*)}{(1+\beta x^*)^2} + D_x\left(\left(\frac{j\pi}{M'}\right)^2 + \left(\frac{i\pi}{N'}\right)^2\right)\right) \\ & \times \left(\gamma_1 y^* + D_y\left(\left(\frac{j\pi}{M'}\right)^2 + \left(\frac{i\pi}{N'}\right)^2\right)\right) + \frac{bcm^2 x^* y^*}{(b+x^*)^2}. \end{aligned}$$

Characteristic equation at the coexistence equilibrium E^* is

$$\lambda^2 + J_1'\lambda + J_2' = 0. \tag{4.38}$$

The coexistence equilibrium is locally asymptotically stable under the following condition:

$$J_1' > 0, \;\; J_2' > 0.$$

Remark: $E^*(x^*, y^*)$ is locally asymptotically stable if

$$bmy^*(1+\beta x^*)^2 > (1+x^*(\beta-1)(2+\beta x^*))(b+x^*)^2.$$

Remark: If $trace(J_{E^*}) > 0$ or $det(J_{E^*}) < 0$, then the corresponding coexistence equilibrium is unstable for the temporal system.

- **Case I:** If $trace(J_{E^*}) > 0$, then the sufficiently higher value of D_x and D_y can stabilize the corresponding equilibrium in the spatiotemporal system.
- **Case II:** If $det(J_{E^*}) < 0$, then the sufficiently higher value of D_x can stabilize the corresponding equilibrium in the spatiotemporal system.

4.5.1 Conditions derived for Turing instability

From the Eq. (4.38), we have

$$J_1' = -trace(J_{E^*}) + (D_x + D_y)\left[\left(\frac{j\pi}{M'}\right)^2 + \left(\frac{i\pi}{N'}\right)^2\right],$$

$$J_2' = D_x D_y\left[\left(\frac{j\pi}{M'}\right)^2 + \left(\frac{i\pi}{N'}\right)^2\right]^2 - (A_1 D_y + A_4 D_x)\left[\left(\frac{j\pi}{M'}\right)^2 + \left(\frac{i\pi}{N'}\right)^2\right] + det\left(J_{E^*}\right), \tag{4.39}$$

where

$$trace(J_{E^*}) = \frac{-bmy^*}{(b+x^*)^2} + \frac{(1+x^*(\beta-1)(2+\beta x^*)}{(1+\beta x^*)^2} - \gamma_1 y^*,$$
$$det(J_{E^*}) = \left[\left(\frac{-bmy^*}{(b+x^*)^2} + \frac{(1+x^*(\beta-1)(2+\beta x^*)}{(1+\beta x^*)^2}\right)(-\gamma_1 y^*) + \left(\frac{bcmy^*}{(b+x^*)^2}\right)\left(\frac{mx^*}{(b+x^*)}\right)\right].$$

The conditions for diffusion-driven instability is either $J_1' < 0$ or $J_2' < 0$ holds. As we can see clearly, $J_1' > 0$ if $trace(J_{E^*}) < 0$. The only possibility left for the occurence of Turing instability

is $J_2' < 0$ with $det(J_{E^*}) > 0$. Defining a function as

$$G(\zeta) = D_x D_y \zeta^2 - (A_1 D_y + A_4 D_x)\zeta + det(J_{E^*}), \tag{4.40}$$

where $\zeta = \left(\frac{j\pi}{M'}\right)^2 + \left(\frac{i\pi}{N'}\right)^2$.

Turing instability occurs if $G(\zeta) < 0$,

$$\text{i.e., } D_x D_y \zeta^2 - (A_1 D_y + A_4 D_x)\zeta + det(J_{E^*}) < 0.$$

Now, let us assume that $G(\zeta)$ attains its minima at $\zeta = \zeta_M$. Hence,

$$G'(\zeta_M) = 0 \Rightarrow 2D_x D_y \zeta_M - (A_1 D_y + A_4 D_x) = 0,$$

leading to

$$\zeta_M = \frac{(A_1 D_y + A_4 D_x)}{2D_x D_y} > 0. \tag{4.41}$$

At $\zeta = \zeta_M$, the condition for diffusion-driven instability is

$$(A_1 D_y + A_4 D_x)^2 > 4 D_x D_y det(J_{E^*}).$$

From Eq. (4.40), the roots of the quadratic equation are

$$\zeta_{1,2} = \frac{(A_1 D_y + A_4 D_x) \pm \sqrt{(A_1 D_y + A_4 D_x)^2 - 4 D_x D_y det(J_{E^*})}}{2 D_x D_y}.$$

Therefore,

$$G(\zeta) < 0 \quad \text{for} \quad \zeta_1 < \zeta < \zeta_2.$$

Also, we have $trace(J_{E^*}) < 0$ and hence,

$$A_1 + A_4 < 0.$$

We know A_4 is always negative, thus,

$$-\frac{A_1}{A_4} < 1. \tag{4.42}$$

Equation (4.41) may lead to

$$A_1 D_y + A_4 D_x > 0,$$

$$\Rightarrow \qquad A_1 D_y > -A_4 D_x,$$

$$\frac{-A_1}{A_4} > \frac{D_x}{D_y}. \tag{4.43}$$

Combining Eqs. (4.42) and (4.43), we get

$$\frac{D_x}{D_y} < \frac{-A_1}{A_4} < 1,$$

$$\Rightarrow D_x < D_y \quad \text{for diffusion-driven instability.}$$

4.5.2 Dynamics of delayed spatiotemporal system

This section investigates the combined consequences of delay and diffusion on Hopf-bifurcation.

Take the transformation $\bar{x}(u,v,t) = x(u,v,t) - x^*$, $\bar{y}(u,v,t) = y(u,v,t) - y^*$ for the system (4.4). The aforementioned system is linearized as (ignoring the variables' bar for simplification of symbols)

$$\begin{array}{rcl} \frac{\partial x(u,v,t)}{\partial t} & = & a_1 x(u,v,t) + a_2 y(u,v,t) + a_5 y(u,v,t-\tau) + D_x \nabla^2 x(u,v,t), \\ \frac{\partial y(u,v,t)}{\partial t} & = & a_4 x(u,v,t) + a_6 x(u,v,t-\tau_2) + a_7 y(u,v,t-\tau_2) + D_y \nabla^2 y(u,v,t). \end{array} \tag{4.44}$$

By perturbing the coexistence equilibrium in both time and space, consider the solution of the form

$$\begin{aligned} x &= A e^{\lambda t} sin\left(\frac{n\pi}{M'}u\right) cos\left(\frac{m\pi}{N'}v\right), \\ y &= B e^{\lambda t} sin\left(\frac{n\pi}{M'}u\right) cos\left(\frac{m\pi}{N'}v\right). \end{aligned}$$

The above-mentioned solutions are substituted in the system (4.44) and simplifying, we get

$$J = \begin{bmatrix} a_1 - D_x\left(\left(\frac{n\pi}{M'}\right)^2 + \left(\frac{m\pi}{N'}\right)^2\right) & a_2 \\ 0 & a_4 - D_y\left(\left(\frac{n\pi}{M'}\right)^2 + \left(\frac{m\pi}{N'}\right)^2\right) \end{bmatrix}$$

$$+ \begin{bmatrix} a_5 & 0 \\ 0 & 0 \end{bmatrix} e^{-\lambda\tau_1} + \begin{bmatrix} 0 & 0 \\ a_6 & a_7 \end{bmatrix} e^{-\lambda\tau_2},$$

$$\Rightarrow J = \begin{bmatrix} a_1 - D_x\kappa^2 + a_5 e^{-\lambda\tau_1} & a_2 \\ a_6 e^{-\lambda\tau_2} & a_4 - D_y\kappa^2 + a_7 e^{-\lambda\tau_2} \end{bmatrix},$$

where all a_i's have same expression as given in Eq. (4.20), and

$$\kappa = \sqrt{\left(\frac{n\pi}{M'}\right)^2 + \left(\frac{m\pi}{N'}\right)^2}.$$

Now, we have the following characteristic equation:

$$\lambda^2 + N_1\lambda + N_2 + N_3 e^{-\lambda\tau_1} + N_4 e^{-\lambda\tau_2} + N_5 e^{-\lambda(\tau_1+\tau_2)} = 0, \tag{4.45}$$

where

$$\begin{aligned}
N_1 &= (D_x + D_y)\kappa^2 - (a_1 + a_4),\\
N_2 &= a_1a_4 - (a_1D_y + a_4D_1)\kappa^2 + D_xD_y\kappa^4,\\
N_3 &= a_5\lambda + a_5a_4 - a_5D_y\kappa^2,\\
N_4 &= a_7\lambda + a_1a_7 - a_7D_x\kappa^2 - a_2a_6,\\
N_5 &= a_5a_7.
\end{aligned}$$

Let us assume $\lambda = i\omega(\omega > 0)$ and substitute it into the above equation, we have

$$\begin{aligned}
-\omega^2 + N_2 + N_3 cos(\omega\tau_1) &= cos(\omega\tau_2)[-N_4 - N_5 cos(\omega\tau_1)] + sin(\omega\tau_2)[N_5 sin(\omega\tau_1)],\\
-N_1\omega + N_3 sin(\omega\tau_1) &= cos(\omega\tau_2)[-N_5 sin(\omega\tau_1)] + sin(\omega\tau_2)[-N_4 - N_5 cos(\omega\tau_1)].
\end{aligned} \tag{4.46}$$

Considering τ_1 is in the interval $(0, \tau_{10}^*)$ and τ_2 is treated as parameter. The two equations above can be squared, added, and simplified to yield

$$\begin{aligned}
&\omega^4 + R\omega^2 + S = 0, \qquad (4.47)\\
\text{where}\quad &R = N_1^2 - 2N_2 - 2N_3 cos(\omega\tau_1),\\
&S = N_3^2 - N_4^2 - N_5^2 + 2N_1N_3\omega sin(\omega\tau_1) - 2cos(\omega\tau_1)(N_2N_3 + N_4N_5).
\end{aligned}$$

Taking $z = \omega^2$, Eq. (4.47) gives

$$\begin{aligned}
z^2 + Rz + S &= 0, \qquad (4.48)\\
z^{\pm} &= \frac{-R \pm \sqrt{R^2 - 4S}}{2}.
\end{aligned}$$

Now, we have the following possible cases:

(H1′): Let $R > 0$, $S > 0$, $R^2 - 4S > 0$.

Then, there is no positive root for the Eq. (4.48). Hence, all the roots of Eq. (4.45) has negative real parts for any κ when $\tau_2 > 0$.

(H2′): If $\exists$ a constant $\kappa_0 \in \mathbb{N}$ such that $S < 0$ holds, then Eq. (4.48) has a unique positive root $\omega^+ = \sqrt{z^+}$.

Then, simplifying Eq. (4.46), we can calculate the bifurcation parameter as

$$\tau_{2_j} = \frac{1}{\omega^+}\left[cos^{-1}\left(\frac{P_1'Q_1' - P_2'R_1'}{{Q_1'}^2 + {R_1'}^2}\right)\right] + \frac{2j\pi}{\omega^+} \quad ; \quad j = 0,1,2,...$$

where

$$P_1' = -\omega^2 + N_2 + N_3 cos(\omega\tau_1), \;\; Q_1' = -N_4 - N_5 cos(\omega\tau_1),$$
$$R_1' = N_5 sin(\omega\tau_1), \;\; P_2' = -N_1\omega + N_3 sin(\omega\tau_1).$$

From the above analysis, we can conclude the following theorem.

Theorem 4.5.1. *The following results can be derived for the delayed diffusive system.*

1. *$E^*(x^*, y^*)$ is locally asymptotically stable for all $\tau_2 > 0$ and for any value of κ under (H1′).*

2. *Let (H2′) hold true:*

   (i) The coexistence equilibrium $E^*(x^*, y^*)$ is locally asymptotically stable for $\tau_2 \in (0, \tau_{2_0})$ and unstable for $\tau_2 > \tau_{2_0}$.

   (ii) When $\tau_2 = \tau_{2_j}, \quad j = 0,1,2,3,...,$ the model (4.4) undergoes Hopf-bifurcation near $E^*(x^*, y^*)$ and we obtain a family of periodic solutions bifurcating from $E^*(x^*, y^*)$.

4.6 Numerical simulations

In this section, we perform a series of qualitative numerical simulations for the temporal and spatially extended proposed system to get a better understanding of the dynamics of the system.

4.6.1 Temporal system

In this subsection, we analyze how the system (4.5) behaves on the variation of the parameters β and γ_0. The parameter values used for simulations are $m = 2$, $b = 0.3$, $c = 0.25$, $\gamma_1 = 0.3$ and the remaining parameters β and γ_0 are varied. Figure 4.5 depicts the stability behavior when the system (4.5) has a unique coexistence equilibrium. For $\gamma_0 = 0.2$, the unique coexistence equilibrium $E_1^*(0.3463, 0.2263)$ is a spiral source, i.e., there is a stable limit cycle around E_1^* (see

Fig. 4.5(a)). For this case, any trajectory that begins very close (or farther away) to the equilibrium point spirals outward (or inward) and finally converges to the stable limit cycle. Further, an increase in the value of γ_0 i.e., for $\gamma_0 = 0.4$, the system is locally asymptotically stable about $E_1^*(1.5908, 0.0689)$ (see Fig. 4.5(b)). From an ecological standpoint, a stable equilibrium in the prey-predator dynamics denotes an ecosystem in balance. If a stable coexistence equilibrium occurs, then both prey and predator species can survive without either species going extinct. Here, the trivial equilibrium E_0 and the axial equilibrium E_1 are saddle points.

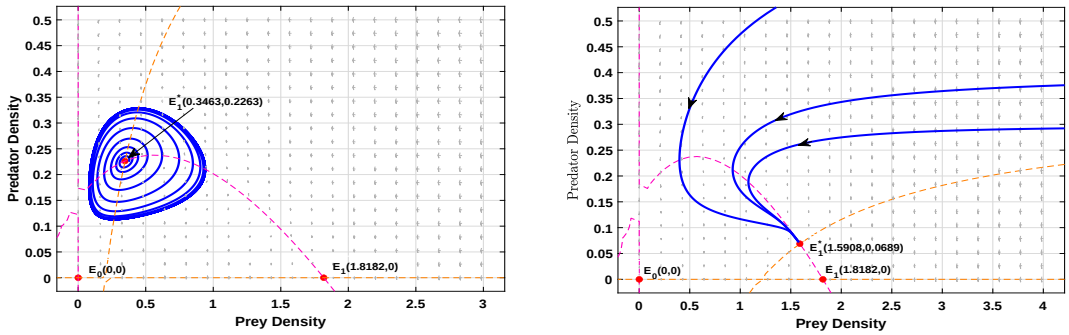

(a) E_1^* is spiral source for $\gamma_0 = 0.2$.

(b) E_1^* is nodal sink for $\gamma_0 = 0.4$.

Fig. 4.5: Stability behavior of unique coexistence equilibrium for the system (4.5) with varying γ_0. Here, $\beta = 0.45$.

Figure 4.6 refers to the case when the system has three coexistence equilibria. For $\gamma_0 = 0.05$, $E_1^*(0.0758, 0.1695)$ is a spiral source and $E_2^*(0.4591, 0.8413)$ is a nodal sink (see Fig. 4.6(a)). In this case, the stable limit cycle around E_1^* and the stable equilibrium E_2^* are the two possible attractors for the system (4.5). Moreover for $\gamma_0 = 0.075$, the system exhibits bi-stability attribute between the two coexistence equilibria $E_1^*(0.1015, 0.1715)$ and $E_2^*(0.5063, 1.0759)$ (see Fig. 4.6(b)). In a prey-predator dynamics, bistability between two coexistence equilibriums symbolizes two stable ecological states. In the above mentioned scenarios, the trivial equilibrium E_0, the axial equilibrium E_1, and the coexistence equilibrium E_3^* are saddle points.

Next, we perform a co-dimension one bifurcation analysis with respect to the parameter β and analyze the system dynamics. From Fig. 4.7, we observe that prey and predator species co-exist for lower values of β. As the value of β increases, the stable coexistence switches the stability behavior, and the limit cycle emerges, i.e., for higher values of β, both the populations of prey and predator exhibit periodic fluctuations. Hence, the system (4.5) experiences supercritical Hopf-bifurcation with respect to the parameter β.

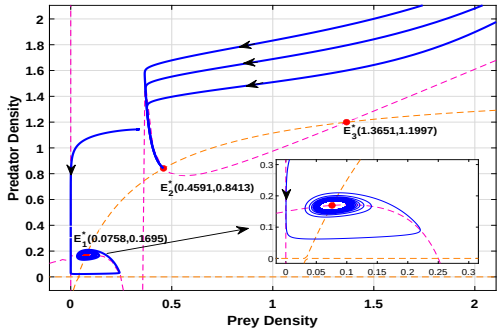

(a) E_1^* is spiral source and E_2^* is a nodal sink for $\gamma_0 = 0.05$.

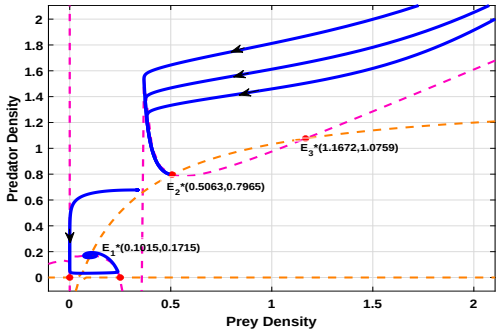

(b) E_1^* and E_2^* are spiral sink for $\gamma_0 = 0.075$.

Fig. 4.6: Stability behavior of different equilibria when the system has three coexistence equilibria with varying γ_0. Here, $\beta = -3$.

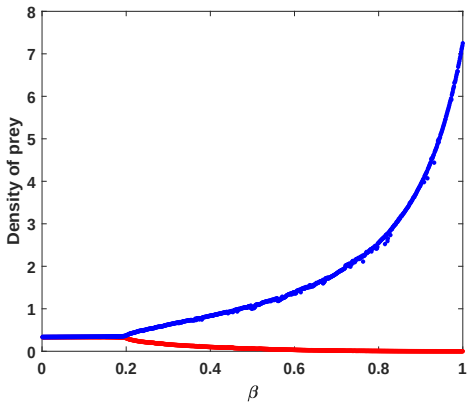

(a) For prey.

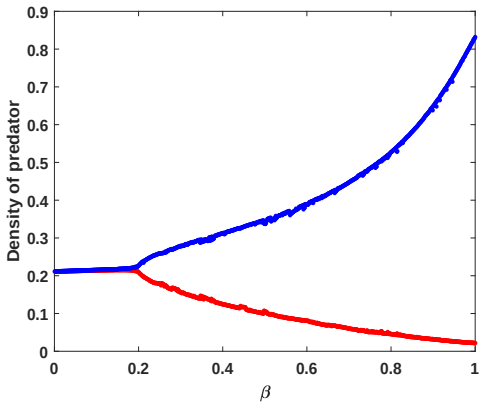

(b) For predator.

Fig. 4.7: Hopf-bifurcation plot with respect to the parameter β. Here, $\gamma_0 = 0.2$.

4.6.2 Delayed temporal system

This part illustrates numerical results for the delayed system when τ_1 is treated as a parameter, and the gestation delay τ_2 is fixed. The parametric values are considered as $m = 2$, $b = 0.3$, $c = 0.25$, $\gamma_1 = 0.3$, $\gamma_0 = 0.2$ and $\beta = 0.8$. From Figs. 4.8(a) and 4.8(b), we observe a stable limit cycle of period 1 and 2, respectively. Increasing the value of τ_1 drifts the system's dynamics from stable to chaotic with a fixed value of gestation delay τ_2 (see Fig. 4.8(c)). In a chaotic system, a small change in the initial conditions can lead to drastically different dynamics. We introduced a small amount of perturbation in initial conditions to confirm the chaotic behavior

of the system. From Fig. 4.9, we observe a significant change in the time series plot with the different initial conditions, ensuring that the system is sensitive towards initial conditions and, hence, chaotic. Figure 4.10 depicts the plot for the Maximal Lyapunov exponent with varying the delay parameter τ_1. The positivity of the Maximal Lyapunov exponent confirms the chaotic behavior of the delayed system.

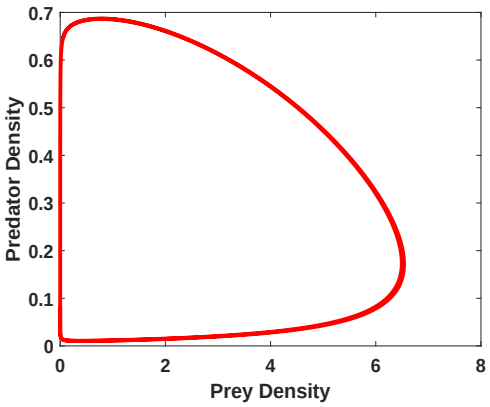

(a) Limit cycle of period 1 for $\tau_1 = 1$.

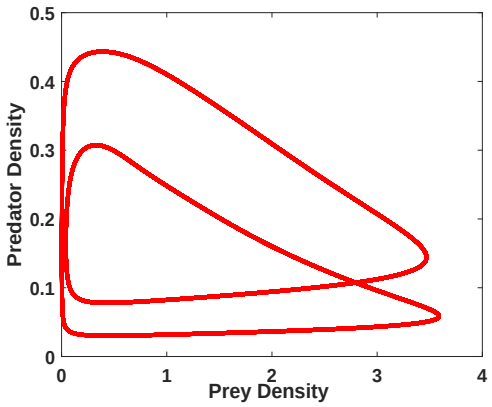

(b) Limit cycle of period 2 for $\tau_1 = 30$.

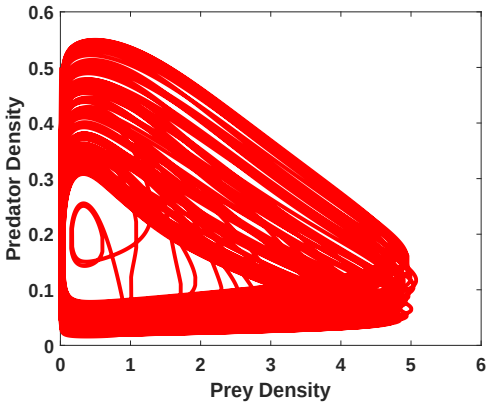

(c) Chaotic behavior for $\tau_1 = 70$.

Fig. 4.8: Limit cycles of various periods exhibited on changing the value of τ_1. Here, $\tau_2 = 1$.

4.6.3 Non-delayed spatial system

This subsection consists of the stationary Turing patterns obtained by perturbing the positive non-trivial solutions. We used Forward Euler Method for the reaction equations, and the Finite Difference scheme has been employed to solve the diffusion terms with Neumann boundary

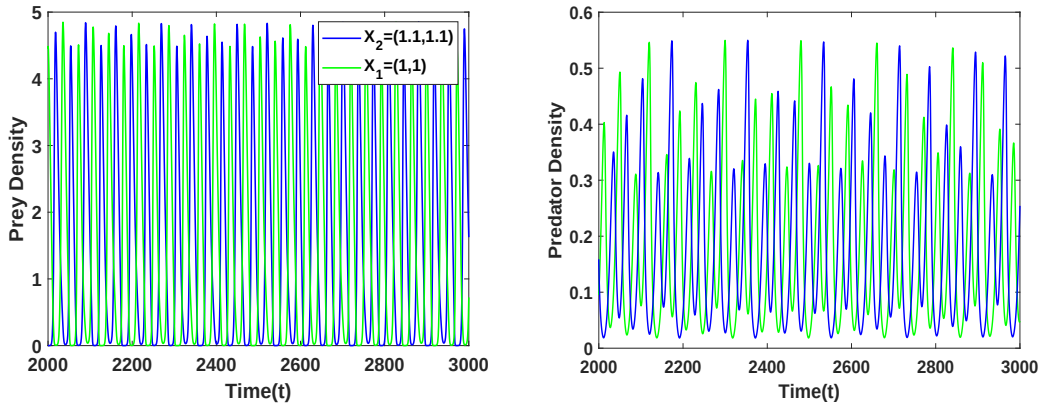

(a) For prey (b) For predator

Fig. 4.9: Sensitivity Analysis with initial conditions for $\tau_1 = 70$.

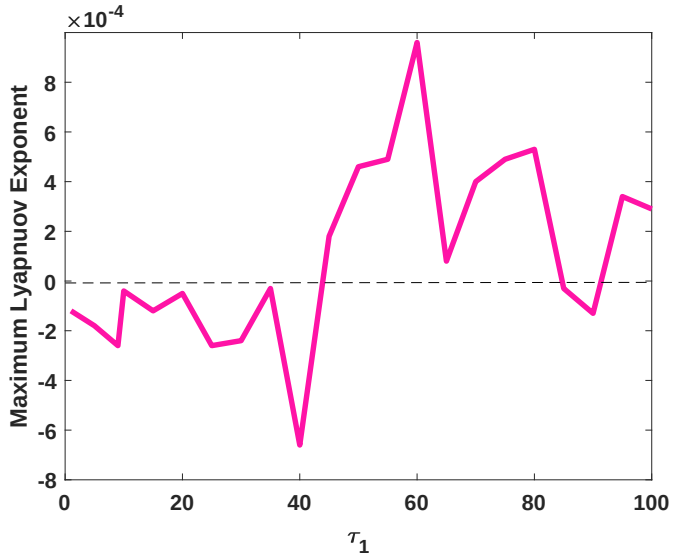

Fig. 4.10: Maximum Lyapnuov Exponent with repect to τ_1.

conditions. To ensure that the scheme will converge, the space and time step sizes were carefully chosen. Prey and predator Turing patterns have a one-to-one correspondence, so we included only Turing patterns for the prey population. The axes in the Turing patterns represent the spatial coordinates within a rectangular two-dimensional domain. The initial condition is considered with the random perturbation of following form:

$$\begin{aligned} x(u,v,0) &= x^* + 5\varepsilon\xi_{i,j}, \\ y(u,v,0) &= y^* + 5\varepsilon\theta_{i,j}, \end{aligned}$$

where $\varepsilon = 0.0001$, (x^*, y^*) is the positive equilibrium point, $\xi_{i,j}$ and $\theta_{i,j}$ denotes standard Gaussian white noise.

Numerical simulations are carried out with the following parameter values: $m = 2$, $b = 0.3$, $c = 0.25$, $\gamma_1 = 0.3$, and the remaining parameters are varied along with the diffusion coefficients. All the parameters are chosen from the Turing Instability region.

From Fig. 4.11, we observe that the system exhibits highly dense coldspot patterns for lower values of prey diffusion coefficients. As the value of D_x increases, these patterns start evolving, i.e., the number of spots decreases. Figure 4.12 depicts that the coldspots prevail in the whole spatial domain for the lower value of predator diffusion coefficient. The prey population becomes more dense as the value of the predator diffusion coefficient increases. For a higher value of the predator diffusion coefficient, such as $D_y = 5$, the area containing a moderate population of prey species nearly disappears (see Fig. 4.12(c)). It is observed that the movement of both prey and predator species plays a significant role in pattern formation.

4.6.4 Delayed spatiotemporal system

In this subsection, we consider the effect of both the delay parameters τ_1 and τ_2 on spatial pattern formation. We performed simulations to demonstrate the effect of the delay parameters on the spatiotemporal dynamics. First, the value of gestation delay τ_2 is taken as zero, and the delay parameter τ_1 is varied (see Fig. 4.13). From Fig. 4.13(a), we observe that the prey species resides at high density in the isolated patch, whereas the prey density is sparse in the remaining region. Gradual increase in the value of the delay parameter τ_1 changes the spatial distribution to Labyrinth pattern (see Figs. 4.13(b) and 4.13(c)). As the value of τ_1 increases, high prey density occupies most of the region (see Figs. 4.13(d) and 4.13(e)). From an ecological perspective, we observe that the density of the prey population increases with an increase in the delay parameter τ_1.

Next, we take the value of τ_1 to be zero and observe the impact of gestation delay τ_2 on the pattern formation. The transition in the Turing patterns determined by the gestation delay τ_2 can be seen in Fig. 4.14. It is observed that the spatial distribution of prey species varies significantly with respect to the delay parameter τ_2. The time series plot with respect to τ_2 depicts that the amplitude, as well as the period of the oscillations, increases as the value of τ_2 is incremented (see Fig. 4.15).

Further, we analyze the spatial distribution of the species when both the delay parameters are non-negative. For lower values of the delay parameter τ_1, the system exhibits hot-spot Turing patterns in the two-dimensional spatial domain, as can be seen in Fig. 4.16(a). As the delay parameter τ_1 is increased gradually, Turing patterns transit from hot-spot to patchy patterns. Higher values of τ_1 lead to increased density of the prey population (see Fig. 4.16).

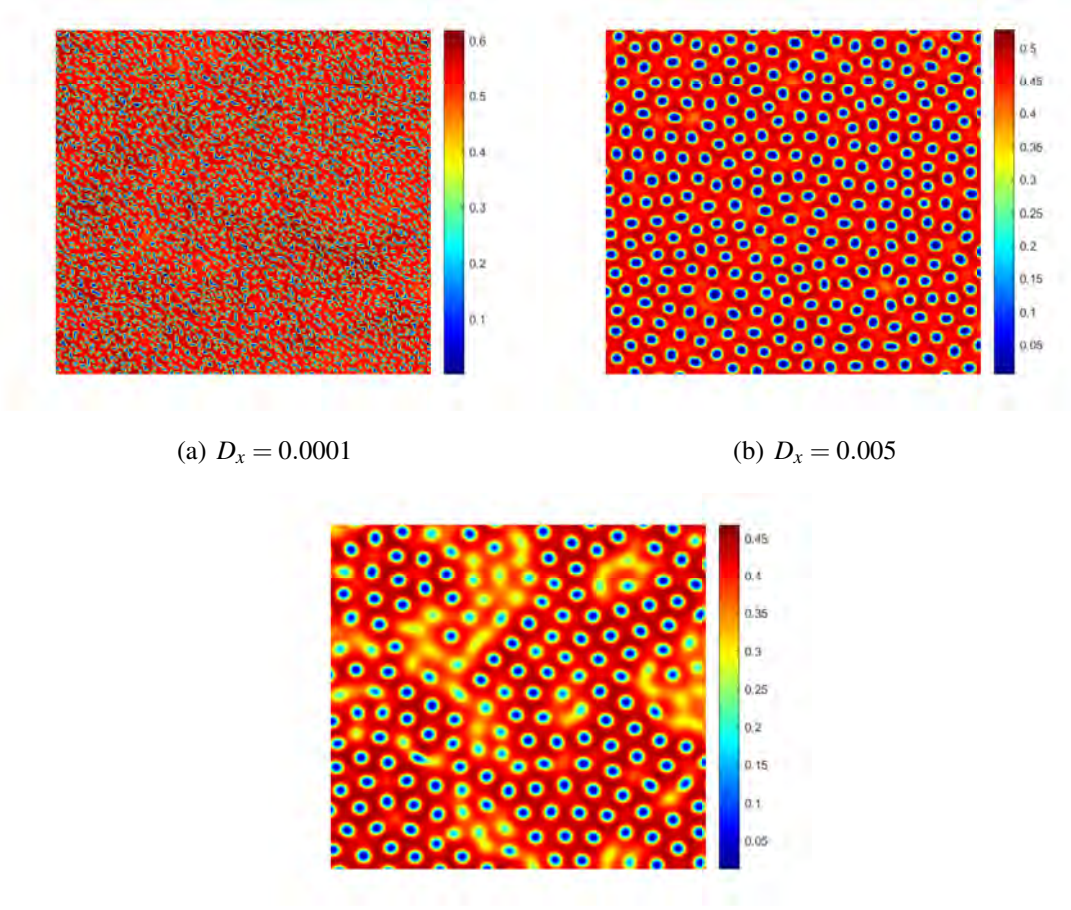

(a) $D_x = 0.0001$ (b) $D_x = 0.005$

(c) $D_x = 0.01$

Fig. 4.11: Stationary Turing patterns obtained for prey population with different prey diffusion coefficient. Here, $\beta = 0.19$, $\gamma_0 = 0.2$ and $D_y = 1$.

Increased value of the delay parameter τ_1 can lead to higher amplitude and period of oscillations as illustrated in Fig. 4.17.

4.7 Discussion and concluding remarks

We have proposed a prey-predator system where the past activities of prey species can alter the present carrying capacity and, consequently, the system's dynamics. Since the effect of past actions is not immediate, we incorporated a delayed carrying capacity as a function of prey density. Further, we included gestation delay τ_2 for the model's realism from an ecological perspective. The temporal and spatiotemporal models are analyzed with and without diffusion to investigate the intriguing dynamics. Pati and Ghosh [122] investigated the temporal dynamics of the proposed model with the linear functional response and without considering gestation

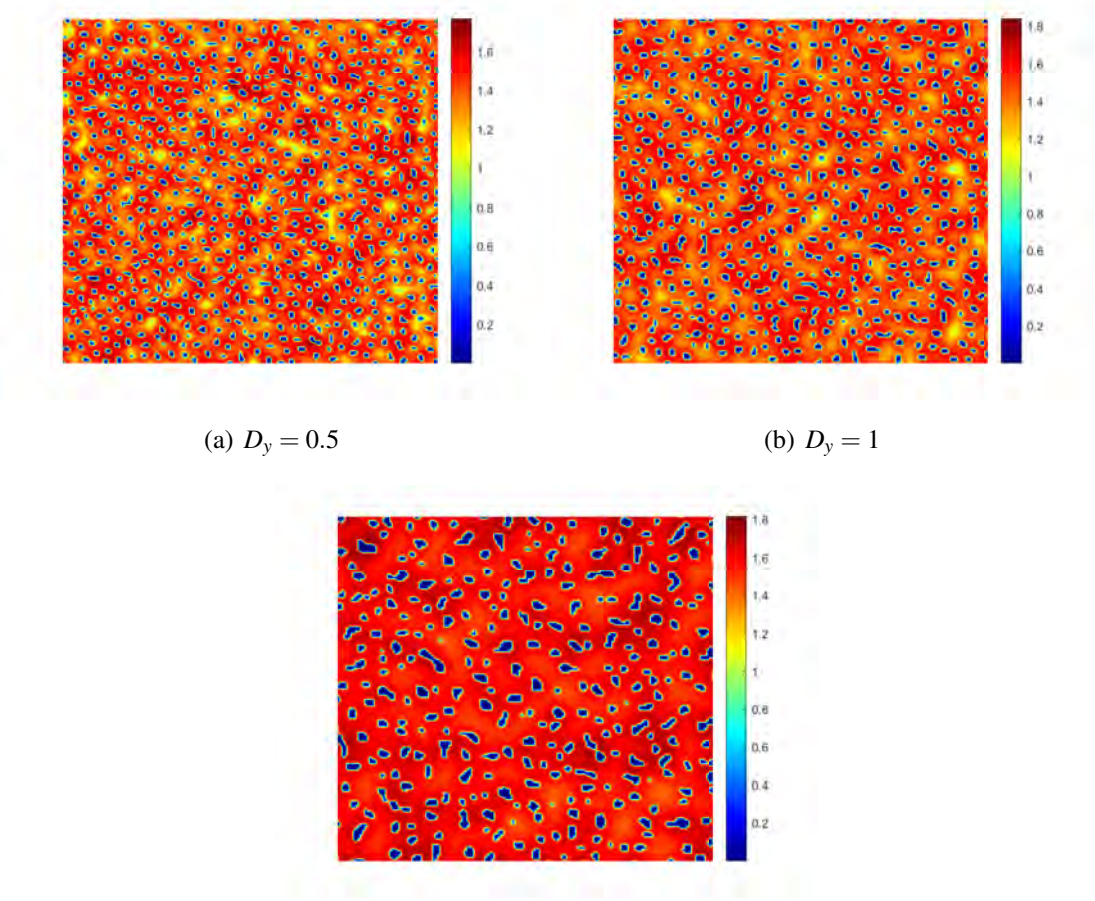

(a) $D_y = 0.5$ (b) $D_y = 1$

(c) $D_y = 5$

Fig. 4.12: Stationary Turing patterns obtained for prey population with different predator diffusion coefficient. Here, $\beta = 0.7$, $\gamma_0 = 0.29$ and $D_x = 0.001$.

delay. The present study assumes that prey and predator interact via Holling Type II functional response, which is more realistic from an ecological perspective as the resources are limited in nature. The positivity and boundedness of the temporal system are investigated. We examined the conditions for the existence of the biologically feasible equilibrium points, and stability analysis is performed. It is observed that the coexistence equilibrium is globally asymptotically stable under a certain condition. We analyzed that the system experiences co-dimension one Hopf-bifurcation with respect to the parameter β. For the spatiotemporal system, Turing instability conditions are derived by performing the linear stability analysis. Moreover, we investigated the system's dynamics by incorporating the discrete delays τ_1 and τ_2. The local stability and Hopf-bifurcation analysis are performed considering the delay parameters. Further, we analyzed Hopf-bifurcation for the delayed spatiotemporal system analytically.

We carried out numerical simulations to validate the analytical results for both the temporal

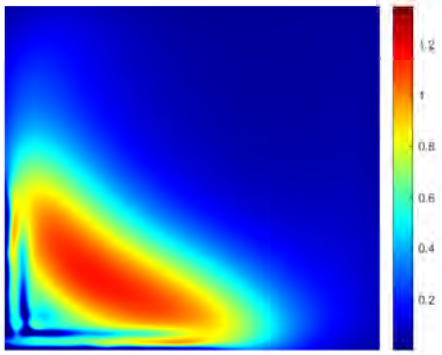

(a) $\tau_1 = 0.1$

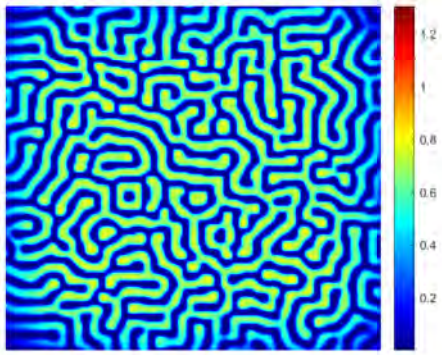

(b) $\tau_1 = 0.5$

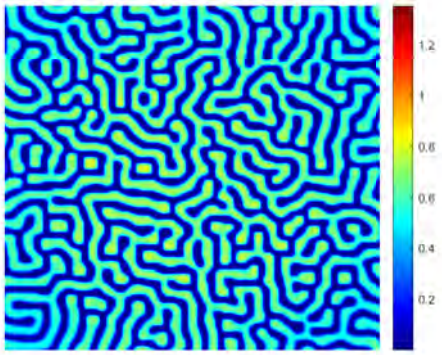

(c) $\tau_1 = 1$

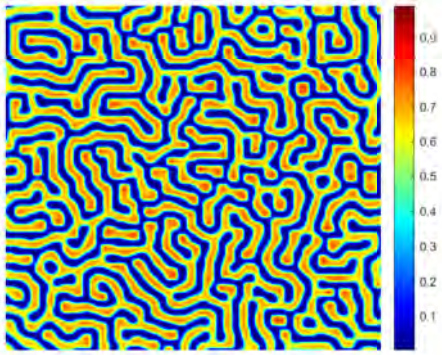

(d) $\tau_1 = 5$

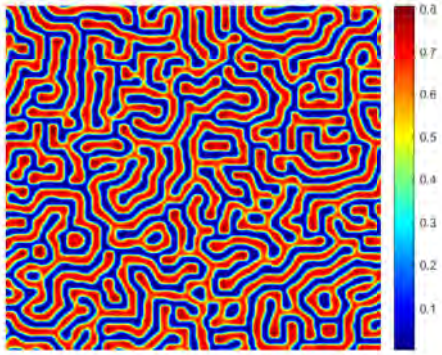

(e) $\tau_1 = 10$

Fig. 4.13: Role of the delay parameter τ_1 in the transition of the Turing Patterns obtained in two-dimensional spatial domain. All the other parameters are fixed as $\tau_2 = 0$, $m = 3$, $b = 0.3$, $c = 0.25$, $\gamma_1 = 0.3$, $\gamma_0 = 0.3$, $\beta = 0.5$, $D_x = 0.005$ and $D_y = 1$.

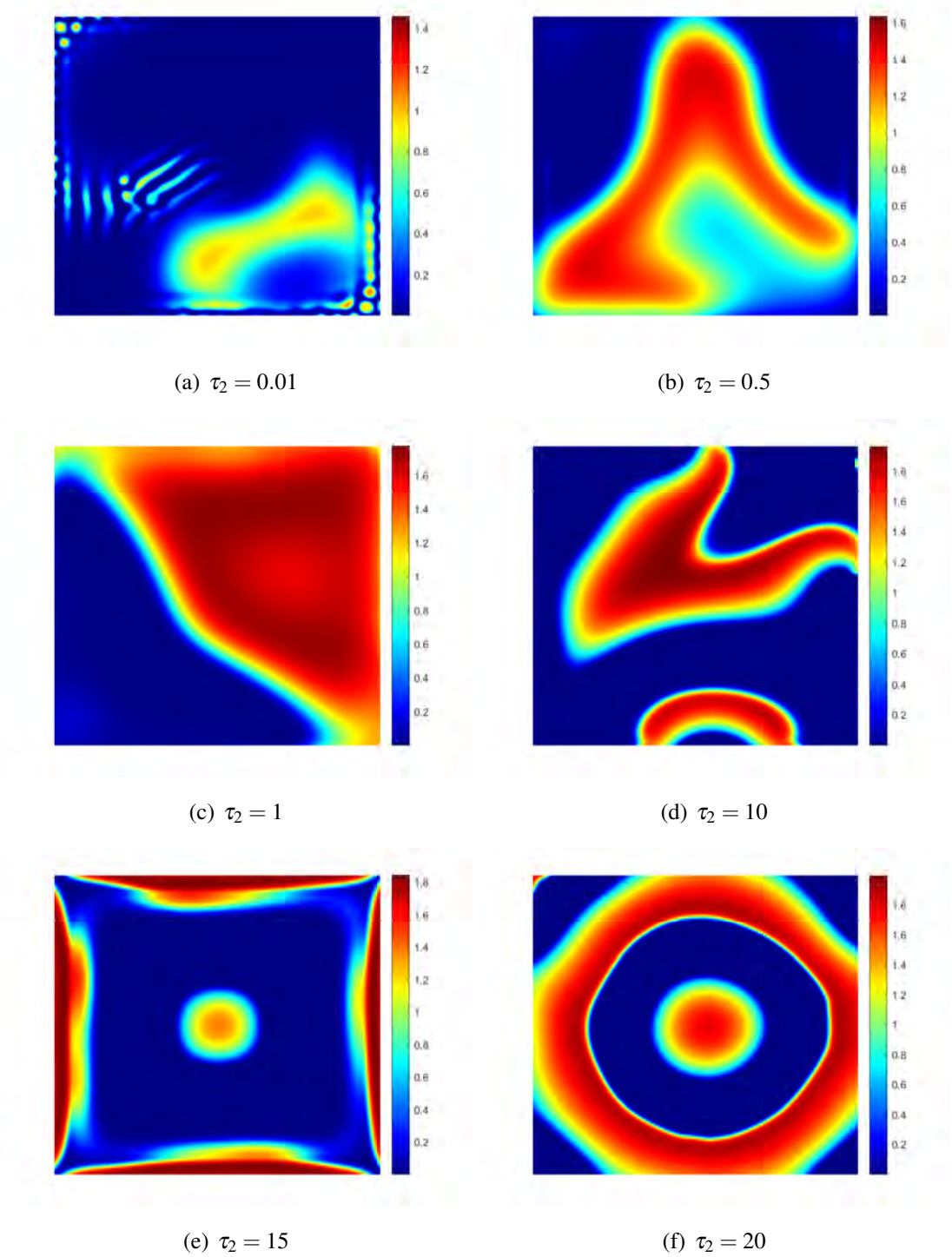

(a) $\tau_2 = 0.01$ (b) $\tau_2 = 0.5$

(c) $\tau_2 = 1$ (d) $\tau_2 = 10$

(e) $\tau_2 = 15$ (f) $\tau_2 = 20$

Fig. 4.14: Role of the gestation delay τ_2 in the transition of the Turing Patterns obtained in two-dimensional spatial domain. All the other parameters are fixed as $\tau_1 = 0$, $m = 3$, $b = 0.3$, $c = 0.25$, $\gamma_1 = 0.3$, $\gamma_0 = 0.2$, $\beta = 0.5$, $D_x = 0.005$ and $D_y = 1$.

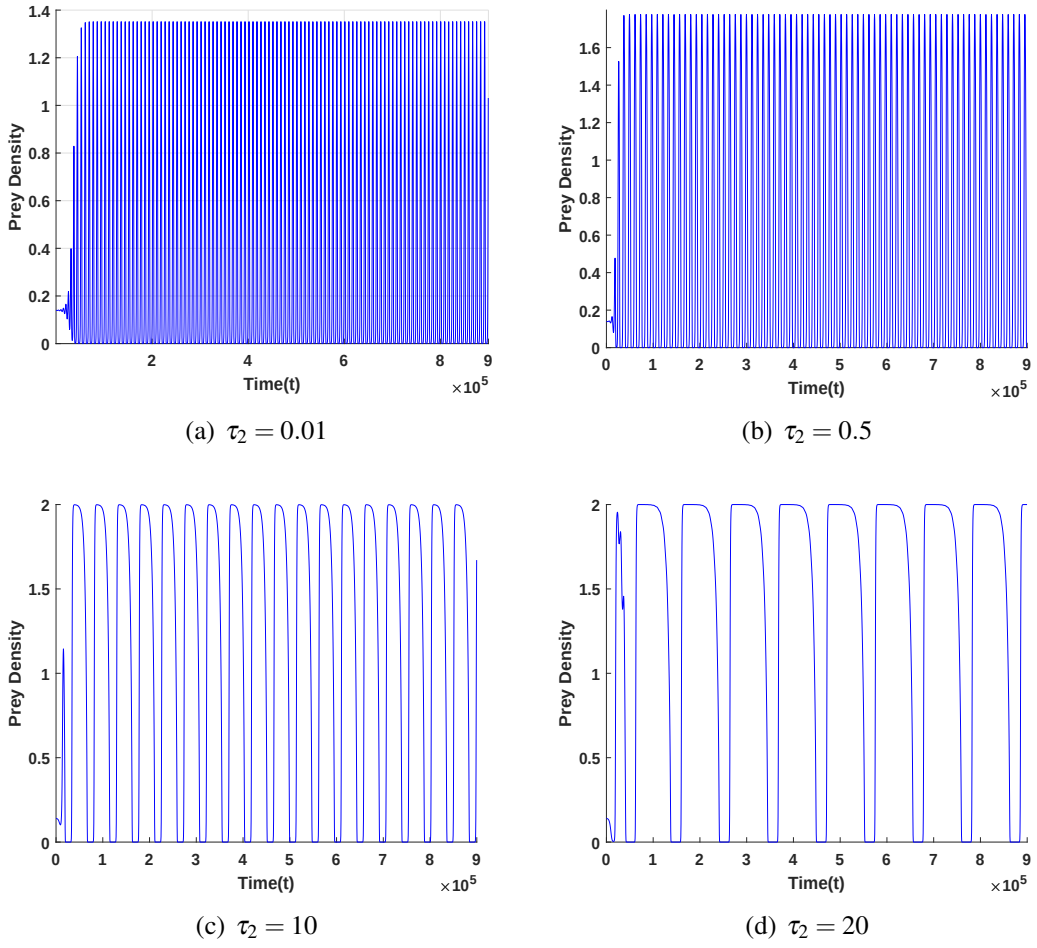

(a) $\tau_2 = 0.01$ (b) $\tau_2 = 0.5$

(c) $\tau_2 = 10$ (d) $\tau_2 = 20$

Fig. 4.15: Time series plot obtained for prey population with varying gestation delay τ_2. All the parameters assume the same values as in Fig. 4.14.

and spatiotemporal system with and without delay. For the temporal system, the local stability behavior of the unique coexistence equilibrium is investigated (see Fig. 4.5). We observed that the system exhibits bi-stability behavior between two coexistence equilibria (see Fig. 4.6). The analysis demonstrates that as the value of β increases, the system loses its stability, and limit cycles are produced via supercritical Hopf-bifurcation (see Fig. 4.7). For the delayed system, the sensitivity analysis is carried out for different initial conditions with regard to the delay parameter τ_1. It is concluded that the system is highly sensitive towards the initial conditions with respect to the delay parameter τ_1 (see Fig. 4.9). Our analysis illustrates that for a fixed value of gestation delay τ_2, the higher values of the delay parameter τ_1 drift the system into a chaotic region. Furthermore, we plotted the maximal Lyapunov exponent to confirm the chaotic nature of the system as depicted in Fig. 4.10. These findings contrast with the work done by Pati and Ghosh [122], as they investigated that the coexistence equilibrium remains stable in

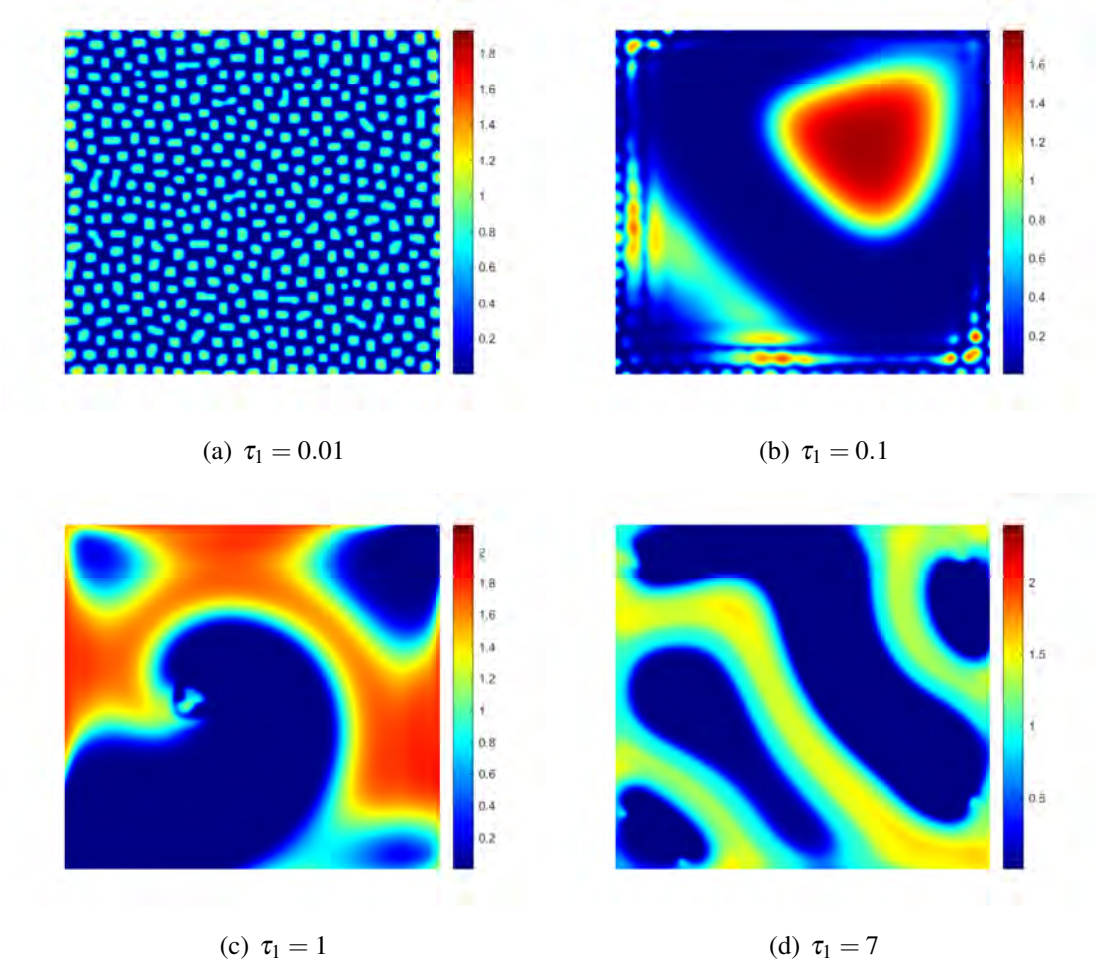

(a) $\tau_1 = 0.01$ (b) $\tau_1 = 0.1$

(c) $\tau_1 = 1$ (d) $\tau_1 = 7$

Fig. 4.16: Role of the delay parameters τ_1 and τ_2 in the transition of the Turing Patterns obtained in two-dimensional spatial domain. All the other parameters are fixed as $\tau_2 = 1$, $m = 3$, $b = 0.3$, $c = 0.25$, $\gamma_1 = 0.3$, $\gamma_0 = 0.2$, $\beta = 0.6$, $D_x = 0.005$ and $D_y = 1$.

the absence of a delay parameter and for the delayed system, their model experiences stability switching. Therefore, our model is more complex and intriguing to explore. For the spatially extended system, numerical simulations are done to comprehend the movement of species and their spatial distribution across time. The derived Turing instability conditions are satisfied numerically for a chosen set of parameters. Further, Turing patterns such as cold-spot and hot-spot are obtained for different diffusive rates as illustrated in Figs. 4.11 and 4.12. The obtained Turing patterns depict a significant change in the density of the prey species as the diffusivity coefficient varies. Moreover, the combined effect of both delay parameters is investigated for the delayed spatiotemporal system. Here, we observed that these findings are comparable to the results given by Bhunia *et al.* [14], where they examined a spatiotemporal prey-predator model with delayed carrying capacity and linear functional response. They analyzed that in

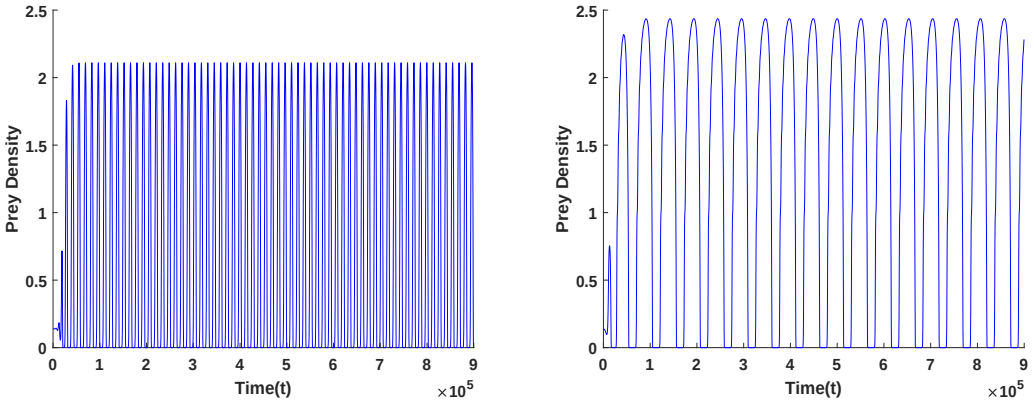

(a) $\tau_1 = 0.01$ (b) $\tau_1 = 7$

Fig. 4.17: Time series plot obtained for prey population with varying delay parameter τ_1. All the parameters assume the same values as in Fig. 4.16.

the absence of cross-diffusion, Turing patterns are not feasible for the delayed system when the activities are constructive. A variety of Turing patterns such as stripes, a combination of stripes and holes, patchy patterns, etc., are obtained for the two-dimensional habitat (Figs. 4.13, 4.14, 4.16). The amplitude of the periodic solutions changes as the value of delay parameters is altered.

Throughout the study, we noticed that the past activities of prey species significantly affect the population dynamics, which could provide valuable insights into strategies for sustainable management. The present piece of research exhibits rich spatial patterns in the rectangular habitat. These patterns provide useful information about species distribution across habitats and can help ecologists implement effective strategies to protect and manage species and their environments.

Chapter 5

Study of a cannibalistic prey-predator model with Allee effect in prey under the presence of diffusion[1]

5.1 Introduction and model formulation

A two dimensional predator-prey model with a generalist or specialist predator can presented by the following system of two ODEs:

$$\begin{aligned} \frac{dU}{dt} &= F_1(U) - F_2(U,P)P, \\ \frac{dP}{dt} &= cF_2(U,P)P + F_3(P)P, \end{aligned} \tag{5.1}$$

where, U and P signify the population densities of prey and predator, respectively. Functions F_1 and F_3 depict the kinetics of each population in the absence of another. Function F_1 can be logistic or logistic with the Allee effect (for example), whereas function $F_3(P) < 0$ for specialist predator and $F_2(0,P) + F_3(P) > 0$ for generalist predator [148]. The concept of the Allee effect was first established by ecologist Warder Clyde Allee in 1931. This concept pertains to the distinct growth dynamics observed in prey populations at low population densities. At lower population densities, prey populations can exhibit either negative or positive growth rates, contingent upon the intensity of the Allee effect. Empirical evidence substantiating the existence of the Allee effect is observed in a diverse array of natural species, covering insects [80], plants [43], marine invertebrates [43], birds and mammals [30]. Based upon negative and positive growth rate at lower population densities, the Allee effect can be classified into two distinct categories: strong and weak, respectively. A critical threshold population density can be observed in communities exhibiting the strong Allee effect. Once the population density falls below this specific level, the per capita growth rate experiences a negative trend, leading to a decrease in population size. On the other hand, within populations exhibiting a weak Allee

[1]This chapter is based on our paper published in *Chaos, Solitons & Fractals*, **182**, 114797, 2024.

effect, the absence of a distinct threshold density is observed, whereby the per capita growth rate never turns negative. In contrast, it is seen that the growth rate maintains a positive when population densities are low, exhibiting a growth pattern similar to that observed in logistic growth models. The term $A(U) = \frac{U}{U+\theta}$ portrays the weak Allee effect in prey population, and it gives the probability of finding a male by the female during the reproduction period [18]. Here, $\theta \geq 0$, known as the Allee parameter, is the reciprocal of search efficacy for mating, and gives the strength of the Allee effect. Thus the increment in θ decreases individual's search efficacy, which is also referred as strong-mate finding Allee effect [31]. Thus a predator-prey model with logistic growth in prey who is suffering with weak Allee effect can be described as

$$\begin{aligned} \frac{dU}{dt} &= \frac{rU^2}{U+\theta}\left(1-\frac{U}{k}\right) - F_2(U,P)P, \\ \frac{dP}{dt} &= cF_2(U,P)P + F_3(P)P, \end{aligned} \tag{5.2}$$

where r is the maximum intrinsic growth rate, k is habitat's carrying capacity for prey-species and c is the rate at which prey biomass is transformed to predator biomass. Sen et al. [148] explored a generalist predator-prey model under the influence of weak Allee effect. They examined their model with and without the Allee effect. Both the models exhibited very rich dynamics by showing different types of local and global bifurcations.

Cannibalism has been observed in a variety of animal species, including bank voles, house finches, wolf spiders, fish, and zooplankton, according to experimental zoologists. Size-structured cannibalism, in which larger individuals of the same species eat smaller ones, may contribute substantially to the total mortality, with rates ranging from 8 percent in Belding's ground squirrels to 95 percent in dragonfly larvae [128]. This demonstrates how greatly it affects population dynamics and interactions within communities [27, 134] . Kohlmeier and Ebenhoh [70] studied a two dimensional prey-predator model with cannibalistic predators. They included cannibalism in their model by taking the total food available for predator equal to the weighted sum of the biomass of prey and the biomass of predator. They investigated the existence and stability of equilibrium points of their system. Following the above work, Chakraborty and Chattopadhyay [22] resolved the paradox of enrichment with a high rate of cannibalism, i.e., they observed that for the high value of the cannibalistic parameter, their system remained stable. Prasad and Prasad [130] studied a predator-prey model with a cannibalistic predator who also has a supply of additional food. They showed that their work could help in determining the suitable additional food to supply in order to increase the effectiveness of cannibalistic predators as biocontrol agents. Recently, Zhang et al. [190] worked on a cannibalistic prey-predator model with incorporation of prey refuge in the presence of self-diffusion. According to their findings,

predator cannibalism increases predator biomass density and stabilizes predator-prey ecosystems. Cannibalism at high levels was observed to prevent the paradox of enrichment. They also discussed the Turing-instability, and nonexistence and existence of nonconstant steady state solutions.
Inspired from the above notions and existing studies, we formulate our model using the following assumption:

1. In our predator-prey system, we consider that the prey follows the logistic growth and this growth is also influenced by weak Allee effect. Thus, in the absence of predator, its growth is represented by the following equation:

$$\frac{dU}{dt} = \frac{rU^2}{U+\theta}\left(1-\frac{U}{k}\right), \tag{5.3}$$

   where r, θ and k have same meanings as defined for model (5.2).

2. We also consider that the predator species is a specialist thus, depends completely on the prey for survival. The second quality of our predator is that it is cannibalistic, i.e., they also eat their conspecifics. Therefore, we use the approach of cannibalism from [70] for predator population to formulate its growth rate governing equation.
   Using all above assumptions, we can set up the following system:

$$\begin{cases} \frac{dU}{dt} = \frac{rU^2}{U+\theta}\left(1-\frac{U}{k}\right) - \frac{c_1UP}{h+U+\beta P} = U f_1(U,P) =: G_1(U,P), & t>0, \\ \frac{dP}{dt} = \frac{c_1c_2UP - c_1\beta\alpha P^2}{h+U+\beta P} - \delta P = P f_2(U,P) =: G_2(U,P), & t>0, \\ U(0) = U_0 \geq 0,\ P(0) = P_0 \geq 0. \end{cases} \tag{5.4}$$

   Here, c_1 is the maximum intake rate of predator over prey, h is predator's coefficient of half-saturation, β is predator's net preference for feeding on members of the same species (cannibalism rate), c_2 is rate of conversion for consumed prey biomass into predator biomass, α is uptake effect due to cannibalism, and δ is mortality rate of predator.

The study of reaction-diffusion systems has received much attention in recent years as an effective tool for exploring the concepts underlying pattern formation. Predators move to catch their prey, and prey migrate to avoid the predators, causing fluctuations in population densities throughout space. This interplay between space and time causes the population to expand under each individual's irregular motions. This irregular movement (dispersal or migration) can be mathematically represented using the Fickian diffusion law [108]. Diffusion, in general, is the process of moving something randomly from a location of higher concentration to one of lower concentration [104]. The movement of individuals may be related to other factors, such

as the need to find food, avoid predators to avoid being caught, flee from areas where there is a severe danger of infection, and so forth. The diffusion of individuals in a system can leads to instability, known as Turing-instability [166], and this diffusion driven instability can further lead to formation of spatial patterns. In a model of interactions between algae and herbivores, Bhattacharyya and Pal [12] found that the spatiotemporal system did not show diffusion-driven instability. In fact, motional states of interaction also exist, which acknowledge potential biases, such as the motion of a predator towards its prey and that of the prey away from the predator [67]. According to theoretical and numerical analyses of ecological systems, phenomena of cross-diffusion may be generating a wide range of diverse pattern [14, 45, 79, 100, 101, 156].

Form the previous studies, we observed that the Allee effect in prey, property of cannibalism in predator, and the mechanism of diffusion play some vital roles in ecological interactions, whereas the combination of all these biological factors have not been studied yet. Thus motivated from it we intend to study a prey-predator model with weak Allee effect in prey, cannibalism in predator under the presence of self and cross-diffusion. We investigate both temporal and spatiotemporal models in great depth. We explore the separate and combined roles of both the parameters responsible for the Allee effect and cannibalism in the occurrence of different kinds of bifurcations. The importance of the diffusion coefficients is also studied for the spatiotemporal model in fine detail. We did a comprehensive analytical study, thoroughly exploring various characteristics associated with the models, and have also presented them through numerical examples in the corresponding sections of this paper. Now, the model to be studied is given below.

$$\begin{cases} \frac{\partial U}{\partial t} = d_U \Delta U + d_1 \Delta P + \frac{rU^2}{U+\theta}\left(1-\frac{U}{k}\right) - \frac{c_1 UP}{h+U+\beta P}, & (x,y)\in\Omega,\ t>0, \\ \frac{\partial P}{\partial t} = d_P \Delta P + d_2 \Delta U + \frac{c_1 c_2 UP - c_1 \beta \alpha P^2}{h+U+\beta P} - \delta P, & (x,y)\in\Omega,\ t>0, \\ \frac{\partial U}{\partial \nu} = \frac{\partial P}{\partial \nu} = 0, & (x,y)\in\partial\Omega,\ t>0, \\ U(x,y,0) = U_0(x,y) \geq 0,\ P(x,y,0) = P_0(x,y) \geq 0, & (x,y)\in\Omega,\ t>0, \end{cases} \tag{5.5}$$

where U and P denotes $U(x,y,t)$ and $P(x,y,t)$, respectively, with Ω as a bounded subset of $\mathbb{R}^2_+$ having a smooth boundary. In (5.5), symbol Δ represents the Laplacian operator; $\frac{\partial^2}{\partial x^2} + \frac{\partial^2}{\partial y^2}$, the constants d_U, d_P are self-diffusion coefficients whereas d_1, d_2 are cross-diffusion coefficients, and we take all these coefficients always positive [45, 125]. The condition $\frac{\partial U}{\partial \nu} = \frac{\partial P}{\partial \nu} = 0$ stands for no flux boundary conditions (homogeneous Neumann boundary conditions) with ν as an outward normal vector to boundary of Ω. We fix the parameters (unless mentioned in text) for both systems (5.4) and (5.5) as given below:

Parameters	Default values	References
r	2	[114]
k	14	[76]
c_1	1.5	Assumed
c_2	0.8	[183]
δ	0.06	[143, 190]
h	3	[96]
α	0.5	[70]
θ	14	Assumed
β	2	Assumed

Table 5.1: Biological signification and parameters' values which are employed in systems (5.4) and (5.5).

We organized this paper as follows: Section 5.2 consists of a detailed analysis of non-spatial model (5.4). This comprises analytical conditions for all feasible steady states' existence and stability. Bifurcations of codimension 1 and 2 are also discussed here analytically and numerically. In Section 5.3, we firstly investigate the existence of non-negativity of solutions for the self-diffusion model and its prior bounds. Next, we drive the conditions for Turing-instability for models with self-diffusion and cross-diffusion. Using numerical simulation, we also present different types of stationary and dynamic patterns. Lastly, concluding remarks of present study are presented in Section 5.4.

5.2 Analysis for temporal model

5.2.1 Model's well-posedness

Theorem 5.2.1. *For system (5.4), its each solution initiating with a non-negative initial condition continue to be non-negative forever and uniformly bounded.*

Proof. From (5.4), it is easy to observe that

$$\begin{aligned} U(t) &= U_0 \exp\left(\int_0^t f_1(U(s),P(s))ds\right) \geq 0, \\ P(t) &= P_0 \exp\left(\int_0^t f_2(U(s),P(s))ds\right) \geq 0, \quad \forall t \geq 0. \end{aligned} \tag{5.6}$$

Now, to prove the boundedness of the solution of (5.4), we first prove the boundedness of variable U and then we prove for P. For U, we take two cases: $U_0 \leq k$ and $U_0 > k$. For the first case, we claim that $U(t) \leq k$ for all $t > 0$. On the contrary of this, we suppose that there exist

$t_1, t_2 > 0$ such that $t_1 < t_2$ and $U(t_1) = k$ where $U(t) > k$ for $t \in (t_1, t_2)$. Using first eq. of (5.6) for $T_1 \in (t_1, t_2)$

$$\begin{aligned} U(T_1) &= U_0 \exp\left(\int_0^{t_1} f_1(U(s), P(s))ds\right) \exp\left(\int_{t_1}^{T_1} f_1(U(s), P(s))ds\right), \\ &= U(t_1) \exp\left(\int_{t_1}^{T_1} f_1(U(s), P(s))ds\right) \leq U(t_1), \end{aligned}$$

holds because $f_1(U(s), P(s)) < 0$ for $t \in (t_1, t_2)$. This leads to a contradiction to the fact that $U(t) > k$ for $t \in (t_1, t_2)$. Thus, we have $U(t) \leq k$ for $t > 0$ in this case.

In the case when $U_0 > k$, there can be two sub-cases, either there exists $T_2 > 0$ such that $U(t) > k$ for $t \in [0, T_2)$ with $U(T_2) = k$ or $U(t) > k$ for $t > 0$. In the first sub-case, $U(t) \leq k$ for $t > T_2$. For $t \in (0, T_2)$, we get

$$U(t) = U_0 \exp\left(\int_0^t f_1(U(s), P(s))ds\right) \leq U_0.$$

With the same argument, we can show that $U(t) < U_0$ in the second sub-case. Hence, combining all the cases we get $U(t) \leq \max\{k, U_0\}$.

For the boundedness of P, we define $W(t) = U(t) + \frac{1}{c_2}P(t)$, then we have

$$\begin{aligned} \frac{dW}{dt} + \delta W &\leq rU\left(1 - \frac{U}{k}\right) + \delta U, \\ &= f(U), \end{aligned}$$

where $f(U) = (r+\delta)U - \frac{r}{k}U^2$. Now, $\max\limits_{U \geq 0} f(U) = f\left(\frac{(r+\delta)k}{2r}\right) = \frac{(r+\delta)^2 k}{4r} = B$ (say). Thus, we have

$$\frac{dW}{dt} + \delta W \leq B,$$

and using the theory of differential inequalities, we get

$$W(t) \leq \frac{B}{\delta} + e^{-\delta t}\left(W_0 - \frac{B}{\delta}\right) \leq \max\left\{\frac{B}{\delta}, W_0\right\}.$$

Therefore, $W(t)$ is bounded and hence $P(t)$ is bounded and all the solutions of (5.4) are bounded.

∎

5.2.2 Equilibrium analysis

Model (5.4) has at most three types of equilibrium points; extinction equilibrium $E_0(0,0)$, predator-free equilibrium $E_1(k,0)$ and the coexistence steady state $E^*(U^*,P^*)$. The equilibrium E^* is the positive solution of following algebraic equations:

$$\frac{rU^*}{U^*+\theta}\left(1-\frac{U^*}{k}\right)-\frac{c_1P^*}{h+U^*+\beta P^*}=0, \tag{5.7}$$

$$\frac{c_1c_2U^*-c_1\beta\alpha P^*}{h+U^*+\beta P^*}-\delta=0. \tag{5.8}$$

From (5.8), we get

$$P^*=\frac{(c_1c_2-\delta)U^*-\delta h}{\beta(\delta+c_1\alpha)}>0 \text{ if } \delta<\frac{c_1c_2U^*}{h+U^*}. \tag{5.9}$$

Using P^* from (5.9) together with (5.7), we have a cubic equation in U^* given by

$$g(U)=A_3U^{*3}+A_2U^{*2}+A_1U^*+A_0=0, \tag{5.10}$$

where

$$\begin{aligned}
A_3&=-r\beta c_1(c_2+\alpha)\ (<0),\\
A_2&=r\beta c_1c_2k-c_1^2c_2k+c_1\delta k-c_1hr\beta\alpha+c_1r\beta\alpha k,\\
A_1&=-c_1^2c_2\theta k+c_1h\delta k+c_1\delta\theta k+c_1hr\beta\alpha k,\\
A_0&=c_1h\delta\theta k\ (>0),
\end{aligned}$$

and define $\Delta=18A_3A_2A_1A_0-4A_2^3A_0+A_2^2A_1^2-4A_3A_1^3-27A_3^2A_0^2$.

Now, the number of coexistence steady states can vary depending upon the sign of A_2, A_1 and Δ. As the parameters θ and β are of most importance, so we study the existence of coexistence steady state in the $\theta\beta$-plane keeping other parameters fixed. We can divide the first quadrant of the $\theta\beta$-plane into following sub-regions (depicted in Fig. 5.1):

$$\begin{aligned}
R_1&=\{(\theta,\beta)\in\mathbb{R}_+^2|A_2>0 \text{ and } A_1>0\},\\
R_2&=\{(\theta,\beta)\in\mathbb{R}_+^2|A_2<0 \text{ and } A_1>0\},\\
R_3&=\{(\theta,\beta)\in\mathbb{R}_+^2|A_2<0 \text{ and } A_1<0\},\\
R_4&=\{(\theta,\beta)\in\mathbb{R}_+^2|A_2>0,\ A_1<0 \text{ and } \Delta<0\},\\
R_5&=\{(\theta,\beta)\in\mathbb{R}_+^2|A_2>0,\ A_1<0 \text{ and } \Delta>0\}.
\end{aligned}$$

Using the above analysis, we can state the following theorem for existence of positive equilibrium.

Theorem 5.2.2. *1. System (5.4) has no coexistence steady state if* $\delta > \frac{c_1c_2U^*}{h+U^*}$.

2. *System (5.4) has an unique coexistence steady state* $E_1^*(U_1^*,P_1^*)$ *if* $(\theta,\beta) \in R_1 \cup R_2 \cup R_3 \cup R_4$ *and* $\delta < \frac{c_1c_2U_1^*}{h+U_1^*}$.

3. *System (5.4) has three coexistence steady states* $E_i^*(U_i^*,P_i^*)$, $i = 1,2,3$ *if* $(\theta,\beta) \in R_5$ *and* $\delta < c_1c_2 \min\left\{\frac{U_1^*}{h+U_1^*}, \frac{U_2^*}{h+U_2^*}, \frac{U_3^*}{h+U_3^*}\right\}$. *In this case, an instantaneous equilibrium* ($E_{z_1} = (U_{z_1},P_{z_1})$ *or* $E_{z_2} = (U_{z_2},P_{z_2})$) *arises when* $g(U_{z_1}) = 0$ *or* $g(U_{z_2}) = 0$, *where* z_1 *and* z_2 *are the roots of* $g'(U) = 0$.

Proof. When condition $\delta > \frac{c_1c_2U^*}{h+U^*}$ holds, then from (5.9), we can observe that under this condition, the predator coordinate of E^* becomes negative, which is biologically insignificant. Thus $\delta < \frac{c_1c_2U^*}{h+U^*}$ is a necessary condition for the existence of coexistence steady state, so from here on next, when we will talk about coexistence steady state, it is preassumed that this condition holds. When we talk about three positive equilibria, the necessary condition becomes $\delta < c_1c_2 \min\left\{\frac{U_1^*}{h+U_1^*}, \frac{U_2^*}{h+U_2^*}, \frac{U_3^*}{h+U_3^*}\right\}$.

Now, we use the theory of cubic equation and Descartes' rule of signs to prove the remaining points. When $(\theta,\beta) \in R_1 \cup R_2 \cup R_3$, one can easily use the above rule of sign and note that $g(U) = 0$ has exactly one positive root; U^* for this choice of parameters. Similarly, when $\{(\theta,\beta) \in \mathbb{R}^2_+ | A_2 > 0$ *and* $A_1 < 0\}$ then $g(U) = 0$ has either one or three positive roots. The discriminant $\Delta < 0$ guarantees the existence of exactly one real root of $g(U) = 0$, so taking it with $A_2 > 0$ and $A_1 < 0$ ensures the existence of exactly one positive root of $g(U) = 0$. In this way, system (5.4) has an unique positive equilibrium for $(\theta,\beta) \in R_1 \cup R_2 \cup R_3 \cup R_4$. In a same way, taking $\Delta > 0$ with $A_2 > 0$ and $A_1 < 0$ gives three positive roots, i.e., for $(\theta,\beta) \in R_5$ system (5.4) has three coexistence steady states.

The case when there are three coexistence steady state i.e., $g(U) = 0$ has three positive roots, say $U_1^* < U_2^* < U_3^*$. Then there exist U_{z_1} and U_{z_2} such that $U_1^* < U_{z_1} < U_2^*$ and $U_2^* < U_{z_2} < U_2^*$ with $g'(U_{z_1}) = g'(U_{z_2}) = 0$, and an instantaneous equilibrium arises when $g(U_{z_1})$ (or $g(U_{z_2})$) becomes zero because of the collision of U_1^* and U_2^* (or U_2^* and U_3^*). Consequently, the collision of E_1^* and E_2^* gives $E_{z_1} = (U_{z_1},P_{z_1})$ (say) and collision of E_2^* and E_3^* gives $E_{z_2} = (U_{z_2},P_{z_2})$. Hence, this completes the proof. ∎

Remark 5.2.1. *In, Fig. 5.1, we can see all the regions defined in the above theorem. Here, we may also note that the boundaries of the region* R_5 *will correspond for saddle-node bifurcation, and the point where these are meeting will be a cusp point. All these things are discussed in detail in Fig. 5.5 in the next section of the bifurcation analysis.*

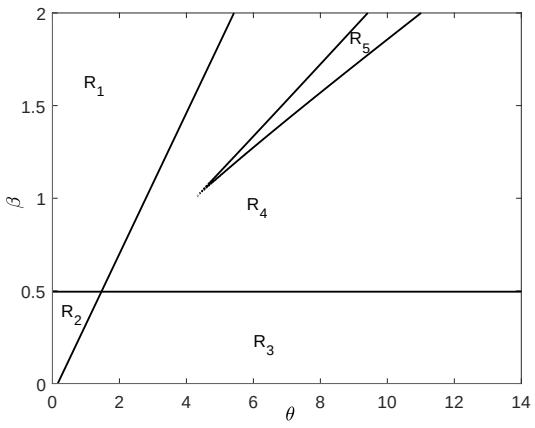

Fig. 5.1: In this figure,the $\theta\beta$-plane is divided into different sub-regions such that $R_1 \cup R_2 \cup R_3 \cup R_4$ has an unique coexistence steady state; R_5 has three coexistence steady states in accordance to conditions stated in Theorem 5.2.2.

5.2.3 Stability analysis for equilibrium points

Here, we execute the local (or global) stability analysis for the feasible equilibrium points.

Theorem 5.2.3. *The extinction equilibrium $E_0(0,0)$ is a non-hyperbolic saddle node with a parabolic sector and two hyperbolic sectors.*

Proof. The eigenvalues of the Jacobian evaluated E_0 are $\lambda_1 = 0$ and $\lambda_2 = -\delta < 0$ which means that E_0 is non-hyperbolic equilibrium, so local stability analysis cannot provide any significant information about its stability. For this, we use Theorem 1, page:151 in [127] and its notations. Now, the system (5.4) can be put into the form

$$\begin{aligned}\dot{U} &= p_2(U,P),\\ \dot{P} &= P + q_2(U,P),\end{aligned}$$

where

$$p_2(U,P) = \frac{r}{\theta}U^2 - \frac{c_1}{h}UP - r\left(\frac{1}{\theta^2} + \frac{1}{k\theta}\right)U^3 + \frac{c_1}{h^2}U^2P - \frac{c_1\beta}{h^2}UP^2 + T_1(U,P),$$

$$q_2(U,P) = -\frac{c_1c_2}{\delta h}UP + \frac{c_1\beta\alpha}{\delta h}P^2 - \frac{c_1\beta^2\alpha}{\delta h^2}P^3 + \frac{c_1c_2}{\delta h^2}U^2P + \left(\frac{c_1c_2\beta}{\delta h^2} - \frac{c_1\beta\alpha}{\delta h^2}\right)UP^2 + T_2(U,P),$$

where, $T_1(U,P)$ and $T_2(U,P)$ are series having terms U^iP^j with $i+j \geq 4$.
Let $P = \phi(U)$ be a solution of $P + q_2(U,P) = 0$ in the neighborhood of origin and write $p_2(U,\phi(U))$ in the form as $\Psi(U) = a_mU^P + \ldots$ in the neighborhood of origin where $m \geq$

2, $a_m \neq 0$. As $\phi(U)$ is solution of $P+q_2(U,P)=0$, thus solving it we get:

$$\phi'(U)p_2(U,\phi(U)) - \phi(U) - q_2(U,\phi(U)) = 0. \tag{5.11}$$

Now, let $P=\phi(U)=aU^2+bU^3+R_1(U)$, where $R_1(U)$ is a series having terms U^i with $i\geq 4$. After some mathematical calculation, we can see that the use of this value of P with (5.11), and comparison of coefficients of U gives $\phi(U)\equiv 0$. Thus $p_2(U,\phi(U))$ becomes

$$p_2(U,\phi(U)) = \frac{r}{\theta}U^2 + R_2(U),$$

where $R_2(U)$ is a series having terms U^i with $i\geq 3$. As $m=2$ thus from the above mentioned theorem from [127], E_0 is a non-hyperbolic saddle node with a parabolic sector and two hyperbolic sectors whereas these sectors are evident from Fig. 5.2(a). ∎

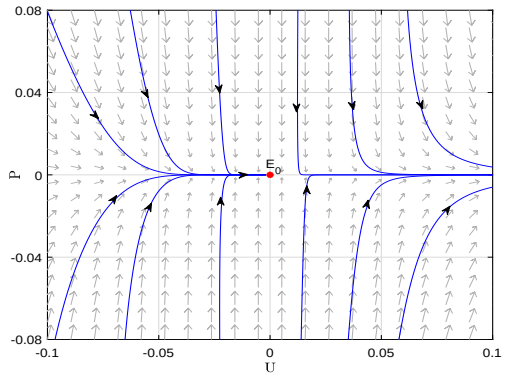

(a) $E_0(0,0)$ is non-hyperbolic saddle node with parabolic sector on the left and hyperbolic sectors on the right.

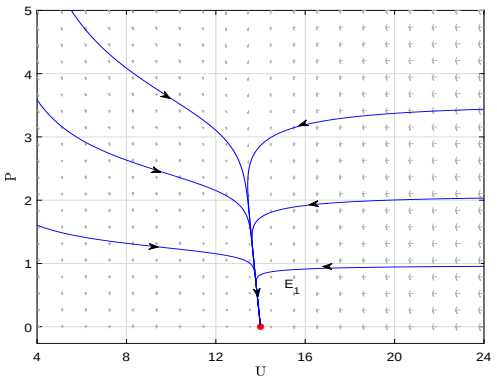

(b) $E_1(k,0)$ is globally asymptotically stable in $\mathbb{R}^2_+$ under the condition $c_1c_2k-\delta(h+k)<0$.

Fig. 5.2: In both figures, $c_1=0.5$, $c_2=0.1$ and $h=10$ with all other parameters from (5.1).

Theorem 5.2.4. *The predator-free equilibrium $E_1(k,0)$ is locally asymptotically stable if $c_1c_2k-\delta(h+k)<0$. Further, E_1 is globally asymptotically stable in $\mathbb{R}^2_+$ if $c_1c_2k-\delta(h+k)<0$.*

Proof. Firstly, from Theorem 5.2.3, we can easily see that no solution of (5.4) in $\mathbb{R}^2_+$ can converge to $E_0(0,0)$. Next, the eigenvalues corresponding to E_1 are $\lambda_1=-\frac{rk}{k+\theta}<0$ and $\lambda_2=\frac{c_1c_2k}{h+k}-\delta$. So, the predator-free equilibrium is locally asymptotically stable if $\lambda_2<0$ i.e., $c_1c_2k-\delta(h+k)<0$. Moreover, $c_1c_2k-\delta(h+k)<0$ gives $\delta>\frac{c_1c_2k}{h+k}$ thus the local stability of E_1

establishes the non-existence of positive steady state. Now, from second equation of (5.4), we have:

$$\begin{aligned}\frac{1}{P}\frac{dP}{dt} &= \frac{c_1c_2U - c_1\beta\alpha P}{h+U+\beta P} - \delta,\\ &\leq \frac{c_1c_2U}{h+U} - \delta.\end{aligned}$$

Let $\Upsilon(U) = \frac{c_1c_2U}{h+U}$, and it is easy to observe that $\Upsilon(U)$ attains its maximum value at $U = k$. Thus

$$\begin{aligned}\frac{1}{P}\frac{dP}{dt} &\leq \frac{c_1c_2k}{h+k} - \delta,\\ &= \frac{c_1c_2k - \delta(h+k)}{h+k}.\end{aligned}$$

Now, we can define $\varepsilon = \delta(h+k) - c_1c_2k$ and as $c_1c_2k - \delta(h+k) < 0$, so we have

$$\begin{aligned}&\frac{1}{P}\frac{dP}{dt} \leq \frac{-\varepsilon}{h+k},\\ \implies &P(t) \leq C\exp\left(\frac{-\varepsilon t}{h+k}\right), \text{ where } C \text{ is some constant}\\ \implies &P(t) \to 0 \text{ as } t \to \infty,\end{aligned}$$

as a result of which the possibility for existence if any periodic orbit get eliminated. In this way, we have established the global stability of $E_0(k,0)$ (depicted in Fig. 5.2(b)). ∎

The Jacobian matrix corresponding to a general interior equilibrium $E^*(U^*,P^*)$ is given as

$$J|_{E(U^*,P^*)} = \begin{pmatrix} E_{11} & E_{12}\\ E_{21} & E_{22}\end{pmatrix}, \tag{5.12}$$

where

$$\begin{aligned}E_{11} &= \frac{rU^*(k(U^*+2\theta) - U^*(2U^*+3\theta))}{k(U^*+\theta)^2} - \frac{c_1P^*(h+\beta P^*)}{(h+U^*+\beta P^*)^2},\\ E_{12} &= -\frac{c_1U^*(h+U^*)}{(h+U^*+\beta P^*)^2}\ (<0),\\ E_{21} &= \frac{c_1c_2P^*(h+\beta P^*) + c_1\beta\alpha P^{*2}}{(h+U^*+\beta P^*)^2}\ (>0),\\ E_{22} &= -\frac{c_1P^*\beta(c_2U^* + \alpha(h+U^*))}{(h+U^*+\beta P^*)^2}\ (<0).\end{aligned}$$

As we are not having the explicit expressions for coexistence steady states so we use graphical method to discuss their stability when it is an unique or more than one (indeed three).

Theorem 5.2.5. *1. When system (5.4) has an unique coexistence steady state $E_1^*(U_1^*, P_1^*)$, then E_1^* is stable (or unstable) if $tr(J|_{E_1^*})$ is negative (or positive).*

2. When system (5.4) has three coexistence steady states $E_i^*(U_i^*, P_i^*)$, $i = 1,2,3$ such that $U_1^* < U_2^* < U_3^*$, then $E_1^*(U_1^*, P_1^*)$ and $E_3^*(U_3^*, P_3^*)$ are stable (or unstable) if the corresponding $tr(J|_{E_1^*}) < 0$ and $tr(J|_{E_3^*}) < 0$, respectively (or $tr(J|_{E_1^*}) > 0$ and $tr(J|_{E_3^*}) > 0$, respectively). Moreover, $E_2^*(U_2^*, P_2^*)$ is a saddle point.

Proof. The above Jacobian $J|_{E^*(U^*,P^*)}$ can also be written as

$$J|_{E^*(U^*,P^*)} = \begin{pmatrix} U\frac{\partial f_1}{\partial U} & U\frac{\partial f_1}{\partial P} \\ P\frac{\partial f_2}{\partial U} & P\frac{\partial f_2}{\partial P} \end{pmatrix}_{(U^*,P^*)}. \tag{5.13}$$

Let $\frac{dP^{(f_1)}}{dU}$ and $\frac{dP^{(f_2)}}{dU}$ denote the slopes of tangents to prey and predator nullclines at E^* , then we have

$$det(J|_{E^*}) = \left(UP\frac{\partial f_1}{\partial P}\frac{\partial f_2}{\partial P}\left(\frac{dP^{(f_2)}}{dU} - \frac{dP^{(f_1)}}{dU}\right)\right)_{(U^*,P^*)}.$$

1. When system (5.4) has an unique coexistence steady state $E_1^*(U_1^*, P_1^*)$, then we draw the possible types of graphical representations for nullclines for our system in Figs. 5.3(a) and 5.3(b). In both the graphs, $f_1 = 0$ (prey nullcline) and $f_2 = 0$ (predator nullcline) are presented by blue and red colors, respectively. The intersection of both these curves gives the unique coexistence steady state E_1^*. Now, for Fig. 5.3(a), we prove $U^*\left(\frac{\partial f_1}{\partial U}\right)_{E_1^*}$ is positive. In this figure, if we take an ε-nbh. at E_1^* in $U-$ direction keeping P constant then using the signs of f_1, it easy to note that $f_1(U_1^* - \varepsilon, y) < 0$ and $f_1(U_1^* + \varepsilon, y) > 0$ which implies $U^*\left(\frac{\partial f_1}{\partial U}\right)_{E_1^*} > 0$. In the same manner, we are able to evaluate the signs of remaining entries of $J|_{E^*(U^*,P^*)}$ at E_1^* in (5.13) from Fig. 5.3(a), and can have

$$Sign(J|_{E_1^*}) = \begin{pmatrix} + & - \\ + & - \end{pmatrix}.$$

Again from Fig. 5.3(a), it is easy to observe that at E_1^* , $\frac{dP^{(f_2)}}{dU} > \frac{dP^{(f_1)}}{dU}$, i.e., $det(J|_{E_1^*}) > 0$. Therefore, for this possibility of figure, E_1^* is stable (or unstable) if $tr(J|_{E_1^*})$ is negative (or positive).

For the Fig. 5.3(b), again $det(J|_{E_1^*}) > 0$, and

$$Sign(J|_{E_1^*}) = \begin{pmatrix} - & - \\ + & - \end{pmatrix}.$$

Thus, for this possibility, E_1^* is stable. Hence, in theorem, we have given the combined statement of both possibilities.

2. The case when system (5.4) has three coexistence steady states $E_i^*(U_i^*, P_i^*)$, $i = 1,2,3$, again we draw the possible ways for intersection of these two nullclines in Figs. 5.3(c) and 5.3(d). From both the figures, it is clear that for E_2^*, $\frac{dP^{(f_2)}}{dU} < \frac{dP^{(f_1)}}{dU}$ which implies that in both the cases $det(J|_{E_2^*}) < 0$ i.e., E_2^* is a saddle point. Now, for Fig. 5.3(c), the signs of Jacobian for E_1^* and E_3^* are given by

$$Sign(J|_{E_1^*}) = \begin{pmatrix} + & - \\ + & - \end{pmatrix}, \; Sign(J|_{E_2^*}) = \begin{pmatrix} + & - \\ + & - \end{pmatrix},$$

whereas $det(J|_{E_1^*}) > 0$ and $det(J|_{E_3^*}) > 0$. Therefore, E_1^* and E_3^* are stable (or unstable) if $tr(J|_{E_1^*}) < 0$ and $tr(J|_{E_3^*}) < 0$, respectively (or $tr(J|_{E_1^*}) > 0$ and $tr(J|_{E_3^*}) > 0$, respectively). Similarly for Fig. 5.3(d), we can conclude that E_3^* is stable but E_1^* is stable (or unstable) if $tr(J|_{E_1^*}) < 0$ (or $tr(J|_{E_1^*}) > 0$).

The theorem's proof is now completed. ∎

5.2.4 Bifurcation investigation

In this subsection, we analyze different types of local bifurcations of co-dimension 1 and 2; Hopf bifurcation, saddle node bifurcation, generalized Hopf bifurcation and Bogdanov-Takens bifurcation under which our system (5.4) may go with certain parametric conditions.

5.2.4.1 Hopf bifurcation

In the last subsection, we have seen that E_2^* is always a saddle point whenever it exist whereas E_1^* and E_3^* are stable or unstable depending upon the signs of trace of their corresponding Jacobians. We consider β as the bifurcation parameter and assess how E_1^* changes its stability when we vary β. A similar analysis can be carried out for E_3^*.

Theorem 5.2.6. *For occurrence of Hopf bifurcation, the following conditions must be satisfied:*

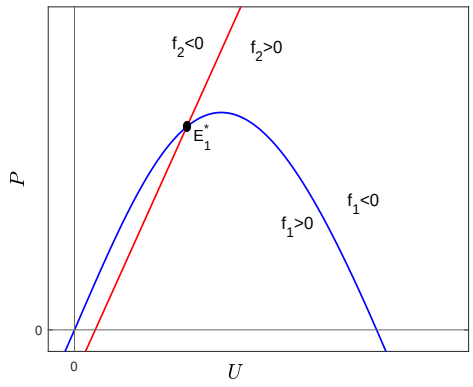

(a) Unique coexistence steady state.

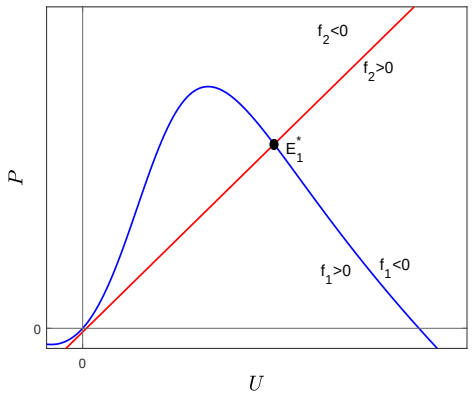

(b) Unique coexistence steady state.

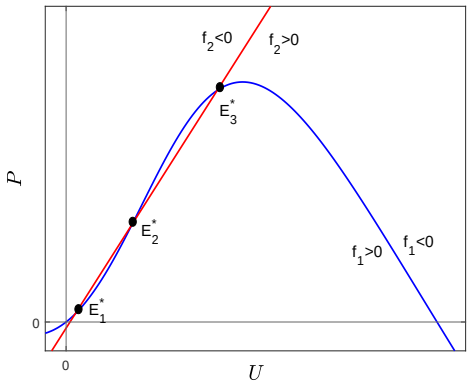

(c) Three coexistence steady states.

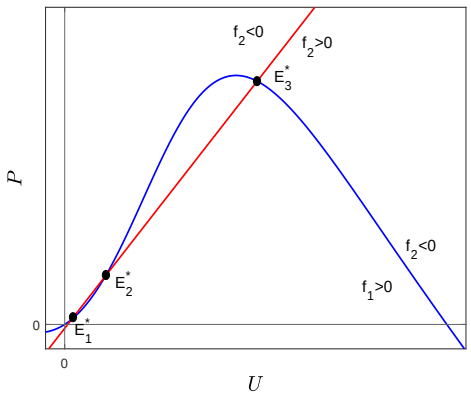

(d) Three coexistence steady states.

Fig. 5.3: This figure describes the graphical method to establish the stability of coexistence steady states.

$\mathscr{H}1$ $tr(J|_{E_1^*};\beta=\beta_H)=E_{11}+E_{22}=0,$

$\mathscr{H}2$ $det(J|_{E_1^*};\beta=\beta_H)=E_{11}E_{22}-E_{12}E_{21}>0,$

$\mathscr{H}3$ $\frac{d}{d\beta}(Re(\lambda(\beta)))_{\beta=\beta_H}=\frac{1}{2}\frac{d}{d\beta}(tr(J|_{E_1^*})_{\beta=\beta_H}\neq 0,$

where $E_{ij};i,j=1,2$ *are the entries of Jacobian* J *(from (5.12)) evaluated at* $(E_1^*;\beta=\beta_H)$ *and* $\lambda(\beta)$ *is eigenvalue of* $J|_{E_1^*}$.

Proof. In Theorem 5.2.5, we have already proved that $det(J|_{E_1^*})>0$ whenever E_1^* exists. The next tasks are; to calculate the critical value β_H which is a positive solution of $tr(J|_{E_1^*})=0$, and to verify the the transversality condition given by $\mathscr{H}3$. The critical value β_H of β for Hopf bifurcation is the root of quadratic equation given below:

$$\Lambda_2\beta^2+\Lambda_1\beta+\Lambda_0=0, \tag{5.14}$$

where

$$\begin{aligned}
\Lambda_2 &= P_1^{*2}rU_1^*(k(U_1^*+2\theta)-U_1^*(2U_1^*+3\theta)),\\
\Lambda_1 &= -c_1kP_1^{*2}(U_1^*+\theta)^2+2hP_1^*rU_1^*(k(U_1^*+2\theta)-U_1^*(2U_1^*+3\theta))\\
&\quad +2P_1^*rU_1^{*2}(k(U_1^*+2\theta)-U_1^*(2U_1^*+3\theta))-c_1kP_1^*(U_1^*+\theta)^2(c_2U_1^*+(h+U_1^*)\alpha),\\
\Lambda_0 &= -c_1hkP_1^*(U_1^*+\theta)^2+h^2rU_1^*(k(U_1^*+2\theta)-U_1^*(2U_1^*+3\theta))\\
&\quad +2hrU_1^{*2}(k(U_1^*+2\theta)-U_1^*(2U_1^*+3\theta))+rU_1^{*3}(k(U_1^*+2\theta)-U_1^*(2U_1^*+3\theta)).
\end{aligned}$$

We can observe that the coefficients Λ_2,Λ_1 and Λ_0 contains, U_1^* and P_1^* which are further implicit functions of β. Thus we evaluate the the value of β_H and the corresponding U_1^* and P_1^* numerically, and the resultant triplet (β_H,U_1^*,P_1^*) satisfy (5.14).

For transversality condition, firstly we need to calculate $\tau_1=U'$ and $\tau_2=P'$ which are given by

$$\begin{aligned}
\tau_1=U' &= -\frac{U(\frac{dA_1}{d\beta}+U\frac{dA_2}{d\beta}+U^2\frac{dA_3}{d\beta})}{3A_3U^2+2A_2U+A_1}\Big|_{(U=U_1^*,P=P_1^*)},\\
&= \frac{-Uc_1(hr\alpha k+U(rc_2\alpha-hr\alpha+r\alpha k)+U^2(-rc_2-rc_2\alpha))}{3A_3U^2+2A_2U+A_1}\Big|_{(U=U_1^*,P=P_1^*)},\\
\tau_2=P' &= \frac{h\delta+(c_1c_2-\delta)(\tau_1\beta-U)}{\beta^2(\delta+c_1\alpha)}\Big|_{(U=U_1^*,P=P_1^*)},
\end{aligned}$$

where $'$ signifies the derivative with respect to β and A_1, A_2, A_3 are taken from (5.10). Now, doing the further calculations, we get that the transversality condition holds if

$$\begin{aligned}\frac{d}{d\beta}(tr(J|_{E_1^*})_{\beta=\beta_H} = \Bigg[&- \frac{c_1}{(h+\beta P_1^* + U_1^*)^3}\Big[-\beta P_1^{*3} + (h+U_1^*)(h+h\beta\alpha+\beta(c_2+\alpha)U_1^*)\tau_2 \\ &- P_1^{*2}[h+h\beta\alpha+(-1+c_2\beta+\beta\alpha)U_1^* - \beta(-2+c_2\beta+\beta\alpha)\tau_1] \\ &+ P_1^*[(c_2+\alpha)U_1^{*2} + U_1^*(h(c_2+2\alpha) - \beta(-2+c_2\beta+\beta\alpha)\tau_2 - \beta(c_2+\alpha)\tau_1) \\ &+ h(h\alpha + (\beta-\beta^2\alpha)\tau_2 + (-2+c_2\beta-\beta\alpha)\tau_1)]\Big] \\ &+ \frac{2r(k\theta^2 - 3\theta^2 U_1^* - 3\theta U_1^{*2} - U_1^{*3})\tau_1}{k(\theta+U_1^*)^3}\Bigg]\Bigg|_{\beta=\beta_H} \\ &\neq 0.\end{aligned}$$

This completes the proof this theorem. ∎

5.2.4.2 Saddle-node bifurcation

Theorem 5.2.7. *When System (5.4) has three interior coexistence steady states, then it undergoes saddle-node bifurcation with respect to parameter θ when either $g(U_{z_1}) = 0$ or $g(U_{z_2}) = 0$ where U_{z_1} and U_{z_2} are the roots of $g'(U) = 0$.*

Proof. We assume that the condition $g(U_{z_1}) = 0$ holds, i.e. the coexistence equilibria $E_1^*(U_1^*, P_1^*)$ and $E_2^*(U_2^*, P_2^*)$ collides and U_{z_1} becomes the double root of $g(U)$ at $\theta = \theta_{SN_1}$. Moreover, at $E_{z_1} = (U_{z_1}, P_{z_1})$ for $\theta = \theta_{SN_1}$, both the nullclines f_1 and f_2 touch each other which implies $\frac{dP^{(f_2)}}{dU} - \frac{dP^{(f_1)}}{dU} = 0$. Thereby, we have $det(J|_{E_{z_1}}) = 0$, which implies one of the eigenvalues of $J|_{(E_{z_1}, \theta_{SN_1})}$ becomes zero. Let R and S be the eigenvectors of $J|_{(E_{z_1}, \theta_{SN_1})}$ and $J^T|_{(E_{z_1}, \theta_{SN_1})}$, respectively, corresponding to zero eigenvalue; are given by $R = (1, R_{21})^T$, $S = (1, S_{21})^T$, where

$$R_{21} = \frac{(h+U_{z_1}+\beta P_{z_1})^2}{c_1 U_{z_1}(h+U_{z_1})}\left(\frac{rU_{z_1}(k(U_{z_1}+2\theta_{SN_1}) - U_{z_1}(2U_{z_1}+3\theta_{SN_1}))}{k(U_{z_1}+\theta_{SN_1})^2} - \frac{c_1 P_{z_1}(h+\beta P_{z_1})}{(h+U_{z_1}+\beta P_{z_1})^2}\right),$$

$$\begin{aligned}S_{21} = &\frac{(h+U_{z_1}+\beta P_{z_1})^2}{c_1 c_2 P_{z_1}(h+\beta P_{z_1}) + c_1\beta\alpha {P_{z_1}}^2} \\ &\times\left(-\frac{rU_{z_1}(k(U_{z_1}+2\theta_{SN_1}) - U_{z_1}(2U_{z_1}+3\theta_{SN_1}))}{k(U_{z_1}+\theta_{SN_1})^2} + \frac{c_1 P_{z_1}(h+\beta P_{z_1})}{(h+U_{z_1}+\beta P_{z_1})^2}\right).\end{aligned}$$

Then the transversality conditions [127] for saddle-node bifurcation are given by

$$S^T G_\theta(E_{z_1}, \theta_{SN_1}) = -\frac{rU_{z_1}^2}{(\theta_{SN_1} + U_{z_1})^2}\left(1 - \frac{U_{z_1}}{k}\right) \neq 0,$$

$$S^T[D^2 G_\theta(E_{z_1}, \theta_{SN_1})(R,R)] = (A_{11} + R_{21}A_{12} + A_{13} + R_{21}A_{14}) + S_{21}(A_{21} + R_{21}A_{22} + A_{23} + R_{21}A_{24}),$$

where

$$\begin{aligned}
A_{11} &= \frac{2c_1(h + P_{z_1}\beta)}{(h + U_{z_1} + P_{z_1}\beta)^3} - \frac{2r(U_{z_1}^3 + 3U_{z_1}^2\theta_{SN_1} - k\theta_{SN_1}^2 + 3U_{z_1}\theta_{SN_1}^2)}{k(U_{z_1} + \theta_{SN_1})^3},\\
A_{12} &= -\frac{c_1(h^2 + 2P_{z_1}U_{z_1}\beta + h(U_{z_1} + P_{z_1}\beta))}{(h + U_{z_1} + P_{z_1}\beta)^3},\\
A_{13} &= -\frac{c_1(h^2 + 2P_{z_1}U_{z_1}\beta + h(U_{z_1} + P_{z_1}\beta))}{(h + U_{z_1} + P_{z_1}\beta)^3},\ A_{14} = \frac{2c_1U_{z_1}(h + U_{z_1})\beta}{(h + U_{z_1} + P_{z_1}\beta)^3},\\
A_{21} &= -\frac{2c_1P_{z_1}(c_2(h + P_{z_1}\beta) + P_{z_1}\beta\alpha)}{(h + U_{z_1} + P_{z_1}\beta)^3},\\
A_{22} &= -\frac{c_1P_{z_1}\beta(c_2(h - U_{z_1} + P_{z_1}\beta) - (h + U_{z_1} - P_{z_1}\beta)\alpha)}{(h + U_{z_1} + P_{z_1}\beta)^3},\\
A_{23} &= \frac{c_1\left(c_2\left(h^2 + 2P_{z_1}U_{z_1}\beta + h(U_{z_1} + P_{z_1}\beta)\right) + 2P_{z_1}(h + U_{z_1})\beta\alpha\right)}{(h + U_{z_1} + P_{z_1}\beta)^3},\\
A_{24} &= -\frac{c_1\beta(h + U_{z_1} - P_{z_1}\beta)(c_2U_{z_1} + (h + U_{z_1})\alpha)}{(h + U_{z_1} + P_{z_1}\beta)^3}.
\end{aligned}$$

Therefore, the transversality conditions for saddle-node bifurcation hold if

$$\begin{aligned}
S^T[D^2 G_\theta(E_{z_1}, \theta_{SN_1})(R,R)] &= (A_{11} + R_{21}A_{12} + A_{13} + R_{21}A_{14})\\
&\quad + S_{21}(A_{21} + R_{21}A_{22} + A_{23} + R_{21}A_{24})\\
&\neq 0.
\end{aligned}$$

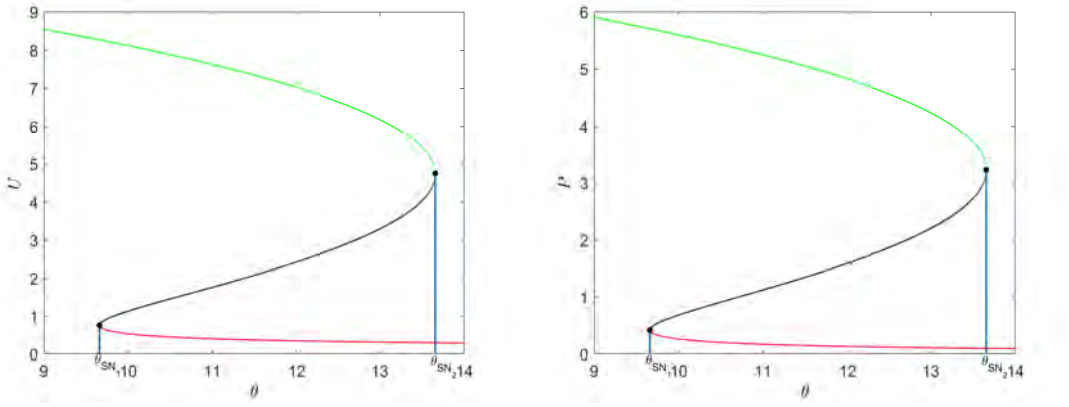

(a) (b)

Fig. 5.4: (a) and (b) illustrates the saddle-node bifurcations at θ_{SN_1} and θ_{SN_2}, respectively, where green line, black line and red line represent stable E_3^*, saddle point E_2^* and stable E_1^*, respectively.

For the fixed parameters from (5.1), we get $\theta_{SN_1} = 9.660692$, $E_{z_1}(U_{z_1}, P_{z_1}) = (0.752202, 0.418216)$. Thus, we can infer that system (5.4) undergo saddle-node bifurcation for $\theta = \theta_{SN_1}$. A similar analysis can be done when $E_2^*(U_1^*, P_1^*)$ and $E_3^*(U_3^*, P_3^*)$ collides at $E_{z_2}(U_{z_2}, P_{z_2}) = (4.741278, 3.225344)$ for $\theta = \theta_{SN_2} = 13.654735$. We have also presented the saddle-node bifurcation diagrams for both the species U and P in Figs. 5.4(a) and 5.4(b), respectively. From these figures, we can also observe that for these set of parameters with $\theta \in (\theta_{SN_1}, \theta_{SN_2})$ there is existence of three coexistence steady states out of which two are stable and one saddle, and beyond this range there is only one coexistence steady state because of saddle-node bifurcation of other two. In other words, we can say that for the coexistence of all three interior equilibria, the strength of the Allee effect must belong a to a particular interval and refraining this will cause the saddle-node bifurcation, resulting in annihilation of E_1^*, E_2^* or E_3^*, E_2^*. ∎

5.2.4.3 Generalized Hopf-bifurcation

Here, we discuss a co-dimension two bifurcation known as Bautin or generalized Hopf bifurcation. In this bifurcation, interior equilibrium has imaginary eigenvalues at the point of bifurcation, called as GH-point. The another attribute of this bifurcation is that the first Lyapunov coefficient also vanishes at GH-point which implies that, at this point the direction of Hopf bifurcation changes from supercritical to subcritical or vice versa. We analyze this bifurcation in the $\theta\beta$-plane with respect to E_1^*.

Theorem 5.2.8. *System (5.4) undergoes generalized Hopf bifurcation about the coexistence equilibrium E_1^* at the critical point (β_G, θ_G) in the $\theta\beta$-plane under the following conditions:*

$\mathscr{G}1$ $tr(J|_{E_1^*}; \theta = \theta_G, \beta = \beta_G) = 0$,

$\mathscr{G}2$ $det(J|_{E_1^*}; \theta = \theta_G, \beta = \beta_G) > 0$,

$\mathscr{G}3$ $l_1(E_1^*; \theta = \theta_G, \beta = \beta_G) = 0$.

Proof. The conditions $\mathscr{G}1$, $\mathscr{G}2$ are similar to $\mathscr{H}1$ and $\mathscr{H}2$ in Theorem 5.2.6, so omit them, Now, we evaluate the first Lyapunov coefficient l_1 at E_1^* with $\theta = \theta_G, \beta = \beta_G$. Firstly, we translate E_1^* to origin using the transformation $x = U - U_1^*$ and $y = P - P_1^*$. Then, using Taylor's series expansion up to order three, system (5.4) in the neighborhood of origin can be written as

$$\begin{aligned}
\dot{x} &= a_{10}x + a_{01}y + a_{20}x^2 + a_{11}xy + a_{02}y^2 + a_{30}x^3 + a_{21}x^2y + a_{12}xy^2 + a_{03}y^3 + H_1(x,y),\\
\dot{y} &= b_{10}x + b_{01}y + b_{20}x^2 + b_{11}xy + b_{02}y^2 + b_{30}x^3 + b_{21}x^2y + b_{12}xy^2 + b_{03}y^3 + H_2(x,y),
\end{aligned}$$

where H_1 and H_2 are C^∞ functions with terms $x^i y^j$ satisfying $i + j \geq 4$ and

$$\begin{aligned}
a_{10} &= \frac{rU_1^*\left(k\left(U_1^*+2\theta\right)-U_1^*\left(2U_1^*+3\theta\right)\right)}{k\left(U_1^*+\theta\right)^2} - \frac{c_1P_1^*\left(h+\beta P_1^*\right)}{\left(h+U_1^*+\beta P_1^*\right)^2},\ a_{01} = -\frac{c_1U_1^*\left(h+U_1^*\right)}{\left(h+U_1^*+\beta P_1^*\right)^2},\\
a_{20} &= \frac{r\left(k\theta^2-3\theta^2U_1^*-3\theta U_1^{*2}-U_1^{*3}\right)}{k\left(\theta+U_1^*\right)^3} + \frac{c_1P_1^*\left(h+\beta P_1^*\right)}{\left(h+U_1^*+\beta P_1^*\right)^3},\\
a_{11} &= -\frac{c_1\left(h\left(h+U_1^*\right)+\beta P_1^*\left(h+2U_1^*\right)\right)}{\left(h+U_1^*+\beta P_1^*\right)^3},\ a_{02} = \frac{\beta c_1U_1^*\left(h+U_1^*\right)}{\left(h+U_1^*+\beta P_1^*\right)^3},\\
a_{30} &= -\frac{c_1P_1^*\left(h+\beta P_1^*\right)}{\left(h+U_1^*+\beta P_1^*\right)^4} - \frac{r\theta^2(k+\theta)}{k\left(\theta+U_1^*\right)^4},\ a_{21} = \frac{c_1\left(-\beta^2P_1^{*2}+2\beta P_1^*U_1^*+h\left(h+U_1^*\right)\right)}{\left(h+U_1^*+\beta P_1^*\right)^4},\\
a_{12} &= \frac{\beta c_1\left(h^2-U_1^{*2}+\beta P_1^*\left(h+2U_1^*\right)\right)}{\left(h+U_1^*+\beta P_1^*\right)^4},\ a_{03} = -\frac{\beta^2c_1U_1^*\left(h+U_1^*\right)}{\left(h+U_1^*+\beta P_1^*\right)^4},\\
b_{10} &= \frac{c_1c_2P_1^*\left(h+\beta P_1^*\right)+c_1\beta\alpha P_1^{*2}}{\left(h+U_1^*+\beta P_1^*\right)^2},\ b_{01} = \frac{-c_1P_1^*\beta\left(c_2U_1^*+\alpha\left(h+U_1^*\right)\right)}{\left(h+U_1^*+\beta P_1^*\right)^2},\\
b_{20} &= -\frac{\left(\beta\alpha c_1P_1^{*2}+c_1c_2P_1^*\left(h+\beta P_1^*\right)\right)}{\left(h+U_1^*+\beta P_1^*\right)^3},\\
b_{11} &= \frac{c_1\left(2\beta\alpha P_1^*\left(h+U_1^*\right)+c_2\left(h\left(h+U_1^*\right)+\beta P_1^*\left(h+2U_1^*\right)\right)\right)}{\left(h+U_1^*+\beta P_1^*\right)^3},
\end{aligned}$$

$$b_{02}=-\frac{\beta c_1\left(h-\beta P_1^*+U_1^*\right)\left(h\alpha+(\alpha+c_2)U_1^*\right)}{2\left(h+U_1^*+\beta P_1^*\right)^3},\ b_{30}=\frac{\left(\beta\alpha c_1 P_1^{*2}+c_1c_2P_1^*\left(h+\beta P_1^*\right)\right)}{\left(h+U_1^*+\beta P_1^*\right)^4},$$
$$b_{21}=-\frac{c_1\left(\beta\alpha P_1^*\left(-\beta P_1^*+2\left(h+U_1^*\right)\right)+c_2\left(-\beta^2P_1^{*2}+2\beta P_1^*U_1^*+h\left(h+U_1^*\right)\right)\right)}{\left(h+U_1^*+\beta P_1^*\right)^4},$$
$$b_{12}=\frac{\beta c_1\left(\alpha\left(h+U_1^*\right)\left(h-2\beta P_1^*+U_1^*\right)-c_2\left(h^2-U_1^{*2}+\beta P_1^*\left(h+2U_1^*\right)\right)\right)}{\left(h+U_1^*+\beta P_1^*\right)^4},$$
$$b_{03}=-\frac{\beta^2c_1\left(h\alpha+(\alpha+c_2)U_1^*\right)\left(\beta P_1^*-2\left(h+U_1^*\right)\right)}{\left(h+U_1^*+\beta P_1^*\right)^4}.$$

Now, we calculate l_1 to determine the direction (stability) of limit cycle by using the formula [127] given as

$$\begin{aligned}l_1=&-\frac{3\pi}{2a_{01}\Theta^{\frac{3}{2}}}\Big\{\Big[a_{10}b_{10}\left(a_{11}^2+a_{11}b_{02}+a_{02}b_{11}\right)+a_{10}a_{01}\left(b_{11}^2+a_{20}b_{11}+a_{11}b_{02}\right)\\&+b_{10}^2\left(a_{11}a_{02}+2a_{02}b_{02}\right)-2a_{10}b_{10}\left(b_{02}^2-a_{20}a_{02}\right)-2a_{10}a_{01}\left(a_{20}^2-b_{20}b_{02}\right)\\&-a_{01}^2\left(2a_{20}b_{20}+b_{11}b_{20}\right)+\left(a_{01}b_{10}-2a_{10}^2\right)\left(b_{11}b_{02}-a_{11}a_{20}\right)\Big]\\&-\left({a_{10}}^2+a_{01}b_{10}\right)\Big[3\left(b_{10}b_{03}-a_{01}a_{30}\right)+2a_{10}\left(a_{21}+b_{12}\right)\\&+\left(b_{10}a_{12}-a_{01}b_{21}\right)\Big]\Big\}\Big|_{(E_1^*;\theta=\theta_G,\beta=\beta_G)},\end{aligned}\tag{5.15}$$

with $\Theta=(a_{10}b_{01}-a_{01}b_{10})|_{(E_1^*;\theta=\theta_G,\beta=\beta_G)}$. Therefore, we infer that our system (5.4) admits GH bifurcation at E_1^* for $\theta=\theta_G,\beta=\beta_G$ if $l_1=0$. ∎

5.2.4.4 Bogdanov-Takens bifurcation

The second type of co-dimension 2 bifurcation under which our system (5.4) may go is Bogdanov–Takens (BT) bifurcation. Varying two parameters, this bifurcation takes place at a point in the bi-parametric plane where saddle-node curve meet with Hopf curve. Two eigenvalues associated with the equilibrium at this point of meet become zero which makes this equilibrium a degenerate equilibrium [127]. As our system has encountered Hopf bifurcation with respect to β and saddle-node bifurcation with respect to θ, thus we study BT-bifurcation in the $\theta\beta$-plane.

Theorem 5.2.9. *If θ and β are picked as the bifurcation parameters then system (5.4) undergoes Bogdanov–Takens (BT) bifurcation of codimension 2 in the vicinity of $E_{BT}=(\bar{U},\bar{P})$ at $(\theta,\beta)=(\theta_{BT},\beta_{BT})$ when the the following conditions holds:*

$\mathscr{BT}1$ $tr(J|_{E_{BT}};\theta=\theta_{BT},\beta=\beta_{BT})=0,$

$\mathscr{BT}2$ $det(J|_{E_{BT}};\theta=\theta_{BT},\beta=\beta_{BT})=0.$

Proof. The above two conditions $\mathscr{BT}1$ and $\mathscr{BT}2$ are equivalent to following:

$$\frac{r\bar{U}(k(\bar{U}+2\theta)-\bar{U}(2\bar{U}+3\theta))}{k(\bar{U}+\theta)^2}-\frac{c_1\bar{P}(h+\beta\bar{P})}{(h+\bar{U}+\beta\bar{P})^2}-\frac{c_1\bar{P}\beta(c_2\bar{U}+\alpha(h+\bar{U}))}{(h+\bar{U}+\beta\bar{P})^2}\Bigg|_{(\theta=\theta_{BT},\beta=\beta_{BT})}=0,$$

$$\left(\frac{r\bar{U}(k(\bar{U}+2\theta)-\bar{U}(2\bar{U}+3\theta))}{k(\bar{U}+\theta)^2}-\frac{c_1\bar{P}(h+\beta\bar{P})}{(h+\bar{U}+\beta\bar{P})^2}\right)\left(-\frac{c_1\bar{P}\beta(c_2\bar{U}+\alpha(h+\bar{U}))}{(h+\bar{U}+\beta\bar{P})^2}\right)$$

$$+\left(\frac{c_1\bar{U}(h+\bar{U})}{(h+\bar{U}+\beta\bar{P})^2}\right)\left(\frac{c_1c_2\bar{P}(h+\beta\bar{P})+c_1\beta\alpha\bar{P}^2}{(h+\bar{U}+\beta\bar{P})^2}\right)\Bigg|_{(\theta=\theta_{BT},\beta=\beta_{BT})}=0,$$

respectively. Now, we use the techniques discussed in [25, 58] to deduce system (5.4) to its the normal form for Bogdanov-Takens bifurcation. Consider the system

$$\begin{cases}\frac{dU}{dt}=\frac{rU^2}{U+\theta_{BT_1}+\varepsilon_1}\left(1-\frac{U}{k}\right)-\frac{c_1UP}{h+U+(\beta_{BT_1}+\varepsilon_2)P},\\ \frac{dP}{dt}=\frac{c_1c_2UP-c_1(\beta_{BT_1}+\varepsilon_2)\alpha P^2}{h+U+(\beta_{BT_1}+\varepsilon_2)P}-\delta P,\end{cases}\tag{5.16}$$

with $\theta=\theta_{BT_1}+\varepsilon_1$ and $\beta=\beta_{BT_1}+\varepsilon_2$, where $\varepsilon=(\varepsilon_1,\varepsilon_2)$ is very small vector in vicinity of $(0,0)$. We make $(0,0)$ as the bifurcation point with use of transformation $u=U-\bar{U}$, $v=P-\bar{P}$ in (5.16), and then we obtain

$$\begin{cases}\dot{u}=m_{00}+m_{10}u+m_{01}v+m_{11}uv+m_{20}u^2+m_{02}v^2+M_1(u,v,\varepsilon),\\ \dot{v}=n_{00}+n_{10}u+n_{01}v+n_{11}uv+n_{20}u^2+n_{02}v^2+M_2(u,v,\varepsilon),\end{cases}\tag{5.17}$$

where

$$\begin{aligned}
m_{00}&=\frac{r\bar{U}^2}{\bar{U}+\theta+\varepsilon_1}\left(1-\frac{\bar{U}}{k}\right)-\frac{c_1\bar{U}\bar{P}}{h+\bar{U}+(\beta+\varepsilon_2)\bar{P}},\\
m_{10}&=-\frac{c_1\bar{P}(h+\bar{P}(\beta+\varepsilon_2))}{(h+\bar{U}+\bar{P}(\beta+\varepsilon_2))^2}+\frac{r\bar{U}(k(\bar{U}+2(\varepsilon_1+\theta))-\bar{U}(2\bar{U}+3(\varepsilon_1+\theta)))}{k(\bar{U}+\varepsilon_1+\theta)^2},\\
m_{01}&=-\frac{c_1\bar{U}(h+\bar{U})}{(h+\bar{U}+\bar{P}(\beta+\varepsilon_2))^2},\ m_{11}=-\frac{c_1\left(h^2+2\bar{P}\bar{U}(\beta+\varepsilon_2)+h(\bar{U}+\bar{P}(\beta+\varepsilon_2))\right)}{(h+\bar{U}+\bar{P}(\beta+\varepsilon_2))^3},\\
m_{20}&=\frac{c_1\bar{P}(h+\bar{P}(\beta+\varepsilon_2))}{(h+\bar{U}+\bar{P}(\beta+\varepsilon_2))^3}-\frac{r\left(\bar{U}^3+3\bar{U}^2(\theta+\varepsilon_1)-k(\theta+\varepsilon_1)^2+3\bar{U}(\theta+\varepsilon_1)^2\right)}{k(\bar{U}+\varepsilon_1+\theta)^3},
\end{aligned}$$

$$m_{02} = \frac{c_1\bar{U}(h+\bar{U})(\beta+\varepsilon_2)}{(h+\bar{U}+\bar{P}(\beta+\varepsilon_2))^3},\ n_{00} = \frac{c_1c_2\bar{U}\bar{P} - c_1(\beta+\varepsilon_2)\alpha\bar{P}^2}{h+\bar{U}+(\beta+\varepsilon_2)\bar{P}} - \delta\bar{P},$$
$$n_{10} = \frac{c_1\bar{P}(c_2(h+\bar{P}(\beta+\varepsilon_2)) + \bar{P}(\beta+\varepsilon_2)\alpha)}{(h+\bar{U}+\bar{P}(\beta+\varepsilon_2))^2},$$
$$n_{01} = -\delta + \frac{c_1(c_2\bar{U} - 2\bar{P}(\beta+\varepsilon_2)\alpha)}{h+\bar{U}+\bar{P}(\beta+\varepsilon_2)} + \frac{c_1\bar{P}(\beta+\varepsilon_2)(-c_2\bar{U}+\bar{P}(\beta+\varepsilon_2)\alpha)}{(h+\bar{U}+\bar{P}(\beta+\varepsilon_2))^2},$$
$$n_{11} = \frac{\left(c_1(c_2\left(h^2+2\bar{P}\bar{U}(\beta+\varepsilon_2)+h(\bar{U}+\bar{P}(\beta+\varepsilon_2))\right)+2\bar{P}(h+\bar{U})(\beta+\varepsilon_2)\alpha\right)}{(h+\bar{U}+\bar{P}(\beta+\varepsilon_2))^3},$$
$$n_{20} = -\frac{c_1\bar{P}(c_2(h+\bar{P}(\beta+\varepsilon_2)) + \bar{P}(\beta+\varepsilon_2)\alpha)}{(h+\bar{U}+\bar{P}(\beta+\varepsilon_2))^3},\ n_{02} = -\frac{c_1(h+\bar{U})(\beta+\varepsilon_2)(c_2\bar{U}+(h+\bar{U})\alpha)}{(h+\bar{U}+\bar{P}(\beta+\varepsilon_2))^3},$$

and $M_1(u,v,\varepsilon)$, $M_2(u,v,\varepsilon)$ are are C^∞ functions with terms u^iv^j satisfying $i+j\geq 3$.

Next, we use the change of coordinates

$$\begin{cases} p = u, \\ q = m_{00} + m_{10}u + m_{01}v + m_{11}uv + m_{20}u^2 + m_{02}v^2 + M_1(u,v,\varepsilon), \end{cases} \tag{5.18}$$

and write (5.17) as

$$\begin{cases} \dot{p} = q, \\ \dot{q} = r_{00} + r_{10}p + r_{01}q + r_{11}pq + r_{20}p^2 + r_{02}q^2 + M_3(p,q,\varepsilon), \end{cases} \tag{5.19}$$

with

$$r_{00} = \frac{m_{00}^2m_{02}m_{10}}{m_{01}^2} - \frac{m_{00}^3m_{02}m_{11}}{m_{01}^3} + m_{01}n_{00} - m_{00}n_{01} + \frac{m_{00}^2n_{02}}{m_{01}},$$
$$r_{10} = \frac{2m_{00}m_{02}m_{10}^2}{m_{01}^2} - \frac{5m_{00}^2m_{02}m_{10}m_{11}}{m_{01}^3} + \frac{3m_{00}^3m_{02}m_{11}^2}{m_{01}^4} + \frac{2m_{00}^2m_{02}m_{20}}{m_{01}^2} + m_{11}n_{00} - m_{10}n_{01}$$
$$+ \frac{2m_{00}m_{10}n_{02}}{m_{01}} - \frac{m_{00}^2m_{11}n_{02}}{m_{01}^2} + m_{01}n_{10} - m_{00}n_{11},$$
$$r_{01} = m_{10} - \frac{2m_{00}m_{02}m_{10}}{m_{01}^2} - \frac{m_{00}m_{11}}{m_{01}} + \frac{3m_{00}^2m_{02}m_{11}}{m_{01}^3} + n_{01} - \frac{2m_{00}n_{02}}{m_{01}},$$

$$
\begin{aligned}
r_{20} =& \frac{m_{02}m_{10}^3}{m_{01}^2} - \frac{7m_{00}m_{02}m_{10}^2m_{11}}{m_{01}^3} + \frac{12m_{00}^2m_{02}m_{10}m_{11}^2}{m_{01}^4} - \frac{6m_{00}^3m_{02}m_{11}^3}{m_{01}^5} + \frac{6m_{00}m_{02}m_{10}m_{20}}{m_{01}^2} \\
& - \frac{7m_{00}^2m_{02}m_{11}m_{20}}{m_{01}^3} - m_{20}n_{01} + \frac{m_{10}^2n_{02}}{m_{01}} - \frac{2m_{00}m_{10}m_{11}n_{02}}{m_{01}^2} + \frac{m_{00}^2m_{11}^2n_{02}}{m_{01}^3} + \frac{2m_{00}m_{20}n_{02}}{m_{01}} \\
& + m_{11}n_{10} - m_{10}n_{11} + m_{01}n_{20}, \\
r_{11} =& -\frac{2m_{02}m_{10}^2}{m_{01}^2} - \frac{m_{10}m_{11}}{m_{01}} + \frac{10m_{00}m_{02}m_{10}m_{11}}{m_{01}^3} + \frac{m_{00}m_{11}^2}{m_{01}^2} - \frac{9m_{00}^2m_{02}m_{11}^2}{m_{01}^4} + 2m_{20} \\
& - \frac{4m_{00}m_{02}m_{20}}{m_{01}^2} - \frac{2m_{10}n_{02}}{m_{01}} + \frac{2m_{00}m_{11}n_{02}}{m_{01}^2} + n_{11}, \\
r_{02} =& \frac{m_{02}m_{10}}{m_{01}^2} + \frac{m_{11}}{m_{01}} - \frac{3m_{00}m_{02}m_{11}}{m_{01}^3} + \frac{n_{02}}{m_{01}},
\end{aligned}
$$

and $M_3(p,q,\varepsilon)$ is C^∞ function with terms p^iq^j satisfying $i+j \geq 3$.
Now, we introduce a time variable τ by $dt = (1-r_{02}p)d\tau$. Rewriting τ as t, (5.19) can be written as

$$
\begin{cases}
\dot{p} = (1-r_{02}p)q, \\
\dot{q} = (1-r_{02}p)(r_{00}+r_{10}p+r_{01}q+r_{11}pq+r_{20}p^2+r_{02}q^2+M_3(p,q,\varepsilon)).
\end{cases} \tag{5.20}
$$

Let $z_1 = p,\ z_2 = q(1-r_{02}p)$, then we can write (5.20) as

$$
\begin{cases}
\dot{z_1} = z_2, \\
\dot{z_2} = \eta_{00}+\eta_{10}z_1+\eta_{01}z_2+\eta_{11}z_1z_2+\eta_{20}z_1^2+M_4(z_1,z_2,\varepsilon),
\end{cases} \tag{5.21}
$$

where

$$
\begin{aligned}
\eta_{00} =& r_{00},\ \eta_{10} = -2r_{00}r_{02}+r_{10},\ \eta_{01} = r_{01},\ \eta_{11} = -r_{01}r_{02}+r_{11}, \\
\eta_{20} =& r_{00}r_{02}^2 - 2r_{02}r_{10}+r_{20},
\end{aligned}
$$

$M_4(z_1,z_2,\varepsilon)$ is C^∞ function with terms $w_1^iw_2^j$ satisfying $i+j \geq 3$. It can be noted that the sign of η_{20} is not known, thus we take the two cases while making following transformations.
Case 1. If $\eta_{20} > 0$, then we make the following transformations

$$
w_1 = z_1,\ w_2 = \frac{z_2}{\sqrt{\eta_{20}}},\ \tau = \sqrt{\eta_{20}}t.
$$

Writing τ as t, (5.21) can be written as

$$\begin{cases} \dot{w_1} = w_2, \\ \dot{w_2} = \theta_{00} + \theta_{10}w_1 + \theta_{01}w_2 + \theta_{11}w_1w_2 + w_1^2 + M_5(w_1, w_2, \varepsilon), \end{cases} \tag{5.22}$$

where

$$\theta_{00} = \frac{\eta_{00}}{\eta_{20}},\ \theta_{10} = \frac{\eta_{10}}{\eta_{20}},\ \theta_{01} = \frac{\eta_{01}}{\sqrt{\eta_{20}}},\ \theta_{11} = \frac{\eta_{11}}{\sqrt{\eta_{20}}},$$

and $M_5(w_1, w_2, \varepsilon)$ is C^∞ function with terms $w_1^i w_2^j$ satisfying $i + j \geq 3$.

Let $g_1 = w_1 + \frac{\theta_{10}}{2},\ g_2 = w_2$, then (5.22) can be written as

$$\begin{cases} \dot{g_1} = g_2, \\ \dot{g_2} = \mu_{00} + \mu_{01}g_2 + \mu_{11}g_1g_2 + g_1^2 + M_6(g_1, g_2, \varepsilon), \end{cases} \tag{5.23}$$

where

$$\mu_{00} = \theta_{00} - \frac{1}{4}\theta_{10},\ \mu_{01} = \theta_{01} - \frac{1}{2}\theta_{11}\theta_{10},\ \mu_{11} = \theta_{11},$$

and $M_6(g_1, g_2, \varepsilon)$ is C^∞ function with terms $w_1^i w_2^j$ satisfying $i + j \geq 3$.

For next transformation, we suppose that $\eta_{11} \neq 0$ which implies that $\mu_{11} = \theta_{11} = \frac{\eta_{11}}{\sqrt{\eta_{20}}} \neq 0$. Now, let $x = \mu_{11}^2 g_1,\ y = \mu_{11}^3 g_2,\ \tau = \frac{1}{\mu_{11}}t$ and using this we get

$$\begin{cases} \dot{x} = y, \\ \dot{y} = \chi_1 + \chi_2 y + x^2 + xy + M_7(x, y, \varepsilon), \end{cases} \tag{5.24}$$

which is versal unfolding of system (5.16), where

$$\chi_1 = \mu_{00}\mu_{11}^4,\ \chi_2 = \mu_{11}\mu_{01},$$

and $M_7(x, y, \varepsilon)$ is C^∞ function with terms $w_1^i w_2^j$ satisfying $i + j \geq 3$.

Now, if the determinant $\left|\frac{\partial(\chi_1, \chi_2)}{\partial(\varepsilon_1, \varepsilon_2)}\right|_{\varepsilon=0} \neq 0$ then it will imply that the parameter transformation (5.24) is homeomorphism in a small vicinity of $(0, 0)$, and $\varepsilon_1, \varepsilon_2$ are independent parameters.

Case 2. When $\eta_{20} < 0$, a similar set of transformation can be applied to obtain similar kind of versal unfolding of system (5.16). Thus we omit it whereas interested researchers can look here [58] for more details.

Using [127], we come to know that system (5.24) undergoes Bogdanov-Takens bifurcation when ε is in a tiny vicinity of $(0,0)$. The local representation of bifurcation curves are given as ($'+'$ for $\eta_{20} > 0$ and $'-'$ for $\eta_{20} < 0$):

1. The saddle node bifurcation curve is $SN = \{(\varepsilon_1, \varepsilon_2) : \chi_1(\varepsilon_1, \varepsilon_2) = 0, \chi_2(\varepsilon_1, \varepsilon_2) \neq 0\}$,
2. The Hopf bifurcation curve is $H = \{(\varepsilon_1, \varepsilon_2) : \chi_2(\varepsilon_1, \varepsilon_2) = \pm\sqrt{-\chi_1(\varepsilon_1, \varepsilon_2)}, \chi_1(\varepsilon_1, \varepsilon_2) < 0\}$,
3. The Homoclinic bifurcation curve is $HL = \{(\varepsilon_1, \varepsilon_2) : \chi_2(\varepsilon_1, \varepsilon_2) = \pm\frac{5}{7}\sqrt{-\chi_1(\varepsilon_1, \varepsilon_2)}, \chi_1(\varepsilon_1, \varepsilon_2) < 0\}$.

∎

Now, using the Matcont software, we try to illustrate all the bifurcations mentioned above in a single bi-parametric bifurcation diagram shown in Fig. 5.5. In this figure, all the observed singularities are marked with a black dot, whereas the meaning of the abbreviations used for them, their type, and the corresponding pair of (θ, β) are provided in Table 5.2. In Fig. 5.5, the blue curve stands for the subcritical Hopf bifurcation, and moving on this curve from right to left, the point where the direction of Hopf bifurcation changes is marked as GH_1. The curve joining the points GH_1 and BT_1 is the curve for supercritical Hopf bifurcation. The curve joining the two BT-bifurcation points, i.e., BT_1 and BT_2 corresponds to a neutral saddle; on this curve, both eigenvalues of the saddle point E_2^* have the same absolute values. Although this curve is not responsible for any bifurcation, but it often connects the BT points, which defines its significance [47]. The black colored lines, SN_1 and SN_2, represent the saddle-node bifurcation curves which join each other tangentially at the cusp point (CP-point). Between these SN_1 and SN_2 curves, all three coexistence equilibria exist, whereas, on SN_1, E_1^* and E_2^* annihilates through saddle-node bifurcation and E_3^* persists on the left of SN_1. Similarly, E_3^* and E_2^* annihilate on SN_2, and E_1^* persists on the right of SN_2. The curve from BT_2 to GH_2 causes the supercritical Hopf bifurcation whose direction changes at GH_2-point, and the further extension of this curve is not shown due to negative values of the parameters.

Abbreviation	Singularity type	(θ, β)
GH_1	Generalized Hopf bifurcation	$(10.116429, 1.927051)$
BT_1	Bogdanov-Takens bifurcation	$(9.190538, 1.909723)$
BT_2	Bogdanov-Takens bifurcation	$(5.887359, 1.126037)$
CP	Cusp Point	$(3.071196, 0.756838)$
GH_2	Generalized Hopf bifurcation	$(0.263186, 0.355407)$

Table 5.2: This table explains the abbreviation, corresponding type of singularity for a particular pair of (θ, β), shown in Fig. 5.5.

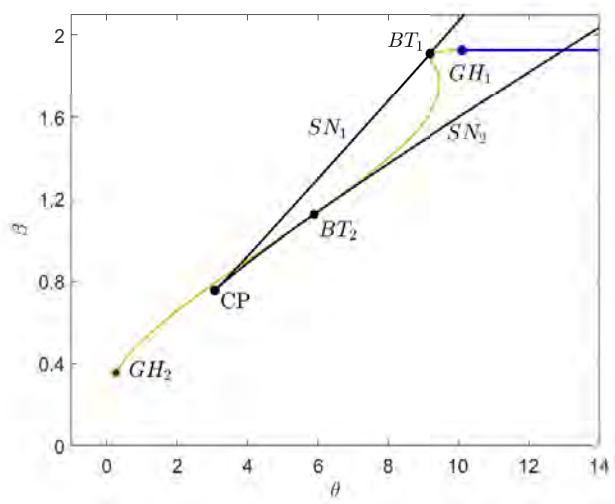

Fig. 5.5: This bi-parametric bifurcation diagram illustrates all the important local bifurcations of co-dimension 1 and 2 associated with system (5.4) for parameters fixed from (5.1).

Now, we analyze the dynamics of our system (5.4) in the neighborhood of *GH* and *BT* points for which we pick GH_1 and BT_1 points from Fig. 5.5.

Firstly, we investigate the kinetics of the system around the GH_1-point by plotting a bi-parametric bifurcation diagram in the $\theta\beta$-plane with $(\theta,\beta) \in [9,11]\times$ [1.922,1.932] in Fig. 5.6(a). To understand this bifurcation diagram, we divide this plane into three sub-regions: GR-I, GR-II, and GR-III, and make a trip about the GH_1-point counterclockwise, starting from part GR-I. In GR-I, the equilibrium E_1^* is locally stable, which is evident from the phase portrait given in Fig. 5.6(b), E_2^* is saddle whereas E_3^* is also locally stable (not shown for better view). Next, when we move from GR-I to GR-II via crossing the olive-colored curve by decreasing rate of cannibalism, the system encounters supercritical Hopf bifurcation about E_1^*, giving rise to a stable limit cycle around it, making E_1^* unstable, an example for this is portraited in Fig. 5.6(c). Further, from GR-II to GR-III by increasing both θ and β via blue colored curve, the system experiences subcritical Hopf bifurcation, which creates an unstable limit cycle (blue colored orbit in Fig. 5.6(d)) around E_1^* and inside the previous stable limit cycle. Moreover, crossing the red-colored curve by further increment in β leads to saddle-node bifurcation of these limit cycles, which results in stable E_1^* without any orbit around it (Fig. 5.6(e)). In this last phase diagram, we also portraited the stability of E_3^*, present in all three previous cases. From this, we can also conclude that system (5.4) possess the attribute of focus-focus and cycle-focus bi-stability with attractors having their corresponding basins of attraction.

Now, we explore the dynamics of system (5.4) in the neighborhood of BT_1-point (from Fig. 5.5) with $(\theta,\beta) \in [9,10] \times [1.9,1.935]$ as shown in Fig. 5.7(a). In this figure, we divide the

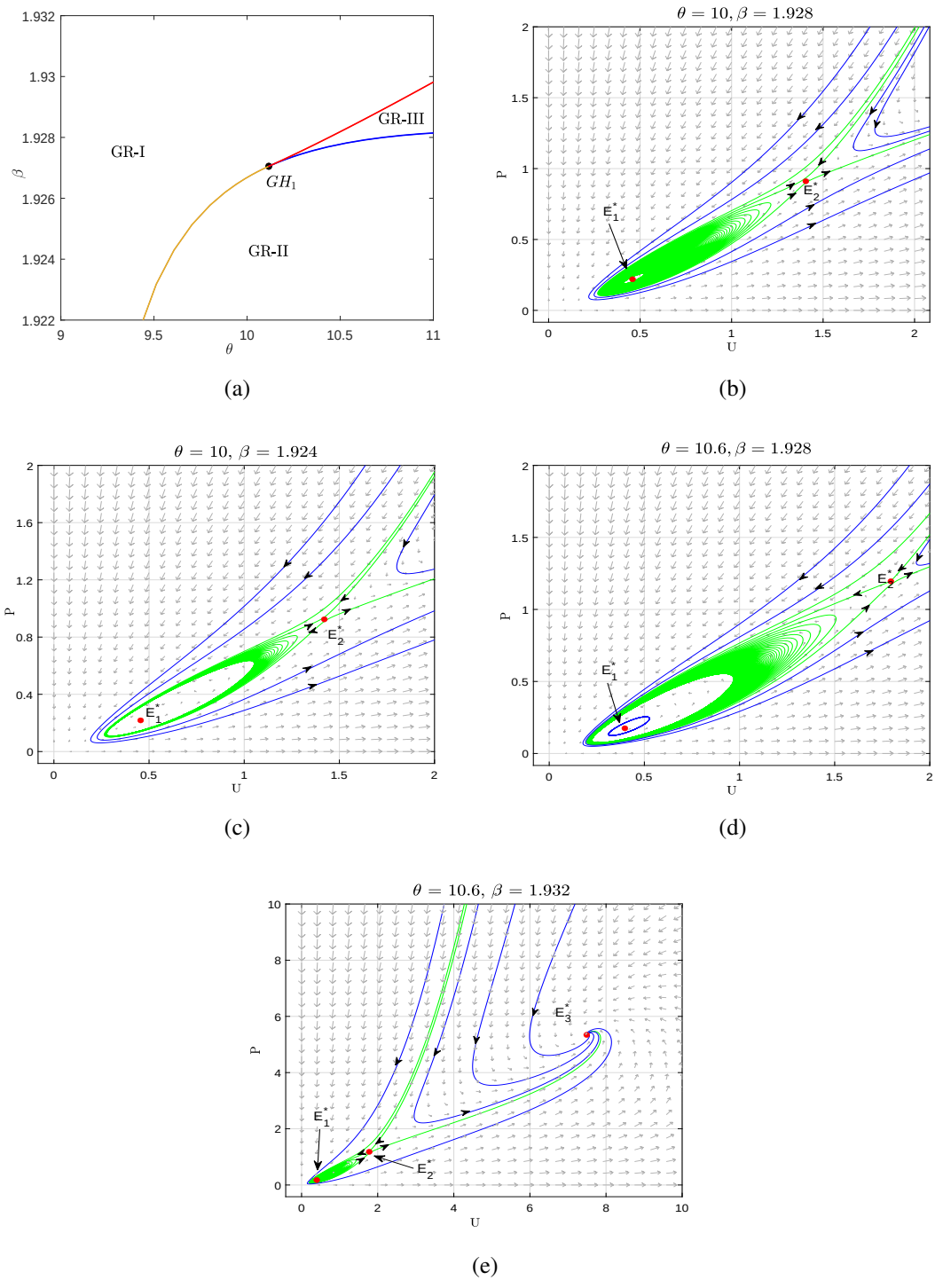

Fig. 5.6: Fig. (a) shows the division of neighborhood of GH_1-point (from Fig. 5.5) into three sub-regions; $GR-I, GR-II$ and $GR-III$; olive, blue and red colored curves denotes supercritical Hopf curve, subcritical Hopf curve and saddle-node curve for periodic orbits, respectively. Fig. (b) corresponds for local stability of E_1^* with $(\theta,\beta) \in GR-I$, whereas Fig. (c) illustrates the arise of a stable limit cycle around E_1^* (after passing through supercritical Hopf curve) for $(\theta,\beta) \in GR-II$. Fig. (d) shows the appearance of an unstable limit cycle about E_1^* (after passing through subcritical Hopf curve) for $(\theta,\beta) \in GR-III$. Lastly, Fig. (e) depicts stable E_1^* without any orbit around it, saddle point E_2^* and stable E_3^* with $(\theta,\beta) \in GR-I$.

vicinity of BT_1-point into four sub-regions; $BR-I, BR-II, BR-III$, and $BR-IV$. We use three curves; saddle-node curve (blacked one), Hopf curve (olive one), and homoclinic curve (cyan one) to develop the above sub-regions. We have a degenerate equilibrium E_{BT_1} at the BT_1-point for $(\theta_{BT}, \beta_{BT}) = (9.190538, 1.909723)$, depicted in Fig. 5.7(b), and we move counterclockwise around BT_1-point starting from sub-region $BR-I$. Here, E_3^* is the only coexistence equilibrium that is stable as well, evident from Fig. 5.7(c). As we increase the Allee effect's strength, we enter into $BR-II$ where stable E_1^* and saddle E_2^* comes into the picture (Fig. 5.7(d)) after passing through the saddle-node curve. Ecologically, this portrays that the decrement in Allee effect's strength can cause the annihilation of two interior equilibria. Next, we move from $BR-II$ to $BR-III$ by decreasing the rate of cannibalism, and a stable limit cycle is created around E_1^* through Hopf bifurcation (Fig. 5.7(e)). We further decrease β and choose a point on the homoclinic curve, where the previously mentioned stable limit cycle collides with the saddle E_2^* to form a homoclinic loop (Fig. 5.7(f)). The additional decrement in β takes us to $BR-IV$, leading to the disappearance of the above homoclinic loop and leaving behind E_1^* as a spiral source, E_2^* as saddle and E_3^* as a spiral sink (Fig. 5.7(g)).

5.3 Analysis for spatiotemporal model

5.3.1 Existence and boundedness of solution

Firstly, we derive the sufficient conditions for existence of non-negative solutions of model (5.5) in absence of cross-diffusion i.e., of (5.25) Following this, we also determine the solution's prior bounds using the techniques discussed in [49, 178]. Here, we define $\mathscr{D} = \Omega \times (0,\infty)$, $\mathscr{H} = \partial\Omega \times (0,\infty)$.

$$\begin{cases} \frac{\partial U(x,y,t)}{\partial t} = d_U \Delta U + \frac{rU^2}{U+\theta}\left(1-\frac{U}{k}\right) - \frac{c_1 UP}{h+U+\beta P}, & (x,y,t) \in \mathscr{D}, \\ \frac{\partial P(x,y,t)}{\partial t} = d_P \Delta P + \frac{c_1 c_2 UP - c_1 \beta \alpha P^2}{h+U+\beta P} - \delta P, & (x,y,t) \in \mathscr{D}, \\ \frac{\partial U}{\partial \nu} = \frac{\partial P}{\partial \nu} = 0, & (x,y,t) \in \mathscr{H}, \\ U(x,y,0) = U_0(x,y) \geq 0,\ P(x,y,0) = P_0(x,y) \geq 0, & (x,y) \in \Omega. \end{cases} \tag{5.25}$$

Theorem 5.3.1. *For system (5.25), we have the following results:*

1. *If $U_0(x,y) \not\equiv 0$, $P_0(x,y) \not\equiv 0$ then reaction-diffusion system (5.25) has a unique solution $(U(x,y,t), P(x,y,t))$ satisfying $U(x,y,t) > 0$ and $P(x,y,t) > 0$ for $(x,y,t) \in \mathscr{D}$.*

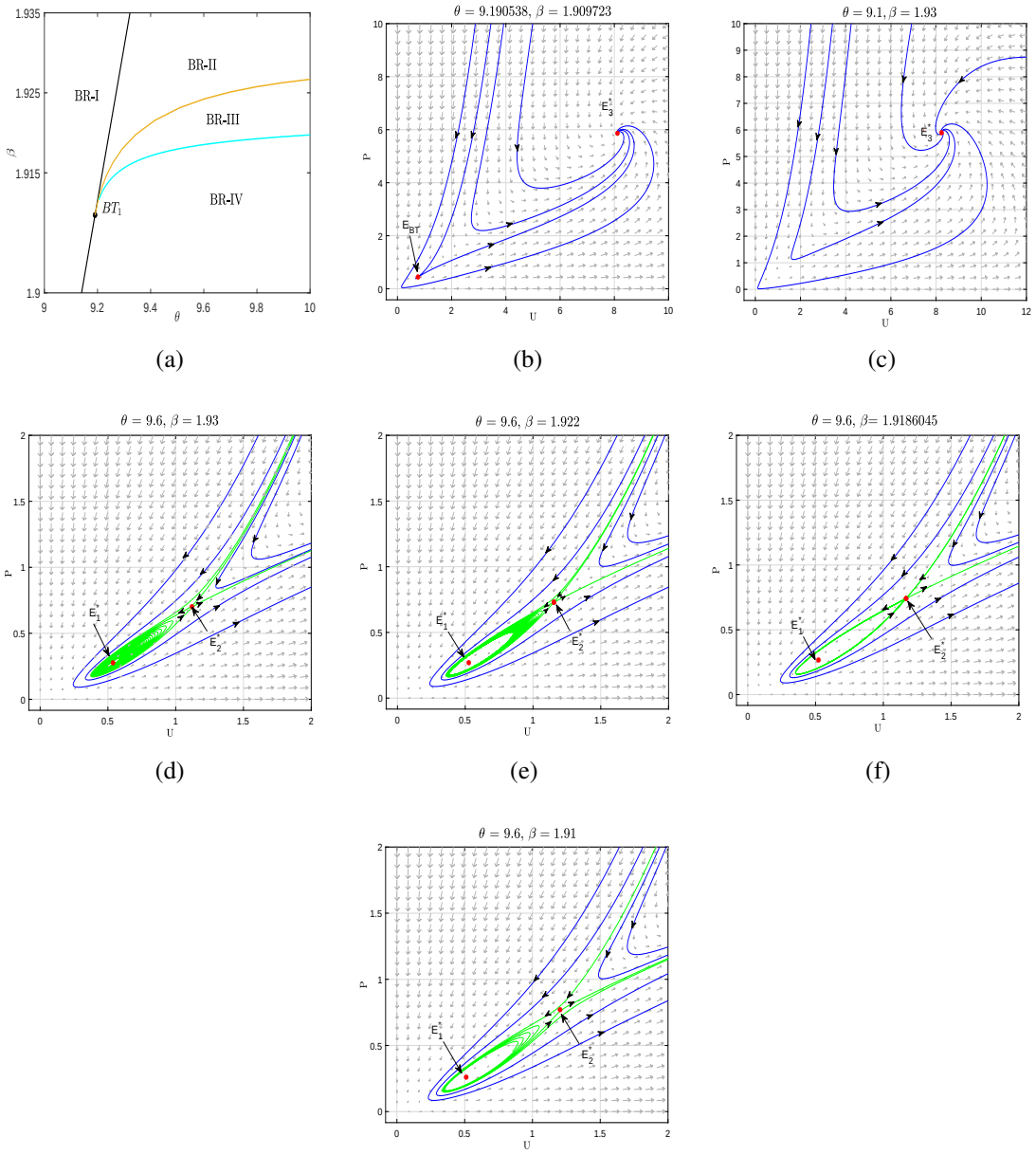

Fig. 5.7: Fig. (a) shows the division of neighborhood of BT_1-point (from Fig. 5.5) into four sub-regions; $BR-I, BR-II, BR-III$ and $BR-IV$; blacked, olive and cyan colored curves denotes saddle-node, Hopf and homoclinic curves, respectively. Fig. (b) shows the degenerate equilibrium E_{BT_1} and stable equilibrium E_3^*. whereas Fig. (c) corresponds for $BR-I$ where E_3^* is the only coexistence equilibrium. Fig. (d) shows the appearance of stable E_1^* and saddle E_2^* through SN_1 curve for $(\theta,\beta) \in BR-III$. Fig. (e) depicts the creation of a stable limit cycle around E_1^* (after passing through Hopf curve) for $(\theta,\beta) \in BR-IV$. In Fig. (f), (θ,β) is taken on the homoclinic curve which leads to formation of a homoclinic loop around E_1^*. Lastly, in Fig. (g), $(\theta,\beta) \in BR-IV$ where E_1^* is unstable focus, E_2^* is a saddle and E_3^* is stable focus.

2. *For a solution* $(U(x,y,t),P(x,y,t))$ *of system (5.25), we have*

$$\limsup_{t\to\infty} U(x,y,t) \le k,\ \limsup_{t\to\infty} \iint_\Omega \frac{\partial P(x,y,t)}{dt} dxdy \le c_2\left(\frac{rM+\delta}{\delta}\right) k|\Omega|.$$

Moreover, for $d_U = d_P = d$ *and* $(x,y) \in \Omega$, *we have*

$$\limsup_{t\to\infty} P(x,y,t) \le \frac{c_2(rM+\delta)k}{\delta}.$$

Proof. As, $\frac{\partial G_1(U,P)}{\partial P} = -\frac{c_1U(h+U)}{(h+U+\beta P)^2} \le 0$, $\frac{\partial G_2(U,P)}{\partial U} = \frac{c_1c_2(h+\beta P)+c_1\beta(1-\alpha)P^2}{(h+U+\beta P)^2} \ge 0$ for $(U,P) \in \overline{\mathbb{R}^2_+} = \{(U,P)|U \ge 0, P \ge 0\}$. Thus, system (5.25) is composed of weakly coupled parabolic equations with mixed quasimonotone terms [120]. Let $(\underline{U}(x,y),\underline{P}(x,y)) = (0,0)$ and $(\overline{U}(x,y),\overline{P}(x,y)) = (U^*(t),P^*(t))$ where $(U^*(t),P^*(t))$ is the unique solution to

$$\begin{cases} \frac{dU}{dt} = \frac{rU^2}{U+\theta}\left(1-\frac{U}{k}\right), t > 0, \\ \frac{dP}{dt} = \frac{c_1c_2UP-c_1\beta\alpha P^2}{h+U+\beta P} - \delta P, t > 0, \\ U(0) = U^* \ge 0,\ P(0) = P^* \ge 0. \end{cases} \tag{5.26}$$

where $U^* = \sup_{\overline{\Omega}} U_0(x,y)$, $P^* = \sup_{\overline{\Omega}} P_0(x,y)$. Since

$$\begin{aligned} &\frac{\partial \overline{U}(x,y,t)}{\partial t} - d_U\Delta\overline{U}(x,y,t) - G_1(\overline{U}(x,y,t),\underline{P}(x,y,t)) = 0 \\ &\qquad \ge 0 = \frac{\partial \underline{U}(x,y,t)}{\partial t} - d_U\Delta\underline{U}(x,y,t) - G_1(\underline{U}(x,y,t),\overline{P}(x,y,t)), \\ &\frac{\partial \overline{P}(x,y,t)}{\partial t} - d_P\Delta\overline{P}(x,y,t) - G_2(\overline{U}(x,y,t),\overline{P}(x,y,t)) = 0 \\ &\qquad \ge 0 = \frac{\partial \underline{P}(x,y,t)}{\partial t} - d_P\Delta\underline{P}(x,y,t) - G_2(\underline{U}(x,y,t),\underline{P}(x,y,t)), \end{aligned}$$

for $(x,y,t) \in \mathscr{D}$. It is easy to note that the following boundary conditions

$$\frac{\partial \overline{U}(x,y,t)}{\partial \nu} \ge 0 \ge \frac{\partial \underline{U}(x,y,t)}{\partial \nu},\ \frac{\partial \overline{P}(x,y,t)}{\partial \nu} \ge 0 \ge \frac{\partial \underline{P}(x,y,t)}{\partial \nu} \text{ for } (x,y,t) \in \mathscr{H},$$

and initial conditions

$$\overline{U}(x,y,0) \ge U_0(x,y) \ge \underline{U}(x,y,0),\ \overline{P}(x,y,0) \ge P_0(x,y) \ge \underline{P}(x,y,0) \text{ for } (x,y) \in \Omega.$$

holds. Thus $(\underline{U}(x,y),\underline{P}(x,y)) = (0,0)$ and $(\overline{U}(x,y),\overline{P}(x,y)) = (U^*(t),P^*(t))$ are lower and upper solutions, respectively, to system (5.25). Using Theorem 8.3.3 from [120], we conclude

that system (5.25) possess a unique solution $(U(x,y,t),\ P(x,y,t))$ satisfying

$$0 \leq U(x,y,t) \leq U^*(t),\ 0 \leq P(x,y,t) \leq P^*(t).$$

Since, $U_0(x,y) \not\equiv 0,\ P_0(x,y) \not\equiv 0$ so using strong parabolic maximum principle from [153], it follows that $U(x,y,t) > 0,\ P(x,y,t) > 0$ for $(x,y,t) \in \mathscr{D}$.

Further, we estimate the prior bounds of solutions of system (5.25). Now, one can observe that $U(x,y,t)$ and k are ordered lower and upper solutions, respectively, of the system given below.

$$\begin{cases} \frac{\partial U(x,y,t)}{\partial t} = d_U \Delta U + \frac{rU^2}{U+\theta}\left(1-\frac{U}{k}\right), & (x,y,t) \in \mathscr{D}, \\ \frac{\partial U}{\partial v} = 0, & (x,y,t) \in \mathscr{H}, \\ U(x,y,0) = U_0(x,y) \geq 0, & (x,y) \in \Omega. \end{cases} \tag{5.27}$$

Then using comparison theorem for semilinear parabolic equations from Theorem 2.4.1 in [120], we get

$$\limsup_{t\to\infty} U(x,y,t) \leq k. \tag{5.28}$$

Now, we set $u(t) = \iint_\Omega U(x,y,t)dxdy,\ p(t) = \iint_\Omega P(x,y,t)dxdy$. Using Green's Theorem and Neumann boundary conditions, we obtain

$$\begin{aligned} \frac{du}{dt} &= \iint_\Omega \frac{\partial U(x,y,t)}{dt}dxdy = \iint_\Omega \left[\frac{rU^2}{U+\theta}\left(1-\frac{U}{k}\right) - \frac{c_1UP}{h+U+\beta P}\right]dxdy, \\ \frac{dp}{dt} &= \iint_\Omega \frac{\partial P(x,y,t)}{dt}dxdy = \iint_\Omega \left[\frac{c_1c_2UP - c_1\beta\alpha P^2}{h+U+\beta P} - \delta P\right]dxdy. \end{aligned} \tag{5.29}$$

Since, $\limsup_{t\to\infty} U(x,y,t) \leq k,\ (x,y) \in \Omega$ which implies $\limsup_{t\to\infty} u(t) \leq k|\Omega|$. Thus for $\varepsilon > 0\ \exists\ t_1 > 0$ such that $u(t) \leq k(|\Omega| + \varepsilon)$.

Using (5.29), we further get

$$\frac{d}{dt}\left(u(t) + \frac{p(t)}{c_2}\right) \leq \iint_\Omega \left(\frac{rU^2}{U+\theta}\left(1-\frac{U}{k}\right) - \frac{\delta P}{c_2}\right)dxdy.$$

Now, define $H(U) = \frac{U}{U+\theta}\left(1-\frac{U}{k}\right)$ which has a global maximum; $M = \frac{(k-U_M)U_M}{k(U_M+\theta)}$ at $U = U_M = -\theta + \sqrt{\theta^2 + k\theta}$.

Thus, we have

$$\begin{aligned}\frac{d}{dt}\left(u(t)+\frac{p(t)}{c_2}\right) &\leq -\delta\left(u(t)+\frac{p(t)}{c_2}\right)+u(t)(rM+\delta),\\ &\leq -\delta\left(u(t)+\frac{p(t)}{c_2}\right)+k(|\Omega|+\varepsilon)(rM+\delta),\ t>t_1.\end{aligned}$$

This yields

$$\limsup_{t\to\infty}\left(u(t)+\frac{p(t)}{c_2}\right)\leq\left(\frac{rM+\delta}{\delta}\right)k|\Omega|,$$

which implies

$$\limsup_{t\to\infty}p(t)=\limsup_{t\to\infty}\iint_{\Omega}\frac{\partial P(x,y,t)}{dt}dxdy\leq c_2\left(\frac{rM+\delta}{\delta}\right)k|\Omega|.$$

For the case $d_U=d_P=d$, it is obvious that $\exists,\ t_2>0$ such that $0\leq U(x,y,t)\leq k+\varepsilon,\ t>t_2,\ (x,y)\in\Omega$. On further setting $Z(x,y,t)=U(x,y,t)+\frac{P(x,y,t)}{c_2}$, we get

$$\begin{cases}\frac{\partial Z(x,y,t)}{\partial t}=d\Delta Z+\frac{rU^2}{U+\theta}\left(1-\frac{U}{k}\right)-\frac{c_1\beta\alpha P^2}{c_2(h+U+\beta P)}-\frac{\delta P}{c_2}, & (x,y)\in\Omega,\ t>t_2\\ \frac{\partial Z}{\partial\nu}=0, & (x,y)\in\Omega,\ t>t_2,\\ Z(x,y,t_2)=U(x,y,t_2)+\frac{P(x,y,t_2)}{c_2}, & (x,y)\in\Omega.\end{cases}\tag{5.30}$$

As for $t>t_2$

$$\frac{rU^2}{U+\theta}\left(1-\frac{U}{k}\right)-\frac{c_1\beta\alpha P^2}{c_2(h+U+\beta P)}-\frac{\delta P}{c_2}\leq(rM+\delta)(k+\varepsilon)-\delta Z.$$

Thus for the system

$$\begin{cases}\frac{\partial Q(x,y,t)}{\partial t}\leq d\Delta Q+(rM+\delta)(k+\varepsilon)-\delta Q, & (x,y)\in\Omega,\ t>t_2\\ \frac{\partial Q}{\partial\nu}=0, & (x,y)\in\Omega,\ t>t_2,\\ Q(x,y,t_2)=U(x,y,t_2)+\frac{P(x,y,t_2)}{c_2}, & (x,y)\in\Omega.\end{cases}\tag{5.31}$$

$Q(x,y,t)$ and $Q'=\frac{(rM+\delta)(k+\varepsilon)}{\delta}$ are ordered lower and upper solutions. This implies

$$\limsup_{t\to\infty}Q(x,y,t)\leq\frac{(rM+\delta)k}{\delta},$$

which further implies

$$\limsup_{t\to\infty}P(x,y,t)\leq\frac{c_2(rM+\delta)k}{\delta}.$$

■

5.3.2 Turing-instability

In this section, we investigate that how the mechanism of self-diffusion can destabilize the interior equilibrium E^* under certain conditions. Next, we analyse the Turing-instability caused by cross-diffusion with those conditions under which self-diffusion is unable to induce it. The linearized form of system (5.5) at $E^*(U^*,P^*)$ can be presented as:

$$\begin{pmatrix} \frac{\partial U}{\partial t} \\ \frac{\partial P}{\partial t} \end{pmatrix} = \begin{pmatrix} d_U & d_1 \\ d_2 & d_P \end{pmatrix} \begin{pmatrix} \Delta U \\ \Delta P \end{pmatrix} + \begin{pmatrix} E_{11} & E_{12} \\ E_{21} & E_{22} \end{pmatrix} \begin{pmatrix} U \\ P \end{pmatrix}. \tag{5.32}$$

For Turing-instability, $E^*(U^*,P^*)$ is assumed to be stable, and thus we have

$$T_0 = -(E_{11}+E_{22}) > 0,\ D_0 = E_{11}E_{22} - E_{12}E_{21} > 0. \tag{5.33}$$

From stability analysis of interior equilibrium without diffusion, we also have $E_{12} < 0,\ E_{21} > 0$ and $E_{22} < 0$. Now, we consider the solution of (5.32) as

$$\begin{pmatrix} U \\ P \end{pmatrix} = \begin{pmatrix} U^* \\ P^* \end{pmatrix} + \begin{pmatrix} U^* \\ P^* \end{pmatrix} \exp(\xi t + i(\omega.r)),$$

where $\omega = \sqrt{\omega_x^2 + \omega_y^2}$ is known as wave number and $r = (x,y)$ is two-dimensional row vector with $x,\ y$ as the spatial variables.

First of all, we investigate the behavior of the system in the presence of self-diffusion and in the absence of cross-diffusion. In this case ($d_1 = d_2 = 0$), characteristic equation for (5.32) is given by

$$\lambda^2 + T(\omega^2)\lambda + D(\omega^2) = 0, \tag{5.34}$$

where

$$T(\omega^2) = T_0 + \omega^2(d_U + d_P) > 0,\ D(\omega^2) = \omega^4(d_U d_P) - \omega^2(E_{11}d_P + E_{22}d_U) + D_0. \tag{5.35}$$

As the sign of E_{11} is unknown, so we discuss the possibilities when E_{11} takes negative or positive value. The case when $E_{11} < 0$, it can be easily observed that $D(\omega^2) > 0$ thus with $E_{11} < 0$ there can be no diffusion driven instability. Now, taking $E_{11} > 0$, we have the following cases:

Case I When $d_U \geq d_P > 0$,
then

$$-(E_{11}d_P + E_{22}d_U) \geq -(E_{11} + E_{22})d_U = T_0 d_U > 0, \tag{5.36}$$

so using (5.36) with $D(\omega^2)$ in (5.35), we get $D(\omega^2) > 0$ under the condition $d_U \geq d_P > 0$. This shows that Turing-instability cannot occur when $d_U \geq d_P > 0$. In other words, we can say that for our model, the necessary condition for occurrence of Turing-instability in presence of self-diffusion only is $\frac{d_U}{d_P} < 1$.
Case II $0 < d_U < d_P$,
Let

$$H_{11} = -(E_{11}d_P + E_{22}d_U),\ H_{12} = (E_{11}d_P + E_{22}d_U)^2 - 4d_U d_P D_0.$$

Then self-diffusion mechanism will induce the Turing-instability when $H_{11} < 0$ and $H_{12} > 0$. The condition $H_{11} < 0$ with $d_U < d_P$ corresponds to $d_P > \max\left\{1, -\frac{E_{22}}{E_{11}}\right\} d_U$. In the $d_U d_P$-plane, this represents an upper-half plane above the line a straight line $C_{11} : d_P = \max\left\{1, -\frac{E_{22}}{E_{11}}\right\} d_U$ which have slope; $\max\left\{1, -\frac{E_{22}}{E_{11}}\right\} > 0$ and passes through origin. The condition $H_{12} = 0$ is equivalent to $C_{12} : E_{11}^2 d_P^2 + E_{22}^2 d_U^2 + (2E_{11}E_{22} - 4D_0)d_U d_P = 0$, which represents a pair of straight lines in the $d_U d_P$-plane whose explicit equations are not easy to drive, thus we analyze $H_{12} > 0$ graphically. The Turing bifurcation threshold, denoted by d_P^T, is determined by $D(\omega^2)_{\min} = 0$, and is given by

$$d_P^T = \frac{d_U}{E_{22}^2}\left[(E_{11}E_{22} - 2E_{12}E_{21}) + \sqrt{(E_{11}E_{22} - 2E_{12}E_{21})^2 - E_{22}^2 E_{11}^2}\right]. \tag{5.37}$$

For the set of parameters from (5.1), we have an unique stable coexistence steady state $E^*(0.287446, 0.091166)$ with

$$E_{11} = 0.041057,\ E_{12} = -0.117734,\ E_{21} = 0.029952,\ E_{22} = -0.042564.$$

For above parameters, we have drawn the region of instability, R_{11} (cyan colored) whereas R_{12} (white colored) is the region of stability in Fig. 5.8(a). Thereby, for the above parameters, the spatial model with only self-diffusion undergo Turing-instability in region R_{11} of the $d_U d_P$-plane. Now from this analysis, we can also state the following theorem.

Theorem 5.3.2. *Assume that $E_{11} > 0$ and condition (5.33) holds. Then self-diffusion induces Turing-instability under the conditions:*

$$d_P > \max\left\{1, -\frac{E_{22}}{E_{11}}\right\} d_U,\ H_{12} > 0,$$

and the system will be unstable for $\omega_-^2 \leq \omega_\pm^2 \leq \omega_+^2$, *where* $\omega_\pm^2 = \frac{-H_{11} \pm \sqrt{H_{12}}}{2d_U d_P}$.

Now, we shall study the behavior of the system in the presence of self as well as cross-diffusion. Here, we discuss the case ($E_{11} > 0,\ d_U \geq d_P > 0$) where self-diffusion is not able to generate Turing-instability and observe how the incorporation of cross-diffusion make the system unstable. In presence of cross-diffusion, the characteristic equation for system (5.32) becomes

$$\lambda^2 + T(\omega'^2)\lambda + D(\omega'^2) = 0, \tag{5.38}$$

where

$$\begin{aligned} T(\omega'^2) =& T_0 + \omega'^2(d_U + d_P) > 0, \\ D(\omega'^2) =& \omega'^4(d_U d_P - d_1 d_2) - \omega'^2(E_{11}d_P + E_{22}d_U - E_{21}d_1 - E_{12}d_2) + D_0, \end{aligned} \tag{5.39}$$

and let us define

$$H_{21} = -(E_{11}d_P + E_{22}d_U - E_{21}d_1 - E_{12}d_2),\ H_{22} = H_{21}^2 - 4(d_U d_P - d_1 d_2)D_0.$$

Using the theory of quadratic equation, it is easy to state the following theorem.

Theorem 5.3.3. *Assume that* $E_{11} > 0,\ d_U \geq d_P > 0$ *and (5.33) holds. Then the system can undergo Turing-instability with the following possibilities.*

1. *If* $d_U d_P = d_1 d_2$ *and* $H_{21} < 0$, *then* $D(\omega'^2) > 0$ *for* $0 \leq \omega' < \sqrt{\frac{D_0}{H_{21}}}$ *and* $D(\omega'^2) < 0$ *for* $\omega' > \sqrt{\frac{D_0}{H_{21}}}$.

2. *If* $d_U d_P - d_1 d_2 < 0$, *then* $D(\omega'^2) < 0$ *for* $\omega' > \omega_2'$ *and* $D(\omega'^2) > 0$ *for* $0 \leq \omega' \leq \omega_2'$, *where* ω_2' *is the unique positive root of* $D(\omega'^2) = 0$, *under this condition.*

3. *If* $d_U d_P - d_1 d_2 > 0,\ H_{21} < 0$ *and* $H_{22} > 0$ *then* $D(\omega'^2) > 0$ *for* $0 \leq \omega'^2 < \omega'^2_-$ *or* $\omega'^2 > \omega'^2_+$ *and* $D(\omega'^2) < 0$ *for* $\omega'^2_- < \omega'^2 < \omega'^2_+$ *where* $\omega'^2_\pm = \frac{-H_{21} \pm \sqrt{H_{22}}}{2(d_U d_P - d_1 d_2)}$.

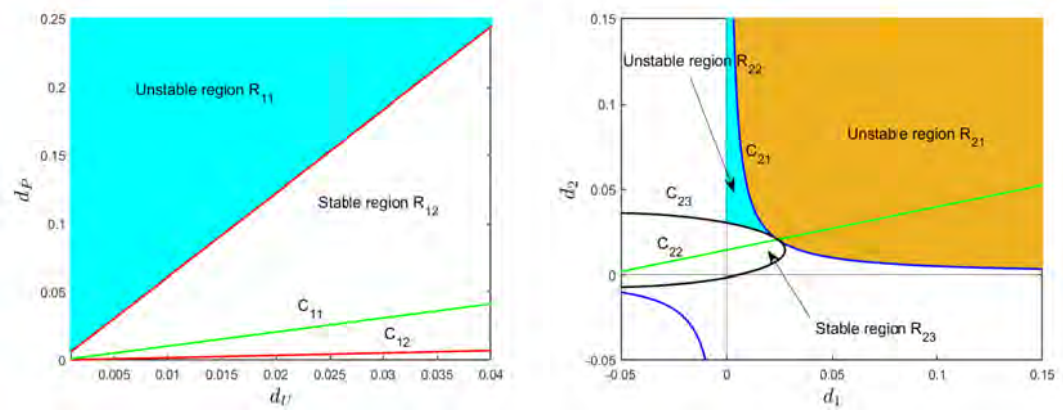

(a) (b)

Fig. 5.8: In Fig. (a), cyan colored region stands for Turing-instability due to self-diffusion only whereas the white region is the region of stability in $d_U d_P$-plane. Fig (b) shows the regions of stability and instability in the presence of cross-diffusion in the $d_1 d_2$-plane with $d_U = 0.05 > d_P = 0.01$. In both the figures, parameters are from (5.1), and the rest details of curves are given in the text.

Now, we shall discuss the regions of stability and instability of the system in presence of cross-diffusion in the $d_1 d_2$-plane (Fig. 5.8(b)). The condition $d_U d_P = d_1 d_2$ corresponds to curve $C_{21} : d_2 = \frac{d_U d_P}{d_1}$ which is a hyperbola and $d_2 > \frac{d_U d_P}{d_1}$ (equivalent of $d_U d_P - d_1 d_2 < 0$) is the region above this hyperbola whereas $d_2 < \frac{d_U d_P}{d_1}$ (equivalent of $d_U d_P - d_1 d_2 > 0$) is the region below it.

The condition $H_{21} = 0$ corresponds to a straight line $C_{22} : d_2 = -\frac{E_{21}}{E_{12}} d_1 + \frac{E_{11} d_P + E_{22} d_U}{E_{12}}$ in the $d_1 d_2$-plane, having slope $-\frac{E_{21}}{E_{12}} > 0$ and intercept $\frac{E_{11} d_P + E_{22} d_U}{E_{12}} > 0$. Thus $H_{21} < 0$ is the region above this line.

The condition $H_{22} = 0$ is equivalent to

$$C_{23} : E_{21}^2 d_1^2 + E_{12}^2 d_2^2 + 2(E_{21}E_{12} + 2D_0) d_1 d_2 - 2(E_{11} d_P + E_{22} d_U)(E_{21} d_1 + E_{12} d_2) + (E_{11} d_P + E_{22} d_U)^2 - 4 D_0 d_U d_P = 0$$

which represent an ellipse in the $d_1 d_2$-plane whose center is given by (d_1^C, d_2^C), where

$$d_1^C = \frac{E_{12}(E_{11} d_P + E_{22} d_U)}{2 E_{11} E_{22}} < 0, \; d_2^C = \frac{E_{21}(E_{11} d_P + E_{22} d_U)}{2 E_{11} E_{22}} > 0.$$

Using the above analysis, and the same set of parameters given in (5.1) with $d_U = 0.05 > d_P = 0.01$, we draw the regions for cases (ii) and (iii) given in Theorem 5.3.3 in first quadrant of the $d_1 d_2$-plane. For these fixed parameters $H_{22} > 0$ represent the region outside the ellipse. In

Fig. 5.8(b), the unstable region R_{21} which is filled with olive color corresponds to case (ii) in above theorem. The unstable region R_{22}, marked with cyan color, corresponds for case (iii), whereas the white region R_{23} in first quadrant stands for region of stability. As a result, with conditions given in Theorem 5.3.3 under which the model with self-diffusion does not have Turing-instability, cross-diffusion induces it in region $R_{21} \cup R_{22}$ of the $d_1 d_2$-plane.

The critical value of d_2 can be determined from $D(\omega'^2)_{\min} = D_0 - \frac{(E_{11}d_P + E_{22}d_U - E_{21}d_1 - E_{12}d_2)^2}{4(d_U d_P - d_1 d_2)}$, and it is given as

$$\begin{aligned} d_2^T = & \frac{1}{E_{12}^2}\left(E_{12}E_{22}d_U - 2E_{11}E_{22}d_1 + E_{12}E_{21}d_1 + E_{11}E_{12}d_P\right) \\ & + \frac{2}{E12^2}\sqrt{(E_{11}E_{22} - E_{12}E_{21})(E_{12}d_U - E_{11}d_1)(E_{12}d_P - E_{22}d_1)}. \end{aligned} \tag{5.40}$$

In the last theorem, we assumed $E_{11} > 0$ but now we present a theorem for Turing-instability in system (5.5) irrespective of the sign of E_{11}.

Theorem 5.3.4. *For system (5.5), the spatially homogeneous stable state becomes prone to Turing-instability under the following conditions:*

1. $T_0 = -(E_{11} + E_{22}) > 0$,
2. $D_0 = E_{11}E_{22} - E_{12}E_{21} > 0$,
3. $H_{21} = -(d_P E_{11} + d_U E_{22} - d_1 E_{21} - d_2 E_{12}) < 0$,
4. $H_{22} = H_{21}^2 - 4(d_U d_P - d_1 d_2)D_0 > 0$.

Proof. The analysis of this theorem is similar to Theorem 5.3.3 so we omit it whereas one can look here [111] for more details. ∎

5.3.3 Turing patterns

Here, we execute numerical simulations to obtain Turing patterns. In order to accomplish this, we discretize the governing equations using the central difference formula for space and the forward Euler method for time. We use space step size $\Delta x = \Delta y = 1/3$ and time step size $\Delta t = 1/125$. Here, we found a one-to-one correlation between the Turing patterns produced for prey and predator species; as a result, we only display the patterns appeared for the predator population.

Firstly, we do a series of simulations taking $d_1 = d_2 = 0$ in (5.5), i.e., for the system with only self-diffusion. With parameters from (5.1), we have the stable unique equilibrium $E^*(0.287446, 0.091166)$, and we inject some random perturbation near this stable E^*. With

$d_U = 0.01$, we get $d_P^T = 0.056932$, and now we study the formation of stationary patterns by varying the value of d_P which will be greater than d_P^T. In Fig. 5.9(a), taking $d_P = 0.07$ shows the formation of hot spots where the predator population density is high. In Fig. 5.9(b), with $d_P = 0.08$, strip patterns are generated. Next, when we take $d_P = 0.1$ (Fig. 5.9(c)), there is a mixture of strips and hollow disks. One more thing can also be noted from this figure, on increasing this diffusion coefficient, the region of low predator population is contracting. On further increment of d_P to 0.4, the stripes disappear, and there are only hollow disk type patterns in Fig. 5.9(d) having only moderate and high predator density all over the space.

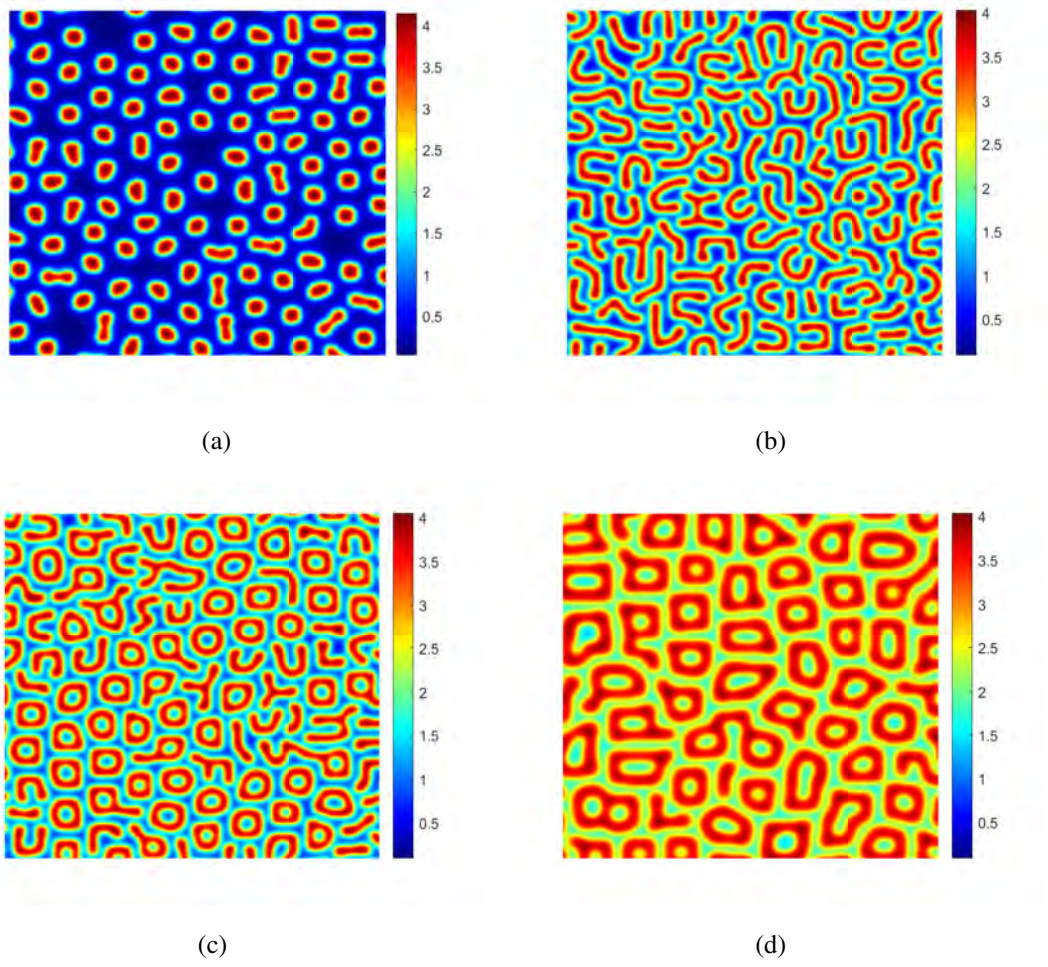

Fig. 5.9: With parameters from (5.1) and $d_U = 0.01$, stationary patterns on increasing d_P away from $d_P^T = 0.056932$. (a) $d_P = 0.07$; (b) $d_P = 0.08$; (c) $d_P = 0.1$; (d) $d_P = 0.4$.

Next, we study the evolution of patterns with variation of diffusion coefficient d_U, keeping $d_P = 0.1$, and all other parameters fixed from (5.1). Taking $d_U = 0.001$, we have isolated hot spots in Fig. 5.10(a), and as we increase d_U to 0.0046, the pattern evolves, and we get a

mixture of spots and strips (Fig. 5.10(b)). The further raise of d_U changes this previous pattern to mixture of strips and hollow disks with high predator density, in Fig. 5.10(c). Now, taking $d_U = 0.013$, the disks disappears and only strips exists, as shown in Fig. 5.10(d).

Now, we talk about the pattern formation in the presence of self as well as cross-diffusion. For this, we study the behavior of model (5.5) around the stable focus (6.090800,3.821193), taking $\alpha = 0.55$ and remaining parameters from (5.1). Here, we fix $dU = 0.02$, $dP = 0.4$, $d_1 = 0.01$ and using (5.40), we get $d_2^T = 0.0165$. Now, we investigate the stationary patterns on the variation of cross-diffusion coefficient d_2 above d_2^T. With $d_2 = 0.02$, we have low density of predator population in isolated spots, i.e, we have cold spot pattern in Fig. 5.11(a). On further increment of d_2, we have a mixture of spots and stripes whereas the population density in non-isolated spaces also changes significantly through this raise in d_2 (Figs. 5.11(b), 5.11(c)). Taking $d_2 = 0.155$, we get a stationary pattern of hot spots and stripes (Fig. 5.11(d)). Thus we can note that increasing the cross diffusivity of prey population (d_2) can affect the spatial distribution of predator population by converting the cold spots into hot spots. By now, we have used small random perturbation in the initial condition but we here we want to explore the change in the spatial distribution of populations by choosing unsymmetrical initial conditions [50, 99]:

$$\begin{aligned} U(x,y,0) &= U^* - \varepsilon_1(x-0.1y-125)(x-0.1y-375), \\ P(x,y,0) &= P^* - \varepsilon_2(x-450) - \varepsilon_3(y-150), \end{aligned} \tag{5.41}$$

with $\varepsilon_1 = 2\times 10^{-7}$, $\varepsilon_2 = 3\times 10^{-5}$, $\varepsilon_3 = 1.2\times 10^{-5}$. Here, we study the patterns formed at different times, i.e., dynamical patterns, using the same parameters as of Fig. 5.11 with $d_2 = 0.15$. For $t = 224$, from Fig. 5.12(a), we can observe that in the center of the space, there is homogeneous distribution of population while due to cross-diffusion there is a formation of aligned stripes pattern on going away from the center. As we increase the time to $t = 280$ (Fig. 5.12(b)), the region of homogeneous distribution diminishes, whereas the area in which patterns are evolved increases. On $t = 400$ (Fig. 5.12(c)), patterns are formed all over the space. Thus, we can see how magnificently cross-diffusion changes the spatial distribution of population density as time passes with the initial conditions given in (5.41).

5.4 Discussion and concluding remarks

Prey-predator interactions primarily drive population dynamics in ecosystems. Their interaction show an intricate relationship between two species, in which one's capacity to capture and eat the other is necessary for its survival and reproduction. In this study, our main objective is to study a prey-predator model involving weak Allee effects in the prey with a specialized cannibalistic predator in the presence of self and cross-diffusion. Allee effects can be classified

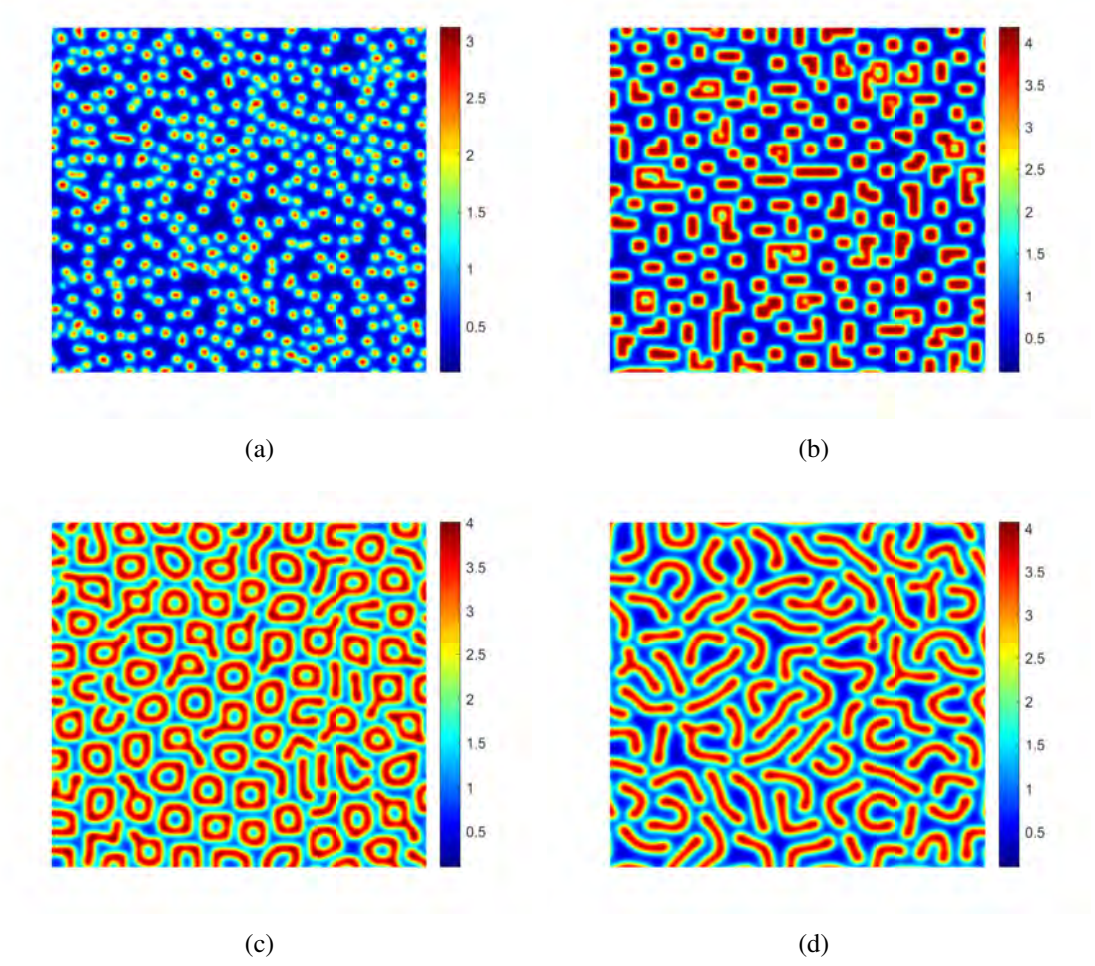

Fig. 5.10: With parameters from (5.1) and $d_P = 0.1$, stationary patterns on increasing d_U. (a) $d_U = 0.001$; (b) $d_U = 0.0046$; (c) $d_U = 0.01$; (d) $d_U = 0.013$.

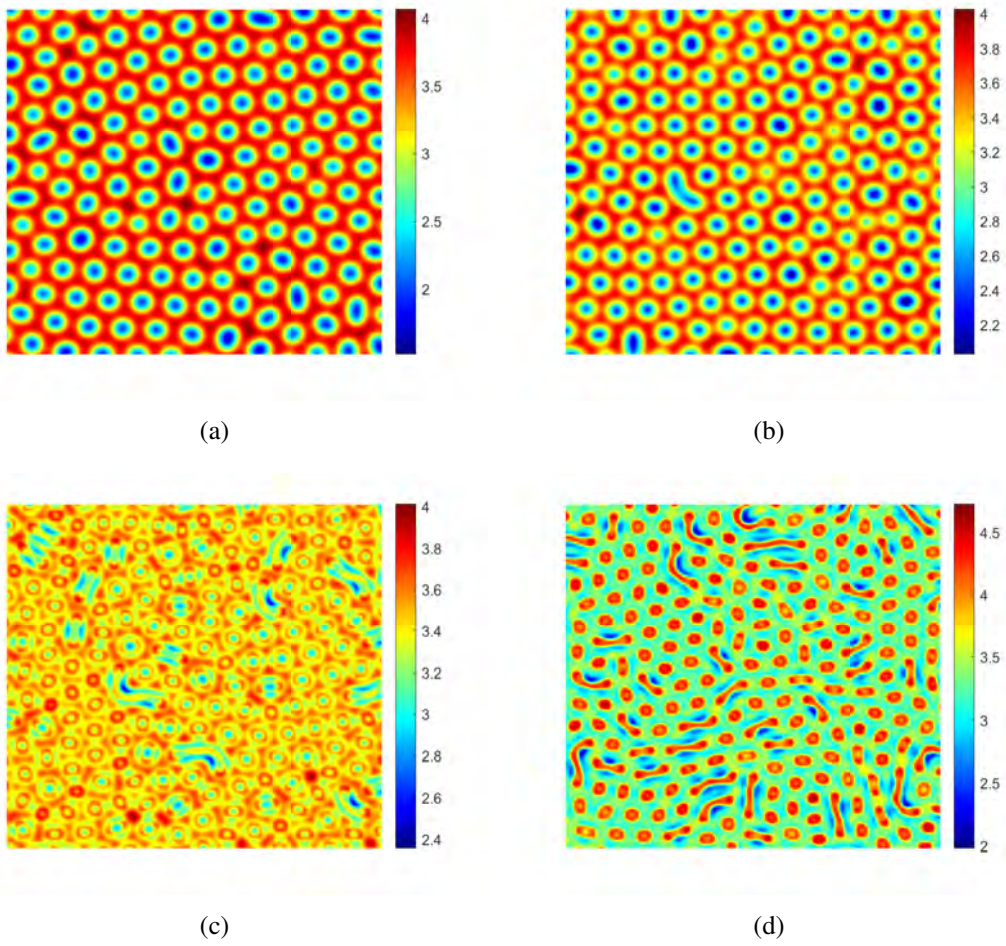

Fig. 5.11: With $\alpha = 0.55$, $dU = 0.02$,$dP = 0.4$, $d_1 = 0.01$ and remaining parameters from (5.1), stationary patterns on increasing $d_2 > d_2^T = 0.0165$. (a) $d_2 = 0.02$; (b) $d_2 = 0.05$; (c) $d_2 = 0.1$; (d) $d_2 = 0.155$.

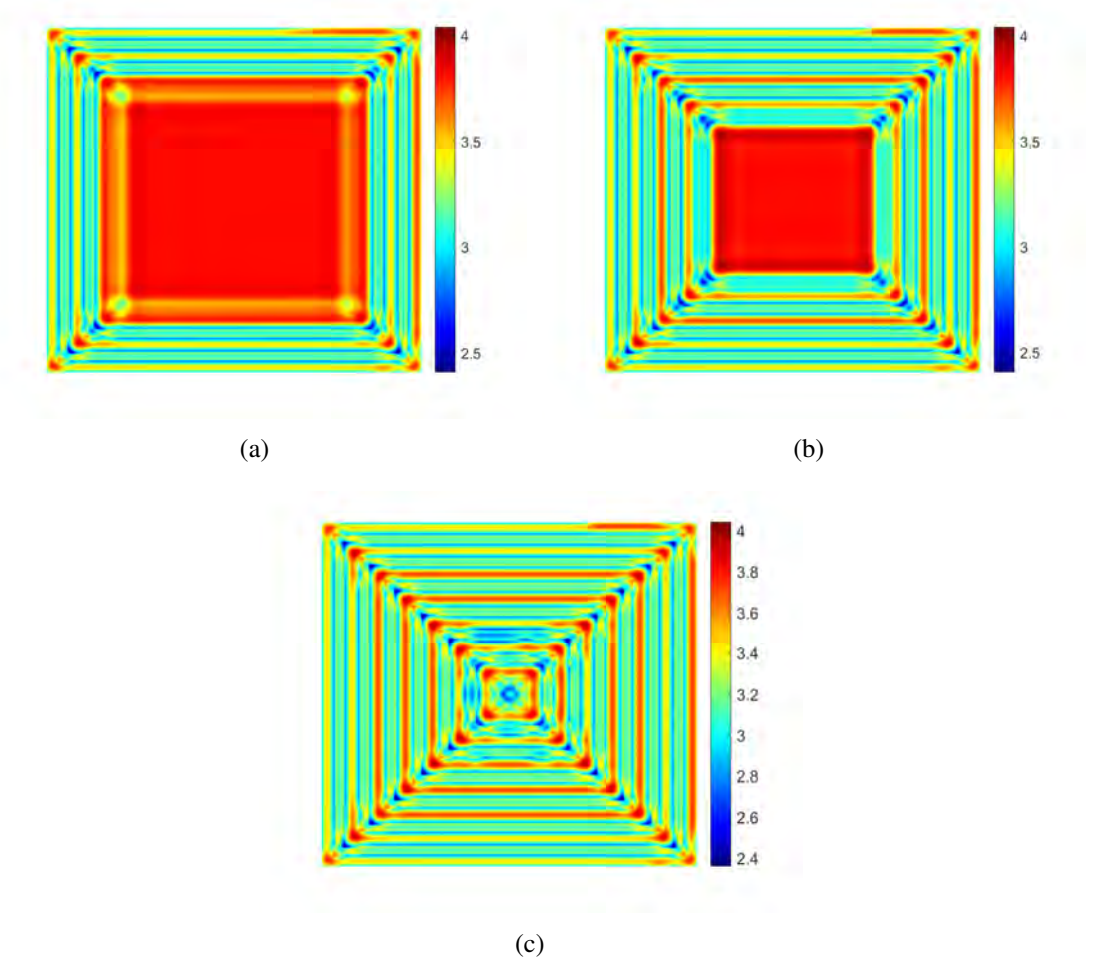

Fig. 5.12: With $\alpha = 0.55$, $dU = 0.02$, $dP = 0.4$, $d_1 = 0.01$, $d_2 = 0.15$ and remaining parameters from (5.1), dynamics patterns at different time: (a) $t = 224$; (b) $t = 280$; (c) $t = 400$.

into two primary types: component Allee effects and demographic Allee effects. They both use various kinds of parameterization and formulation [31]. The demographic Allee effect, typically observed by cats, foxes or rodents; wolves, bears, etc. The weak Allee effect is a further sub-type of demographic Allee effect which has been considered in this research. Cannibalism is an important phenomena in aquatic species. It has been observed that up to 90 percent of species in aquatic ecosystems exhibit cannibalistic behavior at some point throughout their life cycle, suggesting that cannibalism is particularly common in these environments. Adult Dreissena mussels, for instance, eat a variety of minute zooplankton species, such as rotifers like Keratella quadrata, Polyarthra vulgaris, and Euchlanis dilatata, as well as protozoans [152]. In addition, sexual cannibalism occurs often in a variety of spider and scorpion families, having a substantial impact on traits like population size [193] , sex ratio [61]. The cannibalistic character of predator is incorporated in the model using the approach given in [70].

In the analysis of the temporal model, we established the existence of various coexistence steady states and divide the $\theta\beta$-plane into five sub-regions; $R_i, i = 1,2...5$.. We obtained the conditions under which system (5.4) has unique steady state in sub-region $R_1 \cup R_2 \cup R_3 \cup R_4$ and three coexistence steady states in sub-region R_5 (Fig: 5.1). Thus, we can see that how the number of equilibrium points changes on varying the Allee and cannibalism parameter. In the stability analysis, we showed that the extinction equilibrium E_0 is a non-hyperbolic saddle node with a parabolic sector and two hyperbolic sectors. Further, we discussed the global stability of predator-free equilibrium E_1 in the absence of interior equilibrium. Next, for the interior equilibria $E_i^*, i = 1,2,3$, we derived the conditions under which E_1^* and E_3^* are stable and also proved that E_2^* is always a saddle point. In bifurcation analysis, we did the theoretical analysis for all local bifurcations such as saddle-node, Hopf, Generalized Hopf (Bautin), Bogdanov-Takens. We also performed the extensive numerical simulations, presented in Figs. 5.4, 5.5, 5.6, 5.7, to depict the occurrence of all above bifurcations. From these bifurcations, we can corroborate that the proposed type of Allee effect (given in (5.2)) and cannibalistic nature of predator can impact the system's dynamics in a significant manner.

For spatiotemporal model (5.25), we evaluated the sufficient conditions for the existence of a non-negative solution, followed by the calculations of prior bounds of the solution. Next, we analyzed Turing-instability for the self-diffusion model (5.25). Then, we demonstrated that cross-diffusion can cause Turing-instability while self-diffusion cannot in the case of $d_U \geq d_P > 0$. Doing some novel geometric and mathematical analysis, we also drew the region of Turing-instability in the presence of self-diffusion and cross-diffusion in Fig. 5.8(a) and Fig. 5.8(b), respectively. Talking about the pattern formation, firstly, we presented different kinds of stationary patterns in the absence of cross-diffusion on the variation of self-diffusion coefficients d_P and d_U in Fig. 5.9 and Fig. 5.10, respectively. In Fig. 5.11, we demonstrated how

the increment in cross-diffusion coefficient d_2 changes the pattern of cold spots into a mixture of hot spots and stripes. Next, to show the dependence of the patterns on initial conditions, we used unsymmetrical initial conditions in the presence of cross-diffusion. We presented the dynamic patterns in Fig. 5.12 using this initial condition. From this figure, one can perceive how cross-diffusion is changing the spatial distribution of the population from the center of space to its boundaries as time passes. This illustrates the sensitivity of spatial patterns with respect to initial conditions.

Motivated from the studies on predator cannibalism [22, 130, 190], we proposed to investigate a cannibalistic prey-predator with incorporation of weak Allee effect in prey. The inclusion of self and cross-diffusion was the second novelty in the formulation of the present model. The addition of weak Allee effect made the trivial equilibrium E_0 a hyperbolic saddle-node. The property of E_0 being a hyperbolic equilibrium point encouraged us to explore a meticulous mathematical analysis (presented in Theorem 5.2.3) to study its behavior. We also showed that the temporal model undergoes Hopf bifurcation with respect to cannibalism parameter which illustrates the role of β in the stability change of the model. Temporal model also suffered saddle-node bifurcation with respect to θ, and in the analysis of this bifurcation we also provided an interval $(\theta_{SN_1}, \theta_{SN_2})$ in which three coexistence steady states exist out of which two are stable and one saddle (Fig. 5.4). This also depicts the phenomena of bistability. For the combination of θ and β, we further presented codimension-2 bifurcations. The occurrence of codimension-2 bifurcations also shows the impact of cannibalism in addition to Allee effect. In the spatiotemporal model using rigorous mathematical analysis, we discussed about the regions of stability and instability due to the presence of diffusion. The effect of variation of diffusion coefficients is also well explained thorough the two dimensional spatial patterns which can assist in examining spatial heterogeneity, spatial complexity, sensitivity to initial condition. All the above-discussed attributes make the current study more credible and advanced in both mathematical and ecological directions than the previous ones, and we anticipate that this work will assist researchers in investigating spatiotemporal prey-predator models with the Allee effect and cannibalism in greater depth.

In nature, another form of cannibalism can also be found in a stage-structure prey-predator model, having an adult and a juvenile predator [88, 188]. In this type of cannibalism, the adult predator consumes over prey and the juvenile predator, leading to the formation of a three-dimensional model. Thus, this type of stage-structure cannibalistic model can be chaotic too [78], which is again an interesting phenomenon to study. Secondly, in biological systems, the dynamics of different components are influenced by the diffusion coefficient's periodic fluctuations in addition to its constant value [14]. Therefore, in future work, we intend to explore stage-structure cannibalism along with the periodic diffusion.

Chapter 6

Bifurcation analysis and spatiotemporal dynamics in a diffusive predator-prey system incorporating a Holling type II functional response[1]

6.1 Introduction

Prey-predator modelling serves as the crucial component in comprehending the dynamics of ecological systems, offering valuable insights into the interactions between species within an ecosystem. The concept of prey and predator interactions have its roots from the innovative work of Alfred [91] and Vito [177] in the early 20th century, whose equations served the foundation for modelling these dynamic relationships. Leslie [84, 85] modified the simplest form given by Lotka and Volterra and assumed a direct proportionality between the predator's carrying capacity and the density of the prey population. In their studies, they took into account the idea that a predator relies only on prey for food and has no alternative food source. Later on, this notion has been altered by the researchers who assumed that additional food can be provided as an alternative food source to the predators [129, 136, 149]. Many researchers studied the consequent effects of supplying additional food to predators on the system's dynamics [15, 172, 53, 157, 167]. Alves [1] analyzed a predator-prey system with additional food provided to the predators. He concluded that providing additional food has negative impact on predators' growth rate whereas it is beneficial for the prey population in the long term. Onana *et al.* [109] analyzed the interacting species dynamics incorporating food preference rate for the predators. He remarked that increasing the preference rate reduces the prey population initially but subsequently it increases while the density of predators decreases.

In the realm of ecological dynamics, prey refuge emerges as a pivotal behavioral characteristics that has a substantial impact on the dynamics and persistence of both prey and predator

[1]This chapter is based on our paper published in *International Journal of Bifurcation and Chaos*, **34**, 2450105, 2024.

populations. Several researchers incorporated prey refuge in a dynamical model and analyzed that providing spatial refuge can stabilize the system dynamics [28, 64, 60, 24, 179]. In ecological systems, functional response is essential in comprehending the intricate interplay between prey and predator. It defines how predators feed and regulate their populations in response to fluctuating densities of prey. Some investigations have been made using various functional responses such as Holling-type functional responses, Beddington–DeAngelis-type, and Monod-Haldane-type and Crowley-Martin type response functions [55, 68, 69, 93, 137, 16]. Holling type II functional response assumes that the predator's feeding rate initially escalates linearly with prey density until reaching a saturation point when additional increase in prey density no longer boost the predator's feeding rate [7]. In a study by Dash and Khajanchi [36], a three-dimensional intraguild predation model employing a Holling type II functional response between prey and predator was proposed and analyzed. They determined that this intraguild predation model is prone to have coexistence of all the three populations.

In addition to the widespread direct killing witnessed in nature, many preys alter their characteristics in reaction to the perceived risk of predation. These responses could take the form of modified foraging techniques, altered habitat utilisation, increased cognition, decreased exposure times, or modified reproductive practices. Several researchers speculated that these indirect effects might have an impact that is comparable to or greater than direct predation effects [32, 131, 34]. Zanette *et al.* [187], in their study on song sparrows, conducted an experiment illustrating the impact of predation fear. They noted a significant reduction, up to 40%, in the reproduction rate of song sparrows attributable to the perceived risk of predation. Wang *et al.* [180] first incorporated the cost of fear in the predator-prey system and investigated that the fear factor stabilize the system dynamics by preventing the occurrence of periodic oscillations. Kumar and Kumari [75] explored a prey-predator model incorporating predation fear and found that a large degree of fear can stabilize the chaotic dynamics in the system. Sarkar and Khajanchi [139] took into account the minimum fear cost in prey-predator system and studied how the fear effect allowed both species to coexist via stable oscillations. Zhao and Shao [192] proposed a dynamical system with fear, additional food and prey refuge and noticed that creating reserved areas and providing additional food for predators are two strategies that work well to mitigate the effects of predation fear. Pal *et al.* [116] analyzed a multi-species food chain model and examined the complex dynamics induced by the fear effect. Additionally, they observed the deep cascading effects initiated by predation fear in the system.

Within the framework of predator-prey systems, the term carry-over effect refer to the lingering consequences of past interactions between the species and experiences that subsequently influence the current behaviors, physiological states, or population dynamics [107]. Several

studies observed the experimental proof of carry-over effects in amphibians [162], marine invertebrates [98], etc. The aforementioned factors have led to an increase in the investigation of ecological carry-over effects in modeling area. Sasmal and Takeuchi [145], in their study, analyzed the influence of perceived risk of predation and its carry-over effects in a dynamical system and remarked that altering the carry-over effect parameter can significantly affect the stability of the coexistence equilibrium. In addition, they concluded that suitable selection of non-lethal effect parameters can eliminate the phenomenon of "paradox of enrichment". Sajan *et al.* [138] investigated the impact of carry-over effect parameter on the system dynamics and demonstrated that significantly low and high values of carry-over effect parameter eliminate the chaos from the system's dynamics and ultimately the system converges to a coexistence equilibrium.

Furthermore, spatiotemporal pattern formation in biological and ecological communities is a central theme in the population dynamics nowadays. These patterns are essential in comprehending the dynamic interactions, population dynamics, and spatial distributions of different species within ecosystems. Predators have an inherent tendency to migrate as they pursue their prey, and prey may possess the ability to detect the predator and escape in order to avoid being captured, resulting in spatial variations across the habitat. The pioneering work of Turing [166] on chemical morphogenesis first introduced the concept of pattern-forming instabilities. Several studies have been carried out to analyze the pattern formation due to diffusion-driven instabilies in a reaction-diffusion system [51, 35, 142, 4]. Chakraborty *et al.* [21] investigated how alterations in prey species' behavior, induced by predation fear, can give rise to diverse spatiotemporal patterns in population distribution. Pal *et al.* [111] qualitatively analyzed the patterns induced due to cross-diffusion coefficients in a prey-predator reaction-diffusion model incorporating fear effect. Anshu and Dubey [3] investigated a diffusive prey-predator system and concluded that considering spatial variations can instigate intricate and complex population dynamics in the system. Sarkar and Khajanchi[140] proposed and examined a mathematical model that integrates fear-induced birth reduction in prey resulting from predation risk. They obtained warm spots in the two-dimensional spatial model using three distinct initial datasets.

Motivated by the afore-mentioned aspects, we propose and analyze a spatiotemporal prey-predator model to investigate the effects of additional food for predators, indirect predation fear and its carry-over effects with Holling type II functional response. In the present study, our main focus is to achieve the following objectives:

- To investigate the intricate and complex system dynamics associated with the additional food for predators.
- To understand the impact of the parameters linked with the non-lethal effects on the stability behavior of the coexistence equilibrium.

- To analyze the diffusion-induced instability in the spatially extended system.
- To explore the stationary and dynamic pattern formation resulting in a diverse range of Turing and non-Turing space.

This chapter is structured in the subsequent manner: Section 6.2 comprises of the model formulation with and without diffusion. In Section 6.3, we explored the existence and stability of the equilibria along with the bifurcation analysis for the temporal model. In the first subsection of Section 6.4, the existence and boundedness for the spatially extended system has been explained in addition to the priori-bounds of the solutions and in second subsection, the conditions for diffusion-driven intstability incorporating both self and cross-diffusion are derived. Section 6.5 delves into the numerical experiments conducted to validate the analytical results obtained for both temporal and spatiotemporal model. Finally, in Section 6.6, we summarized the vital outcomes and discussion of our study.

6.2 Formulation of mathematical model

Motivated by the afore-mentioned notions and the studies done by Alves [1]; Onana *et al.* [109]; Gupta *et al.* [48], we propose our model with the following assumptions:

- The perceived predation risk affects the prey's growth rate due to change in habitat, increased vigilance, etc. This fear effect also has an associated carry-over effect which can have a significant impact on the birth rate of prey species. Hence, we assume the subsequent function to incorporate the said effects given by:

$$\psi(c,f,u,v) = \frac{1+cu}{1+cu+fv},$$

where f is the fear parameter and c is the carry-over effect parameter. The assumed function satisfy all the properties associated with the parameters f and c as specified in the study done by Sasmal and Takeuchi [145].
Thus, the temporal population growth model for the interacting species is:

$$\begin{aligned} \frac{du}{dt} &= ru\left(\tfrac{1+cu}{1+cu+fv}\right) - r_0 u - r_1 u^2 - \tfrac{q\alpha(1-m)uv}{a+q(1-m)u}, \\ \frac{dv}{dt} &= sv\left(1 - \frac{\beta v}{q\alpha(1-m)u+(1-q)\alpha_A q_A}\right), \end{aligned} \tag{6.1}$$

where u and v denote the density of prey and predator species at any time t, respectively. All the parameter associated are assumed to be positive and their meaning are described in Table 6.1.

- Taking into account the spatial variations across the space, the temporal model (6.1) transforms over a two-dimensional bounded domain as follows:

$$\begin{aligned} \frac{\partial u}{\partial t} &= ru\left(\tfrac{1+cu}{1+cu+fv}\right) - r_0 u - r_1 u^2 - \tfrac{q\alpha(1-m)uv}{a+q(1-m)u} + d_{11}\nabla^2 u + d_{12}\nabla^2 v, \\ \frac{\partial v}{\partial t} &= sv\left(1 - \tfrac{\beta v}{q\alpha(1-m)u+(1-q)\alpha_A q_A}\right) + d_{21}\nabla^2 u + d_{22}\nabla^2 v. \end{aligned} \tag{6.2}$$

The above model is subjected to non-negative initial conditions:

$$u(x,y,0) \geq 0, v(x,y,0) \geq 0,$$

and the zero-flux Neumann boundary conditions given by:

$$\frac{\partial u}{\partial \nu} = \frac{\partial v}{\partial \nu} = 0,$$

where ν represents the outward unit normal vector to the smooth boundary $\partial\Omega$.

Here, $\nabla^2 = \frac{\partial^2}{\partial x^2} + \frac{\partial^2}{\partial y^2}$ depicts the Laplacian operator in two-dimensional space $\Omega = [0,L]\times[0,L] \subset \mathbb{R}^2$. The self-diffusion coefficients $d_{11} > 0$ and $d_{22} > 0$ of prey and predator populations (respectively) represent the random movement of individuals across the habitat. But, the migration of species within a given domain need not be random. The movement of predator population can be affected by the mobility of prey population and vice-versa. Such scenarios are modelled using cross-diffusion terms. The cross-diffusion coefficients may assume positive as well as negative values. Here d_{12} and d_{21} depict the prey's and predator's cross-diffusion coefficients, respectively. Generally, prey has a tendency to avoid large group of predators and migrate to the lower dense region of predators whereas predators in search of prey tend to migrate towards highly dense region of prey, therefore $d_{12} > 0$ and $d_{21} < 0$. Furthermore, $d_{21} > 0$ takes into account the situations in which prey organize into a group defense against predators, and predators prefer to avoid areas where prey is densely concentrated in order to capture prey from smaller groups. In this study, we assume that $(d_{11}d_{22} - d_{12}d_{21}) > 0$ based on the thermodynamic implications of diffusion principles [176]. This condition implies that the movement of each population density within the spatial domain is predominantly influenced by its own density, rather than the densities of other populations.

The proposed ecological model encapsulates the intricacies of real-world ecosystems by integrating various environmental factors. This model includes additional food sources to represent alternative resources, impacting prey-predator interactions and population dynamics. For instance, supplementary feeding programs for carnivores exemplify providing extra food to predators in conservation efforts. Acknowledging the fear effect in prey

Parameter Symbol	Parameter Description	Value	References
r	Prey's intrinsic growth rate	3.5	[48]
r_0	Prey's natural death rate	0.5	[48]
s	Intrinsic growth rate of predator species	0.2	[48]
f	Fear parameter	0.05	Assumed
c	Carry-over effect parameter	0.6	Assumed
r_1	Prey's death rate due to intraspecies competition	0.03	Assumed
q	Food preference rate for predator	0.3	[48]
α	Maximum value of prey's per-capita removal due to predation	2	[48]
a	Half-saturation constant	1	Assumed
β	Maximum value of predator's per-capita removal	1	[48]
α_A	Quantifies the amount of energy assimilated into predators's energy	1	Assumed
q_A	Density of the additional food	1.7	[48]
m	Refuge parameter	0.6	Assumed

Table 6.1: Biological significance of the parameters and their corresponding values.

considers their behavioral responses to predation risk, affecting movement, reproduction, and survival rates. In Yellowstone National Park, elk alter behavior in response to perceived wolf predation risk. The carry-over effect recognizes past interactions' enduring impacts on current population dynamics, influencing species persistence. Additionally, prey refuge areas provide shelter from predation, impacting predator hunting rates and prey persistence. Small fish in coral reef ecosystems seek refuge to evade larger predators. Integrating these factors enriches our understanding of population dynamics and species coexistence in natural ecosystems.

6.3 Temporal model analysis

This part examines the properties of the solutions for the temporal model (6.1).

6.3.1 The well-posedness

Theorem 6.3.1. *For system (6.1), all the solutions with the initial condition* (u_0, v_0) *satisfying* $u_0 \geq 0$ *and* $v_0 \geq 0$ *will remain non-negative for all* $t \geq 0$.

Proof. From the system (6.1), we observe that both equations are continuous smooth functions in $\mathbb{R}^2$. Hence,

$$u(t) = u_0 \exp\left[\int_0^t \left(r\left(\frac{1+cu(s)}{1+cu(s)+fv(s)}\right) - r_0 - r_1 u(s) - \frac{q\alpha(1-m)v(s)}{a+q(1-m)u(s)}\right)ds\right] \geq 0,$$

$$v(t) = v_0 \exp\left[\int_0^t \left(s\left(1 - \frac{\beta v(s)}{q\alpha(1-m)u(s)+(1-q)\alpha_A q_A}\right)\right)ds\right] \geq 0, \quad \forall t \geq 0.$$

This implies the positivity of all the solutions of system (6.1). ∎

Theorem 6.3.2. *The following conditions ensure the system (6.1) to be dissipative:*

$$\limsup_{t\to\infty} u(t) \leq \frac{r-r_0}{r_1} =: u_{max},$$
$$\limsup_{t\to\infty} v(t) \leq \frac{1}{\beta}\left(\frac{q\alpha(1-m)(r-r_0)}{r_1} + (1-q)\alpha_A q_A\right) =: v_{max}.$$

Proof. From the first equation of the system (6.1), we have

$$\frac{du}{dt} \leq ru - r_0 u - r_1 u^2.$$

The solution of the above equation satisfies:

$$\limsup_{t\to\infty} u(t) \leq \left(\frac{r-r_0}{r_1}\right) =: u_{max}.$$

Next, we have the system (6.1)'s second equation, which yields

$$\frac{dv}{dt} \leq sv\left(1 - \frac{\beta v}{q\alpha(1-m)u_{max}+(1-q)\alpha_A q_A}\right),$$
$$\Rightarrow \limsup_{t\to\infty} v(t) \leq \frac{1}{\beta}\left(q\alpha(1-m)u_{max} + (1-q)\alpha_A q_A\right) =: v_{max}.$$

The proof of the theorem is now concluded. ∎

Theorem 6.3.3. *System (6.1) is uniformly persistent if*

$$r > (1+fv_{max})\left[r_0 + \frac{q\alpha(1-m)v_{max}}{a}\right].$$

Proof. From system (6.1), we have

$$\begin{aligned}\frac{du}{dt} &= ru\left(\frac{1+cu}{1+cu+fv}\right) - r_0u - r_1u^2 - \frac{q\alpha(1-m)uv}{a+q(1-m)u},\\ &\geq \left(\frac{r}{(1+fv_{max})} - r_0 - \frac{q\alpha(1-m)v_{max}}{a}\right)u - r_1u^2,\\ \Rightarrow \liminf_{t\to\infty} u(t) &\geq \frac{1}{r_1}\left(\frac{r}{(1+fv_{max})} - r_0 - \frac{q\alpha(1-m)v_{max}}{a}\right) =: u_{min}.\end{aligned}$$

Similarly,

$$\begin{aligned}\frac{dv}{dt} &\geq sv\left(1 - \frac{\beta v}{(1-q)\alpha_A q_A}\right),\\ \Rightarrow \liminf_{t\to\infty} v(t) &\geq \frac{1}{\beta}(1-q)\alpha_A q_A =: v_{min}.\end{aligned}$$

From Theorem 6.3.2, it is evident that

$$0 < u_{min} < \liminf_{t\to\infty} u(t) \leq \limsup_{t\to\infty} u(t) \leq u_{max},\ \ 0 < v_{min} < \liminf_{t\to\infty} v(t) \leq \limsup_{t\to\infty} v(t) \leq v_{max}.$$

This indicates that the species will persist in the future if they are present initially.

Hence, the theorem follows. ∎

6.3.2 Equilibrium analysis

We have the following ecologically feasible equilibria:

1. The trivial equilibrium $E_0(0,0)$.

2. Predator-free equilibrium $E_1(\frac{r-r_0}{r_1},0)$, which exists when $r-r_0>0$.

3. Prey-free equilibrium $E_2(0,\frac{(1-q)\alpha_A q_A}{\beta})$.

4. The positive roots of the following algebraic equations give the coexistence equilibrium points:

$$\begin{aligned} f_1(u,v) &= r\left(\tfrac{1+cu}{1+cu+fv}\right) - r_0 - r_1u - \tfrac{q\alpha(1-m)v}{a+q(1-m)u} = 0,\\ f_2(u,v) &= s\left(1 - \frac{\beta v}{q\alpha(1-m)u+(1-q)\alpha_A q_A}\right) = 0.\end{aligned} \tag{6.3}$$

From the second equation of (6.3), we get $v = \frac{1}{\beta}(q\alpha(1-m)u + (1-q)\alpha_A q_A$. Substituting the value back in the first equation of (6.3), a cubic polynomial is obtained, and it is given by

$$M_3u^3 + M_2u^2 + M_1u + M_0 = 0, \tag{6.4}$$

where

$$\begin{aligned}
M_3 &= q\beta(1-m)r_1(c\beta + fq\alpha(1-m)),\\
M_2 &= c\beta^2(ar_1 - q(1-m)(r-r_0) + q(1-m)[\alpha q(1-m)(c\alpha\beta + r_0\beta f\\
&\quad + fq\alpha^2(1-m)) + \beta r_1(\beta + a\alpha f + f(1-q)\alpha_A q_A)],\\
M_1 &= -(r-r_0)\beta^2(ac + q(1-m)) + ar_1\beta^2 + (1-m)\alpha\beta q((1-m)\alpha q + ar_0 f)\\
&\quad + (1-m)(1-q)q\alpha_A q_A(c\alpha\beta + r_0\beta f + 2fq\alpha^2(1-m)) + ar_1 f\beta(1-q)\alpha_A q_A,\\
M_0 &= -a\beta^2(r-r_0) + \alpha_A q_A(1-q)[af\beta r_0 + q\alpha(1-m)(\beta + f(1-q)\alpha_A q_A)].
\end{aligned}$$

The discriminant for the equation (6.4) is given as:

$$\Delta = 18M_3M_2M_1M_0 - 4M_2^3M_0 + M_2^2M_1^2 - 4M_3M_1^3 - 27M_3^2M_0^2.$$

The number of the possible coexistence equilibrium depends upon the sign of M_0, M_1, M_2 and Δ. The feasible scenarios are as follows:

1. No coexistence equilibrium
   - If $M_0 > 0$, $M_1 > 0$ and $M_2 > 0$, then the system (6.1) has no coexistence equilibrium.
   - Additionaly, the system (6.1) lacks coexistence equilibrium if ($M_0 > 0$, $M_2 < 0$) or ($M_0 > 0$, $M_1 < 0$) and $\Delta = 0$ hold.
2. Unique coexistence equilibrium
   - If ($M_0 < 0$, $M_1 > 0$,$M_2 > 0$) or ($M_0 < 0$, $M_1 < 0$,$M_2 > 0$) or ($M_0 < 0$, $M_1 < 0$,$M_2 < 0$), then the system (6.1) has unique coexistence equilibrium.
   - Also, the system (6.1) has unique coexistence equilibrium under the conditions $M_0 < 0$, $M_1 > 0$, $M_2 < 0$ and $\Delta < 0$.
3. Two coexistence equilibria
   - The system (6.1) has two coexistence equilibrium if ($M_0 > 0$, $M_2 < 0$) or ($M_0 > 0$, $M_1 < 0$) and $\Delta \neq 0$.
4. Three coexistence equilibria

- The system (6.1) has three coexistence equilibrium if $M_0 < 0$, $M_1 > 0$, $M_2 < 0$ and $\Delta > 0$.

Remark: Using the above analysis, the number of possible coexistence equilibrium points is depicted in Fig. 6.1. The conditions mentioned above divide the $\alpha_A - c$ parameter plane into three regions: blue for no coexistence equilibrium; green for unique coexistence equilibrium and yellow for two coexistence equilibria.

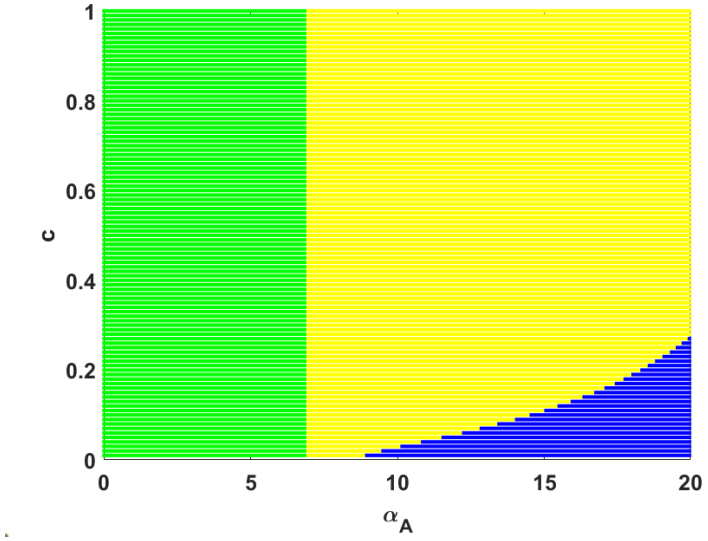

Fig. 6.1: Region depicting the possible number of positive equilibria in the α_A-c plane. Blue: no positive equilibrium, green: unique positive equilibrium and yellow: two positive equilibria. All the remaining parameters are pre-defined in the Table 6.1.

6.3.3 Stability analysis of various equilibria

Now, we perform stability analysis (local or global) for various feasible equilibrium points. By evaluating the variational matrix at the equilibrium points E_0, E_1 and E_2, we get the following results:

1. The trivial equilibrium $E_0(0,0)$ is consistently unstable.
2. The predator-free equilibrium $E_1(\frac{r-r_0}{r_1},0)$ is always a saddle point.
3. The prey-free equilibrium $E_2(0,\frac{(1-q)\alpha_A q_A}{\beta})$ is locally asymptotically stable if

$$r\beta < \frac{(\beta + f(1-q)\alpha_A q_A)^2}{f(1-q)\alpha_A q_A}\left(r_0 + \frac{\alpha q(1-m)(1-q)\alpha_A q_A}{a\beta}\right).$$

Theorem 6.3.4. *For the system (6.1), we have the following qualitative results regarding the stability behavior of the coexistence equilibrium:*

1. *The unique coexistence equilibrium E_1^* is locally aysmptotically stable (or unstable) if $tr(J|_{E_1^*}) < 0$ (or $tr(J|_{E_1^*}) > 0$).*

2. *When the system has two coexistence equilibrium points $E_i^*(u_i^*, v_i^*)$, $i = 1,2$ in a way that $u_1^* < u_2^*$, then E_2^* is always locally asymptotically stable. Additionally, E_1^* is a saddle point.*

Proof. The variational matrix mentioned above can be rewritten as:

$$J|_{E^*(u^*,v^*)} = \begin{bmatrix} u\frac{\partial f_1}{\partial u} & u\frac{\partial f_1}{\partial v} \\ v\frac{\partial f_2}{\partial u} & v\frac{\partial f_2}{\partial v} \end{bmatrix}_{E^*(u^*,v^*)}.$$

Let us assume that the slope of tangents to prey and predator nullclines at $E^*(u^*, v^*)$ is given as $\frac{dv^{(f_1)}}{du}$ and $\frac{dv^{(f_2)}}{du}$, respectively. Now, we have

$$det(J|_{E^*}) = \left(uv\frac{\partial f_1}{\partial v}\frac{\partial f_2}{\partial v}\left(\frac{dv^{(f_2)}}{du} - \frac{dv^{(f_1)}}{du} \right) \right).$$

Further, we have the following possible cases:

Case 1. For the system (6.1) to possess a unique coexistence equilibrium, we have two possibilities for the graphical representation of prey and predator nullclines as depicted in Figs. 6.2(a) and 6.2(b). The prey ($f_1 = 0$)and predator ($f_2 = 0$) nullclines are represented with green and blue color, respectively.

- For Fig. 6.2(a), we take a small ε-nbd near E_1^*. Then, analyzing the sign of the nullclines as we move in u and v direction, we get

$$sign(J|_{E_1^*(u^*,v^*)}) = \begin{bmatrix} - & - \\ + & - \end{bmatrix}.$$

  Also, we can easily observe that $\frac{dv^{(f_1)}}{du} < 0$ and $\frac{dv^{(f_2)}}{du} > 0$. Hence, $tr(J|_{E_1^*}) < 0$ and $det(J|_{E_1^*}) > 0$). It follows that E_1^* is locally asymptotically stable.

- Similarly, for Fig. 6.2(b), we have

$$sign(J|_{E_1^*(u^*,v^*)}) = \begin{bmatrix} + & - \\ + & - \end{bmatrix}.$$

For this graphical possibility, $\frac{dv^{(f_2)}}{du} > \frac{dv^{(f_1)}}{du}$ i.e., $det(J|_{E_1^*}) > 0)$. Therefore, the coexistence equilibrium in this case is stable (or unstable) if $tr(J|_{E_1^*}) < 0$ (or $tr(J|_{E_1^*}) > 0$).

Case 2. When the system (6.1) has two coexistence equilibria, we have only one possibility of intersection of nullclines which is depicted in Fig. 6.2(c). Proceeding in the same manner as in case 1, we have the sign of the variational matrix for E_1^* and E_2^* as follows:

$$sign(J|_{E_1^*(u^*,v^*)}) = \begin{bmatrix} + & - \\ + & - \end{bmatrix},$$

and

$$sign(J|_{E_2^*(u^*,v^*)}) = \begin{bmatrix} - & - \\ + & - \end{bmatrix}.$$

At $E_1^*(u_1^*, v_1^*)$, $\frac{dv^{(f_2)}}{du} < \frac{dv^{(f_1)}}{du}$ i.e., $(det(J|_{E_1^*}) < 0)$. Hence, E_1^* is always unstable irrespective of any condition. Further, at E_2^*, $\frac{dv^{(f_2)}}{du} > \frac{dv^{(f_1)}}{du}$ i.e., $(det(J|_{E_1^*}) > 0)$. The trace of the variational matrix is always negative at E_2^*. Therefore, E_2^* is always locally asymptotically stable.

Hence, the proof. ∎

Remark: The system also exhibits bistability behavior in which the system's solution converges to different equilibrium points for the same parametric set depending on the initial conditions. Fig. 6.3 presents that the trajectories initiating from different initial conditions converges either to the prey-free equilibrium $E_2(0, 17.85)$ or to the coexistence equilibrium $E_2^*(64.8809, 33.4214)$. From ecological perspective, bistability can significantly affect the system's stability as well as survival of both the species.

Theorem 6.3.5. *Let the following inequalities hold:*

(i) $r_1 > \frac{rcfv^*}{(1+fv^*)(1+cu^*+fv^*)} + \frac{\alpha q^2(1-m)^2v^*}{a(a+q(1-m)u^*)}$,

(ii) $a_{12}^2 < 4a_{11}a_{22}$,

where

$$a_{12} = \frac{s\beta q\alpha(1-m)v^*}{((1-q)\alpha_A q_A)(q\alpha(1-m)u^* + (1-q)\alpha_A q_A)} - \frac{rf}{(1+cu_{max}+fv_{max})(1+cu_{max}+fv^*)} - \frac{q\alpha(1-m)}{(a+q(1-m)u_{max})},$$

$$a_{11} = r_1 - \frac{rcfv^*}{(1+fv^*)(1+cu^*+fv^*)} - \frac{\alpha q^2(1-m)^2v^*}{a(a+q(1-m)u^*)}, \quad a_{22} = \frac{s\beta}{(q\alpha(1-m)u_{max} + (1-q)\alpha_A q_A},$$

u_{max} and v_{max} are defined in Theorem 6.3.2.

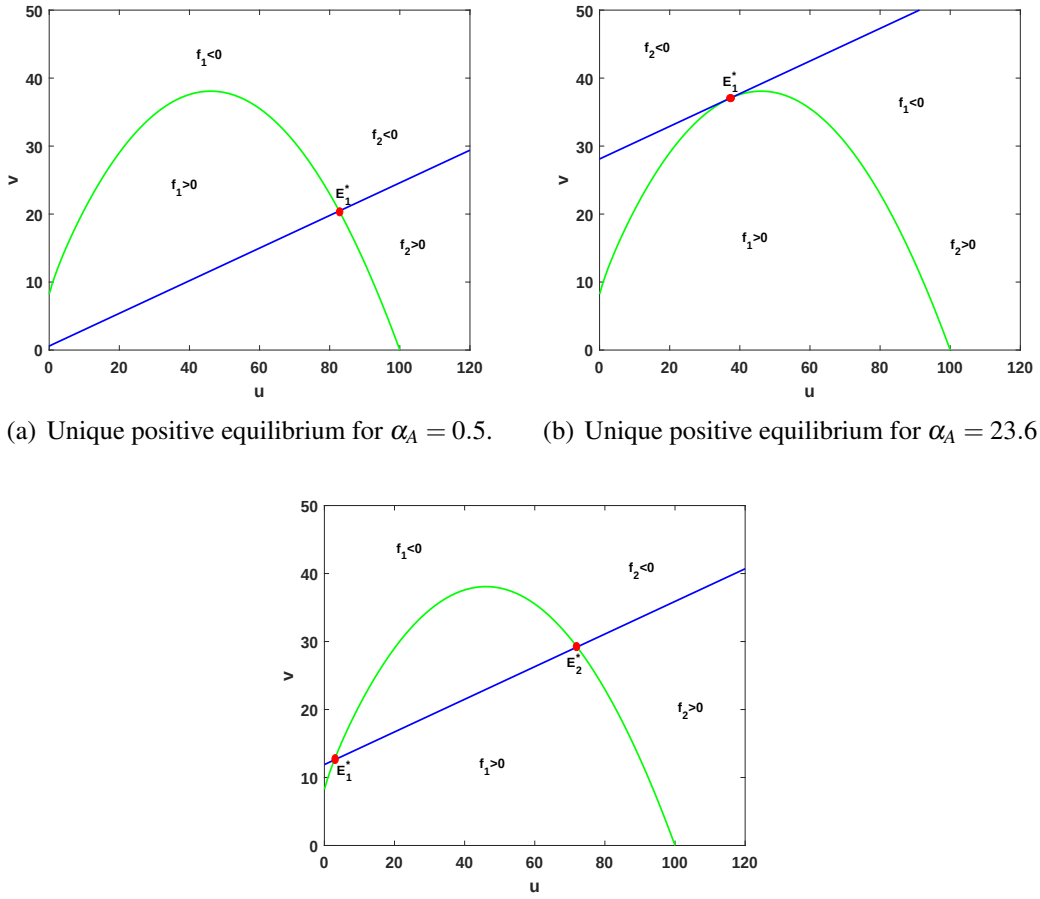

(a) Unique positive equilibrium for $\alpha_A = 0.5$.

(b) Unique positive equilibrium for $\alpha_A = 23.61$.

(c) Two positive equilibria for $\alpha_A = 10$.

Fig. 6.2: This figure illustrates the possible cases for the existence of positive equilibrium. All the other parameteric values are pre-defined in the Table 6.1.

Then the unique coexistence equilibrium $E^*(u^*, v^*)$ is globally asymptotically stable.

Proof. We consider an appropriate Lyapunov function as follows:

$$V(u,v) = \left(u - u^* - u^* ln\frac{u}{u^*}\right) + \left(v - v^* - v^* ln\frac{v}{v^*}\right).$$

Now differentiating the above defined function with respect to t, we have the following expression

$$\dot{V} \quad = \quad -\Theta_{11}(u-u^*)^2 + \Theta_{12}(u-u^*)(v-v^*) - \Theta_{22}(v-v^*)^2,$$

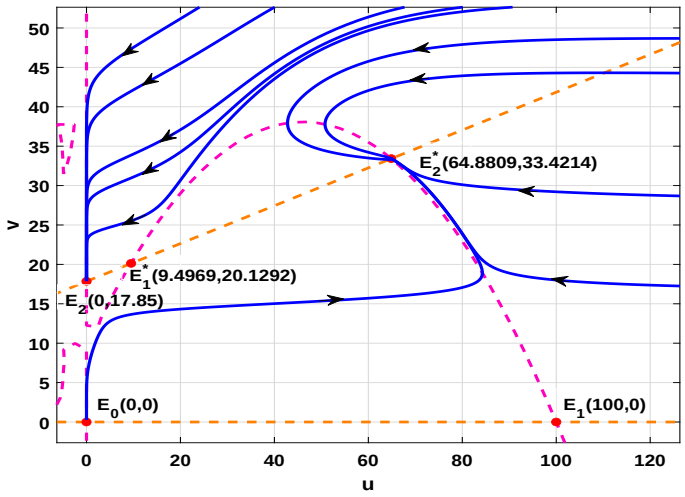

Fig. 6.3: This figure depicts the bistability attribute between the prey-free equilibrium $E_2(0,17.85)$ and the coexistence equilibrium $E_2^*(64.8809,33.4214)$. Here, $\alpha_A = 15$ and all the other parameteric values are pre-defined in the Table 6.1.

where

$$\Theta_{11} = r_1 - \frac{rcfv^*}{(1+cu+fv^*)(1+cu^*+fv^*)} - \frac{\alpha q^2(1-m)^2v^*}{(a+q(1-m)u^*)(a+q(1-m)u)},$$

$$\Theta_{22} = \frac{s\beta}{(q\alpha(1-m)u+(1-q)\alpha_A q_A},$$

$$\Theta_{12} = \frac{s\beta q\alpha(1-m)v^*}{(q\alpha(1-m)u+(1-q)\alpha_A q_A)(q\alpha(1-m)u^*+(1-q)\alpha_A q_A)} - \frac{rf(1+cu)}{(1+cu+fv)(1+cu+fv^*)} - \frac{q\alpha(1-m)}{(a+q(1-m)u)}.$$

Following the Sylvester's criterion, $\dot{V}(u,v)$ is negative definite if and only if $\Theta_{11} > 0$ and ${\Theta_{12}}^2 < 4\Theta_{11}\Theta_{22}$. It may be noted that these two conditions are satisfied under the two conditions mentioned in the statement of the theorem.
Hence, the result follows. ∎

Remark: The global stability behavior of unique coexistence equilibrium is illustrated in Fig. 6.4. Fig. 6.4(a) depicts the region (blue region) in $\alpha_A - r_1$ plane where the unique coexistence equilibrium is globally asymptotically stable. The phase portrait presented in Fig. 6.4(b) demonstrates trajectories converging towards the coexistence equilibrium E_1^*, originating from any point within the phase space.

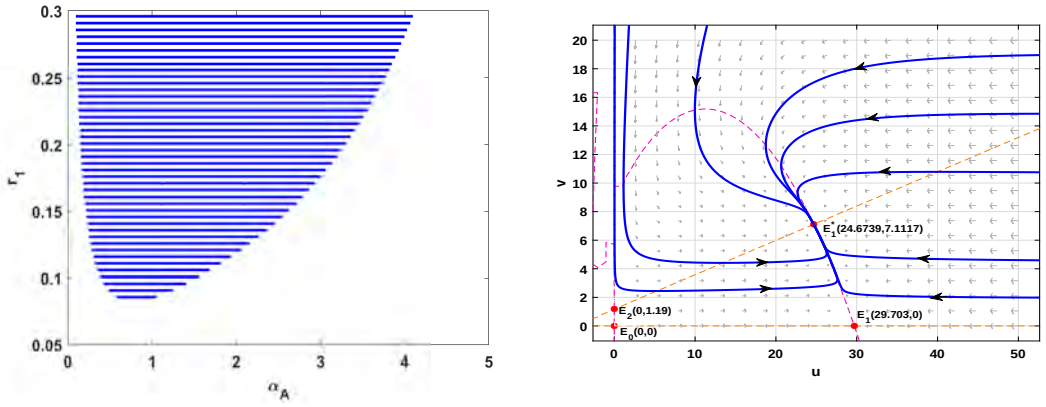

(a) The blue region illustrates the global stability behavior of unique coexistence equilibrium in α_A-r_1 plane.

(b) This phase portrait depicts the global asymptotic stability of E_1^*. Here, $\alpha_A = 1$ and $r_1 = 0.101$.

Fig. 6.4: All the other parameteric values are pre-defined in the Table 6.1.

6.3.4 Bifurcation analysis

The system experiences bifurcation when a slight modification in the parameter values (bifurcation parameters) leads to a qualitative or quantitative change in the system's behavior. This section comprises various kinds of local bifurcations of co-dimension one that help us comprehend how system change their behavior under varying conditions.

Theorem 6.3.6. *The system* (6.1) *undergoes transcritical bifurcation near the prey-free equilibrium* $E_2(0, \frac{(1-q)\alpha_A q_A}{\beta})$ *when the additional food parameter passes through a critical value* $\alpha_A = \alpha_A^*$ *under the following properties:*

(i) $-\frac{\alpha q(1-m)(1-q)q_A}{a\beta} + \frac{rf\beta(1-q)q_A(\beta - f(1-q)\alpha_A^* q_A)}{(\beta + f(1-q)\alpha_A^* q_A)^3} \neq 0,$

(ii) $\frac{2rf\beta}{(\beta+f(1-q)\alpha_A^* q_A)^2}(c(1-q)\alpha_A^* q_A - q\alpha(1-m)) + \frac{2(1-m)^2 q^2 \alpha}{a^2\beta}((1-q)\alpha_A^* q_A - a\alpha) - 2r_1 \neq 0.$

Proof. The variational matrix at the prey-free equilibrium $E_2(0, \frac{(1-q)\alpha_A q_A}{\beta})$ is

$$DF(E_2, \alpha_A) = \begin{bmatrix} -r_0 - \frac{\alpha q(1-m)(1-q)\alpha_A q_A}{a\beta} + \frac{rf\beta(1-q)\alpha_A q_A}{(\beta+f(1-q)\alpha_A q_A)^2} & 0 \\ \frac{s(1-m)\alpha q}{\beta} & -s \end{bmatrix}.$$

The eigenvalues of the above matrix are $\lambda_1 = -s(< 0)$ and $\lambda_2 = -r_0 - \frac{\alpha q(1-m)(1-q)\alpha_A q_A}{a\beta} + \frac{rf\beta(1-q)\alpha_A q_A}{(\beta+f(1-q)\alpha_A q_A)^2}$. E_2 is a non-hyperbolic equilibrium at the critical point $\alpha_A = \alpha_A^*$. Therefore,

$$-r_0 - \frac{\alpha q(1-m)(1-q)\alpha_A^* q_A}{a\beta} + \frac{rf\beta(1-q)\alpha_A^* q_A}{(\beta + f(1-q)\alpha_A^* q_A)^2} = 0.$$

The variational matrix at $\alpha_A = \alpha_A^*$ becomes

$$A = \begin{bmatrix} 0 & 0 \\ \frac{s(1-m)\alpha q}{\beta} & -s \end{bmatrix}.$$

Further, $E_A = [1, \frac{q\alpha(1-m)}{\beta}]^T$ and $E_{A^T} = [1,0]^T$ are the eigenvectors corresponding to the zero eigenvalue of the matrix A and A^T, respectively.

Assuming $F = (g,h)^T$, we have

$$F_{\alpha_A} = \begin{bmatrix} 0 \\ \frac{s\beta v^2(1-q)q_A}{(q\alpha(1-m)u+(1-q)\alpha_A q_A)^2} \end{bmatrix}.$$

Now, $E_{A^T}^T F_{\alpha_A}(E_2, \alpha_A^*) = 0$ ensures that the system doesn't possess any saddle-node bifurcation at E_2.
Let us consider

$$E_{A^T}^T [DF_{\alpha_A}(E_2, \alpha_A^*)E_A] = -\frac{\alpha q(1-m)(1-q)q_A}{a\beta} + \frac{rf\beta(1-q)q_A(\beta - f(1-q)\alpha_A^* q_A)}{(\beta + f(1-q)\alpha_A^* q_A)^3} \neq 0. \tag{6.5}$$

Additionally,

$$E_{A^T}^T [D^2 F_{\alpha_A}(E_2, \alpha_A^*)(E_A, E_A)] = \frac{2rf\beta}{(\beta + f(1-q)\alpha_A^* q_A)^2}(c(1-q)\alpha_A^* q_A - q\alpha(1-m)) + \frac{2(1-m)^2 q^2 \alpha}{a^2\beta}((1-q)\alpha_A^* q_A - a\alpha) - 2r_1 \neq 0. \tag{6.6}$$

Under conditions (6.5) and (6.6), the theorem follows. ∎

Theorem 6.3.7. *The system undergoes saddle-node bifurcation at the critical point $c = c_s$ around the coexistence equilibrium $E^*(u^*, v^*)$ if the following conditions hold:*

(i) $\frac{rfu^{*2}v^*}{(1+c_s u^* + fv^*)^2} \neq 0$,

(ii) $g_{uu} - \frac{g_u}{g_v}(2g_{uv} + h_{uu}) + \frac{g_u^2}{g_v^2}(g_{vv} + 2h_{uv}) - \frac{g_u^3}{g_v^3}h_{vv} \neq 0$.

Proof. The variational matrix matrix at the coexistence equilibrium is

$$J\big|_{E^*(u^*,v^*)} = \begin{bmatrix} \frac{r((1+cu)^2 + f(1+2cu)v}{(1+cu+fv)^2} - \frac{a(1-m)\alpha qv}{(a+q(1-m)u)^2} - r_0 - 2r_1 u & -\left(\frac{ru(1+cu)f}{(1+cu+fv)^2} + \frac{\alpha q(1-m)u}{(a+q(1-m)u)}\right) \\ \frac{s(1-m)q\alpha\beta v^2}{(q\alpha(1-m)u+(1-q)\alpha_A q_A)^2} & s - \frac{2s\beta v}{q(1-m)\alpha u+(1-q)\alpha_A q_A} \end{bmatrix}_{E^*(u^*,v^*)}.$$

Since, the variational matrix has a zero eigenvalue at the critical point $c = c_s$, therefore,

$$det(J\Big|E^*(u^*,v^*)) = 0.$$

Let us define

$$B = DF(E^*, c_s) = \begin{bmatrix} g_u & g_v \\ h_u & h_v \end{bmatrix}_{E^*(u^*,v^*)}.$$

Now, the eigenvectors corresponding to the zero eigenvalue of B and B^T are $w_B = [1 \ \ \frac{-g_u}{g_v}]^T$ and $w_{B^T} = [1 \ \ \frac{-g_u}{h_u}]^T$, respectively.

By proceeding the computations in the same way as in Theorem 10 done by Anshu *et al.* [4], we can conclude that the system undergoes saddle-node bifurcation with respect to the parameter c at $c = c_s$ near the coexistence equilibrium E^* under the following conditions:

$$w_B^T F_c\Big(E^*(u^*,v^*), c_s\Big) = \frac{rfu^{*2}v^*}{(1+c_su^*+fv^*)^2} \neq 0,$$

and

$$w_B^T\Big[\Big(D^2F(E^*(u^*,v^*), a_s)\Big)(w_B, w_B)\Big] = g_{uu} - \frac{g_u}{g_v}(2g_{uv}+h_{uu}) + \frac{g_u^2}{g_v^2}(g_{vv}+2h_{uv}) - \frac{g_u^3}{g_v^3}h_{vv} \neq 0,$$

where

$$\begin{aligned}
g_{uu} &= 2\left(\frac{cfrv^*(1+fv^*)}{(1+cu^*+fv^*)^3} + \frac{a(1-m)^2q^2\alpha v^*}{(a+q(1-m)u^*)^3} - r_1\right),\\
g_{uv} = g_{vu} &= -\left(\frac{rf(1+c(u^*+2fu^*v^*)+fv^*)}{(1+cu^*+fv^*)^3} + \frac{a(1-m)q\alpha}{(a+q(1-m)u^*)^2}\right),\\
g_{vv} &= \frac{2rf^2u^*(1+cu^*)}{(1+cu^*+fv^*)^3},\\
h_{uu} &= \frac{-2(1-m)^2q^2s\alpha^2\beta v^{*2}}{(q\alpha(1-m)u^*+(1-q)\alpha_Aq_A)^3},\\
h_{uv} &= \frac{2(1-m)q\alpha\beta v^*}{(q\alpha(1-m)u^*+(1-q)\alpha_Aq_A)^2},\\
h_{vv} &= \frac{-2s\beta}{(q\alpha(1-m)u^*+(1-q)\alpha_Aq_A)}.
\end{aligned}$$

Hence, for saddle-node bifurcation to occur, the transversality conditions hold true. ∎

Theorem 6.3.8. *For the system to experience Hopf-bifurcation, the following properties must be satisfied:*

1. $tr(J|_{E_1^*}; \alpha_A = \alpha_A^H) = 0$,
2. $det(J|_{E_1^*}; \alpha_A = \alpha_A^H) > 0$,
3. $\frac{\partial}{\partial \alpha_A}(tr(J|_{E_1^*})|_{\alpha_A = \alpha_A^H} \neq 0$.

Proof. In Theorem (6.3.4), we have already established that $det(J_{E_1^*}) > 0$ whenever coexistence equilibrium E_1^* exists. Now, the stability of the coexistence equilibrium depends on the sign of $tr(J|_{E_1^*})$. Assuming α_A as the bifurcation parameter, E_1^* alters the stability behavior as $tr(J|_{E_1^*})$ switches its sign from positive to negative. Further, we get the critical value of the bifurcation parameter by solving $tr(J|_{E_1^*}) = 0$ as

$$\alpha_A = \alpha_A^H = \frac{1}{(1-q)q_A}\left(\frac{2s\beta v_1^*}{\phi + s} - q(1-m)\alpha u_1^*\right),$$

where

$$\phi = \frac{r((1+cu_1^*)^2 + f(1+2cu_1^*)v_1^*}{(1+cu_1^* + fv_1^*)^2} - \frac{a(1-m)\alpha q v_1^*}{(a+q(1-m)u_1^*)^2} - r_0 - 2r_1 u_1^*.$$

The above expression of α_A is an implicit expression because u_1^* and v_1^* depends on α_A. Now, for the system to undergo Hopf-bifurcation, we verify the tranversality condition given by

$$\frac{\partial}{\partial \alpha_A}(tr(J|_{E_1^*})|_{\alpha_A = \alpha_A^H} = \left.\frac{2s\beta(1-q)q_A v_1^*}{(q(1-m)\alpha u_1^* + (1-q)\alpha_A q_A)^2}\right|_{\alpha_A = \alpha_A^H} \neq 0.$$

This completes the proof. ∎

6.4 Analysis of spatiotemporal model

This section investigates the spatiotemporal model (6.2) with Neumann boundary conditions. First, we derive the conditions for the existence and boundedness of the solutions in the absence of cross-diffusion. Then, we analyze the diffusion-induced instability and pattern formation that provides deeper insights into the system's dynamics.

6.4.1 Existence and boundedness

We consider the following system without cross-diffusion:

$$\begin{aligned}
\frac{\partial u}{\partial t} &= d_{11}\Delta u + ru\Big(\frac{1+cu}{1+cu+fv}\Big) - r_0 u - r_1 u^2 - \frac{q\alpha(1-m)uv}{a+q(1-m)u}, && (x,y,t)\in M,\\
\frac{\partial v}{\partial t} &= d_{22}\Delta v + sv\left(1 - \frac{\beta v}{q\alpha(1-m)u+(1-q)\alpha_A q_A}\right), && (x,y,t)\in M,\\
\frac{\partial u}{\partial \nu} &= \frac{\partial v}{\partial \nu} = 0, && (x,y,t)\in N,\\
u(x,y,0) &= u_0(x,y)\geq 0, v(x,y,0) = v_0(x,y)\geq 0, && (x,y)\in\Omega,
\end{aligned} \tag{6.7}$$

where $M=\Omega\times(0,\infty)$ and $N=\partial\Omega\times(0,\infty)$.

For system (6.7), we are able to establish the following theorem.

Theorem 6.4.1.

- *For the non-zero initial conditions $u_0(x,y)$ and $v_0(x,y)$, system (6.7) possess a unique solution $(u(x,y,t),v(x,y,t))$ such that $u(x,y,t)>0$ and $v(x,y,t)>0$ for all $(x,y,t)\in M$.*
- *The solution $(u(x,y,t),v(x,y,t))$ of system (6.7) satisfy the following inequalities:*

$$\begin{aligned}
\limsup_{t\to\infty} u(x,y,t) &\leq \frac{r-r_0}{r_1},\\
\limsup_{t\to\infty}\iint_\Omega \frac{\partial v(x,y,t)}{dt}dxdy &\leq \frac{1}{\beta}\left(\frac{q\alpha(1-m)(r-r_0)(|\Omega|+\varepsilon)}{r_1}+(1-q)\alpha_A q_A\right).
\end{aligned}$$

Proof. Denote

$$\begin{aligned}
G_1(u,v) &= ru\Big(\frac{1+cu}{1+cu+fv}\Big) - r_0 u - r_1 u^2 - \frac{q\alpha(1-m)uv}{a+q(1-m)u},\\
G_2(u,v) &= sv\left(1 - \frac{\beta v}{q\alpha(1-m)u+(1-q)\alpha_A q_A}\right).
\end{aligned}$$

From the above expressions, we have

$$\begin{aligned}
\frac{\partial G_1(u,v)}{\partial v} &= -\left[\frac{rfu(1+cu)}{(1+cu+fv)^2}+\frac{q\alpha(1-m)u}{(a+q(1-m)u)}\right]\leq 0,\\
\frac{\partial G_2(u,v)}{\partial u} &= \frac{s\beta q\alpha(1-m)uv^2}{(q\alpha(1-m)u+(1-q)\alpha_A q_A)^2}\geq 0,
\end{aligned}$$

for $(u,v)\in\mathbb{R}^2_+=\{(u,v)|u\geq 0,v\geq 0\}$. Thus, the system (6.7) consists of weakly coupled parabolic equations with mixed quasimonotonic expressions [120]. Consider $(\underline{u}(x,y),\underline{v}(x,y))=$

$(0,0)$ and $(\bar{u}(x,y),\bar{v}(x,y)) = (u^*(t),v^*(t))$ where $(u^*(t),v^*(t))$ is the unique solution to

$$\begin{aligned}
&\frac{du}{dt} = ru\Big(\frac{1+cu}{1+cu+fv}\Big) - r_0u - r_1u^2 - \frac{q\alpha(1-m)uv}{a+q(1-m)u}, \quad t>0\\
&\frac{dv}{dt} = sv\left(1 - \frac{\beta v}{q\alpha(1-m)u+(1-q)\alpha_A q_A}\right), \quad t>0,\\
&u(0) = u^*, v(0) = v^*,
\end{aligned}$$

where $u^* = \sup_{\bar{\Omega}} u_0(x,y)$ and $v^* = \sup_{\bar{\Omega}} v_0(x,y)$. Since

$$\begin{aligned}
\frac{\partial \bar{u}(x,y,t)}{\partial t} - d_{11}\Delta\bar{u}(x,y,t) - G_1(\bar{u}(x,y,t),\underline{v}(x,y,t)) &= 0\\
\geq 0 = \frac{\partial \underline{u}(x,y,t)}{\partial t} - d_{11}\Delta\underline{u}(x,y,t) - G_1(\underline{u}(x,y,t),\bar{v}(x,y,t)),&\\
\frac{\partial \bar{v}(x,y,t)}{\partial t} - d_{22}\Delta\bar{v}(x,y,t) - G_2(\bar{u}(x,y,t),\bar{v}(x,y,t)) &= 0\\
\geq 0 = \frac{\partial \underline{v}(x,y,t)}{\partial t} - d_{22}\Delta\underline{v}(x,y,t) - G_2(\underline{u}(x,y,t),\underline{v}(x,y,t)),&
\end{aligned}$$

for $(x,y,t) \in M$, we can easily observe the given boundary conditions

$$\frac{\partial \bar{u}(x,y,t)}{\partial \nu} \geq 0 \geq \frac{\partial \underline{u}(x,y,t)}{\partial \nu}, \frac{\partial \bar{v}(x,y,t)}{\partial \nu} \geq 0 \geq \frac{\partial \underline{v}(x,y,t)}{\partial \nu} \quad for \ \ (x,y,t) \in N,$$

and initial conditions

$$\bar{u}(x,y,0) \geq u_0(x,y) \geq \underline{u}(x,y,0), \bar{v}(x,y,0) \geq v_0(x,y) \geq \underline{v}(x,y,0) \ \ for \ \ (x,y) \in \Omega,$$

hold. Therefore, for system (6.7), $(\underline{u}(x,y),\underline{v}(x,y)) = (0,0)$ and $(\bar{u}(x,y),\bar{v}(x,y)) = (u^*(t),v^*(t)$ constitute the lower and upper solutions, respectively. From Theorem 8.3.3 from [120], we may conclude that the system (6.7) admits a unique solution $(u(x,y,t),v(x,y,t))$ satisfying

$$0 \leq u(x,y,t) \leq u^*(t), 0 \leq v(x,y,t) \leq v^*(t).$$

As $u_0(x,y) \neq 0$ and $v_0(x,y) \neq 0$, so from strong parabolic maximum principle [[153], Lemma 2.1.8], it follows that $u(x,y,t) > 0$, $v(x,y,t) > 0$ for $(x,y,t) \in M$.
This completes the first part of the theorem.

Next, we compute the priori bounds of solutions for the system (6.7). For the estimation of $u(x,y,t)$, we can observe that $u(x,y,t)$ satisfies the system given below:

$$\begin{aligned}
&\frac{\partial u}{\partial t} = d_{11}\Delta u + ru\Big(\frac{1+cu}{1+cu+fv}\Big) - r_0 u - r_1 u^2, && (x,y,t) \in M,\\
&\frac{\partial u}{\partial \nu} = 0, && (x,y,t) \in N,\\
&u(x,y,0) = u_0(x,y) \geq 0, && (x,y) \in \Omega.
\end{aligned}$$

From the standard comparison theorem for parabolic equations [[120],Theorem 2.4.1], it follows that

$$\limsup_{t\to\infty} u(x,y,t) \leq \frac{r-r_0}{r_1}. \tag{6.8}$$

To estimate the priori bound of $v(x,y,t)$, we denote $U(x,y,t) = \iint_\Omega u(x,y,t)dxdy$ and $V(x,y,t) = \iint_\Omega v(x,y,t)dxdy$. Following the Neumann boundary conditions and Green's theorem , we get

$$\begin{aligned}
\frac{dU}{dt} &= \iint_\Omega \frac{\partial u(x,y,t)}{\partial t}dxdy = \iint_\Omega \left[ru\Big(\frac{1+cu}{1+cu+fv}\Big) - r_0 u - r_1 u^2 - \frac{q\alpha(1-m)uv}{a+q(1-m)u}\right]dxdy,\\
\frac{dV}{dt} &= \iint_\Omega \frac{\partial v(x,y,t)}{\partial t}dxdy = \iint_\Omega \left[sv\left(1 - \frac{\beta v}{q\alpha(1-m)u + (1-q)\alpha_A q_A}\right)\right]dxdy.
\end{aligned} \tag{6.9}$$

Since, $\limsup_{t\to\infty} u(x,y,t) \leq \frac{r-r_0}{r_1}$ implying $\limsup_{t\to\infty} U(x,y,t) \leq \frac{r-r_0}{r_1}|\Omega|$. Hence, for $\varepsilon > 0$, there exists $t_1 > 0$ such that $U(t) < \frac{r-r_0}{r_1}(|\Omega| + \varepsilon)$. From (6.9), we have

$$\frac{dV}{dt} = \iint_\Omega \left[sv\left(1 - \frac{\beta v}{q\alpha(1-m)u + (1-q)\alpha_A q_A}\right)\right]dxdy,$$

which implies

$$\frac{dV}{dt} \leq \left[sV\left(1 - \frac{\beta V}{\frac{q\alpha(1-m)(r-r_0)(|\Omega|+\varepsilon)}{r_1} + (1-q)\alpha_A q_A}\right)\right], \quad t > t_1.$$

Thus,

$$\limsup_{t\to\infty} V(t) \leq \frac{1}{\beta}\left(\frac{q\alpha(1-m)(r-r_0)(|\Omega|+\varepsilon)}{r_1} + (1-q)\alpha_A q_A\right),$$

which further yields

$$\limsup_{t\to\infty} V(t) = \limsup_{t\to\infty} \iint_{\Omega} \frac{\partial v(x,y,t)}{\partial t} dxdy \leq \frac{1}{\beta}\left(\frac{q\alpha(1-m)(r-r_0)(|\Omega|+\varepsilon)}{r_1} + (1-q)\alpha_A q_A\right). \tag{6.10}$$

This completes the proof of the second part of the theorem. ∎

6.4.2 Turing instability induced by self and cross-diffusion

In this subsection, we shall derive the conditions for diffusion induced instability in the presence of self and cross-diffusion. Consider the linearized form of the model (6.2) about the coexistence equilibrium $E^*(u^*, v^*)$:

$$\begin{aligned} \frac{\partial u}{\partial t} &= \Upsilon_{11}u + \Upsilon_{12}v + d_{11}\nabla^2 u + d_{12}\nabla^2 v, \\ \frac{\partial v}{\partial t} &= \Upsilon_{21}u + \Upsilon_{22}v + d_{21}\nabla^2 u + d_{22}\nabla^2 v, \end{aligned} \tag{6.11}$$

where

$$\begin{aligned} \Upsilon_{11} &= u^*\left[\frac{rcfv^*}{(1+cu^*+fv^*)^2} - r_1 + \frac{q^2\alpha(1-m)v^*}{(a+q(1-m)u^*)^2}\right], \\ \Upsilon_{12} &= -u^*\left[\frac{rf(1+cu^*)}{(1+cu^*+fv^*)^2} - \frac{q\alpha(1-m)}{(a+q(1-m)u^*)}\right], \\ \Upsilon_{21} &= \frac{s(1-m)q\alpha\beta v^{*2}}{(q\alpha(1-m)u^* + (1-q)\alpha_A q_A)^2}, \\ \Upsilon_{22} &= \frac{-s\beta v^*}{(q\alpha(1-m)u^* + (1-q)\alpha_A q_A)}. \end{aligned}$$

We are keen in examining the linear stability behavior of the system (6.2) near the coexistence equilibrium $E(u^*, v^*)$ by introducing a slight perturbations as follows

$$\begin{aligned} u &= u^* + u_\kappa \exp(\lambda t + i(\kappa.r)), \\ v &= v^* + v_\kappa \exp(\lambda t + i(\kappa.r)), \end{aligned}$$

where (u_κ, v_κ) is a constant column vector, $\kappa = (\kappa_x, \kappa_y)$ is a row vector, $\kappa = \sqrt{\kappa_x^2 + \kappa_y^2}$ is wave number and (x, y) are spatial coordinates.
The linearized system (6.11) has the following characteristic equation:

$$\xi^2 + T(\kappa^2)\xi + D(\kappa^2) = 0, \tag{6.12}$$

where

$$T(\kappa^2) = -(\Upsilon_{11}+\Upsilon_{22}) + \kappa^2(d_{11}+d_{22}) = -tr(J|_{E^*}) + \kappa^2(d_{11}+d_{22}),$$
$$D(\kappa^2) = (d_{11}d_{22}-d_{12}d_{21})\kappa^4 - (\Upsilon_{11}d_{22}+\Upsilon_{22}d_{11}-\Upsilon_{12}d_{21}-\Upsilon_{21}d_{12})\kappa^2 + (\Upsilon_{11}\Upsilon_{22}-\Upsilon_{12}\Upsilon_{21}),$$
$$= (d_{11}d_{22}-d_{12}d_{21})\kappa^4 - (\Upsilon_{11}d_{22}+\Upsilon_{22}d_{11}-\Upsilon_{12}d_{21}-\Upsilon_{21}d_{12})\kappa^2 + det(J|_{E^*}).$$

For $E^*(u^*,v^*)$ to be initially stable in the absence of diffusion, $(\Upsilon_{11}+\Upsilon_{22}) < 0$ and $(\Upsilon_{11}\Upsilon_{22} - \Upsilon_{12}\Upsilon_{21}) > 0$. Therefore, $T(\kappa^2) > 0$. Now, the required condition for diffusion driven instability is $Re[\xi(\kappa^2)] > 0$. Using Routh-Hurwitz criterion, $D(\kappa^2) < 0$ (for some $\kappa \neq 0$) provided that $det(J|_{E^*}) > 0$ is the only possibility for Turing instability.
Solution of Eq. (6.12) for ξ is given as:

$$\xi_{1,2}(\kappa^2) = \frac{-T(\kappa^2) \pm \sqrt{(T(\kappa^2))^2 - 4D(\kappa^2)}}{2}. \tag{6.13}$$

Since $D(\kappa^2)$ is a quadratic in κ^2, therefore, the extremum of $D(\kappa^2)$ is a minimum for some κ^2. So, $D(\kappa^2)$ is minimum at

$$\kappa^2_{min} = \frac{(\Upsilon_{11}d_{22}+\Upsilon_{22}d_{11}-\Upsilon_{12}d_{21}-\Upsilon_{21}d_{12})}{2(d_{11}d_{22}-d_{12}d_{21})}.$$

The corresponding minima is

$$D(\kappa^2_{min}) = det(J|_{E^*}) - \frac{(\Upsilon_{11}d_{22}+\Upsilon_{22}d_{11}-\Upsilon_{12}d_{21}-\Upsilon_{21}d_{12})^2}{4(d_{11}d_{22}-d_{12}d_{21})}.$$

If $D(\kappa)^2 < 0$ for some κ^2, then $D(\kappa^2_{min}) < 0$. Thus,

$$\frac{(\Upsilon_{11}d_{22}+\Upsilon_{22}d_{11}-\Upsilon_{12}d_{21}-\Upsilon_{21}d_{12})^2}{4(d_{11}d_{22}-d_{12}d_{21})} > det(J|_{E^*}).$$

The critical value of Turing bifurcation for system (6.2) can be determined when $D(\kappa^2) = 0$, i.e.,

$$(\Upsilon_{11}d_{22}+\Upsilon_{22}d_{11}-\Upsilon_{12}d_{21}-\Upsilon_{21}d_{12})^2 - 4(d_{11}d_{22}-d_{12}d_{21})det(J|_{E^*}) = 0. \tag{6.14}$$

Further the critical wave number is given as

$$\kappa_c = \sqrt{\frac{det(J|_{E^*(u^*,v^*)})}{d_{11}d_{22}-d_{12}d_{21}}}.$$

Now from the above analysis, we have the following four conditions that must be satisfied for Turing instability:

(i) $(\Upsilon_{11}+\Upsilon_{22})<0$,

(ii) $(\Upsilon_{11}\Upsilon_{22}-\Upsilon_{12}\Upsilon_{21})>0$,

(iii) $(\Upsilon_{11}d_{22}+\Upsilon_{22}d_{11}-\Upsilon_{12}d_{21}-\Upsilon_{21}d_{12})>0$,

(iv) $(\Upsilon_{11}d_{22}+\Upsilon_{22}d_{11}-\Upsilon_{12}d_{21}-\Upsilon_{21}d_{12})^2-4(d_{11}d_{22}-d_{12}d_{21})det(J|_{E^*})>0$.

Remark: When $d_{12}=d_{21}=0$, the above set of four parametric conditions represents the Turing space for self-diffusion.

6.5 Numerical simulations

6.5.1 For temporal model

A series of extensive numerical simulations has been carried out using MATLAB R2019b and MATCONT to validate the theoretical results. To better understand the dynamics of the system, we investigate a number of local bifurcations in this section.

6.5.2 Bifurcation analysis

First, we explore the system's dynamics with respect to the parameter α_A that symbolizes the additional food for the predators. Fig. (6.5) depicts the local bifurcation analysis of co-dimension one in reference to the parameter α_A. In this figure, all the parameters assume values from Table 6.1. As presented in Figs. 6.5(a) and 6.5(b), the coexistence equilibrium is initially stable (blue curve), which then loses its stability behavior through Hopf-bifurcation H_1 occurring at $\alpha_A = 23.3256$. Further, we observe that the system experiences transcritical bifurcation BP at $\alpha_A = 6.9273$ near the prey-free equilibrium E_1^*. Now, as the value of α_A is increased, we notice that the two coexistence equilibria E_1^* and E_2^* collide, and they annihilate each other via saddle-node bifurcation LP at $\alpha_A = 23.6163$. From a biological point of view, for small values of α_A, the species coexist at a relatively constant density over time. But as the value of α_A is increased, the system becomes unstable, exhibiting a recurring pattern of population dynamics between the prey and predator species. However, a significant rise in the additional food might lead to the disapperance of the state where both species coexist.

Next, for deeper insights into the system's dynamics, we presented the bifurcation analysis in varying the fear parameter f (Fig. 6.6). This figure shows that for lower values of the

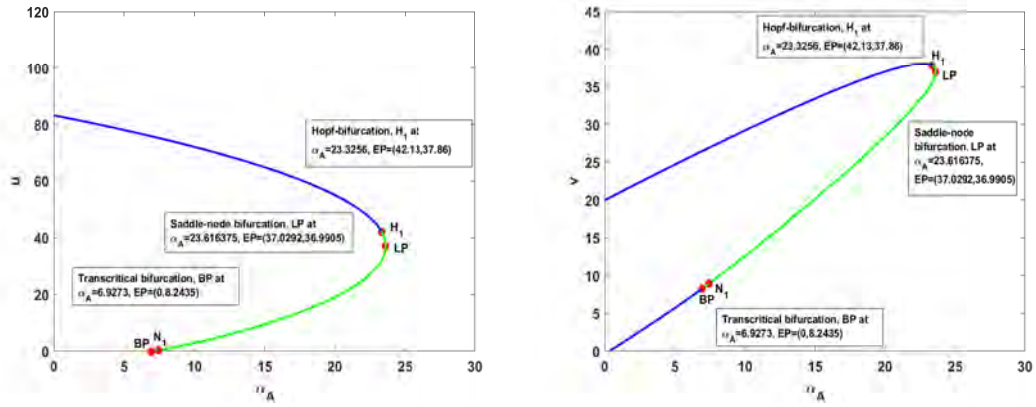

(a) For Prey (b) For Predator

Fig. 6.5: One-dimension bifurcation analysis of the equilibrium point concerning the bifurcation parameter α_A. All other parameters remain consistent as outlined in Table 6.1.

fear parameter, there is a stable coexistence between both species. With a rise in the fear among the prey population, the stable equilibrium becomes unstable via Hopf-bifurcation (H_2) at $f = 1.8858$. Moreover, the axial equilibrium undergoes a transcritical bifurcation (BP) at $f = 2.9035$, which alters the stability behavior of the prey-free equilibrium. Increasing fear level among prey population significantly might cease the coexistence of prey and predator species. This means that as f increases, E_1^* and E_2^* collide via saddle-node bifurcation (LP) at $f = 4.1297$. The blue curve signifies the stable equilibrium while green represents unstable equilibrium point.

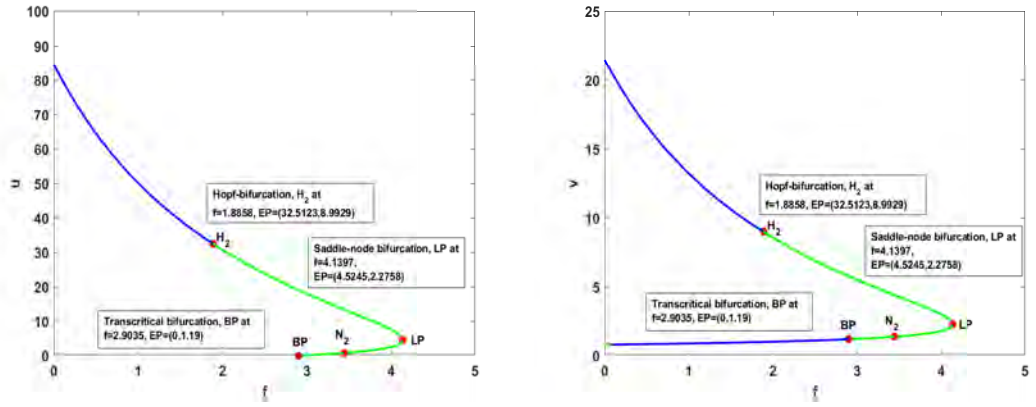

(a) For Prey (b) For Predator

Fig. 6.6: One-dimension bifurcation analysis of the equilibrium point concerning the bifurcation parameter f. All other parameters remain consistent as outlined in Table 6.1.

Further, Fig. 6.7 depicts the kinetics of the system as the value of carry-over effect parameter c is varied. Initially the system is stable near the coexistence equilibrium, which then experiences a Hopf-bifurcation (H_3) at $c = 0.0873$ and becomes unstable. The system now exhibits a recurring pattern dynamics between the species. Again, at $c = 0.4640$, the system experiences a second Hopf-bifurcation (H_4) and the species coexist at a constant density across time. Particularly, we can observe two Hopf-bifurcations for two different values of c. The starting point of oscillation is $c = 0.0873$ with increasing amplitudes. Again, with increasing carry-over effect parameters, the amplitudes decrease, and the oscillation stabilizes at $c = 0.4640$. The oscillations emerging from critical points appear like a bubble, and this effect is generally called a bubbling phenomenon (Fig. 6.8). This type of phenomenon results from the appearance and disappearance of limit cycles due to forward and backward Hopf-bifurcations, respectively. The bubbling loop formed due the occurrence of Hopf bifurcation is different from the classical period bubbling phenomena [82]. Layek and Pati [83] and Pati *et al.* [123] conducted a bi-parameter analysis in a discrete mathematical model and observed that the system demonstrates chaos through period-bubbling routes. Several researchers have also studied the bubbling effect in an ecological context [158, 173].

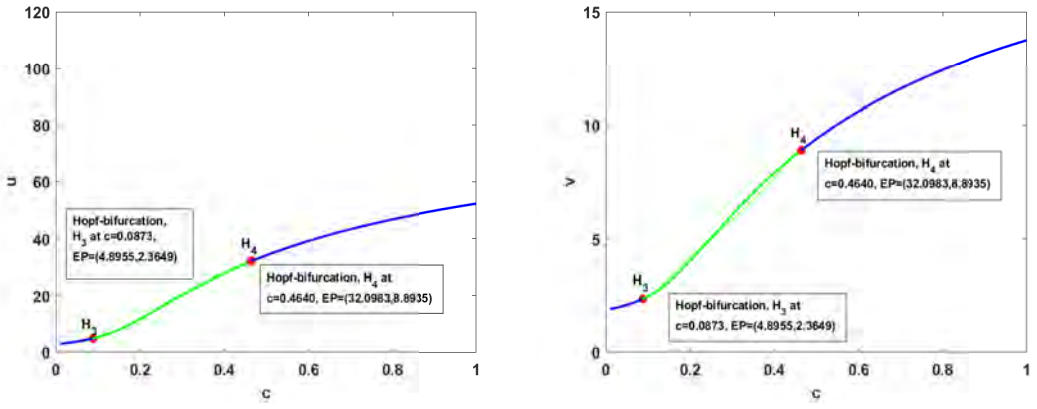

(a) For Prey (b) For Predator

Fig. 6.7: One-dimension bifurcation analysis of the equilibrium point concerning the bifurcation parameter c. Here, $f = 1.5$ and all other parameters remain consistent as outlined in Table 6.1.

Next, as seen in Fig. 6.9(a), we execute our simulation by varying $[c, f]$ about H_3 Hopf-bifurcation. A cusp-bifurcation point is observed at $[c, f] = [0.2892, 2.9035]$ around the prey-free equilibrium point $E_2 = (0, 1.1900)$. In a two-parameter family of autonomous systems, the tangential intersection of two saddle-node bifurcation curves is called the cusp-bifurcation point. Additionally, Bogdanov-Takens bifurcation occurs around the coexistence equilibrium $(1.3112, 1.5046)$ at $[c, f] = [0.3357, 2.9776]$. The specific conditions for Bogdanov-Takens

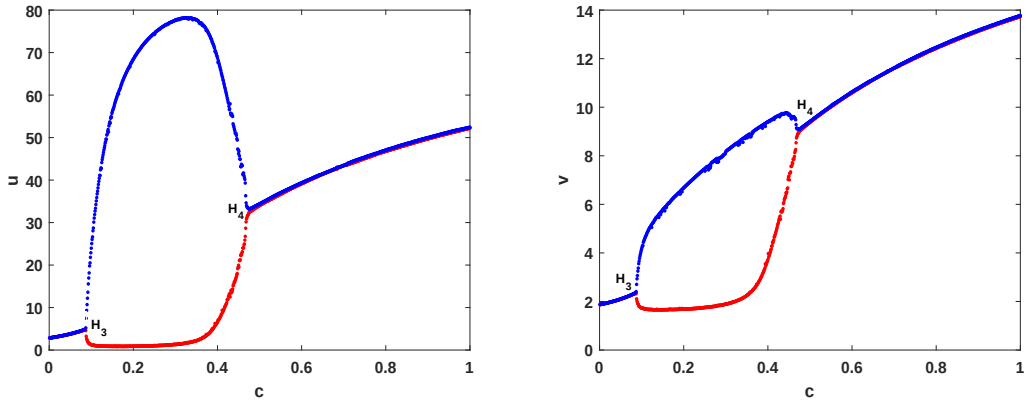

(a) For Prey (b) For Predator

Fig. 6.8: Hopf-bifurcation analysis of the equilibrium point concerning the bifurcation parameter c. Here, $f = 1.5$ and all other parameters remain consistent as outlined in Table 6.1.

bifurcation is that the linearized variational matrix should have two zero real eigenvalues. In Fig. 6.9(a), the magenta curve signifies the saddle-node curve and the red curve denotes the Hopf-bifurcation curve. The intersection of these two depicts the Bogdanov-Takens bifurcation point. Fig. 6.9(b) presents the partition of neighbourhood of the BT point into four different regions namely R_1, R_2, R_3 and R_4. The black, blue and red colored curves represents saddle-node, Hopf and homoclinic curves, respectively.

Now, we investigate the dynamics of system (6.1) in the vicinity of the BT-point with $(c, f) \in [0.3, 0.35] \times [2.91, 2.98]$, as depicted in Fig. 6.9(b). This figure divides the vicinity of the BT-point into four sub-regions: R_1, R_2, R_3, and R_4. Three curves, namely the saddle-node curve (black), Hopf curve (blue), and homoclinic curve (red) are utilized to delineate these subregions. A degenerate equilibrium E_d exists at the BT-point for $(c, f) = (0.3357, 2.9776)$, illustrated in Fig. 6.10(a). In region R_1, E_2 emerges as the only stable coexistence equilibrium, as indicated in Fig. 6.10(b). Upon decreasing the fear parameter, the system transitions into R_2, where the saddle point E_1^* and spiral sink E_2^* become prominent (Fig. 6.10(c)) after traversing the saddle-node curve. Ecologically, this signifies that an increase in the strength of the fear effect can lead to the annihilation of two interior equilibria. Subsequently, progression from R_2 to R_3 occurs by elevating the carry-over effect parameter, resulting in the generation of a limit cycle around the spiral source E_2^* through Hopf-bifurcation (Fig. 6.10(d)). Continuing, we increase the carry-over effect parameter further and choose a point on the homoclinic curve, where the previously noted stable limit cycle collides with the saddle E_2^*, resulting in the formation of a homoclinic loop (Fig. 6.10(e)). Subsequently, a further increment in c takes us into region R_4, causing the homoclinic loop mentioned earlier to vanish, while E_1^* persists as a

saddle point and E_2^* remains a spiral source (Fig. 6.10(f)).

Remark: The influence of prey refuge on system dynamics aligns with the findings of Gupta *et al.* [48]. We have excluded the figures illustrating the results related to prey refuge for brevity.

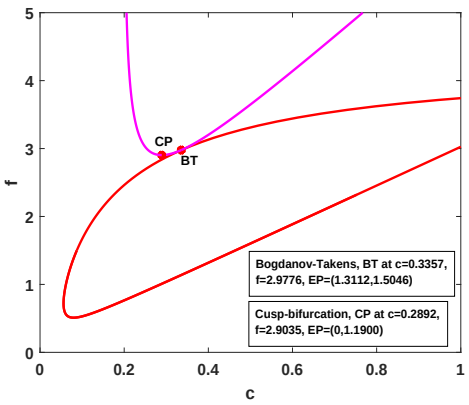

(a) This figure depicts the bi-parametric plot illustrating the local bifurcations of co-dimension 2.

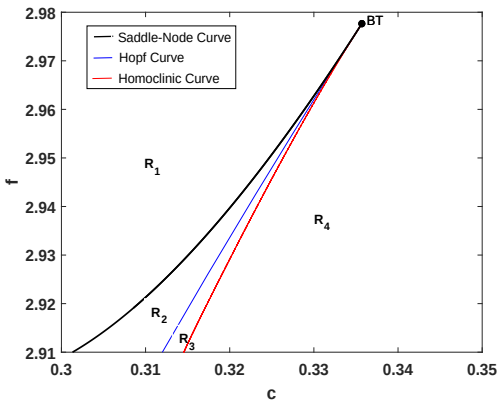

(b) This figure depicts the divison of neighbourhood of BT-point into four sub-regions: R_1, R_2, R_3 and R_4.

Fig. 6.9: Two-dimension bifurcation analysis of the equilibrium point concerning bifurcation parameters $[c, f]$. All other parameters remain consistent as outlined in Table 6.1.

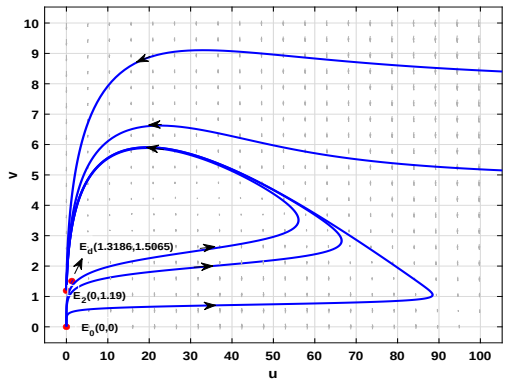

(a) $c = 0.3357$, $f = 2.9976$. This figure shows the degenerate equilibrium E_d.

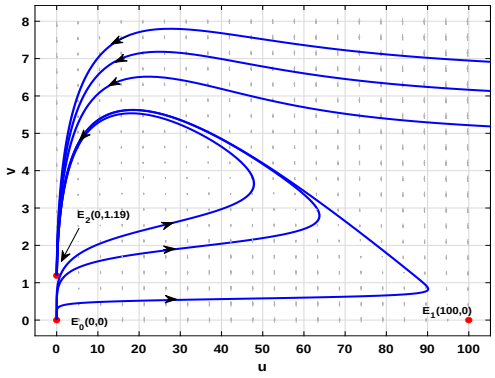

(b) $c = 0.3$, $f = 2.92$. This figure corresponds to R_1 region where E_2 is the only stable equilibrium.

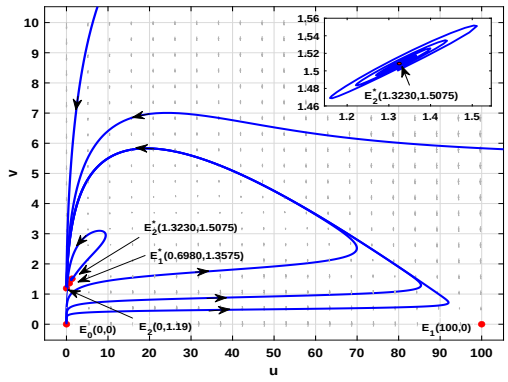

(c) $c = 0.323$, $f = 2.943$. This figure shows the appearance of saddle point E_1^* and spiral sink E_2^* (after passing through the saddle-node curve).

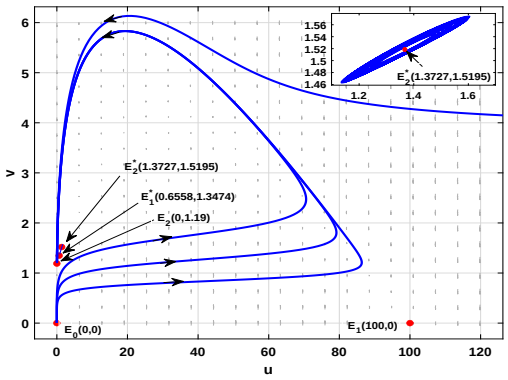

(d) $c = 0.323$, $f = 2.942$. This figure depicts the generation of a limit cycle around the spiral source E_2^* (after passing through the Hopf-bifurcation curve)

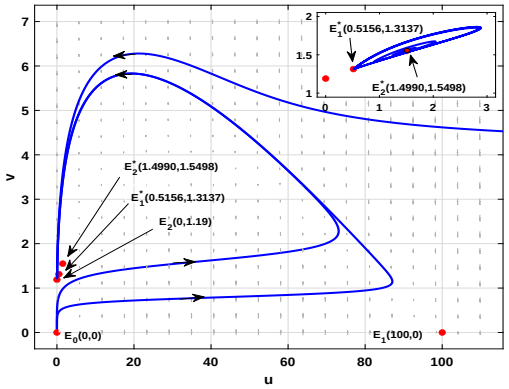

(e) $c = 0.3221$, $f = 2.9365$. This figure depicts the formation of a homoclinic loop connecting the saddle point E_1^* and spiral source E_2^*.

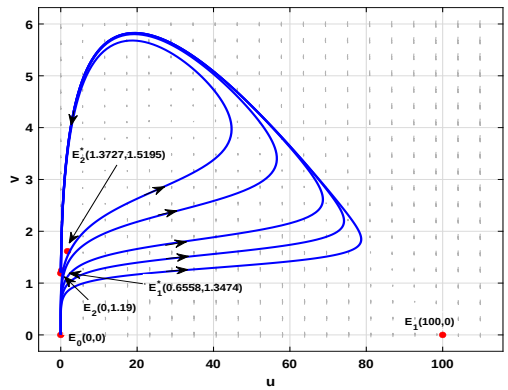

(f) $c = 0.32$, $f = 2.92$. This figure corresponds to R_4 where E_1^* is a saddle point and E_2^* is spiral source (after passing through the Homoclinic curve)

Fig. 6.10: This plot depicts the system's dynamics in a bi-parameteric plane $[c, f]$. All other parameters remain consistent as outlined in Table 6.1.

6.5.3 Pattern formation

This section comprised the numerical simulations conducted to analyze the dynamics of the proposed spatiotemporal model (6.2) in a two-dimensional habitat. In order to carry out the simulations, we took into account a 200×200 spatial grid with the Neumann (zero-flux) boundary conditions, a time step of $\Delta t = 1/300$, and a space step-size of $\Delta x = \Delta y = 1/3$. We employed the forward Euler scheme for the reaction part and the conventional five-point explicit finite difference scheme for the diffusion part. The following two types of initial conditions has been considered to investigate the spatialtemporal patterns:

- $$\begin{aligned} u(x,y,0) &= u^* + \varepsilon_1 G_{i,j}, \\ v(x,y,0) &= v^* + \varepsilon_1 H_{i,j}, \end{aligned} \tag{6.15}$$

  where $G_{i,j}$ and $H_{i,j}$ are conventional Gaussian white noise, (u^*, v^*) is the coexistence equilibrium and $\varepsilon_1 = 0.0001$.

- $$\begin{aligned} u(x,y,0) &= u^* + \varepsilon_2 \sin\big(\frac{2\pi(x-x_0)}{50}\big) + \varepsilon_2 \sin\big(\frac{2\pi(y-y_0)}{50}\big), \\ v(x,y,0) &= v^*. \end{aligned} \tag{6.16}$$

  where $\varepsilon_2 = 0.01$, $x_0 = y_0 = 0.1$ and (u^*, v^*) is the coexistence equilibrium.

6.5.3.1 In the absence of cross-diffusion

First, we set $d_{12} = d_{21} = 0$ in model (6.2) and then explore the effect of diffusion coefficients d_{11} and d_{22} on the Turing patterns. This section considers the coexistence equilibrium from the Turing space, i.e., the coexistence equilibrium that satisfies the analytic Turing conditions. Here, the numerical simulations are performed using the initial state (6.15). Figure 6.11 illustrates the effect of the movement of prey species on the pattern formation. The predator self-diffusion coefficient d_{22} is intentionally set to 1. In Fig. 6.11(a), we observe a patchy pattern of low and high predator populations, whereas the moderate predator population occupies most of the region. With an increase in the value of the prey self-diffusion coefficient, the simulations reveal the emergence of the cold-spot pattern (Fig. 6.11(b)). Further increasing the value of d_{11} results in the evolvement of the cold spots, which are well-connected within the stripe structures (Fig. 6.11(c)).

Next, we investigate the consequences of increased predator movement across the habitat on the Turing patterns. In Fig. 6.12, we fix the prey-diffusion coefficient $d_{11} = 0.01$. Figure 6.12(a) reveals a Turing pattern consisting of spots and stripes that almost have the same predator density as the rest of the habitat. Increasing the predator movement results in forming connected cold-spot patterns illustrated in Fig. 6.12(b). A significant increase in d_{22} demonstrates the emergence of patchy Turing patterns as a combination of low and high-density populations. From an ecological perspective, increased random movement of prey species results in decreased density of predator populations across the habitat.

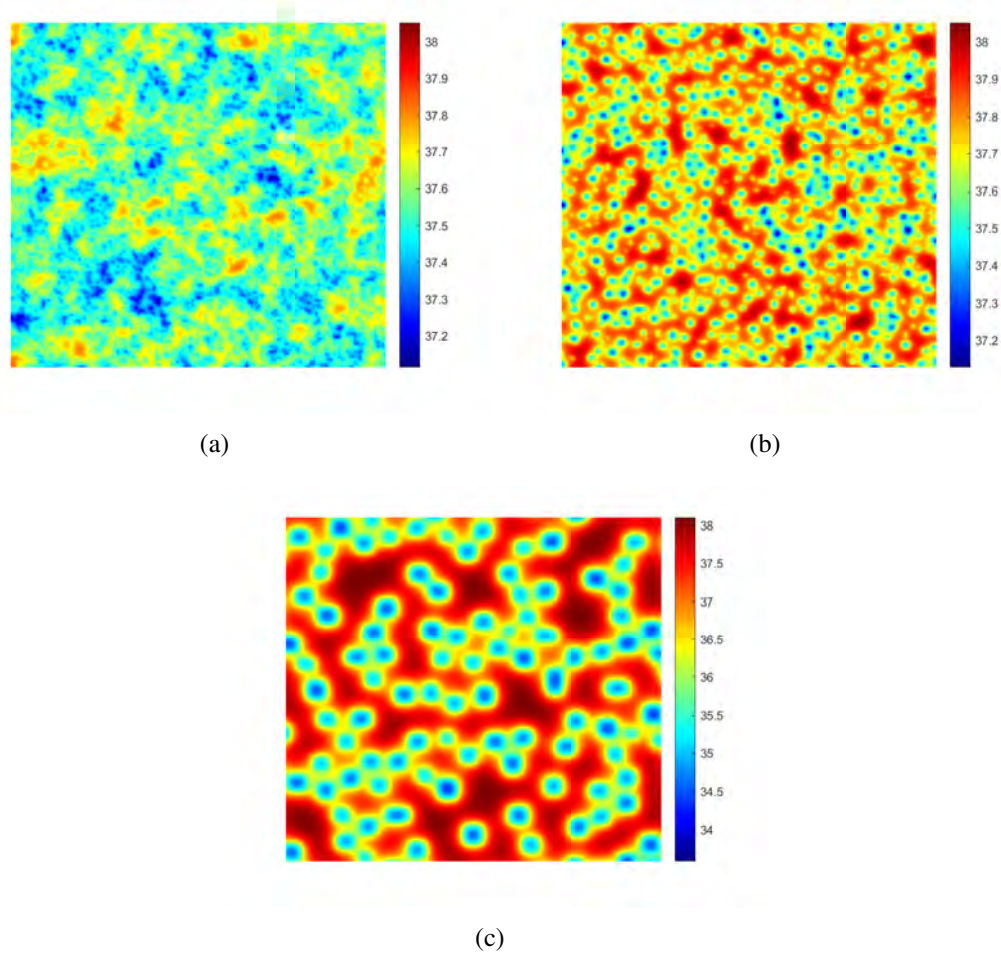

Fig. 6.11: Snapshots of contour pictures of predator species for different values of d_{11} i.e. at (a) $d_{11} = 0.0001$; (b) $d_{11} = 0.001$; and (c) $d_{11} = 0.01$. Here, $c = 0.601$, $\alpha_A = 23$, $d_{22} = 1$ and all the other parameters are same as described in the Table 6.1.

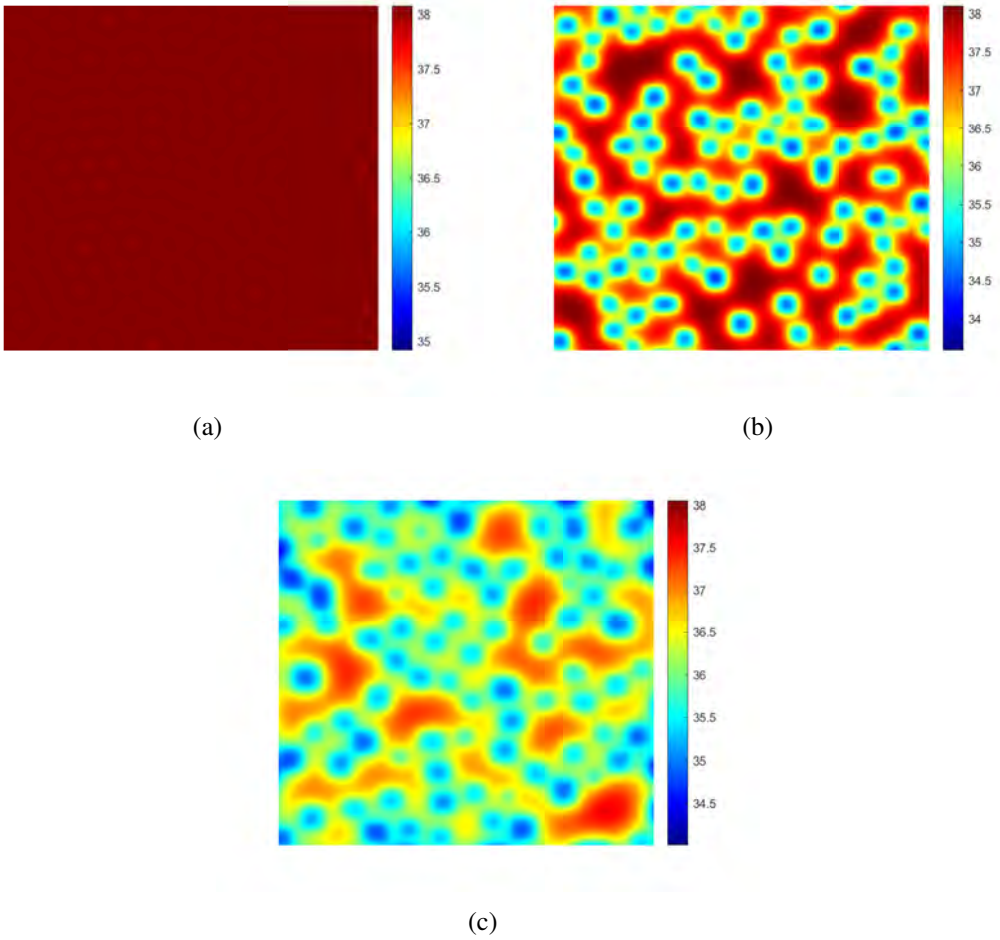

(a) (b)

(c)

Fig. 6.12: Snapshots of contour pictures of predator species for different values of d_{22} i.e. at (a) $d_{22} = 0.6$; (b) $d_{22} = 1$; and (c) $d_{22} = 3$. Here, $c = 0.601$, $\alpha_A = 23$, $d_{11} = 0.01$ and all the other parameters are same as described in the Table 6.1.

6.5.3.2 Stationary and dynamic pattern formation in the presence of both self and cross diffusion

Now, we explore the evolution of patterns in the presence of both self and cross-diffusion. In Fig. 6.13, we simulate the system (6.2) with the random initial conditions (6.15) and study the impact of cross-diffusion coefficient d_{21} on the Turing patterns. For $d_{21} = 0$, as depicted in Fig. 6.13(a), the pattern is composed of cold-spots scattered in high-density environment. As the value of the predator's cross-diffusion coefficient d_{21} increases, the predator density in the majority of the region decreases as illustrated in Fig. 6.13(b). The cold-spots pattern switches to hot-spots pattern with a significant increase in the value of d_{21} (Fig. 6.13(c)).

Till now, we obtained the distribution of population species using random initial conditions. Now, we explore the intriguing pattern formation and spatial dynamics by choosing specific

initial conditions 6.16 [76]. Fig. 6.14 depicts the spatiotemporal bifurcation diagram for the parameter values $f = 1.5$, $d_{11} = 0.01$, $d_{22} = 1$ and $d_{12} = 0.01$ in the $f - d_{21}$ parameter plane. Here, red colour depicts Turing region (TR), blue for Turing-Hopf region (THR), green for stable region (SR) and yellow for non-Turing region (NTR). This figure illustrates that increasing the value of fear parameter f may decrease the critical value for the predator's cross-diffusion coefficient.

Further, Fig. 6.15 demonstrates a graphical plot for $D(\kappa^2)$ vs. κ^2, which helps us better grasp the idea of the Turing instability regime and wave numbers. This figure presents different curves for various fear parameters f values which causes Turing instability i.e. $H(\kappa^2) < 0$. It is noticeable that for a fixed value of predator's cross-diffusion coefficient, fear parameter f less than a critical value fails to touch the κ^2 axis. This figure clearly shows that the range of wave numbers responsible for causing Turing instability increases with increasing fear parameter f.

Next, we analyze the dynamic pattern formation in different regimes. Fig. 6.16 presents the evolution of predators' spatial distribution in the Turing region. Turing instability drives the system towards a more organized state characterized by distinct Turing patterns. This figure reveals that predators exhibit various spatial distributions and keep changing for different time levels at $t = 100$, $t = 900$, and $t = 1400$. Similarly, Fig. 6.17 illustrates the time-varying spatial density of the predator population in the Turing-Hopf region. Turing-Hopf region characterizes the simultaneous occurrence of Hopf in temporal and instability resulting from the diffusion. From here, we can observe how time changes the spatial distribution of the predator species across the habitat, ultimately converging to organized hot-spot patterns.

Additionally, Fig. 6.18 depicts the predator's evolution across the habitat over time in non-Turing regions. Here, it is essential to emphasize that the patterns emerging in the non-Turing area don't adhere to the Turing instability conditions. This figure reveals that the predator species is initially aggregated at the center of the habitat, forming a dense red patch. Over time, the density of the predator species at the center decreases, creating a blue square area in the middle surrounded by moderate-density predators. The concentric circles with different predator densities are formed for a sufficiently higher time value.

6.6 Discussion and concluding remarks

This study analyzed a Leslie-Gower prey-predator model with additional food in the presence of fear and its carry-over effects, with and without diffusion. Detailed analysis has been performed for the proposed ODE model (6.1) to probe the intricate dynamics between the species. We established the well-posedness of the system (6.1) and outlined the prerequisites under which the system (6.1) has none, unique or two coexistence equilibrium points (Fig. 6.1). The local

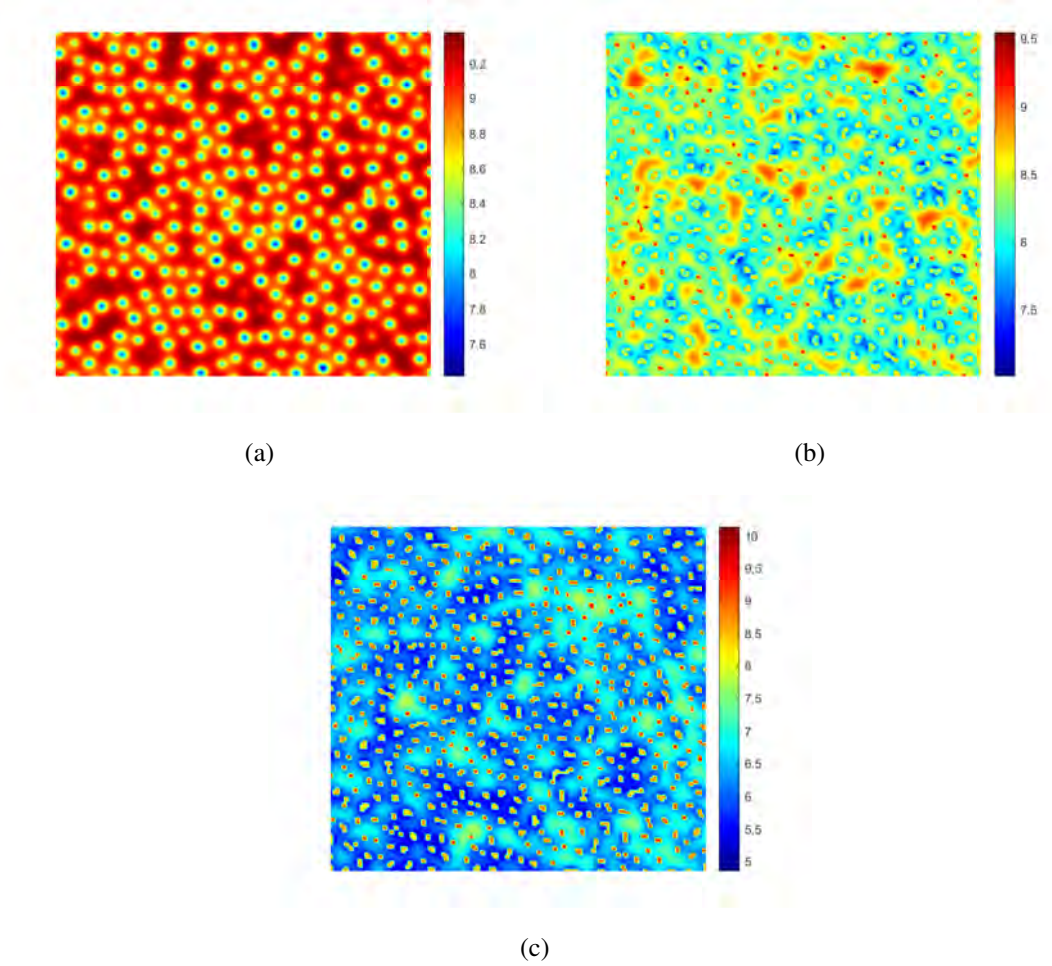

(a) (b)

(c)

Fig. 6.13: Snapshots of contour pictures of predator species for different values of d_{21} i.e. at (a) $d_{21} = 0$; (b) $d_{21} = 0.025$; and (c) $d_{21} = 0.05$. Here, $c = 0.1$, $d_{11} = 0.01$, $d_{22} = 1$, $d_{12} = 0.1$ and all the remaining parameters are consistent as outlined in the Table 6.1.

and global stability behavior of various coexistence equilibria are explored (Figs. 6.2 and (6.4)). The bistability attribute is presented between the coexistence equilibrium and the prey-free equilibrium via graphical representation (Fig. 6.3). Further, we studied the intriguing dynamics of the system by varying crucial parameters via bifurcation analysis. We investigated that the system experiences various co-dimension one bifurcations such as transcritical, saddle-node and Hopf-bifurcation along with the co-dimension two bifurcations such as Bogdanov-Takens and Cusp bifurcation. We noticed that when the density of the additional food is low, the species co-exist in a stable state in ecosystem. However, further increasing the additional food density may destabilize the coexistence of the species disrupting the balance in the ecosystem. Beyond a certain threshold value of the additional food parameter, species cease to co-exist (Fig. 6.5). It has been observed that lower level of fear in prey population maintains a stable coexistence of

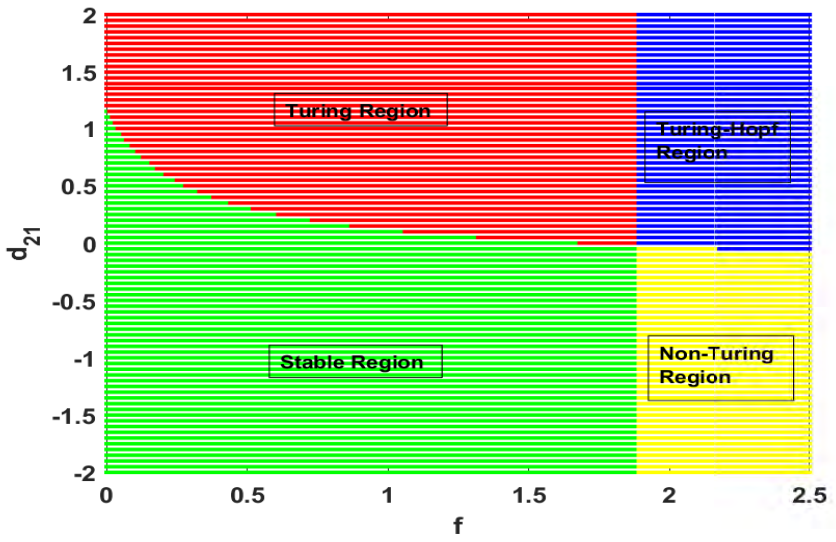

Fig. 6.14: Bifurcation region plot for system (6.2) in f-d_{21} parameteric plane. Here, $f = 1.5$, $d_{11} = 0.01$, $d_{22} = 1$ and $d_{12} = 0.01$. All the other parameters are considered from the Table 6.1.

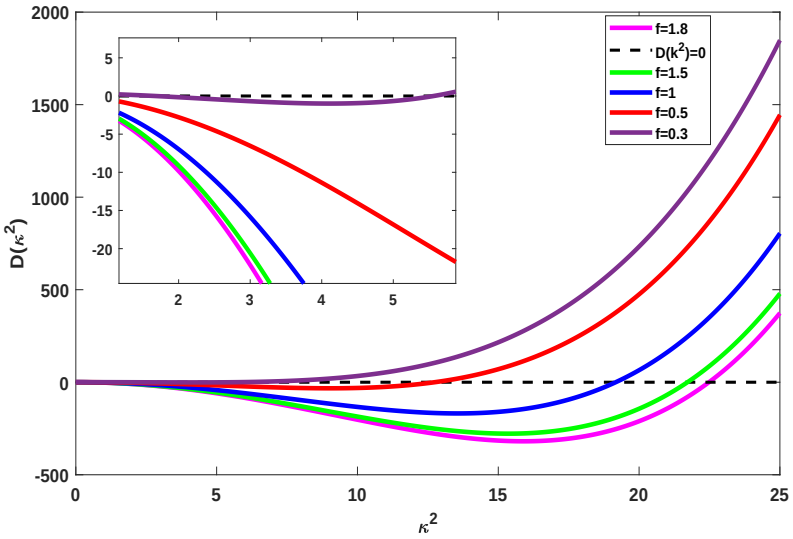

Fig. 6.15: $D(\kappa^2)$ vs. κ^2 plot for different values of fear parameter f. Here, $d_{21} = 0.5$ and all the other parameters are same as pre-defined in Fig. 6.14.

both the species in the ecosystem (Fig. 6.6). Our analysis demonstrates a bubbling phenomenon with respect to the carry-over effect parameter i.e. the system undergoes Hopf-bifurcation twice (Fig. 6.8). The occurrence of these bifurcations is crucial as they help predict how changes in parameters or environmental conditions might impact the stability and behavior of ecological populations. It may be pointed out here that the proposed model in this manuscript

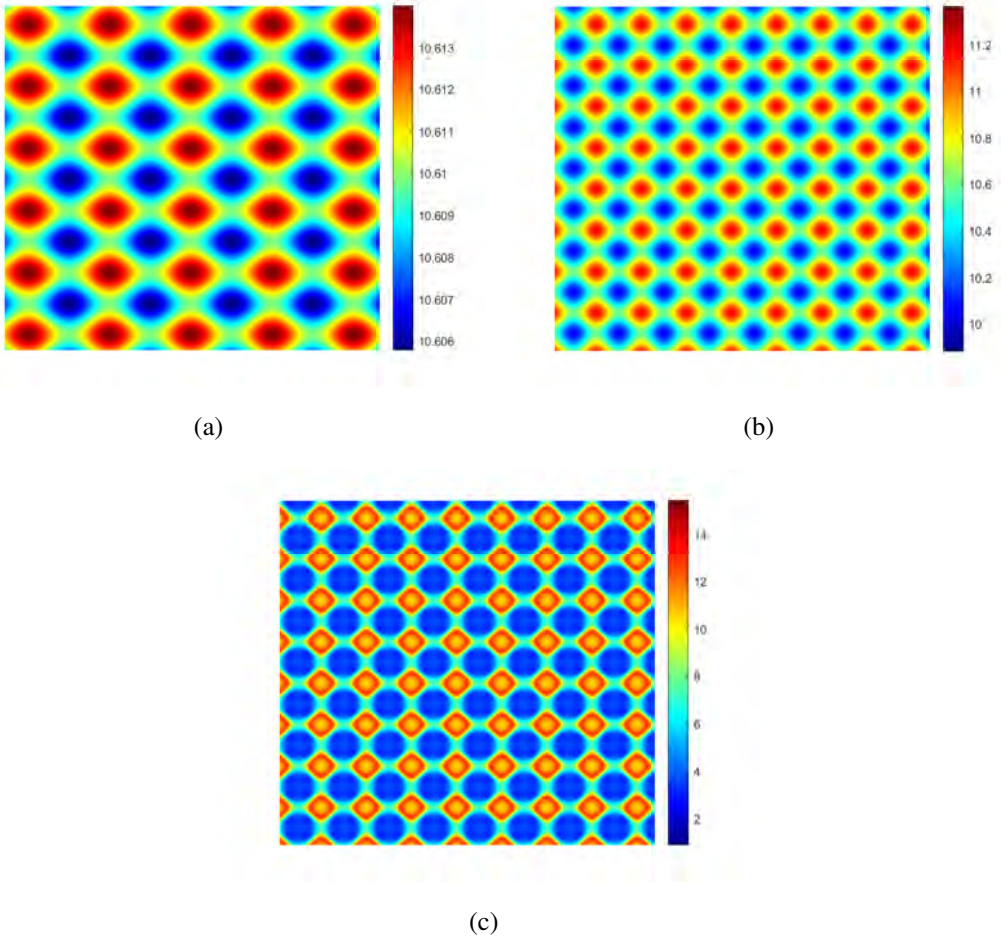

(a) (b)

(c)

Fig. 6.16: Evolution of predator species in Turing region at different time values (a) $t = 100$, (b) $t = 900$ and (c) $t = 1400$. The parameters are taken from the Turing region as described in Fig. 6.14. Here, $f = 1.5$ and $d_{21} = 0.2$.

is a two-dimensional autonomous model, and hence chaos will not appear. In the future, this model could be extended to a three-dimensional framework, enabling the exploration of the route to chaos and offering a more profound understanding of the intricate interactions and bi-parametric dynamics within the system [82].

Further, we extend the temporal model to incorporate the diffusion terms due to the random movement among the species in a pre-defined habitat. For the spatiotemporal model, we outlined the sufficient criteria for the existence of non-negative solution and then, calculated the priori-bounds of the solutions. Our primary focus is to analyze the Turing patterns induced due to diffusion-driven instability by varying different self and cross-diffusion coefficients. For this, we derived the conditions for Turing space in the presence of self and cross diffusion.

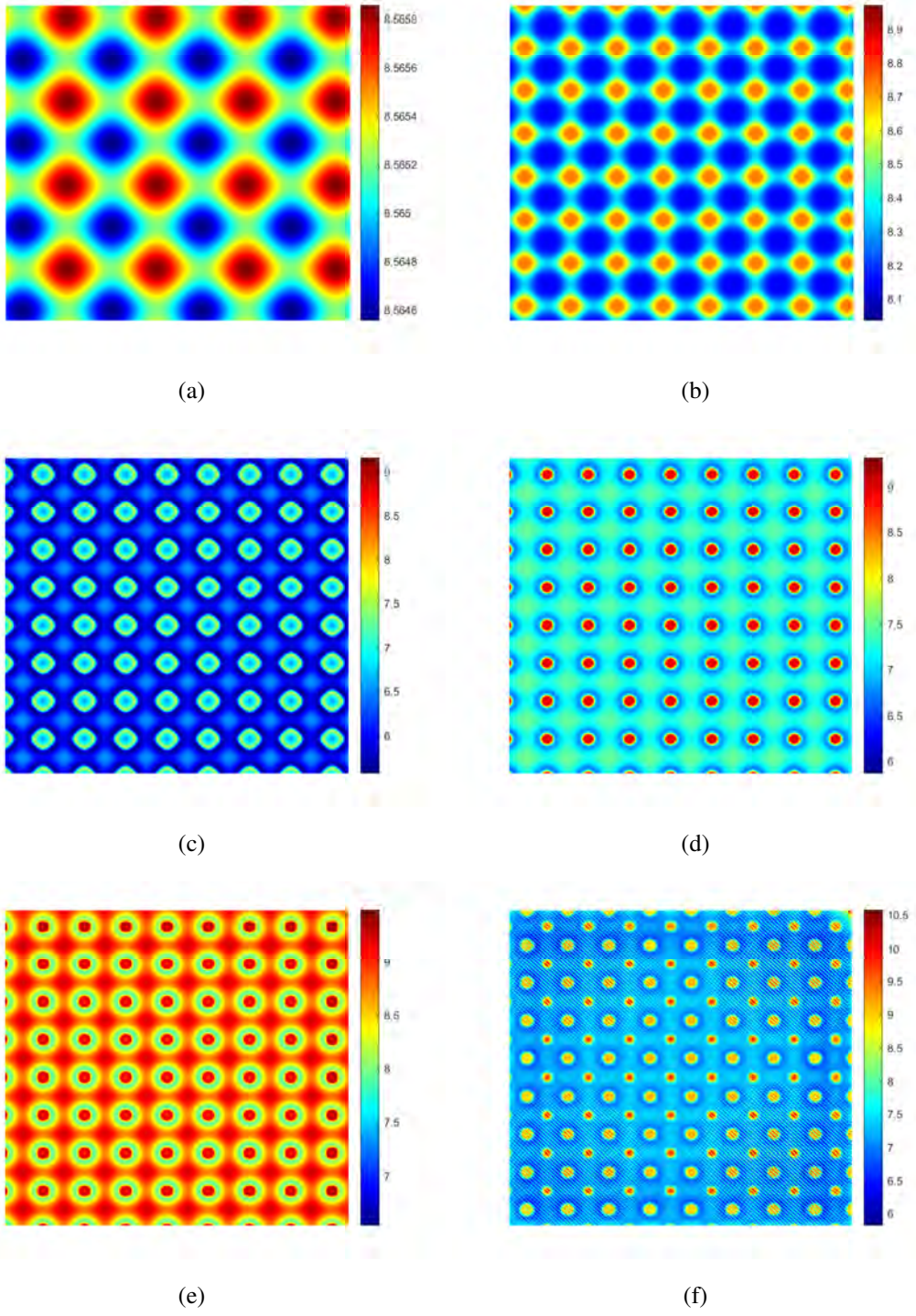

Fig. 6.17: Evolution of predator species in Turing-Hopf region at different time values (a) $t = 100$, (b) $t = 2000$,(c) $t = 2500$, (d) $t = 3500$, (e) $t = 4500$ and (f) $t = 5500$. The parameters are taken from the Turing-Hopf region as described in Fig. 6.14. Here, $f = 2$ and $d_{21} = 0.05$.

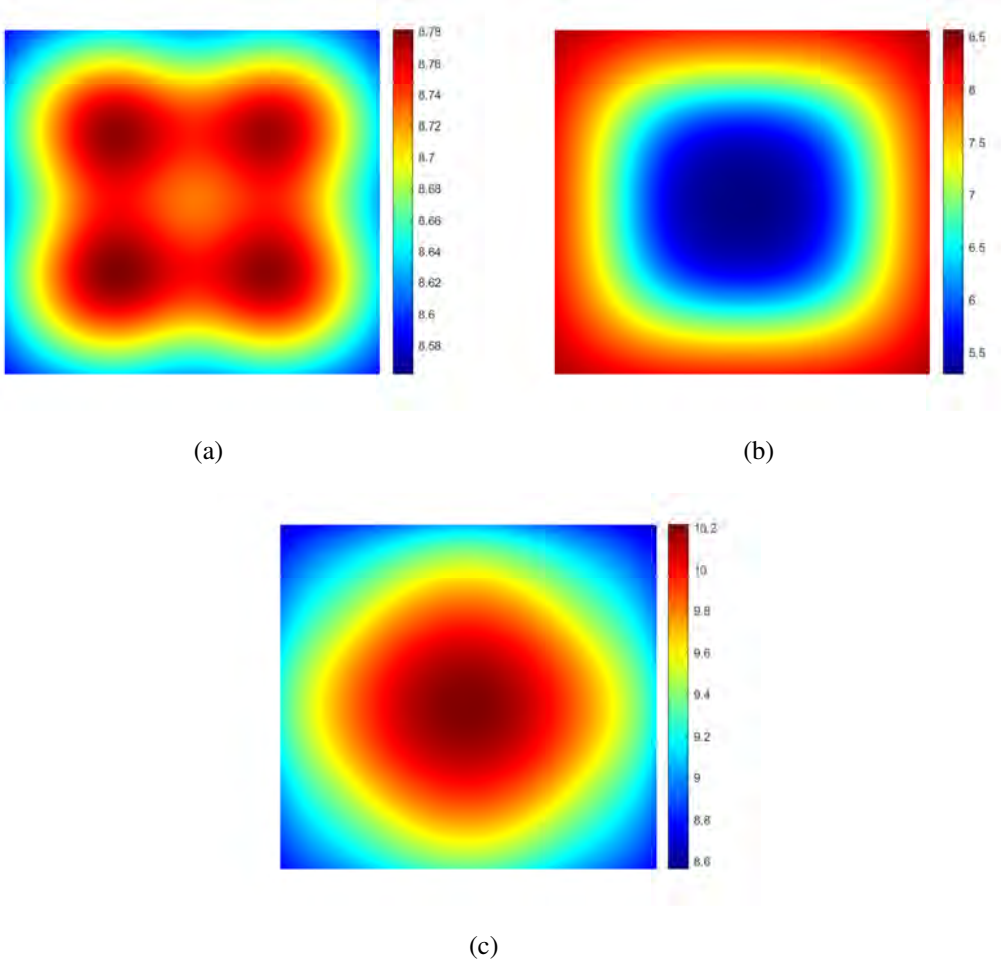

(a) (b)

(c)

Fig. 6.18: Evolution of predator species in Non-Turing region at different time values (a) $t = 50000$, (b) $t = 100000$, and (c) $t = 150000$. The parameters are taken from the Non-Turing region as described in Fig. 6.14. Here, $f = 2$ and $d_{21} = -1$.

Moreover, we used two types of initial conditions to analyze the Turing pattern formation. Using the first initial condition (6.15), we investigated the Turing patterns induced in the absence of cross-diffusion. Here, we noticed emergence of patchy and connected cold spots patterns (Figs. 6.11, (6.12)). Next, we investigated the impact of cross-diffusion coefficients on pattern formation using random initial conditions (6.15). The findings here illustrated the conversion of cold-spots pattern to hot-spots patterns in the Turing domain (Fig. 6.13). Hence, our analysis explored that using the first initial condition, we obtained stationary patterns in Turing space. Furthermore, we divided the $f - d_{21}$ parameteric plane into four regions: Turing region, Turing-Hopf region, stable region and non-Turing region (Fig. 6.14). Then, we investigated the dynamic pattern formation in the three different regions using specific initial conditions (6.16). Studying dynamic patterns reveals the sensitivity of the spatial patterns with respect to

time. The formation of these spatial patterns help elucidate the distribution of species across the habitat.

Motivated by the work done on additional food [1, 109, 48], we proposed the current model to analyze a prey-predator model with fear and its carry-over effects. By considering the random and directed movement among the species, we incorporated self and cross diffusion terms in the proposed model. The findings in the present study demonstrated that when there is no fear among the prey populations, both species co-exist in a stable state and incorporating fear induced periodic oscillations which is in agreement with the results obtained by *Gupta et al.* [48]. We found in our study that the density of the prey and predator populations at the co-existence equilibrium increases as the value of the carry-over effect parameter grows which is consistent with the findings illustrated by Sasmal and Takeuchi [145]. Song *et al.* [154] investigated the pattern formation induced by cross-diffusion driven instability and concluded that self-diffusion alone is not enough to induce Turing instability which is in contrast to the findings of the present study. We illustrated the Turing patterns induced due to self-diffusion driven instability.

In essence, understanding the intriguing dynamics and spatial patterns obtained in this study is helpful for comprehending the complexities of the interacting species, managing natural resources sustainably, and predicting and mitigating the impacts of environmental changes on the ecosystem functioning.

Conclusions and future directions

Conclusions

The interaction between species in the presence of one another is a crucial aspect of ecosystem dynamics. Mathematical modeling serves as a tool to represent real-world scenarios, simplifying and approximating the complexity of ecosystems for analysis and prediction. Through these mathematical models, ecologists can gain insights into the interactions among different species and the influence of environmental factors on them.

This thesis endeavors to investigate prey-predator interactions, modeled as a reaction diffusion system, while incorporating various ecological factors. The study utilizes ordinary, delay, and partial differential equations to analyze the dynamics of the ecosystem comprehensively. Therefore, we analyzed each proposed model theoretically and numerically, focusing on critical parameters. We investigated the well-posedness of the model by demonstrating the positivity and boundedness of its solutions. Subsequently, we explored the existence of different feasible equilibrium points and then assessed their local and global stability behavior. Following this, we analyzed possible local and global bifurcations with respect to the significant parameters occurring in the system. For the spatiotemporal model, conditions for Turing instability have been obtained. Turing patterns are analyzed to understand the spatial distribution of the species in the two-dimensional spatial domain. These Turing patterns suggest that the dynamics of prey-predator interactions can lead to a spatially heterogeneous species distribution, with localized areas of low and high densities. Extensive numerical simulations have been conducted for each proposed model to validate the analytical findings. These simulations illustrate the system's dynamics by generating multiple time-series plots, phase portraits, bifurcation diagrams, and Turing patterns.

In Chapter 2, we proposed a prey-predator model incorporating hunting cooperation among predators and fear-induced birth reduction in prey. We presume that predators consume prey through Type-I functional response. We provided some sufficient conditions for the system to be persistent. Further, we derived the conditions for the persistence and existence of the various equilibria. The system shows a variety of complex dynamics, including one-parameter bifurcations such as saddle-node and Hopf bifurcation. We observed that increasing the hunting cooperation parameter may destabilize the system. Moreover, we noticed that for a fixed value of the hunting cooperation parameter, increasing the value of the fear parameter can make the system stable. The system also exhibits the bi-stability attribute between various equilibria.

Various Turing patterns, such as spots, holes, and stripes, are obtained for different diffusive rates.

Chapter 3 investigated a delayed spatial prey-predator model based on a modified Leslie-Gower scheme incorporating fear induced by predator population and non-constant prey refuge. We observed that the low value of the half-saturation constant annihilates the coexistence of both species. Moreover, we noted that the system demonstrates bistability behavior between prey-free and coexistence equilibrium states. The system experiences double Hopf-bifurcation with respect to the fear parameter. The impact of the refuge parameter on the system's dynamics is also explored, revealing that preserving prey individuals below a certain threshold benefits both species. However, prolonged preservation beyond this threshold negatively affects predators. We observed that introducing fear response delay induces periodic oscillations in the system via Hopf-bifurcation for the non-spatial delayed model. Various Turing patterns, such as cold-spots, hot-spots, stripes, and a combination of holes and stripes are obtained for the spatiotemporal model, which can better explain the spatial distribution of species over time.

Chapter 4 is dedicated to a delayed prey-predator system where the past activities of prey species can alter the present carrying capacity and, hence, the system's dynamics. We incorporated two discrete delays, one to assess a delayed carrying capacity as a function of prey density and the other to account for a gestation delay. Holling type II functional response handles the corresponding interactions. The system exhibits a bi-stability attribute between two coexistence equilibria. Moreover, the system demonstrates stability switching by producing periodic oscillations via supercritical Hopf-bifurcation. Notably, the delayed system exhibits high sensitivity to initial conditions, indicating its transition into a chaotic regime. Turing instability conditions for the spatiotemporal system are derived, revealing a range of Turing patterns illustrating significant shifts in species densities with variations in crucial parameters.

In Chapter 5, we considered a prey-predator model involving weak Allee effects in the prey with a specialized cannibalistic predator in the presence of self and cross-diffusion. For the temporal model, we established the existence of various coexistence equilibria determined by varying the Allee and cannibalism parameters. The stability analysis showed that the extinction equilibrium is a non-hyperbolic saddle-node with a parabolic sector and two hyperbolic sectors. Thorough theoretical analysis and numerical simulations have been conducted to illustrate the occurrence of local bifurcations, including saddle-node, Hopf, Generalized Hopf (Bautin), and Bogdanov-Takens. For the spatiotemporal model, we derived the sufficient conditions for the existence of a non-negative solution, followed by the calculations of the prior bounds of the solution. Furthermore, we demonstrated that self-diffusion fails to induce Turing instability under specific conditions. The effect of variation of diffusion coefficients is also well explained through the two-dimensional spatial patterns that can assist in examining spatial heterogeneity,

spatial complexity, and sensitivity to initial conditions.

In Chapter 6, a Leslie-Gower prey-predator model with additional food in the presence of fear and its carry-over effects, with and without diffusion, has been proposed and analyzed. Including these ecological factors contributes to the system's complexity, resulting in intricate dynamics. For the temporal system, the bistability attribute is presented between the coexistence and prey-free equilibrium. We investigated that the system experiences various co-dimension one bifurcation such as transcritical, saddle-node, and Hopf-bifurcation, along with the co-dimension two bifurcations such as Bogdanov-Takens and Cusp bifurcation. We analyzed that at low densities of additional food, the species coexist in a stable state within the ecosystem. However, species cease to coexist beyond a particular threshold value of the additional food parameter. Moreover, we observed that a lower level of fear in the prey population maintains a stable coexistence of both species in the ecosystem. The system undergoes Hopf bifurcation twice, resulting in bubbling phenomena with respect to the carry-over effect parameter. For the spatiotemporal model, we outlined sufficient criteria for the existence of non-negative solutions and then calculated the priori-bounds of the solutions. We illustrated the formation of various Turing and non-Turing patterns induced by diffusion coefficients. Dynamic patterns are explored that reveal sensitivity of the spatial patterns with respect to time.

Future directions

In this thesis, we worked on various spatial ecological models that depict interactions between prey and predators, considering the incorporation of multiple environmental factors. The following are possible future goals that can be further explored for our work.

- In this thesis, we analyzed ecological models involving two species. However, exploring models with three or more species would add further complexity, which could yield more interesting insights.

- In this thesis, we worked on autonomous models. In the future, we would like to extend our work to nonautonomous phenomena that often occur due to seasonal variations in biological parameters.

- With technological advancements and the ease of data collection and sharing, it would be beneficial to work with real-world data-driven models to predict the spread of invasive species and monitor alterations in species distribution.

Bibliography

[1] M. T. Alves, *Des Interactions Indirectes Entre les Proies: Modélisation et Influence du Comportement du Prédateur Commun*. Ph.D. Thesis, Université Nice Sophia Antipolis, 2013.

[2] M. T. Alves and F. M. Hilker, "Hunting cooperation and Allee effects in predators," *Journal of Theoretical Biology*, vol. 419, pp. 13–22, 2017.

[3] Anshu and B. Dubey, "Spatiotemporal dynamics of a multi-delayed prey–predator system with variable carrying capacity," *Chaos: An Interdisciplinary Journal of Nonlinear Science*, vol. 33, no. 11, p. 113 116, 2023.

[4] Anshu, B. Dubey, S. Kumar Sasmal, and A. Sudarshan, "Consequences of fear effect and prey refuge on the Turing patterns in a delayed predator–prey system," *Chaos: An Interdisciplinary Journal of Nonlinear Science*, vol. 32, no. 12, p. 123 132, 2022.

[5] M. Aziz-Alaoui and M. D. Okiye, "Boundedness and global stability for a predator-prey model with modified Leslie-Gower and Holling-type II schemes," *Applied Mathematics Letters*, vol. 16, no. 7, pp. 1069–1075, 2003.

[6] I. Bailey, J. P. Myatt, and A. M. Wilson, "Group hunting within the carnivora: Physiological, cognitive and environmental influences on strategy and cooperation," *Behavioral ecology and sociobiology*, vol. 67, pp. 1–17, 2013.

[7] C. Baishya, "Dynamics of fractional Holling type-II predator-prey model with prey refuge and additional food to predator," *Journal of Applied Nonlinear Dynamics*, vol. 10, no. 02, pp. 315–328, 2021.

[8] B. Barman and B. Ghosh, "Explicit impacts of harvesting in delayed predator-prey models," *Chaos, Solitons & Fractals*, vol. 122, pp. 213–228, 2019.

[9] L. Berec, "Impacts of foraging facilitation among predators on predator-prey dynamics," *Bulletin of Mathematical Biology*, vol. 72, no. 1, pp. 94–121, 2010.

[10] A. A. Berryman, "The orgins and evolution of predator-prey theory," *Ecology*, vol. 73, no. 5, pp. 1530–1535, 1992.

[11] M. Bhargava, S. Sajan, and B. Dubey, "Trade-off and chaotic dynamics of prey–predator system with two discrete delays," *Chaos: An Interdisciplinary Journal of Nonlinear Science*, vol. 33, no. 5, p. 053 120, 2023.

[12] J. Bhattacharyya and S. Pal, "Algae-herbivore interactions with Allee effect and chemical defense," *Ecological Complexity*, vol. 27, pp. 48–62, 2016.

[13] B. Bhunia, L. T. Bhutia, T. K. Kar, and P. Debnath, "Explicit impacts of harvesting on a fractional-order delayed predator–prey model," *The European Physical Journal Special Topics*, vol. 232, 2629–2644, 2023.

[14] B. Bhunia, S. Ghorai, T. K. Kar, S. Biswas, L. T. Bhutia, and P. Debnath, "A study of a spatiotemporal delayed predator–prey model with prey harvesting: Constant and periodic diffusion," *Chaos, Solitons & Fractals*, vol. 175, p. 113 967, 2023.

[15] T. Bilde and S. Toft, "Quantifying food limitation of arthropod predators in the field," *Oecologia*, vol. 115, pp. 54–58, 1998.

[16] S. Biswas, B. Ahmad, and S. Khajanchi, "Exploring dynamical complexity of a cannibalistic eco-epidemiological model with multiple time delay," *Mathematical methods in the Applied Sciences*, vol. 46, no. 4, pp. 4184–4211, 2023.

[17] C. Boesch, "Cooperative hunting in wild chimpanzees," *Animal Behaviour*, vol. 48, no. 3, pp. 653–667, 1994.

[18] D. S. Boukal and L. Berec, "Single-species models of the Allee effect: Extinction boundaries, sex ratios and mate encounters," *Journal of Theoretical Biology*, vol. 218, no. 3, pp. 375–394, 2002.

[19] S. F. Brosnan and R. Bshary, *Cooperation and deception: From evolution to mechanisms*, 2010.

[20] Y. Cai, Z. Gui, X. Zhang, H. Shi, and W. Wang, "Bifurcations and pattern formation in a predator–prey model," *International Journal of Bifurcation and Chaos*, vol. 28, no. 11, p. 1 850 140, 2018.

[21] B. Chakraborty, H. Baek, and N. Bairagi, "Diffusion-induced regular and chaotic patterns in a ratio-dependent predator–prey model with fear factor and prey refuge," *Chaos: An Interdisciplinary Journal of Nonlinear Science*, vol. 31, no. 3, p. 033 128, 2021.

[22] S. Chakraborty and J Chattopadhyay, "Effect of cannibalism on a predator–prey system with nutritional value: A model based study," *Dynamic Systems, Measurement, and Control*, vol. 26, no. 1, pp. 13–22, 2011.

[23] S. Chakraborty, P. Tiwari, S. Sasmal, S. Biswas, S. Bhattacharya, and J. Chattopadhyay, "Interactive effects of prey refuge and additional food for predator in a diffusive predator-prey system," *Applied Mathematical Modelling*, vol. 47, pp. 128–140, 2017.

[24] F. Chen, L. Chen, and X. Xie, "On a Leslie–Gower predator–prey model incorporating a prey refuge," *Nonlinear Analysis. Real World Applications*, vol. 10, no. 5, pp. 2905–2908, 2009.

[25] J. Chen, J. Huang, S. Ruan, and J. Wang, "Bifurcations of invariant tori in predator-prey models with seasonal prey harvesting," *SIAM Journal on Applied Mathematics*, vol. 73, no. 5, pp. 1876–1905, 2013.

[26] L. Chen, F. Chen, and L. Chen, "Qualitative analysis of a predator–prey model with Holling type II functional response incorporating a constant prey refuge," *Nonlinear Analysis: Real World Applications*, vol. 11, no. 1, pp. 246–252, 2010.

[27] D. Claessen, A. M. De Roos, and L. Persson, "Population dynamic theory of size–dependent cannibalism," *Proceedings of the Royal Society B: Biological Sciences*, vol. 271, no. 1537, pp. 333–340, 2004.

[28] J. B. Collings, "Bifurcation and stability analysis of a temperature-dependent mite predator-prey interaction model incorporating a prey refuge," *Bulletin of Mathematical Biology*, vol. 57, pp. 63–76, 1995.

[29] C. Cosner, D. L. DeAngelis, J. S. Ault, and D. B. Olson, "Effects of spatial grouping on the functional response of predators," *Theoretical Population Biology*, vol. 56, no. 1, pp. 65–75, 1999.

[30] F Courchamp, B. Grenfell, and T. Clutton-Brock, "Impact of natural enemies on obligately cooperative breeders," *Oikos*, vol. 91, no. 2, pp. 311–322, 2000.

[31] F. Courchamp, L. Berec, and J. Gascoigne, *Allee Effects in Ecology and Conservation*. OUP Oxford, 2008.

[32] S. Creel and D. Christianson, "Relationships between direct predation and risk effects," *Trends in ecology & evolution*, vol. 23, no. 4, pp. 194–201, 2008.

[33] S. Creel and N. M. Creel, "Communal hunting and pack size in african wild dogs, lycaon pictus," *Animal Behaviour*, vol. 50, no. 5, pp. 1325–1339, 1995.

[34] W. Cresswell, "Predation in bird populations," *Journal of Ornithology*, vol. 152, pp. 251–263, 2011.

[35] B. Dai and G. Sun, "Turing–Hopf bifurcation of a delayed diffusive predator–prey system with chemotaxis and fear effect," *Applied Mathematics Letters*, vol. 111, p. 106 644, 2021.

[36] S. Dash and S. Khajanchi, "Dynamics of intraguild predation with intraspecies competition," *Journal of Applied Mathematics and Computing*, vol. 69, no. 6, pp. 4877–4906, 2023.

[37] J. Dawes and M. Souza, "A derivation of Holling's type I, II and III functional responses in predator–prey systems," *Journal of Theoretical Biology*, vol. 327, pp. 11–22, 2013.

[38] S. Djilali and C. Cattani, "Patterns of a superdiffusive consumer-resource model with hunting cooperation functional response," *Chaos, Solitons & Fractals*, vol. 151, p. 111 258, 2021.

[39] B. Dubey, B. Das, and J. Hussain, "A predator–prey interaction model with self and cross-diffusion," *Ecological Modelling*, vol. 141, no. 1-3, pp. 67–76, 2001.

[40] B. Dubey and A. Kumar, "Dynamics of prey–predator model with stage structure in prey including maturation and gestation delays," *Nonlinear Dynamics*, vol. 96, pp. 2653–2679, 2019.

[41] B. Dubey, N. Kumari, and R. K. Upadhyay, "Spatiotemporal pattern formation in a diffusive predator-prey system: An analytical approach," *Journal of Computational and Applied Mathematics*, vol. 31, no. 1, pp. 413–432, 2009.

[42] B. Dubey, Sajan, and A. Kumar, "Stability switching and chaos in a multiple delayed prey–predator model with fear effect and anti-predator behavior," *Mathematics and Computers in Simulation*, vol. 188, pp. 164–192, 2021.

[43] J.-B. Ferdy, F. Austerlitz, J. Moret, P.-H. Gouyon, and B. Godelle, "Pollinator-induced density dependence in deceptive species," *Oikos*, vol. 87, no. 3, pp. 549–560, 1999.

[44] C. Ganguli, T. Kar, and P. Mondal, "Optimal harvesting of a prey–predator model with variable carrying capacity," *International Journal of Biomathematics*, vol. 10, no. 05, p. 1 750 069, 2017.

[45] S. Ghorai and S. Poria, "Turing patterns induced by cross-diffusion in a predator-prey system in presence of habitat complexity," *Chaos, Solitons & Fractals*, vol. 91, pp. 421–429, 2016.

[46] K. Gopalsamy, *Stability and Oscillations in Delay Differential Equations of Population Dynamics*. Springer Science & Business Media, 1992.

[47] W. Govaerts, "Numerical bifurcation analysis for ODEs," *Journal of Computational and Applied Mathematics*, vol. 125, no. 1-2, pp. 57–68, 2000.

[48] A. Gupta, A. Kumar, and B. Dubey, "Complex dynamics of Leslie–Gower prey–predator model with fear, refuge and additional food under multiple delays," *International Journal of Biomathematics*, vol. 15, no. 08, p. 2 250 060, 2022.

[49] R. Han and B. Dai, "Spatiotemporal pattern formation and selection induced by nonlinear cross-diffusion in a toxic-phytoplankton–zooplankton model with Allee effect," *Nonlinear Analysis. Real World Applications*, vol. 45, pp. 822–853, 2019.

[50] R. Han, S. Dey, and M. Banerjee, "Spatiotemporal pattern selection in a prey–predator model with hunting cooperation and Allee effect in prey," *Chaos, Solitons & Fractals*, vol. 171, p. 113 441, 2023.

[51] R. Han, L. N. Guin, and B. Dai, "Cross-diffusion-driven pattern formation and selection in a modified Leslie–Gower predator–prey model with fear effect," *Journal of Biological Systems*, vol. 28, no. 01, pp. 27–64, 2020.

[52] R. Han, L. N. Guin, and B. Dai, "Consequences of refuge and diffusion in a spatiotemporal predator–prey model," *Nonlinear Analysis. Real World Applications*, vol. 60, p. 103 311, 2021.

[53] J. P. Harmon, *Indirect Interactions among a Generalist Predator and its Multiple Foods*. Ph.D. Thesis, University of Minnesota, 2003.

[54] D. P. Hector, "Cooperative hunting and its relationship to foraging success and prey size in an avian predator," *Journal of Ethology*, vol. 73, no. 3, pp. 247–257, 1986.

[55] C. S. Holling, "Some characteristics of simple types of predation and parasitism," *The Canadian Entomologist*, vol. 91, no. 7, pp. 385–398, 1959.

[56] C. S. Holling, "The components of predation as revealed by a study of small-mammal predation of the European Pine Sawfly," *The Canadian Entomologist*, vol. 91, no. 5, pp. 293–320, 1959.

[57] C. S. Holling, "The functional response of predators to prey density and its role in mimicry and population regulation," *The Memoirs of the Entomological Society of Canada*, vol. 97, no. S45, pp. 5–60, 1965.

[58] D. Hu and H. Cao, "Stability and bifurcation analysis in a predator–prey system with Michaelis–Menten type predator harvesting," *Nonlinear Analysis. Real World Applications*, vol. 33, pp. 58–82, 2017.

[59] J. Huang, S. Ruan, and J. Song, "Bifurcations in a predator–prey system of Leslie type with generalized Holling type III functional response," *Journal of Differential Equations*, vol. 257, no. 6, pp. 1721–1752, 2014.

[60] Y. Huang, F. Chen, and L. Zhong, "Stability analysis of a prey–predator model with Holling type III response function incorporating a prey refuge," *Applied Mathematics and Computation*, vol. 182, no. 1, pp. 672–683, 2006.

[61] L. Hurd *et al.*, "Cannibalism reverses male-biased sex ratio in adult mantids: Female strategy against food limitation?" *Oikos*, pp. 193–198, 1994.

[62] S. Jana, M. Chakraborty, K. Chakraborty, and T. K. Kar, "Global stability and bifurcation of time delayed prey–predator system incorporating prey refuge," *Mathematics and Computers in Simulation*, vol. 85, pp. 57–77, 2012.

[63] T. K. Kar, "Stability analysis of a prey–predator model incorporating a prey refuge," *Communications in Nonlinear Science and Numerical Simulation*, vol. 10, no. 6, pp. 681–691, 2005.

[64] T. K. Kar, "Modelling and analysis of a harvested prey–predator system incorporating a prey refuge," *Journal of Computational and Applied Mathematics*, vol. 185, no. 1, pp. 19–33, 2006.

[65] T. K. Kar and A. Ghorai, "Dynamic behaviour of a delayed predator–prey model with harvesting," *Applied Mathematics and Computation*, vol. 217, no. 22, pp. 9085–9104, 2011.

[66] T. Kar, A. Ghorai, and S. Jana, "Dynamic consequences of prey refugia in a two-predator–one-prey system," *Journal of Biological Systems*, vol. 21, no. 02, p. 1 350 013, 2013.

[67] E. H. Kerner, "A statistical mechanics of interacting biological species," *Bulletin of Mathematical Biophysics*, vol. 19, pp. 121–146, 1957.

[68] S. Khajanchi, "Dynamic behavior of a Beddington–DeAngelis type stage structured predator–prey model," *Applied Mathematics and Computation*, vol. 244, pp. 344–360, 2014.

[69] S. Khajanchi, "Modeling the dynamics of stage-structure predator-prey system with Monod–Haldane type response function," *Applied Mathematics and Computation*, vol. 302, pp. 122–143, 2017.

[70] C Kohlmeier and W Ebenhoh, "The stabilizing role of cannibalism in a predator-prey system," *Bulletin of Mathematical Biology*, vol. 57, no. 3, pp. 401–411, 1995.

[71] S. Kondo, "The reaction-diffusion system: A mechanism for autonomous pattern formation in the animal skin," *Genes Cells*, vol. 7, no. 6, pp. 535–541, 2002.

[72] S. Kondo and T. Miura, "Reaction-diffusion model as a framework for understanding biological pattern formation," *Science*, vol. 329, no. 5999, pp. 1616–1620, 2010.

[73] A. Korobeinikov, "A Lyapunov function for Leslie-Gower predator-prey models," *Applied Mathematics Letters*, vol. 14, no. 6, pp. 697–699, 2001.

[74] Y. Kuang, *Delay Differential Equations: with Applications in Population Dynamics*. Academic press, 1993.

[75] V. Kumar and N. Kumari, "Controlling chaos in three species food chain model with fear effect," *AIMS Math*, vol. 5, no. 2, p. 828, 2020.

[76] V. Kumar and N. Kumari, "Bifurcation study and pattern formation analysis of a tritrophic food chain model with group defense and Ivlev-like nonmonotonic functional response," *Chaos, Solitons & Fractals*, vol. 147, p. 110 964, 2021.

[77] N. Kumari, "Pattern formation in spatially extended tritrophic food chain model systems: Generalist versus specialist top predator," *International Scholarly Research Notices*, vol. 2013, p. 198 185, 2013.

[78] N. Kumari and V. Kumar, "Controlling chaos and pattern formation study in a tritrophic food chain model with cannibalistic intermediate predator," *The European Physical Journal Plus*, vol. 137, no. 3, pp. 1–23, 2022.

[79] S. Kumari, S. K. Tiwari, and R. K. Upadhyay, "Cross diffusion induced spatiotemporal pattern in diffusive nutrient–plankton model with nutrient recycling," *Mathematics and Computers in Simulation*, vol. 202, pp. 246–272, 2022.

[80] M. Kuussaari, I. Saccheri, M. Camara, and I. Hanski, "Allee effect and population dynamics in the glanville fritillary butterfly," *Oikos*, vol. 82, no. 2, pp. 384–392, 1998.

[81] Y. Lamontagne, C. Coutu, and C. Rousseau, "Bifurcation analysis of a predator–prey system with generalised Holling type III functional response," *Journal of Dynamics and Differential Equations*, vol. 20, no. 3, pp. 535–571, 2008.

[82] G. Layek, *An Introduction to Dynamical Systems and Chaos*. Springer Nature, Singapore, 2nd Edition, 2024.

[83] G. Layek and N. Pati, "Organized structures of two bidirectionally coupled logistic maps," *Chaos: An Interdisciplinary Journal of Nonlinear Science*, vol. 29, no. 9, p. 093 104, 2019.

[84] P. H. Leslie, "Some further notes on the use of matrices in population mathematics," *Biometrika*, vol. 35, no. 3/4, pp. 213–245, 1948.

[85] P. H. Leslie, "A stochastic model for studying the properties of certain biological systems by numerical methods," *Biometrika*, vol. 45, no. 1-2, pp. 16–31, 1958.

[86] P. Leslie and J. Gower, "The properties of a stochastic model for the predator-prey type of interaction between two species," *Biometrika*, vol. 47, no. 3/4, pp. 219–234, 1960.

[87] S. A. Levin and L. A. Segel, "Hypothesis for origin of planktonic patchiness," *Nature*, vol. 259, no. 5545, pp. 659–659, 1976.

[88] J. Li, X. Zhu, X. Lin, and J. Li, "Impact of cannibalism on dynamics of a structured predator–prey system," *Applied Mathematical Modelling*, vol. 78, pp. 1–19, 2020.

[89] S. L. Lima, "Nonlethal effects in the ecology of predator-prey interactions," *Bioscience*, vol. 48, no. 1, pp. 25–34, 1998.

[90] J. Liu, B. Liu, P. Lv, and T. Zhang, "An eco-epidemiological model with fear effect and hunting cooperation," *Chaos, Solitons & Fractals*, vol. 142, p. 110 494, 2021.

[91] A. J. Lotka, "Analytical note on certain rhythmic relations in organic systems," *Proceedings of the National Academy of Sciences*, vol. 6, no. 7, pp. 410–415, 1920.

[92] N. MacDonald and N MacDonald, *Biological Delay Systems: Linear Stability Theory*. Cambridge University Press, 2008.

[93] A. P. Maiti and B. Dubey, "Stability and bifurcation of a fishery model with Crowley–Martin functional response," *International Journal of Bifurcation and Chaos*, vol. 27, no. 11, p. 1 750 174, 2017.

[94] T. R. Malthus, "An essay on the principle of population (1798)," *The Works of Thomas Robert Malthus, London, Pickering & Chatto Publishers*, vol. 1, pp. 1–139, 1986.

[95] M. Manarul Haque and S. Sarwardi, "Dynamics of a harvested prey–predator model with prey refuge dependent on both species," *International Journal of Bifurcation and Chaos*, vol. 28, no. 12, p. 1 830 040, 2018.

[96] A. Mandal, P. K. Tiwari, S. Samanta, E. Venturino, and S. Pal, "A nonautonomous model for the effect of environmental toxins on plankton dynamics," *Nonlinear Dynamics*, vol. 99, pp. 3373–3405, 2020.

[97] K. Manna and M. Banerjee, "Stability of Hopf-bifurcating limit cycles in a diffusion-driven prey-predator system with Allee effect and time delay," *Mathematical Biosciences and Engineering*, vol. 16, no. 4, pp. 2411–2446, 2019.

[98] D. J. Marshall and S. G. Morgan, "Ecological and evolutionary consequences of linked life-history stages in the sea," *Current Biology*, vol. 21, no. 18, R718–R725, 2011.

[99] A. B. Medvinsky, S. V. Petrovskii, I. A. Tikhonova, H. Malchow, and B.-L. Li, "Spatiotemporal complexity of plankton and fish dynamics," *SIAM Journal on Applied Mathematics*, vol. 44, no. 3, pp. 311–370, 2002.

[100] S. Mishra and R. K. Upadhyay, "Spatial pattern formation and delay induced destabilization in predator–prey model with fear effect," *Mathematical Methods in the Applied Sciences*, vol. 45, no. 11, pp. 6801–6823, 2022.

[101] A. K. Misra and A. Gupta, "A reaction–diffusion model for the control of cholera epidemic," *Journal of Biological Systems*, vol. 24, no. 04, pp. 431–456, 2016.

[102] H. Molla, M. S. Rahman, and S. Sarwardi, "Dynamics of a predator–prey model with Holling type II functional response incorporating a prey refuge depending on both the species," *International Journal of Nonlinear Sciences and Numerical Simulation*, vol. 20, no. 1, pp. 89–104, 2019.

[103] J. D. Murray, *Mathematical Biology: I. An introduction*. Springer, 2002.

[104] J. D. Murray, *Mathematical Biology: II: Spatial Models and Biomedical Applications*. Springer, 2003, vol. 3.

[105] A. Nindjin, M. Aziz-Alaoui, and M Cadivel, "Analysis of a predator–prey model with modified Leslie–Gower and Holling-type II schemes with time delay," *Nonlinear Analysis. Real World Applications*, vol. 7, no. 5, pp. 1104–1118, 2006.

[106] K. Nitu and M. Nishith, "Positive solutions and pattern formation in a diffusive tritrophic system with Crowley–Martin functional response," *Nonlinear Dynamics*, vol. 100, no. 1, pp. 763–784, 2020.

[107] C. M. O'Connor, D. R. Norris, G. T. Crossin, and S. J. Cooke, "Biological carryover effects: Linking common concepts and mechanisms in ecology and evolution," *Ecosphere*, vol. 5, no. 3, pp. 1–11, 2014.

[108] A. Okubo, S. A. Levin, *et al.*, *Diffusion and Ecological Problems: Modern Perspectives*. Springer, 2001, vol. 14.

[109] M. Onana, B. Mewoli, and J. J. Tewa, "Hopf bifurcation analysis in a delayed Leslie–Gower predator–prey model incorporating additional food for predators, refuge and threshold harvesting of preys," *Nonlinear Dynamics*, vol. 100, pp. 3007–3028, 2020.

[110] C. Packer, D. Scheel, and A. E. Pusey, "Why lions form groups: Food is not enough," *American Naturalist*, vol. 136, no. 1, pp. 1–19, 1990.

[111] D. Pal, D. Kesh, and D. Mukherjee, "Qualitative study of cross-diffusion and pattern formation in Leslie–Gower predator–prey model with fear and Allee effects," *Chaos, Solitons & Fractals*, vol. 167, p. 113 033, 2023.

[112] S. Pal, N. Pal, S. Samanta, and J. Chattopadhyay, "Effect of hunting cooperation and fear in a predator-prey model," *Ecological Complexity*, vol. 39, p. 100 770, 2019.

[113] S. Pal, N. Pal, S. Samanta, and J. Chattopadhyay, "Fear effect in prey and hunting cooperation among predators in a Leslie-Gower model," *Mathematical Biosciences and Engineering*, vol. 16, no. 5, pp. 5146–5179, 2019.

[114] S. Pal, A. Gupta, A. Misra, and B. Dubey, "Complex dynamics of a predator–prey system with fear and memory in the presence of two discrete delays," *The European Physical Journal Plus*, vol. 138, no. 11, p. 984, 2023.

[115] S. Pal, A. Gupta, A. K. Misra, and B. Dubey, "Chaotic dynamics of a stage-structured prey–predator system with hunting cooperation and fear in presence of two discrete delays," *Journal of Biological Systems*, vol. 31, no. 02, pp. 611–642, 2023.

[116] S. Pal, P. K. Tiwari, A. K. Misra, and H. Wang, "Fear effect in a three-species food chain model with generalist predator," *Mathematical Biosciences and Engineering*, vol. 21, no. 1, pp. 1–33, 2024.

[117] P. Panday, N. Pal, S. Samanta, and J. Chattopadhyay, "A three species food chain model with fear induced trophic cascade," *International Journal of Applied and Computational Mathematics*, vol. 5, pp. 1–26, 2019.

[118] P. Panday, N. Pal, S. Samanta, P. Tryjanowski, and J. Chattopadhyay, "Dynamics of a stage-structured predator-prey model: Cost and benefit of fear-induced group defense," *Journal of Theoretical Biology*, vol. 528, p. 110 846, 2021.

[119] P. Panday, S. Samanta, N. Pal, and J. Chattopadhyay, "Delay induced multiple stability switch and chaos in a predator–prey model with fear effect," *Mathematics and Computers in Simulation*, vol. 172, pp. 134–158, 2020.

[120] C.-V. Pao, *Nonlinear Parabolic and Elliptic Equations*. Springer Science & Business Media, 2012.

[121] R. D. Parshad, N. Kumari, A. R. Kasimov, and H. A. Abderrahmane, "Turing patterns and long-time behavior in a three-species food-chain model," *Mathematical Biosciences*, vol. 254, pp. 83–102, 2014.

[122] N. Pati and B. Ghosh, "Delayed carrying capacity induced subcritical and supercritical Hopf bifurcations in a predator–prey system," *Mathematics and Computers in Simulation*, vol. 195, pp. 171–196, 2022.

[123] N. Pati, G. Layek, and N. Pal, "Bifurcations and organized structures in a predator-prey model with hunting cooperation," *Chaos, Solitons & Fractals*, vol. 140, p. 110 184, 2020.

[124] J. Pearce and D. Lindenmayer, "Bioclimatic analysis to enhance reintroduction biology of the endangered helmeted honeyeater (Lichenostomus melanops cassidix) in south-eastern Australia," *Restoration ecology*, vol. 6, no. 3, pp. 238–243, 1998.

[125] Y. Peng and H. Ling, "Pattern formation in a ratio-dependent predator-prey model with cross-diffusion," *Applied Mathematics and Computation*, vol. 331, pp. 307–318, 2018.

[126] L. Perko, *Differential Equations and Dynamical Systems*. New York, Springler-Verlag, 2001.

[127] L. Perko, *Differential Equations and Dynamical Systems*. Springer Science & Business Media, 2013, vol. 7.

[128] G. A. Polis, "The evolution and dynamics of intraspecific predation," *Annual Review of Ecology, Evolution, and Systematics*, vol. 12, no. 1, pp. 225–251, 1981.

[129] B. Prasad, M. Banerjee, and P. Srinivasu, "Dynamics of additional food provided predator–prey system with mutually interfering predators," *Mathematical Biosciences*, vol. 246, no. 1, pp. 176–190, 2013.

[130] K. D. Prasad and B. Prasad, "Biological pest control using cannibalistic predators and with provision of additional food: A theoretical study," *Theoretical Ecology*, vol. 11, no. 2, pp. 191–211, 2018.

[131] E. L. Preisser and D. I. Bolnick, "The many faces of fear: Comparing the pathways and impacts of nonconsumptive predator effects on prey populations," *PLoS One*, vol. 3, no. 6, e2465, 2008.

[132] L. Pribylova and A. Peniaskova, "Foraging facilitation among predators and its impact on the stability of predator–prey dynamics," *Ecological Complexity*, vol. 29, pp. 30–39, 2017.

[133] E. Reimondo, T. Sisk, and T. Thiemer, "Effects of introduced Bison on wetlands of the Kaibab Plateau, Arizona," *The Colorado Plateau VI: Science and Management at the landscape scale. University of Arizona Press, Tucson, Arizona*, pp. 120–135, 2015.

[134] V. H. Rudolf, "Consequences of stage-structured predators: Cannibalism, behavioral effects, and trophic cascades," *Ecology*, vol. 88, no. 12, pp. 2991–3003, 2007.

[135] H. M. Safuan, H. S. Sidhu, Z. Jovanoski, and I. N. Towers, "A two-species predator-prey model in an environment enriched by a biotic resource," *ANZIAM Journal*, vol. 54, pp. C768–C787, 2012.

[136] B. Sahoo and S. Poria, "Effects of additional food in a delayed predator–prey model," *Mathematical Biosciences*, vol. 261, pp. 62–73, 2015.

[137] Sajan and B. Dubey, "Chaos control in a multiple delayed phytoplankton–zooplankton model with group defense and predator's interference," *Chaos: An Interdisciplinary Journal of Nonlinear Science*, vol. 31, no. 8, p. 083 101, 2021.

[138] Sajan, B. Dubey, and S. K. Sasmal, "Chaotic dynamics of a plankton-fish system with fear and its carry over effects in the presence of a discrete delay," *Chaos, Solitons & Fractals*, vol. 160, p. 112 245, 2022.

[139] K. Sarkar and S. Khajanchi, "Impact of fear effect on the growth of prey in a predator-prey interaction model," *Ecological Complexity*, vol. 42, p. 100 826, 2020.

[140] K. Sarkar and S. Khajanchi, "Spatiotemporal dynamics of a predator-prey system with fear effect," *Journal of the Franklin Institute*, vol. 360, no. 11, pp. 7380–7414, 2023.

[141] S. K. Sasmal, "Population dynamics with multiple Allee effects induced by fear factors–a mathematical study on prey-predator interactions," *Applied Mathematical Modelling*, vol. 64, pp. 1–14, 2018.

[142] S. K. Sasmal, Anshu, and B. Dubey, "Diffusive patterns in a predator–prey system with fear and hunting cooperation," *The European Physical Journal Plus*, vol. 137, no. 2, p. 281, 2022.

[143] S. K. Sasmal, J. Banerjee, and Y. Takeuchi, "Dynamics and spatio-temporal patterns in a prey–predator system with aposematic prey," *Mathematical Biosciences and Engineering*, vol. 16, no. 5, pp. 3864–3884, 2019.

[144] S. K. Sasmal and Y. Takeuchi, "Dynamics of a predator-prey system with fear and group defense," *Journal of Mathematical Analysis and Applications.*, vol. 481, no. 1, p. 123 471, 2020.

[145] S. K. Sasmal and Y. Takeuchi, "Modeling the Allee effects induced by cost of predation fear and its carry-over effects," *Journal of Mathematical Analysis and Applications*, vol. 505, no. 2, p. 125 485, 2022.

[146] L. A. Segel and J. L. Jackson, "Dissipative structure: An explanation and an ecological example," *Journal of Theoretical Biology*, vol. 37, no. 3, pp. 545–559, 1972.

[147] D. Sen, S Ghorai, and M. Banerjee, "Allee effect in prey versus hunting cooperation on predator–enhancement of stable coexistence," *International Journal of Bifurcation and Chaos*, vol. 29, no. 06, p. 1 950 081, 2019.

[148] D. Sen, S Ghorai, S. Sharma, and M. Banerjee, "Allee effect in prey's growth reduces the dynamical complexity in prey-predator model with generalist predator," *Applied Mathematical Modelling*, vol. 91, pp. 768–790, 2021.

[149] M. Sen, P. Srinivasu, and M. Banerjee, "Global dynamics of an additional food provided predator–prey system with constant harvest in predators," *Applied Mathematics and Computation*, vol. 250, pp. 193–211, 2015.

[150] S. Sharma and G. Samanta, "A Leslie–Gower predator–prey model with disease in prey incorporating a prey refuge," *Chaos Solitons & Fractals*, vol. 70, pp. 69–84, 2015.

[151] J. J. Shepherd and L. Stojkov, "The logistic population model with slowly varying carrying capacity," *ANZIAM Journal*, vol. 47, pp. C492–C506, 2005.

[152] L. Shevtsova, G. Zhdanova, V. Movchan, and A. Primak, "Experimental interrelationship between dreissena and planktonic invertebrates," *Hydrobiological Journal*, vol. 22, no. 6, pp. 36–39, 1986.

[153] H. L. Smith, *Monotone Dynamical Systems: an Introduction to the Theory of Competitive and Cooperative Systems*. American Mathematical Soc., 1995.

[154] D. Song, C. Li, and Y. Song, "Stability and cross-diffusion-driven instability in a diffusive predator–prey system with hunting cooperation functional response," *Nonlinear Analysis: Real World Applications*, vol. 54, p. 103 106, 2020.

[155] Y. Song and J. Wei, "Bifurcation analysis for Chen's system with delayed feedback and its application to control of chaos," *Chaos, Solitons & Fractals*, vol. 22, no. 1, pp. 75–91, 2004.

[156] F. Souna, P. K. Tiwari, M. Belabbas, and Y. Menacer, "A predator–prey system with prey social behavior and generalized Holling III functional response: Role of predator-taxis on spatial patterns," *Mathematical Methods in the Applied Sciences*, vol. 46, no. 13, pp. 13 991–14 006, 2023.

[157] P. Srinivasu, B. Prasad, and M Venkatesulu, "Biological control through provision of additional food to predators: A theoretical study," *Theoretical Population Biology*, vol. 72, no. 1, pp. 111–120, 2007.

[158] L. Stone, *Period-doubling reversals and chaos in simple ecological models*, 1993.

[159] X. Tang, Y. Song, and T. Zhang, "Turing–Hopf bifurcation analysis of a predator–prey model with herd behavior and cross-diffusion," *Nonlinear Dynamics*, vol. 86, no. 1, pp. 73–89, 2016.

[160] R. Taylor, "A family of regression equations describing the density distribution of dispersing organisms," *Nature*, vol. 286, no. 5768, pp. 53–55, 1980.

[161] P. K. Tiwari, M. Verma, S. Pal, Y. Kang, and A. K. Misra, "A delay nonautonomous predator–prey model for the effects of fear, refuge and hunting cooperation," *Journal of Biological Systems*, vol. 29, no. 04, pp. 927–969, 2021.

[162] J. C. Touchon, M. W. McCoy, J. R. Vonesh, and K. M. Warkentin, "Effects of plastic hatching timing carry over through metamorphosis in red-eyed treefrogs," *Ecology*, vol. 94, no. 4, pp. 850–860, 2013.

[163] J. P. Tripathi, S. Abbas, G.-Q. Sun, D. Jana, and C.-H. Wang, "Interaction between prey and mutually interfering predator in prey reserve habitat: Pattern formation and the Turing–Hopf bifurcation," *Journal of the Franklin Institute*, vol. 355, no. 15, pp. 7466–7489, 2018.

[164] J. P. Tripathi *et al.*, "Modeling the cost of anti-predator strategy in a predator-prey system: The roles of indirect effect," *Mathematical Methods in the Applied Sciences*, vol. 45, no. 8, pp. 4365–4396, 2022.

[165] A. M. Turing, "The chemical basis of morphogenesis," *Philosophical Transactions of the Royal Society of London. Series B, Biological Sciences*, vol. 237, no. 641, pp. 37–72, 1952.

[166] A. M. Turing, "The chemical basis of morphogenesis," *Bulletin of Mathematical Biology*, vol. 52, pp. 153–197, 1990.

[167] H. M. Ulfa, A. Suryanto, and I. Darti, "Dynamics of Leslie-Gower predator-prey model with additional food for predators," *International Journal of Pure and Applied Mathematics*, vol. 115, no. 2, pp. 751–765, 2017.

[168] R. K. Upadhyay, N. Kumari, and V. Rai, "Wave of chaos in a diffusive system: Generating realistic patterns of patchiness in plankton–fish dynamics," *Chaos, Solitons & Fractals*, vol. 40, no. 1, pp. 262–276, 2009.

[169] R. K. Upadhyay and S. Mishra, "Population dynamic consequences of fearful prey in a spatiotemporal predator-prey system.," *Mathematical Biosciences and Engineering*, vol. 16, no. 1, pp. 338–372, 2018.

[170] R. K. Upadhyay, N. Thakur, and B Dubey, "Nonlinear non-equilibrium pattern formation in a spatial aquatic system: Effect of fish predation," *Journal of Biological Systems*, vol. 18, no. 01, pp. 129–159, 2010.

[171] R. K. Upadhyay, W. Wang, and N. Thakur, "Spatiotemporal dynamics in a spatial plankton system," *Mathematical Modelling of Natural Phenomena*, vol. 5, no. 5, pp. 102–122, 2010.

[172] M. Van Baalen, V. Křivan, P. C. van Rijn, and M. W. Sabelis, "Alternative food, switching predators, and the persistence of predator-prey systems," *The American Naturalist*, vol. 157, no. 5, pp. 512–524, 2001.

[173] J. Vandermeer, "Period 'bubbling'in simple ecological models: Pattern and chaos formation in a quartic model," *Ecological modelling*, vol. 95, no. 2-3, pp. 311–317, 1997.

[174] P.-F. Verhulst, "Notice sur la loi que la population suit dans son accroissement," *Correspondence mathematique et physique*, vol. 10, pp. 113–129, 1838.

[175] M. Verma and A. Misra, "Modeling the effect of prey refuge on a ratio-dependent predator–prey system with the Allee effect," *Bulletin of Mathematical Biology*, vol. 80, no. 3, pp. 626–656, 2018.

[176] V. Vitagliano, "Some phenomenological and thermodynamic aspects of diffusion in multicomponent systems," *Pure and Applied Chemistry*, vol. 63, no. 10, pp. 1441–1448, 1991.

[177] V. Volterra, "Variations and fluctuations of the number of individuals in animal species living together.," *Animal Ecology*, pp. 412–433, 1931.

[178] J. Wang, J. Shi, and J. Wei, "Dynamics and pattern formation in a diffusive predator–prey system with strong Allee effect in prey," *Journal of Difference Equations*, vol. 251, no. 4-5, pp. 1276–1304, 2011.

[179] J. Wang, Y. Cai, S. Fu, and W. Wang, "The effect of the fear factor on the dynamics of a predator-prey model incorporating the prey refuge," *Chaos: An Interdisciplinary Journal of Nonlinear Science*, vol. 29, no. 8, p. 083 109, 2019.

[180] X. Wang, L. Zanette, and X. Zou, "Modelling the fear effect in predator–prey interactions," *Journal of Mathematical Biology*, vol. 73, no. 5, pp. 1179–1204, 2016.

[181] X. Wang and X. Zou, "Modeling the fear effect in predator–prey interactions with adaptive avoidance of predators," *Bulletin of Mathematical Biology*, vol. 79, no. 6, pp. 1325–1359, 2017.

[182] D. Worster, *Dust Bowl: the Southern Plains in the 1930s*. Oxford University Press, 2004.

[183] B. Xie, "Impact of the fear and Allee effect on a Holling type II prey–predator model," *Advances in Difference Equations*, vol. 2021, no. 1, pp. 1–15, 2021.

[184] R. Yang and J. Wei, "Bifurcation analysis of a diffusive predator–prey system with nonconstant death rate and Holling III functional response," *Chaos, Solitons & Fractals*, vol. 70, pp. 1–13, 2015.

[185] V. I. Yukalov, E. P. Yukalova, and D. Sornette, "Extreme events in population dynamics with functional carrying capacity," *The European Physical Journal Special Topics*, vol. 205, no. 1, pp. 313–354, 2012.

[186] V. I. Yukalov, E. Yukalova, and D. Sornette, "Punctuated evolution due to delayed carrying capacity," *Physica D: Nonlinear Phenomena*, vol. 238, no. 17, pp. 1752–1767, 2009.

[187] L. Y. Zanette, A. F. White, M. C. Allen, and M. Clinchy, "Perceived predation risk reduces the number of offspring songbirds produce per year," *Science*, vol. 334, no. 6061, pp. 1398–1401, 2011.

[188] L. Zhang and C. Zhang, "Rich dynamic of a stage-structured prey–predator model with cannibalism and periodic attacking rate," *Communications in Nonlinear Science and Numerical Simulation*, vol. 15, no. 12, pp. 4029–4040, 2010.

[189] X. Zhang, Q. An, and L. Wang, "Spatiotemporal dynamics of a delayed diffusive ratio-dependent predator–prey model with fear effect," *Nonlinear Dynamics*, vol. 105, no. 4, pp. 3775–3790, 2021.

[190] Y. Zhang, X. Rong, and J. Zhang, "A diffusive predator-prey system with prey refuge and predator cannibalism," *Mathematical Biosciences and Engineering*, vol. 16, no. 3, pp. 1445–1470, 2019.

[191] Z. Zhang, R. K. Upadhyay, R. Agrawal, and J. Datta, "The gestation delay: A factor causing complex dynamics in gause-type competition models," *Complexity*, vol. 2018, pp. 1–21, 2018.

[192] J. Zhao and Y. Shao, "Bifurcations of a prey-predator system with fear, refuge and additional food," *Mathematical Biosciences and Engineering*, vol. 20, pp. 3700–3720, 2023.

[193] M. Zimmermann and J. R. Spence, "Adult population dynamics and reproductive effort of the fishing spider dolomedes triton (araneae, pisauridae) in central alberta," *Canadian Journal of Zoology*, vol. 70, no. 11, pp. 2224–2233, 1992.

[194] J. Zu and M. Mimura, "The impact of Allee effect on a predator–prey system with Holling type II functional response," *Applied Mathematics and Computation*, vol. 217, no. 7, pp. 3542–3556, 2010.

List of Publications

Published

1. Sourav Kumar Sasmal, Anshu and Balram Dubey. Diffusive patterns in a predator–prey system with fear and hunting cooperation, The European Physical Journal Plus, 137:281, (2022).
   (Impact Factor **3.4**, **SCI**, Q2)
   https://doi.org/10.1140/epjp/s13360-022-02497-x

2. Anshu, Balram Dubey, Sourav Kumar Sasmal and Anand Sudarshan. Consequences of fear effect and prey refuge on the Turing patterns in a delayed predator–prey system, Chaos: An Interdisciplinary Journal of Nonlinear Science, 32:123132, (2022).
   (Impact Factor **3.741**, **SCI**, Q1)
   https://doi.org/10.1063/5.0126782

3. Anshu and Balram Dubey. Spatiotemporal dynamics of a multi-delayed prey–predator system with variable carrying capacity, Chaos: An Interdisciplinary Journal of Nonlinear Science, 33:113116, (2023).
   (Impact Factor **3.741**, **SCI**, Q1)
   https://doi.org/10.1063/5.0173566

4. Anshu, Sourav Kumar Sasmal and Balram Dubey. Impact of Cooperative Hunting and Fear-Induced in a Prey-Predator System with Crowley-Martin Functional Response, In: Banerjee, S., Saha, A. (eds) Nonlinear Dynamics and Applications. Springer Proceedings in Complexity, 1015-1026, (2022).
   (Indexed in **Scopus**)
   https://doi.org/10.1007/978-3-030-99792-2_86

5. Sajan, Anshu and Balram Dubey. Study of a cannibalistic prey-predator model with Allee effect in prey under the presence of diffusion, Chaos, Solitons & Fractals, 182:114797, (2024).
   (Impact Factor **7.8**, **SCI**, Q1)
   https://doi.org/10.1016/j.chaos.2024.114797

6. Masoom Bhargava, Anshu and Balram Dubey. Spatiotemporal and trade-off dynamics in prey-predator model with domed functional response and fear effect, International Journal of Bifurcation and Chaos, 34:2450061, (2024).
(Impact Factor **2.836**, **SCI**, Q1)
https://doi.org/10.1142/S0218127424500615

7. Balram Dubey, Anand Singh, and Anshu. Spatiotemporal dynamics of prey-predator model incorporating Holling-type II functional response with fear and its carry-over effects, Chaos: An Interdisciplinary Journal of Nonlinear Science, 34:053108, (2024).
(Impact Factor **3.741**, **SCI**, Q1)
https://doi.org/10.1063/5.0203353

8. Anshu, Sajan and Balram Dubey. Bifurcation analysis and spatiotemporal dynamics in a diffusive predator-prey system incorporating a Holling type II functional response, International Journal of Bifurcation and Chaos, 34:2450105, (2024).
(Impact Factor **2.836**, **SCI**, Q1)
https://doi.org/10.1142/S0218127424501050

9. Nawaj Sarif, Arjun Kumar, Anshu, Sahabuddin Sarwardi and Balram Dubey. Spatiotemporal dynamics in a delayed prey-predator model with nonlinear prey refuge and harvesting, Chaos, Solitons & Fractals, 186:115247, (2024).
(Impact Factor **7.8**, **SCI**, Q1)
https://doi.org/10.1016/j.chaos.2024.115247

Workshops/ Schools/ Conferences

1. A Five Days International Seminar on Mathematical Modeling and Turing's Pattern Formation organized by the Department of Mathematics, Vellore Institute of Technology, Vellore, India, (11-15 September 2023).

2. Workshop on Fundamentals of Mathematical Biology organized by Indian Institute of Information Technology Allahabad, India, (11-12 May 2023).

3. Workshop on Nonlinear Phenomena in Mathematical Biology (WoNPMB-2022) organized by the Department of Applied Sciences, ABV- Indian Institute of Information Technology and Management, Gwalior, India, (19-23 December 2022).

4. International Conference on Advances in Biomathematics organized by Amity University, Lucknow, India, (21-23 July 2022).

5. International Conference on Advances in Mechanics, Modelling, Computing and Statistics (ICAMMCS-2022) organized by Department of Mathematics, BITS Pilani, Pilani Campus, India, (19-21 March 2022).

6. International Conference on Nonlinear Dynamics and Applications organized by Sikkim Manipal Institute of Technology, Sikkim, India, (9-11 March 2022).

7. Workshop on Teaching-Learning Workshop for Next Generation Academicians organized by TLC BITS Pilani, Pilani Campus, India, (27 November 2021).

8. Two Week Online Faculty Development Programme on Biomathematics organized by P.G.D.A.V. College, University of Delhi in collaboration with Mahatma Hansraj Faculty Development Centre (MHRFDC), Hansraj College, University of Delhi, India, (15-28 October 2020).

Brief Biography of the Supervisor

Prof. Balram Dubey is a Professor and Former Head of the Department of Mathematics at Birla Institute of Technology & Science, Pilani, Pilani Campus, India. He earned his Bachelor's Degree (B.Sc. Hons) with the first merit rank from Bhagalpur University, Bhagalpur, India, in 1988. He received his Master's degree in 1990 and Ph.D. degree in 1994 from the Department of Mathematics, Indian Institute of Technology Kanpur. Kanpur, India. He was a Research Associate at IIT Kanpur from 1994-1995, and later, he joined IIT Kanpur as visiting faculty during 2000- 2002. He was awarded the "Best Teaching Award" for tutorship in MATH1102 in 2001 at IIT Kanpur. Prof. Dubey served as Lecturer and Senior Lecturer in the Department of Mathematics at Tezpur University, India, from 1995 to 2000. There, he guided two students. In 2002, he joined the Department of Mathematics, Birla Institute of Technology & Science, Pilani, Pilani Campus, as an Assistant Professor. He was promoted to Associate Professor in August 2010 and Professor in February 2013. His research interests are Mathematical Biology, Mathematical Ecology, Ecotoxicology, Soil Erosion and Conservation, Epidemiology, Mathematical Immunology, and Applications of ODEs & PDEs in real-world Problems. As a result of his research accomplishments, he has published more than 100 research articles in national and international journals of repute. He is also the author of the book "Introductory Linear Algebra", Asian Books, Pvt. Ltd. 2007. He has successfully guided 7 Ph.D. students.

Brief Biography of the Candidate

Anshu is a Senior Research Fellow at the Department of Mathematics, BITS Pilani, Pilani Campus, having joined the institute in January 2020. Her research area is mathematical ecology, which mainly focuses on formulation and analysis of mathematical models describing population dynamics. Anshu has actively participated in various workshops and webinars, and she has presented her work at both national and international conferences. Her research is funded by the University Grants Commission, New Delhi, India.

Anshu achieved eligibility for the CSIR-UGC NET Junior Research Fellowship in June 2019 and also qualified the GATE examination in the field of Mathematical Sciences. She obtained her bachelor's degree in Mathematics, Computer Science, and Physics from Delhi University. Subsequently, she completed her Master's degree in Mathematics from Panjab University, Chandigarh.